Transmembrane domain interactions in carnitine palmitoyltransferase I

Zsuzsanna Jenei

A thesis submitted for the degree of Doctor of Philosophy

University of Warwick

Department of Chemistry

February 2010

Table of Contents

LIST OF FIGURES

LIST OF TABLES

ACKNOWLEDGEMENTS

I would like to thank my supervisor, Dr Ann Dixon, for her exceptional guidance and support during my years at the University of Warwick, her enthusiasm to study the fascinating field of membrane protein science, and for her patience and help throughout the writing of this manuscript.

I am very thankful to all Dixon Group members, past and present, for their encouragement and their company in the lab. Special thanks to Dr Joanne Oates for teaching me in the lab, listening to all my worries and for all the helpful discussions, Dr Gavin King for his help with the cross-linking and GALLEX experiments, Dr Andrew Beevers for his advice regarding AUC and CHI data analysis and Dr Gemma Warren for helpful discussions.

Special thanks go to Professor Victor A. Zammit and Dr Karen Matthews, who introduced me to their work with carnitine palmitoyltransferase 1 and gave me helpful advice and support.

I am really grateful to everyone in the Chemical Biology Cluster. Thanks go to the Blindauer group, especially to Dr Oksana Leszczyszyn and Jin Lu for their helpful discussions and friendship. I am also very thankful for Professor Alison Roger and her research group for letting me use their equipment and for all their help "on the 6th floor". I also would like to Professor Greg Challis and Dr Martin Lochner for their help as my academic panel.

My thanks also go to Dr Dirk Schneider for providing plasmids and guidance on performing the GALLEX assay, Professor Donald Engelman for providing plasmids for performing the TOXCAT assay, Dr Tim Dafforn and Rosemary Parslow in Birmingham University and Dr David Staunton in Oxford University for their guidance in collecting AUC data, furthermore to Dr David Scott for SEDFIT tutorial.

I would also like to thank for the Warwick Postgraduate Research Fellowship for financial support.

Most especially I wish to thank my Jenei and Fejér families for their endless support and love, in particular to my husband, Dr Szilárd Fejér, for his continued love and optimism. Finally, I would like to dedicate this thesis to the memory of my grandmother, Józsvai Anna Magdolna.

DECLARATION

I declare that the work recorded in this thesis is original and was conducted by the author, unless otherwise stated. No part of it has previously been presented for any other degree to any institution.

All sources of information have been acknowledged by means of reference.

Funding was provided by the Warwick Postgraduate Research Fellowship (WPRF) studentship.

Some of the work presented in this thesis (CHAPTER 3) has been published in the following journal (appended to the end of the thesis):

Jenei, Z. A., K. Borthwick, V. A. Zammit and A. M. Dixon (2009). Self-association of transmembrane domain 2 (TM2), but not TM1, in carnitine palmitoyltransferase 1A: role of GXXXG(A) motifs. *J Biol Chem* **284**(11): 6988-97.

ABBREVIATIONS

A

aa	Amino acid
ACN	Acetonitrile
Amp	Ampicillin
AU	Absorbance units
AUC	Analytical ultracentrifugation

B

BS^3	Bis(sulfosuccinimidyl)suberate

C

CAM	Chloramphenicol
CAT	Chloramphenicol acetyl transferase
CAT	Carnitine acetyltransferase
CD	Circular dichroism
CHI	CNS searching of helix interactions
CoA	Coenzyme A
COT	Carnitine octanoyltransferase
CPT II	Carnitine palmitoyltransferase II
CNS	Crystallography and NMR system

D

dH_2O	Distilled water
DNA	Deoxyribonucleic acid
dNTP	Deoxynucleotide triphosphate
DPC	Dodecylphosphocholine

E

E. coli	*Escherichia coli*
EDTA	Ethylenediaminetetraacetic acid

	ESI-MS	Electrospray ionisation mass spectrometry
G		
	GpA	Glycophorin A
H		
	HEPES	4-(2-hydroxyethyl)-1-piperazineethanesulfonic acid
	HPLC	High performance liquid chromatography
I		
	IPTG	Isopropyl-beta-D-thiogalactopyranoside
	LB	Luria-Bertani broth
	L-CPT I	Liver type carnitine palmitoyltransferase I
	LPPG	Lyso-palmitoyl phosphatidylglycerol
M		
	MALDI	Matrix-assisted laser desorption/ionisation
	MBP	Maltose binding protein
	M-CPT I	Muscle type carnitine palmitoyltransferase I
	M:P	Micelle to peptide concentration ratio
	MS	Mass spectrometry
	MW	Molecular weight
N		
	NMR	Nuclear magnetic resonance
O		
	OD	Optical density
	OG	Octylglucoside
	OMM	Outer mitochondrial membrane
	ONP	o-nitrophenol
	ONPG	o-nitrophenyl-β-D-galactoside
P		
	PAGE	Poly-acrylamide gel electrophoresis

	PBS	Phosphate buffered saline
	PCR	Polymerase chain reaction
	PSV	Partial specific volume
R		
	RP-HPLC	Reversed phase high performance liquid chromatography
	rpm	Revolutions per minute
S		
	SDS	Sodium dodecyl sulphate
	SV	Sedimentation velocity
T		
	TBA	Tris-borate-EDTA
	TCA	Trichloroacetic acid
	TFA	Trifluoroacetic acid
	TFE	2,2,2-trifluoroethanol
	TM	Transmembrane
	TOF	Time-of-flight
U		
	UV	Ultraviolet
W		
	wt	Wild type

Greek symbols

Δ	Delta (gene knockout)
ε	Extinction coefficient
λ	Wavelength
µL	microliter
µM	micromolar

Amino acid symbols

alanine	A	Ala
arginine	R	Arg
asparagine	N	Asn
aspartic acid	D	Asp
cysteine	C	Cys
glutamic acid	E	Glu
glutamine	Q	Gln
glycine	G	Gly
isoleucine	I	Ile
leucine	L	Leu
lysine	K	Lys
methionine	M	Met
phenylalanine	F	Phe
proline	P	Pro
serine	S	Ser
threonine	T	Thr
tryptophan	W	Trp
tyrosine	Y	Tyr
valine	V	Val

ABSTRACT

Membrane proteins are involved in a wide range of vital cellular processes, responsible for relaying signals and cargo across cell membranes. A deeper molecular understanding of their function is essential to elucidate the mechanisms of numerous diseases and medical conditions. As an example, the carnitine palmitoyltransferase 1 (CPT1) enzymes are responsible for the regulation of mitochondrial fatty acid oxidation thus are central to cell function.

Previous work had shown that the transmembrane (TM) domains of the mitochondrial outer membrane protein CPT1 have a significant influence on the enzyme's kinetics, which is different in the two catalytically active isoforms, CPT1A and CPT1B. It was also shown that TM-domains, and specifically TM2, are involved in driving the oligomerisation of the full length CPT1A. For this reason, the study of TM-TM oligomerisation and their roles in the function of CPT1 are fundamentally important in the design of pharmacological strategies aimed at the modulation of the activities of these enzymes in conditions such as diabetes.

The main focus of this PhD research was to systematically investigate the homo- and hetero-oligomerisation of the TM domains to help better understand the structure-function relationship for CPT1 membrane proteins. In this project, different techniques were used from the areas of chemistry, molecular biology, and biophysics (*in vivo* oligomerisation assays, chemical crosslinking, circular dichroism and analytical ultracentrifugation), in order to examine these interactions.

The membrane spanning sequences of rCPT1A and rCPT1B were found to self-associate, and the order of oligomerisation was also determined. Sequence motifs likely to be responsible for the interactions of these TM domains were identified using *in silico* modelling. Mutagenesis analyses confirmed the role of suggested GxxxG(A) motifs in the homo-oligomerisation of rCPT1A TM2 domains. The hetero-oligomerisation of TM1-TM2 domains was also studied, and was found to be significant in both isoforms. The work presented in this thesis shows that the membrane spanning regions of the CPT1 enzymes are capable of interacting through both homo- and hetero-oligomerisation. The results strongly suggest that these interactions may play a significant role in the complex formation of the full length enzymes and provide further evidence that CPT1 may function as a channel in the outer mitochondrial membrane.

CHAPTER 1

INTRODUCTION

In this chapter basic concepts are introduced about the membrane protein research field, concentrating on α-helical membrane proteins, and the current knowledge about carnitine palmitoyltransferase 1 (CPT1) enzymes is shortly summarized.

1.1 Membrane proteins

Membrane proteins regulate the flow of information across biological membranes. Information flow is crucial for many essential cellular processes such as translocation, respiration, signalling and energy metabolism (Chapman *et al.*, 1998; Chen and Rost, 2002). The multi-level role of membrane proteins in cell function makes them important targets for drug design for many diseases (Sanders and Nagy, 2000; Sanders and Myers, 2004). Despite the biological importance of membrane proteins, the structure and function of relatively few such proteins has been determined to date.

Determining the three-dimensional structure and identifying the mechanisms by which these proteins function is one of the most difficult topics in protein science. The expression, purification, solubilisation and structural investigation of these proteins are very challenging tasks, confirmed by the fact that to date they represent fewer than ~0.5% of the structures in the Protein Data Bank, while they account for over a quarter of all existing proteins (Granseth *et al.*, 2007). The reason for the very limited structural information for membrane proteins is that,

since they exist in their native form in a mostly non-polar environment, the three-dimensional structure gets disrupted during solubilisation. For this reason, they cannot be crystallized in the same way as water soluble proteins.

The complexity of biological membranes explains well the intricacy of membrane protein research. In the fluid-mosaic or Singer-Nicolson model (Singer and Nicolson, 1972) of biological membranes, the fluidity of the membrane is the result of hydrophobic lipid-protein interactions. Globular membrane proteins are considered to be of two different types, extrinsic (peripheral) and intrinsic (integral).

One important subfamily of integral membrane proteins are transmembrane proteins. There are two main types of transmembrane proteins: β-barrel proteins (**Figure 1.1 a**), in which the membrane-spanning regions are made up of β-strands, and α-helical proteins, in which the membrane-spanning regions are made up of α-helices (**Figure 1.1 b**). The current state of understanding of the stability and folding of these proteins has been summarised in several reviews (White and Wimley, 1999; White, 2003; Wimley, 2003; Tamm *et al.*, 2004). These reviews focus on their protein binding and folding in bilayer interfaces, the transmembrane helix insertion, helix-helix interactions, as well as on their effects on the structure and function of lipid bilayers.

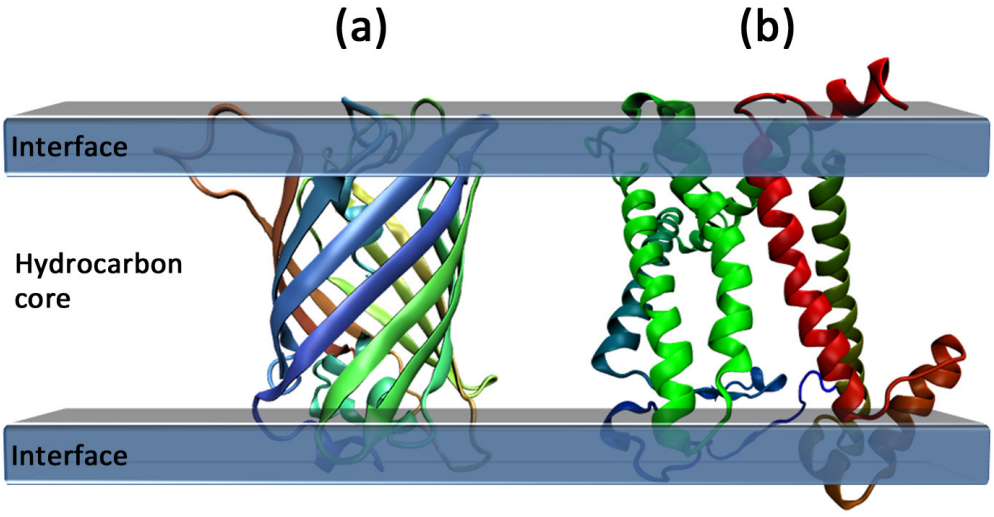

Figure 1.1 - The two types of transmembrane proteins: (a) β-barrel (green fluorescent protein, PDB ID 1ema) and (b) α-helical (reaction centre from *Rhodobacter sphaeroides*, PDB ID 2hj6) structures.

1.2 α-helical integral membrane proteins

As the main topic of this thesis is the oligomerisation of the transmembrane segments within α-helical membrane proteins, in the following sections the concepts about the folding and oligomerisation of helical membrane proteins are reviewed.

1.2.1 The folding of α-helical transmembrane proteins

Involved in a wide range of essential biological functions, α-helical membrane proteins are of great interest in protein science. During the last thirty years, many studies have helped our understanding of the structural determinants of the stability and folding of these proteins. Central aspects about structural stability, folding pathways and association of transmembrane segments in α-helical membrane proteins have improved markedly in recent years, and we now know over 90 unique structures (von Heijne, 1996; Fleishman and Ben-Tal, 2002; Bowie, 2005).

A simplified model of membrane protein folding and complex formation, the "Two-Stage Model" proposed by Popot and Engelman (**Figure 1.2**), hypothesises that the final structure in the transmembrane region is assembled from several smaller elements (helices). According to this model, membrane proteins fold in two thermodynamically distinct stages. In the first stage, hydrophobic sequences insert into the bilayer and form stable helices. In the second stage, these helices associate laterally to form the final fold of the protein (Popot and Engelman, 1990). While the extensively studied bacteriorhodopsin was the first example of a "split" membrane protein capable of refolding *via* association of its transmembrane domains (Liao *et al.*, 1984; Popot *et al.*, 1987), the above model was further supported by several other experimental observations. For example, lateral associations of membrane-embedded protein fragments were found to regenerate and refold into functional proteins in several other systems such as lactose permease (Bibi and Kaback, 1990), rhodopsin (Ridge *et al.*, 1995) or the red cell anion exchanger protein (Groves and Tanner, 1995).

It is possible to apply the two-stage model in order to try to understand the folding of other membrane proteins. By focusing our attention on the second stage, we can investigate structural factors determining transmembrane helix-helix association. However, the complexity of helix-interactions in the membrane

bilayer also needs to be taken into account when considering the assembly of the whole protein.

Apart from the actual helix-helix interactions, there are additional complicating factors in interactions of transmembrane segments that determine the shape and stability of membrane proteins. These are the interaction of helices with water, the bilayer hydrocarbon core, bilayer interfaces, and with cofactors as well (Lemmon and Engelman, 1994; White and Wimley, 1999).

The two-stage model (**Figure 1.2**) has been updated to include a possible third stage of membrane protein folding. This third stage takes into account the involvement of peripheral domains and ligand binding in the quaternary structure forming process (Engelman *et al.*, 2003).

Based on our current understanding, the helix-helix association within the membrane bilayer is most likely driven by non-covalent interactions (van der Waals forces, electrostatic interactions or hydrogen bonding). Sequence motifs from well-studied membrane proteins (see below) were found to have great impact in the association of transmembrane domains. Studies investigating the role of these motifs in the folding of membrane proteins were recently summarized (Senes *et al.*, 2004), while their structural determinants were also studied by *in silico* and statistical analyses (Walters and DeGrado, 2006; Harrington and Ben-Tal, 2009). Typical interaction motifs relevant for this work are illustrated in the following section.

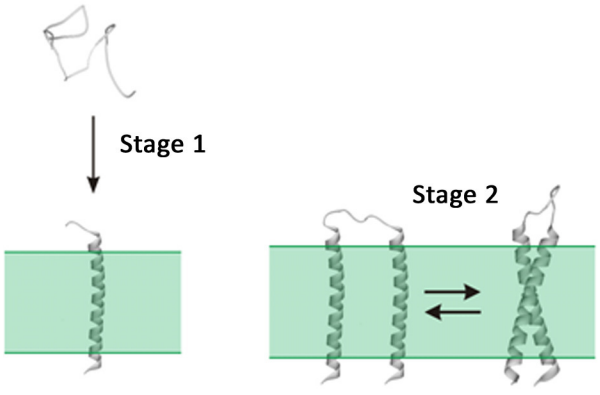

Figure 1.2 - The "Two-Stage Model". Stage 1: Hydrophobic sequences form stable transbilayer α-helices (left). Stage 2: Lateral association of transbilayer α-helices (right).

1.2.2 Interaction motifs in transmembrane helices

The transmembrane spanning regions of α-helical membrane proteins are approximately 20 amino acids in length. These predominantly hydrophobic side chains can contain specific sequence motifs which could support helix interactions: Russ and Engelman identified the GxxxG motif, where glycine residues are separated by three other amino acids (Russ and Engelman, 2000), placing the Gly residues on the same face of the α-helix. The small side chain in Gly allows very close packing of the helices, giving rise to stabilising van der Waals interactions. The GxxxG motif was identified in more than 100 highly dimeric transmembrane domains, while statistical analyses revealed that it is over-represented in genomes. These observations suggest that many (but not all) GxxxG motifs are involved in forming specific helix-helix interactions.

The discovery of the GxxxG motif was the result of the extensive study of glycophorin A (GpA). GpA is an integral membrane protein in human red blood cells, carries several medically important blood group antigens, and its TM domain has been shown to mediate non-covalent dimerisation. Mutagenesis (Lemmon *et al.*, 1992), computational (Treutlein *et al.*, 1992; Adams *et al.*, 1996) and thermodynamic (Fleming *et al.*, 1997; Fisher *et al.*, 1999; Fleming *et al.*, 2004) characterisation also indicated a central role of GxxxG in GpA dimerisation (**Figure 1.3 a**). The variants of this motif, the "*small xxx small*" (where *small* denotes residues with small side chains such as Ala, Gly, Ser) motifs were also found to mediate transmembrane interactions (Senes *et al.*, 2000), although these motifs do not always play a role in forming strong helix-helix interactions (Schneider and Engelman, 2004).

Another example of a structural motif is the heptad repeat, which consists of a repeating pattern of amino acids. Repeated heptad motifs of amino acids characteristic of soluble leucine zipper coiled-coil interaction domains were also found in membrane proteins such as bacteriorhodopsin, the photosynthetic reaction center, and cytochrome C oxidase (Langosch and Heringa, 1998). The importance of leucine zipper-like motifs in transmembrane domain association was investigated by Langosch and colleagues. They have found that leucine residues are involved in the oligomerisation of designed (polyleucines) and biological (erythropoietin) sequences (Gurezka *et al.*, 1999; Gurezka and Langosch, 2001; Ruan *et al.*, 2004). Another example of leucine-isoleucine

zipper interaction motifs (based on mutagenesis data) can be found in the phospholamban pentamer, shown in **Figure 1.3 b** (Simmerman *et al.*, 1996).

Aromatic π-π stacking interactions between pairs of aromatic residues (Phe, Thr, Tyr) in a membrane environment have also been shown to significantly enhance the strength of oligomerisation of designed transmembrane helices, which suggested that similar interactions may also be a significant factor in the folding and stability of native membrane proteins (Dougherty, 1996; Johnson *et al.*, 2007). The mutagenesis and molecular modelling studies of the cholera toxin secretion protein EpsM provided further evidence for the involvement of aromatic residues in the dimerisation of TM domains (Sal-Man *et al.*, 2007). **Figure 1.3 c** contains an example for aromatic interhelical interactions in bacteriorhodopsin, with the aromatic rings oriented perpendicular to each other (Harrington and Ben-Tal, 2009).

The presence of interhelical hydrogen bonds between polar residues (Gln, Asn, Glu or Asp), which help shielding their polarity in the non-polar core of the bilayer, was found to be sufficient to induce strong helix association in model TM helices (Zhou *et al.*, 2000; Zhou *et al.*, 2001). Modelling and mutagenesis of single asparagines and threonine-serine motifs in membrane proteins highlighted their role in creating helical oligomers (Dawson *et al.*, 2002; Dawson *et al.*, 2003; Sal-Man *et al.*, 2004). The modelling of the interface in the erythropoietin receptor transmembrane domain suggests that interhelical hydrogen bonds between Ser and Thr residues are involved in self-association (Seubert *et al.*, 2003). A recent study of conserved polar residues in human nucleoside triphosphate diphosphohydrolase 3 (NTPDase3) transmembrane domain also found that the formation of interhelical hydrogen bonds promotes oligomerisation and protein folding, and is therefore important for optimal protein expression and enzymatic activity (Gaddie and Kirley, 2009).

Furthermore, the presence of proline residues in transmembrane helices causes kinks, as the amide nitrogen of proline cannot form a backbone hydrogen bond. Incorporation of proline residues provides a way to make highly curved helixes, having a great impact on the TM helix packing, as shown by scanning mutagenesis and studies on model TM segments (von Heijne, 1991; Nilsson *et al.*, 1998; Nilsson and von Heijne, 1998; Orzaez *et al.*, 2004). In summary, the above studies suggest that the presence of a variety of residues and sequence motifs can be strong predictors of transmembrane helix-helix interactions.

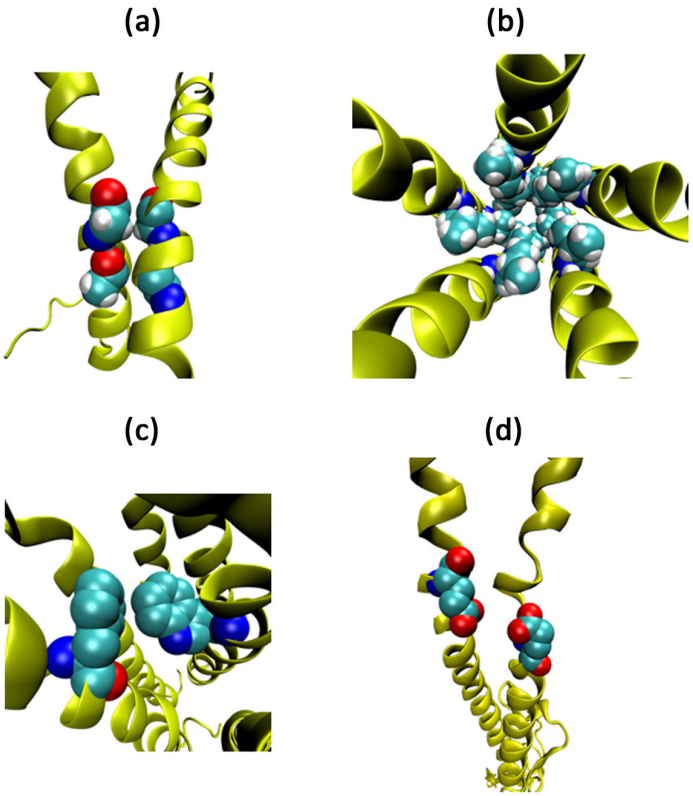

Figure 1.3 - Typical interaction motifs within transmembrane α-helices. (a) GxxxG motif in glycophorin A (PDB ID 1afo); (b) leucine zippers in the phospholamban pentamer (PDB ID 1xnu); (c) interaction between aromatic residues in bacteriorhodopsin (PDB ID 1c3w); (d) Hydrogen bonding between two glutamic acid residues in sodium-potassium channel (PDB ID 3a3y, hydrogen atoms not shown).

1.2.3 Techniques to study helix-helix association

Biological assays developed for measuring helix-helix association have made it possible to study transmembrane domains in a natural membrane environment. The ToxR system (Langosch *et al.*, 1996) was initially created to examine the sequence-dependent homo-oligomerisation of the GpA transmembrane domain in the inner membrane of *E. coli*, and this domain was later used as a positive control to characterise other TM interactions. Other assays such as the TOXCAT assay (Russ and Engelman, 1999) and the POSSYCAT assay (Gurezka and Langosch, 2001) were modifications of the ToxR system. For the study of hetero- (and homo-) oligomerisation, a similar concept was introduced to create the GALLEX assay, having a different transcriptional activator, the asymmetric LexA operator and promoter system (Schneider and Engelman, 2003). From the above mentioned biological assays, the TOXCAT and GALLEX assays are the most relevant for the research presented in this work (for details see § 2.2 and § 2.3).

Many biophysical techniques have also been successfully employed in the research of membrane protein folding, and many of these were initially developed and tested on glycophorin A (MacKenzie and Fleming, 2008). Currently, the interactions *in vitro* between membrane spanning α-helical peptides are usually studied in detergent micelles or in synthetic membranes (lipids) by SDS-PAGE (Fisher *et al.*, 1999), analytical ultracentrifugation (AUC) (Doura *et al.*, 2004), Förster resonance energy transfer (FRET) (Fisher *et al.*, 2003), solution-state nuclear magnetic resonance spectroscopy (NMR) (MacKenzie *et al.*, 1997), or solid state NMR (Liu *et al.*, 2003).

1.3 Carnitine palmitoyltransferase 1 (CPT1)

The main focus of this PhD thesis is the analysis of TM helix-helix interactions in an essential enzyme for fatty acid oxidation, namely carnitine palmitoyltransferase 1 (CPT1). For this reason, in the following paragraphs the existing knowledge underlying the significance of transmembrane domains in the structure and function of this enzyme is reviewed.

Fatty acids are an important source of energy and therefore play a major role in maintaining cell function in many organisms. In order to take part in reactions, fatty acids must first be activated. One such activation process is thioesterification by an acyl-CoA synthetase enzyme. The thioesterified fatty acid can form acylcarnitine in a reaction catalyzed by carnitine acyltransferases (**Figure 1.4**). The carnitine acyltransferases enzyme family includes carnitine palmitoyltransferases (CPT1 and CPT2), carnitine octanoyltransferase (CrOT), and carnitine acyltransferase (CAT), which have substrate preference for long-chain, medium-chain and short-chain acyl groups, respectively.

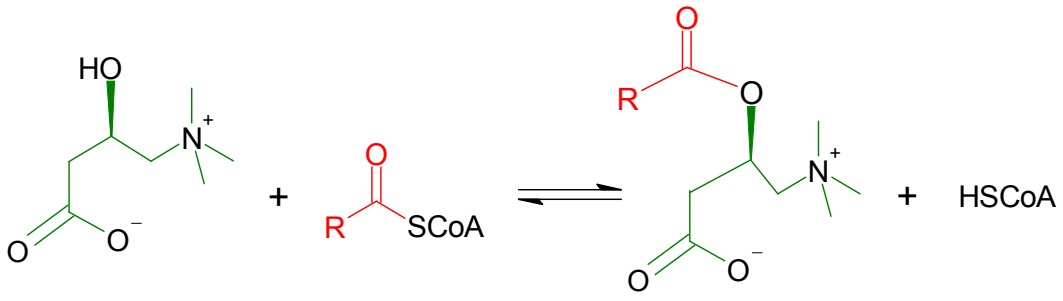

Figure 1.4 - The reaction catalyzed by carnitine acyltransferases. For CPT1 and CPT2: R > 16 C atoms, CrOT: R is between 8-14 C atoms and CAT: R < 8 C atoms.

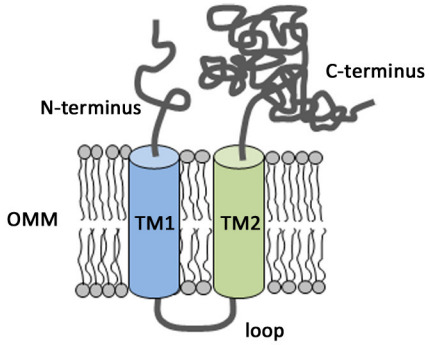

Figure 1.5 - Topology of CPT1 in the outer mitochondrial membrane (OMM).

The CPT1 enzyme exists in three tissue specific isoforms, CPT1A (liver, L-isoform), CPT1B (muscle, M-isoform), and the CPT1C brain-specific isoform. Based on our current knowledge, of the three isoforms, only CPT1A and CPT1B are catalytically active in fatty acid oxidation (McGarry and Brown, 1997), while CPT1C is believed to be involved in appetite control.

The CPT1 enzymes are polytopic integral membrane proteins, localised in the outer mitochondrial membrane (OMM). To date there is no solved 3D crystal structure of CPT1 enzymes. The currently accepted structure is based on experimental studies involving partial proteolysis, immobilised malonyl-CoA and substrates, anti-peptide antibody binding and immunogold electron microscopy (Fraser *et al.*, 1997; van der Leij *et al.*, 1999). The topology of CPT1 includes the N-terminus and the C-terminus, which are both exposed on the cytosolic site of the membrane, while the loop region is extended into the intermembrane space, as shown in **Figure 1.5**. The isoforms also contain two relatively highly conserved hydrophobic transmembrane domains (TM1, TM2: predicted to contain residues 53-75 and 103-122, respectively) in the N-terminal region.

1.3.1 CPT1A and CPT1B

The two catalytically active isoforms, CPT1A and CPT1B (772 aa, 88kDa), have a considerable sequence similarity (63%). They share the same catalytic function, but they have a different sensitivity towards an inhibitor, malonyl-CoA. Their inhibition by malonyl-CoA is crucial because it is the point at which the metabolism of fatty acids (**Figure 1.6**) and glucose come into the most direct 'contact', and can influence each other, and this gives these enzymes a central role in cell function.

It is known that CPT1A is much less sensitive to inhibition by malonyl-CoA (Saggerson, 1982) than CPT1B (Park and Cook, 1998). This kinetic characteristic was found to be dependent on the physical properties of the mitochondrial outer membrane, especially its lipid composition and molecular order (Grantham and Zammit, 1986; Kolodziej and Zammit, 1990; Zammit *et al.*, 1998). These properties can be influenced by physiological conditions, such as fasting or the onset of certain diseases like diabetes, or by experimental manipulation *in vitro*. The membrane microenvironment significantly influences the kinetic properties of the CPT1A isoform, which suggests a high degree of molecular *"flexibility"* in the protein (McGarry and Brown, 2000). By contrast, CPT1B has a permanently high malonyl-CoA sensitivity which is not modulated by physiological state and suggests that this molecule adopts a more *"rigid"* structure (Mynatt *et al.*, 1992; Saggerson *et al.*, 1992).

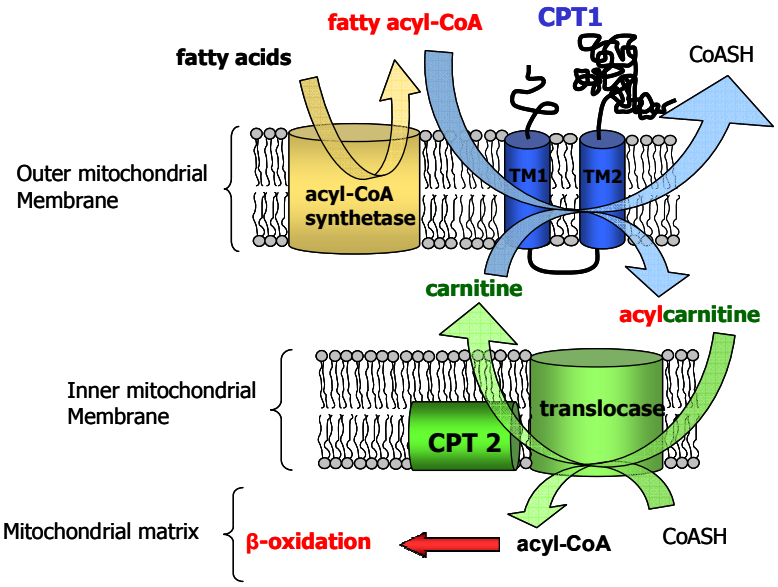

Figure 1.6 - The role of liver and muscle type CPT1 in fatty acid oxidation.

In previous homology modelling studies it was shown that the enzyme inhibitor malonyl-CoA binds to the catalytic C-terminal domain of CPT1 (Morillas *et al.*, 2002). In CPT1A, some specific amino acid residues in the N-terminal segment also modulate the inhibitor binding properties (Shi *et al.*, 1999; Jackson *et al.*, 2000; Jackson *et al.*, 2001). Cross-linking experiments showed that in CPT1A there are close intermolecular interactions between the N- and C-terminal segments which could potentially be modulated by TM1-TM2 interactions (Faye *et al.*, 2005). Consequently, we suggest that the TM1-TM2 interaction is an

important characteristic of the CPT1A isoform function. Since CPT1B does not show a similar adaptation of its kinetic properties to physiological state (Mynatt *et al.*, 1992), it is possible that TM1-TM2 interactions are different in this isoform. A recent report has suggested that the N-terminal region of the protein containing the TM-domains, and specifically TM2, (residues 1-147 in the rat enzyme, rCPT1A) is also involved in driving the oligomerisation of CPT1A (Faye *et al.*, 2007). Studies by Prof. Victor A. Zammit and his research group (Warwick Medical School) have also demonstrated the different oligomerisation properties of the full length rCPT1A and rCPT1B (unpublished data) extracted from yeast or mitochondria. These observations suggest the possibility of CPT1 oligomerisation through the self-association of TM domains, although other structural factors, such as the C-terminal segment, may also be involved in enzyme oligomerisation.

1.3.2 CPT1C function

Recently a third isoform of CPT1, CPT1C been identified in mouse brain (Price *et al.*, 2002; Lavrentyev *et al.*, 2004). CPT1C has a high degree of sequence similarity to CPT1A and B. However, it also has a 33 amino acid residue extension at the C-terminal end of the protein. CPT1C was found in specific regions of the brain that are known to be involved in appetite control and it has been suggested that its function may relate to control of feeding behaviour. CPT1C was studied in a yeast expression system (*Pichia pastoris*), and the membrane fractions contained no detectable activity when assayed using several different acyl-CoA esters and carnitine as substrates. Interestingly, it did have a high affinity for malonyl-CoA binding, suggesting that it is correctly folded and imported into the yeast OMM. CPT1C also binds malonyl-CoA with the same affinity as CPT1A (Price *et al.*, 2002), and it is believed to act as a ‘sink’ for malonyl-CoA in the cell types in which it occurs. Transgenic mice in which the CPT1C gene is disrupted have disturbed energy metabolism, becoming unable to regulate body weight when placed on a high-fat diet (Wolfgang *et al.*, 2006). Also, its localised over-expression in the hypothalamus protects animals against weight gain (Dai *et al.*, 2007). To date this isoform is believed to have a different function from that of CPT1A and B, and was not studied during this work.

1.4 Objectives of the present study

At present it is believed that possible interactions between the CPT1 transmembrane domains are modulated by physicochemical properties of the membrane. A change in membrane fluidity or composition would influence the interaction between N- and C-terminal segments located on the same side of the membrane. The interaction between these segments can therefore alter the protein conformation in the vicinity of the substrate- and inhibitor-binding sites, with consequent modulation of the kinetic characteristics of the protein. Furthermore, a region containing TM2 in CPT1A is thought to control homo-oligomer formation in the full-length protein, and these oligomerisation properties are thought to differ between the muscle and liver forms of the enzyme. In light of the above discussed observations, the interaction of TM domains is suggested to have a critical role in CPT1 structure and function, and was not studied before in detail. Therefore, the present study was designed to investigate the homo- and hetero-oligomerisation of the TM domains in CPT1A and CPT1B (**Figure 1.7**).

As summarised in **Figure 1.7**, the overall aims of the present PhD project were:

- To examine the self-association of the rCPT1A TM domains in order to identify the oligomeric states achieved and compare these with the full length protein's known oligomerisation behaviour (CHAPTER 3).
- Investigation of the role of helix-helix interaction motifs in the possible oligomerisation of rCPT1A TM2 (CHAPTER 4).
- Study the oligomerisation of rCPT1B TM domains, and compare this with what has been observed for rCPT1A TM domains (CHAPTER 5).
- Determine the possible hetero interactions of TM1-TM2 in both isoforms (CHAPTER 6).

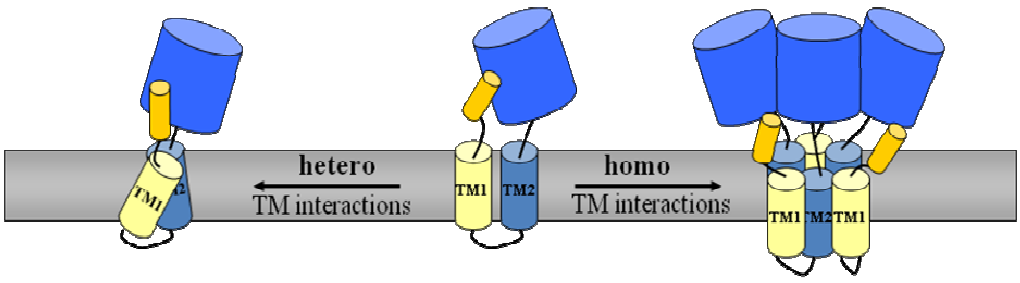

Figure 1.7 - Schematic representation of possible homo and hetero TM interactions in CPT1.

CHAPTER 2

MATERIALS AND METHODS

In this chapter the biochemical and biophysical experimental techniques used are presented, as well as the methods employed in data analysis and theoretical modelling of helix-helix interactions.

2.1 General practice

2.1.1 Chemicals

Throughout this research, unless otherwise stated, all standard laboratory chemicals were purchased from the following companies in analytical reagent or the highest grade for microbiology work: Sigma Aldrich (UK), BDH Merck (UK) or Fisher Scientific (UK). Enzymes and buffers for DNA work were purchased from Fermentas (UK), Invitrogen (UK), New England Biolabs (UK), Promega (UK) or Stratagene (UK).

2.1.2 Reagents and buffers

All buffers were prepared using distilled water (dH_2O, Millipore), and organic solvents were of analytical reagent grade or better. Buffers and dH_2O for DNA work were sterilized by autoclave and/or filtered using 0.22 μM filters (Millipore).

2.1.3 Cloning and modifying of DNA

2.1.3.1 Oligonucleotides

All oligonucleotides used during this work were purchased from Invitrogen (UK), and are listed in **Table 2.2** (sequences listed in **Appendix 1**), **Table 2.3** (sequences listed in **Appendix 2**), and **Table 2.4**. The oligonucleotides were used in 10 µM concentration either to carry out Polymerase Chain Reaction (PCR) (§ 2.1.3.3) or as an insert DNA for ligation reactions (§ 2.1.3.8). The oligonucleotides used as an insert DNA were first phosphorylated and annealed before being ligated into the target plasmid. For phosphorylation, 5 µL of oligonucleotides (10 µM), 2 µL of 10x T4 polynucleotide kinase (PNK) buffer, 1 µL ATP (10 mM), 2 µL T4 PNK (Fermentas, UK) and 10 µL dH_2O were incubated at 37°C for 30 min, followed by 56°C for 10 min to stop the reaction. For annealing, 4 µL each of the forward and reverse primers, 2 µL annealing buffer (200 µL 1 M Tris-HCl (pH=7.5), 20 µL of 1 M $MgCl_2$, 166 µL 3 M NaCl, and 614 µL dH_2O) and 10 µL dH_2O were incubated at 95°C for 7 min. Annealed oligonucleotides were cooled to room temperature before ligation and stored at -20°C.

2.1.3.2 Plasmids

The plasmids used to carry out the TOXCAT and GALLEX biological assays were provided by Professor Donald M. Engelman (Yale University, USA) and Dr Dirk Schneider (Albert-Ludwigs-University, Germany), respectively, and are listed below in **Table 2.1**.

In this study, modifications of the pCC-KAN plasmid were carried out as follows: the KAN cassette was cut out of the vector plasmid (§ 2.1.3.5) and the transmembrane domain (TM) sequences of interest were cloned in (§ 2.1.3.8). These constructs were used as templates to create shorter and/or point mutant TM sequences in the pCC-plasmid by PCR site directed mutagenesis (§ 2.1.3.4). The pCC-KAN modified plasmid vectors were used for the TOXCAT experiments (§ 2.2). All of the pCC-plasmid constructs created during this work carry ampicillin antibiotic resistance and are listed in **Table 2.2**.

In the GALLEX study, pALM148, pBLM100 and their modified vectors were used (see **Table 2.1**) and our TM domains of interest incorporated (**Table 2.3**).

Table 2.1 - List of previously generated plasmid vectors used in this study.

Plasmid	Details	Reference
pCC-KAN	New England Biolabs pMAL-c2 and -p2 vectors (pBR322 + *lacI* and Maltose binding protein). Carries ampicillin antibiotic resistance.	(Russ and Engelman, 1999)
pCC-GpA	pCC-KAN with glycophorin A (GpA) transmembrane (TM) domain. Carries ampicillin antibiotic resistance.	
pCC-G83I	pCC-GpA with Gly83 to Ile substitution. Carries ampicillin antibiotic resistance.	
pALM148	Described in detail in reference. Carries tetracycline antibiotic resistance.	(Schneider and Engelman, 2003)
pBLM100	described in detail in reference. Carries ampicillin antibiotic resistance.	
pALM-Gpa	pALM with glycophorin A (GpA) transmembrane (TM) domain. Carries tetracycline antibiotic resistance.	
pALM-G83I	pALM-GpA with Gly83 to Ile substitution. Carries tetracycline antibiotic resistance.	
pBLM-Gpa	pBLM with glycophorin A (GpA) transmembrane (TM) domain. Carries ampicillin antibiotic resistance.	
pBLM-G83I	pBLM-GpA with Gly83 to Ile substitution. Carries ampicillin antibiotic resistance.	

Table 2.2 - List of plasmid vectors generated from pcc-KAN throughout this study. QC=quick change, T=template plasmid was used in the quick change reaction. "for" denotes forward, "rev" denotes reverse primers.

Plasmid name	Generating Oligonucleotide	Features
pcc_rCPT1A TM1(27)[1]	rCPT1A_TM1(27)for rCPT1A_TM1(27)rev	Oligonucleotide of Lys_{47} to Met_{73}
pcc_rCPT1A TM1(24)[2]	rCPT1A_TM1(24)for rCPT1A_TM1(24)rev	QC primer, deletion of Lys_{47}-Gly_{49}, T[1]
pcc_rCPT1A TM1(21)	rCPT1A_TM1(21)for rCPT1A_TM1(21)rev	QC primer, deletion of Ser_{71} -Met_{73}, T[2]
pcc_rCPT1A TM1(18)	rCPT1A_TM1(18)for rCPT1A_TM1(18)rev	Oligonucleotide of Ile_{50} to Val_{67}
pcc_rCPT1A TM1(16)	rCPT1A_TM1(16)for rCPT1A_TM1(16)rev	Oligonucleotide of Thr_{52} to Val_{67}
pcc_rCPT1A TM2(22)[3]	rCPT1A_TM2(22)for rCPT1A_TM2(22)rev	Oligonucleotide of Lys_{102} to Arg_{123}
pcc_rCPT1A TM2(20)[4]	rCPT1A_TM2(20)for rCPT1A_TM2(20)rev	QC primer, deletion of Met_{122} -Arg_{123}, T[3]
pcc_rCPT1A TM2(18)[5]	rCPT1A_TM2(18)for rCPT1A_TM2(18)rev	QC primer, deletion of Lys_{102} -Asn_{103}, T[4]
pcc_rCPT1A TM2(16)[6]	rCPT1A_TM2(16)for rCPT1A_TM2(16)rev	QC primer, deletion of Met_{120} -Thr_{121}, T[5]
pcc_rCPT1A TM2(16)_G107I[7]	rCPT1A_TM2(16)_G107Ifor rCPT1A_TM2(16)_G107Irev	QC primer, changing Gly_{107} to Ile, T[6]
pcc_rCPT1A TM2(16)_G111I	rCPT1A_TM2(16)_G111Ifor rCPT1A_TM2(16)_G111Irev	Oligonucleotide of Ile_{104} to Ile_{119} where Gly_{111} changed to Ile

Plasmid name	Generating Oligonucleotide	Features
pcc_rCPT1A TM2(16)_G113I[8]	rCPT1A_TM2(16)_G113Ifor rCPT1A_TM2(16)_G113Irev	QC primer, changing Gly_{113} to Ile, T[6]
pcc_rCPT1A TM2(16)_A117I	rCPT1A_TM2(16)_A117Ifor rCPT1A_TM2(16)_A117Irev	QC primer, changing Ala_{117} to Ile, T[6]
pcc_rCPT1A TM2(16)_G107IG111I	rCPT1A TM2(16)_G107IG111Ifor rCPT1A TM2(16)_G107IG111Irev	Oligonucleotide of Ile_{104} to Ile_{119} where Gly_{107} and Gly_{111} changed to Ile
pcc_rCPT1A TM2(16)_G113IA117I	rCPT1A TM2(16)_G113IA117Ifor rCPT1A TM2(16)_G113IA117Irev	QC primer, changing Ala_{117} to Ile, T[8]
pcc_rCPT1A TM2(16)_G107IG113I[9]	rCPT1A TM2(16)_G107IG113Ifor rCPT1A TM2(16)_G107IG113Irev	QC primer, changing Gly_{113} to Ile, T[6]
pcc_rCPT1A TM2(16) G107IG111IG113IA117I[10]	rCPT1A TM2(16)_ G107IG111IG113IA117Ifor rCPT1A TM2(16)_ G107IG111IG113IA117Irev	Oligonucleotide of Ile_{104} to Ile_{119} where Gly_{107}, Gly_{111}, Gly_{113} and Ala_{117} changed to Ile
pcc_rCPT1A TM2(16) _T112A	rCPT1A TM2(16) _T112Afor rCPT1A TM2(16) _T112Arev	QC primer, changing Thr_{112} to Ala, T[6]
pcc_rCPT1A TM2(16)_G107IG113IT112A	rCPT1A TM2(16)_ G107IG113IT112Afor rCPT1A TM2(16)_ G107IG113IT112Arev	QC primer, changing Thr_{112} to Ala, T[9]
pcc_rCPT1A TM2(16)_G107IG113I T112V	rCPT1A TM2(16)_ G107IG113IT112Vfor rCPT1A TM2(16)_ G107IG113IT112Vrev	QC primer, changing Thr_{112} to Val, T[9]
pcc_rCPT1A TM2(16) G107IG111IG113IA117I T112A	rCPT1A TM2(16)_ G107IG111IG113IA117IT112Afor rCPT1A TM2(16)_ G107IG111IG113IA117IT112Arev	QC primer, changing Thr_{112} to Ala, T[10]
pcc_rCPT1A TM2(16) G107IG111IG113IA117I T112V	rCPT1A TM2(16)_ G107IG111IG113IA117IT112Vfor rCPT1A TM2(16)_ G107IG111IG113IA117IT112Vrev	QC primer, changing Thr_{112} to Val, T[10]
pcc_rCPT1B TM1(25)[11]	rCPT1B TM1(25)for rCPT1B TM1(25)rev	Oligonucleotide of Arg_{52} to Lys_{76}
pcc_rCPT1B TM1(22)	rCPT1B TM1(22)for rCPT1B TM1(22)rev	QC primer, deletion of Arg_{52} -Val_{54}, T[11]
pcc_rCPT1B TM1(24)	rCPT1B TM1(24)for rCPT1B TM1(24)rev	QC primer, addition of Asn_{48} -Leu_{51}, T[12]
pcc_rCPT1B TM1(23)	rCPT1B TM1(23)for rCPT1B TM1(23)rev	QC primer, deletion of Cys_{75} -Lys_{76}, T[11]
pcc_rCPT1B TM1(22*)[12]	rCPT1B TM1(22*)for rCPT1B TM1(22*)rev	QC primer, deletion of Tyr_{74} - Lys_{76}, T[11]
pcc_rCPT1B TM1(20*)	rCPT1B TM1(20*)for rCPT1B TM1(20*)rev	QC primer, deletion of Ser_{72} -Asn_{73}, T[12]
pcc_rCPT1B TM2(22)[13]	rCPT1B TM2(22)for rCPT1B TM2(22)rev	Oligonucleotide of Glu_{104} to Arg_{125}
pcc_rCPT1B TM2(20)[14]	rCPT1B TM2(20)for rCPT1B TM2(20)rev	QC primer, deletion of Glu_{104} -Thr_{105}, T[13]
pcc_rCPT1B TM2(19)[15]	rCPT1B TM2(19)for rCPT1B TM2(19)rev	QC primer, deletion of Arg_{125}, T[14]
pcc_rCPT1B TM2(17)	rCPT1B TM2(17)for rCPT1B TM2(17)rev	QC primer, deletion of Leu_{123} -Phe_{124}, T[15]

Table 2.3 - List of plasmid vectors generated from pALM148 and pBLM100 throughout this study. "for" denotes forward, "rev" denotes reverse primers.

Plasmid name	Generating Oligonucleotides	Features
pBLM_ rCPT1A_iTM1(21)	rCPT1A_iTM1(21)for rCPT1A_iTM1(21)rev	Oligonucleotide of Ile_{70}-Ile_{50}
pBLM_ rCPT1A_iTM1(18)	rCPT1A_iTM1(18)for rCPT1A_iTM1(18)rev	Oligonucleotide of Val_{67}-Ile_{50}
pBLM_ rCPT1A_iTM1(16)	rCPT1A_iTM1(16)for rCPT1A_iTM1(16)rev	Oligonucleotide of Ile_{67}-Thr_{52}
pBLM_ rCPT1A_TM2(16)	rCPT1A_TM2(16)for rCPT1A_TM2(16)rev	Oligonucleotide of Ile_{104}-Ile_{119}
pALM_ rCPT1A_TM2(16)	rCPT1A_TM2(16)for rCPT1A_TM2(16)rev	Oligonucleotide of Ile_{104}-Ile_{119}
pBLM_ rCPT1B_iTM1(20)	rCPT1B_iTM1(20)for rCPT1B_iTM1(20)rev	Oligonucleotide of Gly_{71}-Arg_{52}
pBLM _rCPT1B_TM2(19)	rCPT1B_TM2(19)for rCPT1B_TM2(19)rev	Oligonucleotide of Leu_{106}-Phe_{124}
pALM_ rCPT1B_TM2(19)	rCPT1B_TM2(19)for rCPT1B_TM2(19)rev	Oligonucleotide of Leu_{106}-Phe_{124}

2.1.3.3 Amplification of DNA by Polymerase Chain Reaction

We have used the PCR (Polymerase Chain Reaction) technique for amplification of DNA fragments and for deletion and single amino acid quick change mutation experiments of several plasmids. Oligonucleotide PCR primers specific for the regions of DNA of interest were designed following the polymerase enzyme manufacturers' manuals. The list of PCR primers used throughout this study is shown in **Table 2.2**. The reactions were carried out in a Biometra® T-personal PCR machine.

The amplification of DNA fragments was typically performed in 50 µL volumes using 38.5 µL filter sterilized dH_2O, 1 µL template DNA, 1.5 µL of each (forward, reverse) primer (10 µM), 1.5 µL of dNTP mix (contaning 10 mM of each dNTP), 5 µL of Pfx50™10x PCR reaction buffer and 1 µL of Pfx50™ DNA polymerase (Invitrogen, UK). A typical PCR reaction contained 35 cycles with the following three steps in each cycle: denaturation at 94°C for 2 min, annealing at 55°C for 30 sec, and extension at 68°C for 30 sec, followed by a final extension at 68°C for 5 min. PCR reaction mixtures were purified using the Qiaprep PCR purification kit (Qiagen, Germany) according to the manufacturers manual.

2.1.3.4 Site-directed mutagenesis of DNA using PCR

The PCR methods for creating deletion and single amino acid quick change mutations were carried out according to the Stratagene site directed mutagenesis

kit manual. The reaction was performed typically in 50 µL volumes using 40 µL filter sterilized dH_2O, 1 µL wild type template DNA, 1 µL of each quick change (forward, reverse) primer (10 µM), 1 µL of dNTP mix (containing 10 mM of each dNTP), 5 µL of Hot-Start Pfu-TURBO™ 10x PCR reaction buffer and 1 µL of Hot-Start Pfu-TURBO™ DNA polymerase (Stratagene, UK). A typical PCR reaction contained 18 cycles of the following three steps: denaturation at 95°C for 30 sec, annealing at 55°C for 1 min, and extension at 68°C for 2 min.

2.1.3.5 Digestion of DNA by restriction endonucleases

The restriction endonuclease digestion reactions were carried out according to the enzyme manufacturer's manual, typically with an incubation period of 3-4 hours at 37°C in a water bath. The reaction was inactivated by heat (20 min at 65°C) and products were purified using a PCR purification kit (Qiagen, Germany) or agarose gel electrophoresis. The enzymes used in this study are listed below:

- *BamH I, Nhe I* were used for double digestion of the pccKAN plasmid.
- *Sac I, Spe I* were used for double digestion of the pALM148 and pBLM100 plasmids.
- *Dpn I* was used to remove the methylated template DNA from the quick change PCR mutagenesis reaction mixtures.

2.1.3.6 Detection of DNA- Agarose Gel Electrophoresis

Agarose gel electrophoresis was routinely used for detection, concentration determination and purification of DNA samples. Typically 1-2% (w/v) agarose gels were prepared. The required amount of agarose was dissolved by heating in 1x TAE buffer (40 mM Tris-acetate, 2 mM EDTA, 0.12% (v/v) acetic acid), and finally 3 µL of ethidium bromide was added. DNA samples were mixed with 1 µL of 6x Loading Dye sample buffer (Fermentas, UK) and DNA standards were prepared using 1 µL of Gene Ruler™ 1 kb DNA Ladder (Fermentas UK) or 100 bp DNA Ladder (Invitogen, UK) mixed with 1 µL of 6x Loading Dye sample buffer and 4 µL of dH_2O.

2.1.3.7 Purification of DNA fragments

Products of restriction endonuclease double digestions reactions were separated by using agarose gel electrophoresis. The DNA of interest was cut out from the

gel under UV light, and purified by removing the agarose using QIAprep gel extraction kit (Qiagen, Germany) according to the manufacturer's instructions.

2.1.3.8 Ligation of DNA fragments

The digested plasmid vector and the insert DNA concentrations were estimated by comparison to quantitative molecular weight standards on an agarose gel. For ligation reactions, typically a 1:3 vector to insert ratio was used and the ligations were set up as follows: 8.5 µL dH_2O, 2 µL cut plasmid, 6 µL insert DNA fragment, 2 µL 10x ligation buffer and 1.5 µL T4 DNA ligase enzyme (Fermentas, UK). The ligation reactions were performed at 4°C for 16 hours. The enzyme in the ligation reaction samples was then heat inactivated at 65°C for 10 min before transforming competent cells.

2.1.3.9 Plasmid isolation

For plasmid preparation, QIAprep Spin Miniprep kit was purchased from Qiagen (Qiagen, Germany). The DNA plasmid was isolated, purified and concentrated according to the manufacturer's manual.

2.1.3.10 Plasmid sequencing

The sequences of all the plasmids obtained by cloning and PCR mutagenesis were confirmed using the University of Warwick, Department of Biological Sciences Molecular Biology Service or the GATC Biotech Laboratory (Germany). Sequencing primers used in this study are listed in **Table 2.4**.

Table 2.4 - List of sequencing primers generated and used throughout this study.

Primer Name	Sequencing Target	Sequence (5' to 3')
pCC_for	TM insert in pCC-KAN	CCTTCATCAGCCACTGTAGTGAAC
pCC_rev	TM insert in pCC-KAN	CAGTTCAGCGAGACCGTTATAG
pABLM_for	TM insert in pALM or pBLM	GGGATTCGTCTGTTGCAGGAAGAGGAAGAA

2.1.4 Growth and maintenance of *E. coli* strains

2.1.4.1 **E. coli** ***bacterial strains***

The bacterial strains of *Escherichia coli* (*E. coli*) used throughout this study are listed in **Table 2.5**. All of the cloning was performed in a (laboratory stock) DH5α

strain. To perform TOXCAT and GALLEX assays, the NT326 *E. coli* strain (provided by Professor Donald M. Engelman, Yale University) was used. For the GALLEX assay, further *E. coli* strains SU101 and SU202 (provided by Dr Dirk Schneider, Albert-Ludwigs-University) were also used.

Table 2.5 - List of *Escherichia coli* strains used throughout this study.

Strain	Genotype	Reference
DH5α	supE44, ΔlacU169(ϕ80lacZΔM15), hsdR17, recA1, endA1, gyrA96, thi-1, relA1	(Sambrook and Russel, 2001)
NT326	F−(argF-lac)U169, rpsL150, relA1, rbsR, flbB5301, ptsF25, thi-1, deoC1, ΔmalE444, recA, srlA^{+} Strep25 resistance.	(Treptow and Shuman, 1985)
SU101*	*lexA*71::Tn5(Def)*sulA*211 Δ(*lacIPOZYA*)169/F'lacI^{q} *lacZ*ΔM15::Tn9 CAM20, Km30 resistance.	(Dmitrova *et al.*, 1998)
SU202*	*lexA*71::Tn5(Def)*sulA*211 Δ(*lacIPOZYA*)169/F'lacI^{q} *lacZ*ΔM15::Tn9 CAM20, Km30 resistance.	(Dmitrova *et al.*, 1998)

* The strains differ in LexA operator sequence controlling the *lacZ* expression SU101 (wt), SU202 (mut) are the lysogen of JL1434 *E. coli* strain. JL1434 transformed with pGC202 bears *sulA* promoter variant *op+/op+ or* op408/op+ operon fusion to *lacZ* gene respectively.

2.1.4.2 Media for E. coli *culture*

The *E. coli* cells were grown on agar plates (Luria Broth Miller (LB) liquid medium plus agar; Sambrook and Russel, 2001, Appendix A2.5). For liquid culture, *E. coli* cells were cultured in LB liquid medium (Sambrook and Russel, 2001, Appendix A2.2). The cultures were grown by inoculating a volume of 5 mL of the LB/antibiotic medium with a single colony from an agar plate and incubating for 16 hrs under aerobic conditions in an incubator shaker at 37°C and 250 rpm. For making outgrowth liquid cultures, *E. coli* cells were typically prepared as 1 in 100 dilutions of overnight cultures (100 µL overnight culture in 10 mL LB) and were grown in the presence of the required antibiotics until their optical density measured at 600 nm, OD_{600}, reached a value of 0.6; this corresponds to a mid-exponential growth phase.

2.1.4.3 Antibiotics

For the experiments, where it was necessary, we have used several antibiotics with different final concentrations, as detailed below:

- Ampicillin 100 µg/mL (Amp^{100}) or 200 µg/mL (Amp^{200})
- Chloramphenicol 5 µg/mL (CAM^{5})
- Kanamycin 5 µg/mL (Km^{5})
- Tetracycline 12 µg/mL (Tet^{12})

2.1.4.4 Preparation of chemically competent E. coli cells

To generate chemically competent *E. coli* cells for transformation by our DNA of interest, cells were prepared based on the calcium chloride ($CaCl_2$) or rubidium chloride (RbCl) methods.

The calcium chloride method (Sambrook and Russel, 2001) was performed as follows: 10 mL mid-exponential phase culture (OD_{600} reached 0.6) was sedimented at 2500 rpm and resuspended in 10 mL of 100 mM filter sterilized $MgCl_2$ and incubated at 4°C for 5 min. After sedimentation, cells were resuspended in 1 mL of 100 mM filter sterilized $CaCl_2$. The cells were incubated at 4°C for 2-24 hours before transformation and stored as 200 µL aliquots at -80°C.

The RbCl method was used to generate 'super competent' *E. coli* cells, to use with quick change mutagenesis modified DNA plasmids. For this method, 2.5 mL LB media was inoculated with cells grown in liquid media or on plates, and grown for 16 h at 37°C, 250 rpm in a shaker incubator. All were transferred to 250 mL of LB supplemented with 20 mM $MgSO_4$ and grown until OD_{600} reached 0.4 – 0.6. Cells were sedimented at 2500 rpm and resuspended in 100 mL buffer 1 (30 mM CH_3COOK, 10 mM $CaCl_2$, 50 mM $MnCl_2$, 100 mM RbCl, 15% glycerol, adjusted to pH=5.8 with 0.2 M acetic acid and filter sterilized) and left on ice for 5 min. After sedimentation, cells were resuspended in 10 mL buffer 2 (10 mM $C_7H_{15}NO_4S$ (MOPS: 3-(N-morpholino) propanesulfonic acid), 75 mM $CaCl_2$, 10 mM RbCl, 15% glycerol, adjusted to pH=6.8 with 0.1 M NaOH and filter sterilized) and left on ice for 15-30 min. Competent cells were dispensed as 200 µL aliquots into pre-chilled 500 µL centrifuge tubes, flash frozen in an ethanol-dry ice bath and stored immediately at -80°C.

2.1.4.5 Bacterial transformation

The transformation of DH5α with the desired DNA was performed as follows: a 10 µL aliquot of ligated DNA was added to 100 µL chemically competent DH5α

cells, and this was left at 4°C for 30 min. Cells were then heat-shocked at 42°C for 45-70 sec, suspended in 500 µL fresh LB, placed in a shaker incubator at 37°C, 250 rpm for 45 min. The cells were sedimented at 13,000 rpm for 1 min using a bench top mini-centrifuge, and 400 µL of supernatant was removed. Cells were resuspended and plated out on LB-agar plates containing the required antibiotic. The plates were incubated at 37°C for 16 hours.

A 10 µL aliquot of the DNA obtained from quick change PCR mutagenesis was added to 90 µL of filter sterilized TCA buffer (10 mM Tris-HCl (pH=7.5), 10 mM $CaCl_2$, 10 mM $MgCl_2$) before DH5α super competent cells were transformed as described above. Chemically competent DH5α, NT326, SU101, and SU202 *E. coli* cells were transformed as above mentioned, except that 100 µL aliquots of cells and 1-2 µL of plasmid DNA were used.

2.1.5 Detection of proteins

2.1.5.1 SDS-Polyacrylamide Gel Electrophoresis (SDS-PAGE)

The separation of the proteins was carried out using Invitrogen X-Cell Sure Lock™ vertical electrophoresis system, and the samples were loaded on to NuPAGE 12% Bis-Tris ready gels and run in 1x MES-SDS NuPAGE running buffer (Invitrogen, UK). The gels were typically run at 120 mA and 200 V for 35 min at room temperature. However, the electrophoresis conditions for the cross-linking experiments were 120 mA, 200 V, 50 min at 4°C. With all gels, 1-5 µL SeeBlue® Plus2 Pre-Stained Standard (Invitrogen, UK) was loaded.

The protein samples were prepared by sedimenting 500 µL of OD_{600}=0.6 protein culture at 13,400 rpm for 60 sec, adding lysis buffer to normalize the sample concentration to OD_{600}=0.1 and breaking up the pellet by pipetting. To 15 µL of this sample, 5 µL of 4x LDS sample buffer (Invitrogen, UK) was added and samples were heated at 80°C for 10 min before loading on the gel (10 µL).

The TCA precipitated samples (see in § 2.2.2.4) were resuspended in 80 µL 1x LDS sample buffer and heated at 80°C and/or sonicated for 10 min to break up pellets. Typically 10-15 µL of the prepared sample was then loaded on the gel.

The peptide samples from cross-linking experiments were prepared by adding 2 µL of 4x LDS sample buffer to 8 µL of each peptide-detergent sample, and 8 µL of the resulting solution was loaded on the gel.

2.1.5.2 Coomassie staining

After gel-electrophoresis, protein bands were visualized by coomassie staining. The coomassie binds through a combination of hydrophobic interactions and heteropolar binding of the dye to basic amino acids such as arginine, histidine or lysine. This technique is widely used for visualization of peptides bands 5-50 ng range detection.

During the experiments, the gel was first soaked in 50 mL fixing solution (50(v/v)% CH_3OH, 10(v/v)% CH_3COOH) for 15 min and stained in 50 mL coomassie stain solution (0.025 (w/v)% coomassie blue G250 or R250, 10(v/v)% CH_3COOH) for 3-16 h at room temperature. The gels were then destained in 50 mL 10(v/v)% acetic acid solution for 3 h. The destain solution was changed several times until the bands were seen with minimal background. The gel was stored in dH_2O.

2.1.5.3 Silver nitrate staining

The silver staining mechanism for proteins in gels is relatively well understood. The protein detection depends on the binding of silver ions to the amino acid side chains, primary the sulfhydril and carboxyl groups of proteins (Switzer *et al.*, 1979; Merril *et al.*, 1981; Merril and Pratt, 1986) followed by reduction to free metallic silver (Rabilloud, 1990). The protein bands are visualized as brown-black spots where the reduction occurs and, as a result, the image of protein distribution within the gel is based on the difference in oxidation-reduction potential between the gel's area occupied by proteins and the free adjacent sites.

Here, the low concentration protein and peptide bands were visualized by the following silver nitrate method. The gels were electrophoresed with 0.2-0.5 µL protein standard. Coomassie staining was performed before silver staining to help minimise the background discolouration. For silver staining, all solutions were freshly prepared using pre-cleaned glassware, and all soaking steps were carried out at room temperature with gentle shaking in a fume cupboard. First, the gels were soaked in a fixer solution (60 mL 50% acetone, 1.5 mL 50% TCA (16.339 g TCA dissolved in 200mL dH_2O) and 25 µL 37% formaldehyde) for 15 minutes, washed quickly three times with dH_2O, then soaked in dH_2O for 5 minutes, followed by a final three quick washes with dH_2O. Next, the gels were soaked in 50% acetone (500 mL acetone (100%) and 500 mL dH_2O) for 5 min, $Na_2S_2O_3$ solution (10 mg $Na_2S_2O_3$ in 60mL dH_2O) for 1 min, then washed quickly

three times with dH_2O. The gels were then soaked in staining solution (160 mg silver nitrate, 600 µL 37% formaldehyde in 60 mL dH_2O) for 8 minutes and washed quickly two times with dH_2O. In the developing solution (1.2 g Na_2CO_3, 25 µL 37% formaldehyde, 2.5 mg $Na_2S_2O_3$ in 60ml dH_2O), the gels were soaked for 10-20 seconds as protein bands appear very quickly. The reaction was quenched by soaking gels in 1% acetic acid (990 mL acetone dH_2O, 10 mL glacial acetic acid) and finally rinsing and storing in dH_2O.

2.1.5.4 Immunoblotting (Western Blot)

The western blot analyses were used to detect maltose binding protein (MBP) and its fusion proteins (see in § 2.2 and § 2.2.2.1-2.2.2.3). After the proteins were electrophoresed on 12% NuPAGE gels, they were electro blotted onto a 0.45 µm pore size nitrocellulose membrane at 160 mA, 90 V for 1 hour using the transfer XCell II™ Blot Module according to the manufacturer's manual (Invitrogen, UK).

After the transfer the membrane was blocked in TTBS + 3% milk solution for 1 hour (or overnight at 4°C), it was washed with TTBS buffer (30 mM Tris-HCl, 140 mM NaCl, 3 mM KCl, 0.1% Tween-20, pH 7.4) three times at 5 min each. The membrane was incubated for 1 hour with the primary antibody anti-MBP (Sigma), which was diluted 1 in 4000 with TTBS - 3% milk solution, before the washing step was repeated. The secondary antibody, anti-mouse IgG (Sigma), was used in a 1 in 10,000 dilution with TTBS + 3% milk solution and incubated for 1 hour, followed by the washing step. Finally, to detect MBP and its fusion proteins, the SigmaFast™ kit was used according to the manufacturer's instructions (Sigma, UK).

2.2 The TOXCAT assay

The *in vivo* oligomerisation of rCPT1 transmembrane domains was studied using the TOXCAT biological assay, the details of which have been described previously (Russ and Engelman, 1999). TOXCAT employs a chimeric protein, in which the α-helical TM domain of interest is inserted between the N-terminal DNA binding domain of ToxR, a dimerization-dependent transcriptional activator, and maltose binding protein (MBP), a monomeric periplasmic anchor protein. The fusion protein is constitutively expressed in *E. coli* together with a chloramphenicol acetyltransferase (CAT) reporter gene under the control of a ToxR-responsive cholera toxin (ctx) promoter. Oligomerisation of the TM domains within the

bacterial inner membrane results in oligomerisation of the ToxR domain, transcriptional activation of the *ctx* promoter, and CAT expression (**Figure 2.1**). The amount of CAT expressed in this system is proportional to the strength of oligomerisation of the TM domains.

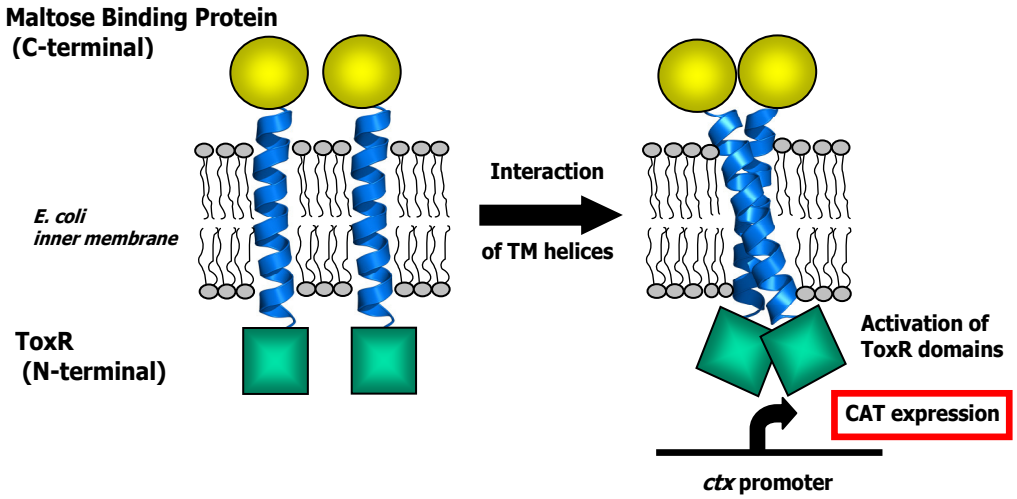

Figure 2.1 - The principle of the TOXCAT assay.

2.2.1 Constructing protein chimeras

The expression vectors (pcc-KAN, pcc-GpA and pcc-$G_{83}I$, see in § 2.1.3.2), and *E. coli* strain NT326 (see in § 2.1.4.1), were kindly provided by Dr Donald M. Engelman (Yale University, USA). To create chimeric proteins containing the TM domains of interest, oligonucleotides corresponding to the predicted rCPT1A and rCPT1B TM domain sequences were ligated into the pcc-KAN plasmid, between the Nhe I and BamH I restriction sites, and the resulting plasmids were used to transform NT326 *E. coli* competent cells (detailed in § 2.1.3 and 2.1.4.5). The oligonucleotides are listed in **Appendix 1**, and the resulting plasmids are summarised in **Table 2.2**.

2.2.1.1 Construction of chimeric protein mutants

The chimeras used in the length optimization and the sequence mutants (GxxxG, GxxxA, Thr) were constructed using quick change PCR as described in § 2.1.3.4. The oligonucleotide quick change primers are listed in **Appendix 1**, the resulting plasmids are summarised in § 2.1.3.2, **Table 2.2**.

The assay controls are the wild type glycophorin A (GpA) TM domain, known to form a strong dimer and therefore used as a positive control, and its dimerisation defective point mutant $G_{83}I$, used as the negative control. Before performing the TOXCAT assay, several tests are performed to ensure that the constructed chimeras are correctly inserted into the *E. coli* membrane and changes to the TM sequence do not change the relative amounts of expressed or membrane inserted chimera. For further discussion of the concept, see also § 3.3.

2.2.2 Control assays

2.2.2.1 Sample preparation for expression level test

To confirm that different CAT activities were not due to differences in the chimeras' expression level, similar expression levels for all constructs were established *via* Western analysis against the MBP domain prior to performing CAT assays. Approximately 200 µL of NT326 cells expressing the chimeric proteins (cells harvested from fresh outgrowth culture, volume normalized to OD_{600}=0.6) were sedimented at 13,000 rpm for 3 min using a bench top mini-centrifuge, the supernatant was removed, and the cell pellet was resuspended in 80 µL of 1x LDS sample buffer (Invitrogen, UK). The proteins were separated by SDS-PAGE, and MBP was detected by immunoblotting (see in § 2.1.5.4).

2.2.2.2 NaOH extraction

Prior to performing the TOXCAT assay, membrane association of all chimeric proteins was confirmed using sodium hydroxide washes (Chen and Kendall, 1995). In this method, 1 mL of an NT326 outgrowth culture expressing the chimeric proteins (normalized to OD_{600}=0.6) was sedimented at 4°C and 13,000 rpm for 3 min using a bench top mini-centrifuge and the pellet was resuspended in 90 µL dH_2O, 2.4 µL $MgCl_2$, 5 µL DNase (10 mg/mL), and 5 µL lysosyme (10 mg/mL) and incubated at room temperature for 1 hour. To the lysed cells, 150 µL of ice cold dH_2O was added and 125 µL was taken as a whole cell fraction (WC). To the remaining cells, 125 µL of ice cold 0.1 M NaOH was added and the solution was vortexed for 1 min and centrifuged at 4°C at 13,000 rpm for 15 min. The supernatant was separated as the soluble protein fraction (SP) and the pellet was taken as the membrane protein fraction (MP). The preparation of the whole cell (WC) and soluble protein (SP) samples was continued with the TCA precipitation.

2.2.2.3 Spheroplast proteolysis assay

Membrane association and correct orientation of the TOXCAT chimeras in the *E. coli* membrane was also confirmed through protease sensitivity in a spheroplast proteolysis assay. In this assay, 1 mL of NT326 outgrowth culture (normalized to OD_{600}=0.6) was sedimented at 4°C and 13,000 rpm for 15 min. The pellet was resuspended in 375 µL buffer A (100 mM Tris-acetate, 500 mM sucrose, pH=8.2), and 1 µL of 187.5 mM EDTA, 6 µL of 10 mg/mL lysosyme, 8 µL of 1 M $MgSO_4$ and 375 µL ice cold dH_2O was added. The sample was incubated at 4°C for 1 hour. After the incubation, the sample was split into 3x250 µL fractions (whole cell (WC), spheroplast (SPH), broken spheroplast (BSP)). To the SPH fraction, 100 µL buffer B (10 mM HEPES, 2 mM EDTA pH=7.6) and 15 µL of 3.5 mg/mL proteinase K were added, and the sample was incubated at 4°C for 40 min. The BSP fraction was sedimented at 4°C and 13,000 rpm for 1 min, the supernatant was retained, and the pellet was resuspended in 100 µL buffer B. The resuspended pellet was frozen in dry ice and then left to defrost (*i.e.* freeze-thaw). After the freeze-thaw procedure was repeated three times and the supernatant was returned to the sample, 15 µL of 3.5 mg/mL proteinase K was added and the sample was incubated at 4°C for 30 min. TCA precipitation was then carried out for each of the WC, SPH, and BSP samples.

2.2.2.4 TCA precipitation

The WC and SP fractions from the NaOH assay, and the WC, SPH and BSP fractions from the spheroplast assay were prepared by TCA precipitation (trichloroacetic acid, CCl_3COOH). 1 mL of 10% TCA was added to each sample, followed by incubation at 4°C for 30 min. The samples were centrifuged at 4°C and 13,000 rpm for 15 min, and all the supernatant was removed. 1 mL of acetone was added to the pellet, and incubated at 4°C for 5 min. Finally, the samples were centrifuged at 4°C and 13,000 rpm for 10 min, the acetone was removed, the pellet was allowed to dry, and the dry pellets were dissolved in 80 µL 1x LDS sample buffer to load on an SDS-PAGE gel. The proteins were separated on the protein gel and MBP was detected by immunoblotting (see in § 2.1.5.4).

2.2.2.5 MalE complementation assay

The correct orientation of the chimera in the membrane was also confirmed using the *mal*E complementation assay. In this assay, maltose minimal media agar plates were prepared by sterilizing 50 mL 5xM9 minimal medium (Sambrook and Russel 2001, A2.2), 0.5 mL of 1 M $MgSO_4$, 25 µL of 1 M $CaCl_2$ and 5 mL 20% maltose solutions and adding these to a sterile, melted agar solution (3.73 g agar in 195 mL dH_2O). The mixture was poured into Petri dishes and allowed to dry and set. Single colonies of NT326 cells were streaked out on these maltose plates and were incubated at 37°C for 3 days.

In this assay the *mal*E deficient (Δ*mal*E) NT326 cells are used as negative controls, as they do not express MBP and cannot grow on maltose minimal media. However, the cells containing the plasmid of the constructed TOXCAT chimeras are able to grow, if the chimera is correctly inserted in the membrane with the MBP in periplasmic orientation.

2.2.3 The qualitative and quantitative CAT assay

To perform the qualitative CAT assay (or disk diffusion assay), NT326 outgrowth cultures (OD_{600} 0.6-0.8) were normalized to OD_{600} 0.1 by dilution with LB. 100 µL of the diluted cells were plated onto LB/agar/Amp^{200} plates and allowed to dry for 1 hour. On a 1 cm diameter Wathman filter paper disk, 42 µL of 90 mg/mL chloramphenicol (CAM) was pipetted and allowed to soak through. These CAM soaked disks were then placed in the centre of each agar plate. The plates were incubated at 37°C for 16 hours.

The quantitative CAT assays were performed using the FAST CAT Kit (Molecular Probes, Invitrogen), where an acetylation reaction yields a fluorescent butyryl-cloramphenicol (butyryl-CAM) product (see reaction scheme in **Figure 2.2**) which was isolated *via* liquid-liquid extraction into a xylene phase. The concentration of butyryl-CAM was measured using a fluorimeter.

Samples were prepared from 200µL of NT326 outgrowth culture (OD_{600} 0.6) which was sedimented at 4°C and 13,000 rpm for 3 min. The pellet was resuspended in 500 µL 100 mM Tris-HCl pH=8.0 and vortexed to mix, then 20 µL of lysis solution (100 mM EDTA, 100 mM DTT, 50 mM Tris-HCl (pH=8.0)) and one drop of toluene was added. The sample was incubated at 30°C for 30 min. The lysed cells were used freshly or after being stored for 1-3 days at -80°C. In

the TOXCAT assay, a 10x dilution of lysed cells was used (6 µL of lysed cells, 54 µL 100 mM Tris-HCl (pH=8.0)). To each sample of diluted cells, 10 µL of fluorescent CAM (FAST CAT® kit) was added and incubated at 37°C for 5 min. Then 10 µL of 5 mg/mL butyryl-CoA (Amersham) was added to the sample and it was returned to incubate at 37°C for 90 min. The reaction was terminated by adding 300 µL of xylene and vortexed to mix for 30 sec.

For solution phase extraction, the samples were centrifuged at 13,000 rpm for 3 min and the upper, organic phase was collected. To the upper phase (xylene) 300 µL of 100 mM Tris-HCl (pH=8.0) buffer was added and it was mixed and centrifuged as before. Finally, this last wash step was repeated and the CAT concentration in the upper phase was measured using a fluorimeter (Jasco, FP-6500).

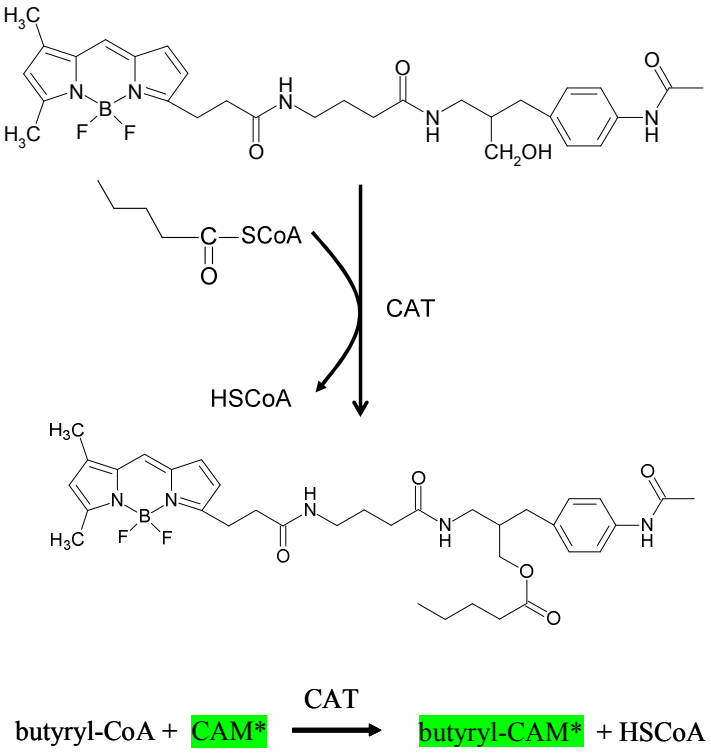

Figure 2.2 - The reaction scheme of the CAT assay.

2.3 GALLEX methods

The GALLEX assay (Schneider and Engelman, 2003) can measure not only homo, but also hetero TM interactions in a natural membrane, and was used to investigate the transmembrane domains of rCPT1A and rCPT1B. To perform this assay, the expression vectors (pALM148 and pBLM100 furthermore pALM148 or pBLM100 GpA and pALM148 or pBLM100 G83I), and *E. coli* strain SU101 and SU202 (see in § 2.1.4.1), were kindly provided by Dr Dirk Schneider (Albert-Ludwigs-University, Germany).

The GALLEX assay, similar to TOXCAT (previously described in § 2.2), also employs a chimeric protein, in which the α-helical TM domain of interest is inserted between an N-terminal DNA binding domain (in this case, the LexA dimerisation-dependent transcriptional activator), and maltose binding protein (MBP), a monomeric periplasmic anchor protein. The fusion protein is constitutively expressed in *E. coli* together with the lacZ reporter gene under the control of the *op+* or *op408* promoter as shown in **Figure 2.3**. When studying homo-oligomerisation, interaction of TM domains within the bacterial inner membrane results in oligomerisation of the wild type LexA domains and transcriptional activation of the *op+* promoters which causes the repression of the β-galactosidase expression of in the *E. coli* cell (SU101). When measuring hetero-oligomerisation, the TM domain interactions results in oligomerisation of the wild type and mutant LexA domains, and this in turn results in the transcriptional activation of the hybrid *op408/op+* promoters. This represses the expression of β-galactosidase in *E. coli* (SU202). The amount of β-galactosidase repression in these systems is proportional to the strength of oligomerisation of the TM domains (**Figure 2.3**).

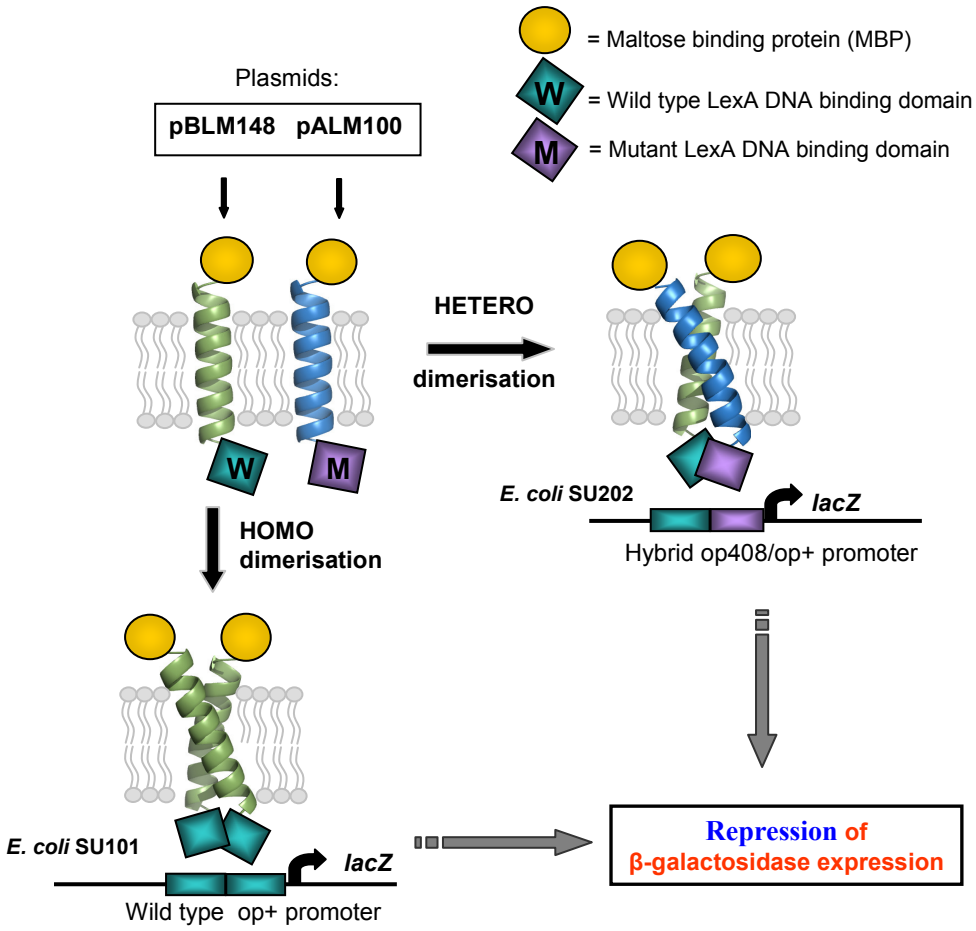

Figure 2.3 - The principle of GALLEX *in vivo* oligomerisation assay.

2.3.1 The construction of chimeric proteins

To create the GALLEX chimeric proteins, primers were ligated into pALM148 and pBLM100 vectors between the Sac I and Spe I restriction sites (see § 2.1.3.5 and § 2.1.3.8).

To perform the homo-oligomerisation assay, SU101 *E. coli* competent cells were transformed with vectors generated from pBLM100 depending on the TM of interest of rCPT1A and rCPT1B domains as well as the GpA and G83I controls. These created the *wt* LexA-TM-MBP protein chimeras.

To measure hetero-oligomerisation, TM1-TM2 domains were cloned into the vector pair pALM148/pBLM100, and used to transform the SU202 *E. coli* cells, as were the pALM148/pBLM100 GpA and G83I controls. These created the *wt* LexA-TM-MBP and *mut* LexA-TM-MBP protein chimera pairs. SU202 competent cells were first transformed with pALM148 plasmids.

After transformation, one single colony from the Tet^{12} selection-plate was cultured and the cells were made competent again. This was followed by transformation of SU202 (pALM148) with the second pBLM100 plasmid DNA (plasmid vectors generated from pALM148 and pBLM100 see in § 2.1.3.2, **Table 2.3**).

2.3.2 Control assays

The GALLEX assay uses the same biological control assays to confirm the correct topology and similar expression levels of chimeric proteins as the TOXCAT assay (see in § 2.2.2).

The culturing and any differences in performing control assays will be discussed below.

To perform the control assays, the MBP deficient NT326 *E. coli* strain was used. For the GALLEX assay, the SU101 (for homo-oligomerisation) and SU202 (for hetero-oligomerisation) strains were used. Overnight cultures of freshly transformed cells were grown in the presence of antibiotics Amp^{100}, Tet^{12}, Km^{5}, CAM^{5} (see § 2.1.4.3 for definitions) and 0.01- 0.1 mM IPTG, at 37°C and 250 rpm for 16 hours. The following morning, 250 µL of the cells were used to innoculate

10 mL of fresh LB media (1:40 dilution) containing the above mentioned antibiotics and IPTG, and the cultures were grown in a 50 mL Erlenmeyer flask until OD_{600} reached 0.6, which were typically 3 hours for SU101 and 5 hours for SU202 cells. To confirm the correct topology of chimera protein constructs, NT326 *E. coli* stain were transformed with vectors generated from pALM148 and pBLM100 plasmids and the *malE* complementation and spheroplast proteolysis assays were performed. To achive the *malE* complementation assay, the maltose minimal media agar plates (above in § 2.1.4.2) here were prepared to contain Amp^{100} and 0.01 mM IPTG.

2.3.3 The β-galactosidase assay

The association capacity of the different GALLEX protein chimeras was measured as a function of the repression of β-galactosidase activity. To measure the β-galactosidase concentration, an enzymatic reaction was carried out, as described below. The synthetic compound o-nitrophenyl-β-D-galactoside (ONPG) was added to the lysed cells. In the reaction catalyzed by the β-galactosidase

(**Figure 2.4**), ONPG was cleaved (hydrolysis) to yield galactose and o-nitrophenol, which has a yellow colour. The production of o-nitrophenol is proportional to the concentration of β-galactosidase; thus the production of the yellow colour followed with UV spectroscopy can be used to determine the β-galactosidase enzyme concentration. The standardized amount of β-galactosidase was calculated in Miller units:

$$\text{Miller units} = \frac{1000 \cdot (Abs_{420} - 1.75 \cdot Abs_{550})}{t(\text{min}) \cdot V(\text{mL}) \cdot OD_{600}}$$

where Abs_{420} is the absorbance of the yellow o-nitrophenol at 420 nm, Abs_{550} is the scatter from cell debris, which, when multiplied by 1.75 approximates the scatter observed at 420 nm, t is the reaction time in minutes, V is the volume of the culture assayed in millilitres. OD_{600} stands for the optical density of the cultures at 600 nm.

Cultures were prepared as described above in § 2.3.2. The OD_{600} of a 1 mL culture was recorded, then 100 µL of the sample was diluted with 900 µL Z-buffer with 50 mM 2-mercaptoethanol (1x Z buffer: 60 mM $Na_2HPO_4x7H_2O$, 40 mM $NaH_2PO_4xH_2O$ 10 mM KCl, 1 mM $MgSO_4x7H_2O$). Cells were lysed with 10 µL of 10% SDS and 2 drops of chloroform, and were mixed with a vortex mixer for 10 seconds. To start the reaction catalysed by β-galactosidase (**Figure 2.4**), 200 µL of ONPG (4 mg/mL in Z buffer), to stop the reaction, 0.5 mL 1M Na_2CO_3 solution was added. The reaction mixture was centrifuged for 10 min and the supernatant was transferred into a plastic cuvette. The absorbance was recorded at 420 and 550 nm for each sample.

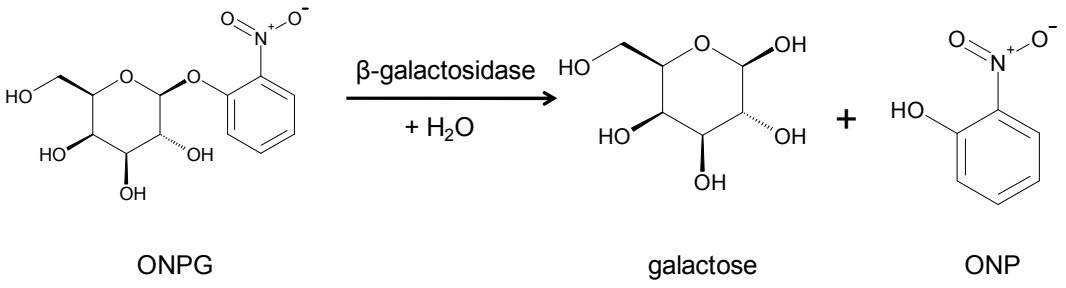

Figure 2.4 - The β-galactosidase reaction scheme.

2.4 Synthetic peptide purification

Peptides corresponding to the TM domains (**Table 2.6**) of rCPT1A and rCPT1B were synthesized by the Keck Facility at Yale University, using F-moc chemistry. Lysine residues were added to the sequences at the N- and C-termini for rCPT1A TM2, and only at the C-terminus for rCPT1A TM1, to aid solubility and to reduce non-specific aggregation, an approach that has been shown in several previous studies not to affect the properties of strongly interacting TM domain peptides (Ding *et al.*, 2001; Melnyk *et al.*, 2003; Lazarova *et al.*, 2004).

Table 2.6 - The amino acid sequences of synthetic peptides used in this study. Non-native lysine residues are shown in bold.

TM domain of interest	Synthetic peptide sequence	Molecular weight (Da)
rCPT1A TM1	$COCH_3$-KNGIITGVFPANPSSWLIVVVGVISSM**K**-$CONH_2$	2957
rCPT1A TM2 wt	$COCH_3$-**K**KNIVSGVLFGTGLWVAVIMTMR**K**-$CONH_2$	2689
rCPT1A TM2 $G_{107}I$	$COCH_3$-**K**KNIVSIVLFGTGLWVAVIMTMR**K**-$CONH_2$	2745
rCPT1A TM2 $G_{107}G_{113}I$	$COCH_3$-**K**KNIVSIVLFGTILWVAVIMTMR**K**-$CONH_2$	2804
rCPT1B TM1	$COCH_3$-**K**ILRGVYPGSPTSWLVVVMATVGSNY**K**-$CONH_2$	2963
rCPT1B TM2	$COCH_3$-**K**ETLLSMVIFSTGVWATGIFLFR**K**-$CONH_2$	2785

These hydrophobic peptides were purified by reversed-phase high performance liquid chromatography (RP-HPLC) using a Phenomenex C4 or phenylhexyl semi-preparative column. The peptides were solubilised adding a solution containing 200 µL trifluoroacetic acid (TFA), 200 µL 2,2,2-trifluoroethanol (TFE) then 400 µL acetonitrile (ACN) to the dried peptide, and injecting this solution onto the HPLC column. For separation, a 30% to 100% linear ACN gradient containing 0.1% TFA was used. The eluent was monitored at 280 nm (**Figure 2.5**). The fractions comprising the major peaks were collected and analyzed by mass spectrometry.

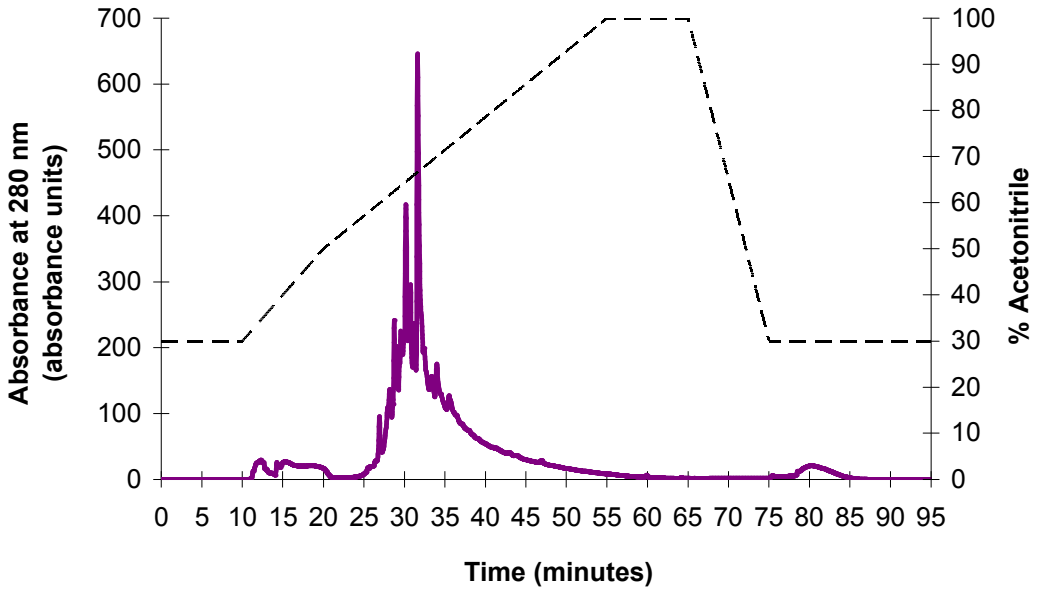

Figure 2.5 - Reverse phase liquid chromatography purification of rCPT1A TM2 peptide on Phenomenex C4 column. The solid purple line represents the chromatogram and the broken line shows the ACN gradient.

2.4.1 Lyophilisation of purified peptides

The pooled HPLC fractions containing peptide were frozen on dry ice to form a thin layer in a round bottomed flask. The flask was placed in liquid nitrogen before being attached to vacuum (Schlenk line) and left under vacuum until all the solvent had been removed. Lyophilised peptide was dissolved in TFE, aliquoted, dried under nitrogen to remove the organic phase and then stored at -20ºC until required. Peptides were stored as dry powders until use.

2.4.2 Determination of peptide concentration

Peptide concentration was determined by measuring UV absorbance. Peptides were dissolved in organic solvent or buffer and their absorbance was measured using a spectrophotometer (Biomate, Thermo Scientific). The extinction coefficients at 280 nm of all studied peptides were ε_{280} = 5500 M^{-1} cm^{-1} and for rCPT1B TM1 peptide it was 8480 M^{-1} cm^{-1}. These values were calculated using ProtParam (http://www.expasy.org), and the peptide concentration was calculated using the Beer-Lambert law:

$$Abs = \varepsilon \cdot \mathrm{b} \cdot c \,,$$

where Abs is the absorbance, ε is the extinction coefficient ($M^{-1}cm^{-1}$), b is the optical path length (cm), and c is the concentration (M).

2.5 Analysis of synthetic peptides

2.5.1 Mass spectrometry

The HPLC peak fractions were analyzed by electro spray ionization time-of-flight mass spectrometry (ESI-TOF-MS micrOTOF, Bruker). Samples were prepared by adding 10 µL 10% formic acid to 90 µL of the HPLC fraction. During analysis, the positive ionisation mode was used and detection was between 50 and 3000 m/z. Spectra were typically recorded for 2 minutes, averaged and deconvoluted to determine the mass of the main species (for spectra see § 3.4.1 **Figure 3.8** and **Figure 3.9**).

For detection and characterization of peptides, matrix-assisted laser desorption/ionisation-time-of-flight mass spectrometry (MALDI-TOF-MS) was also used, mainly to check the purity of the lyophilised peptide samples (for spectra see § 5.4.1, **Figure 5.7** and **Figure 5.8**). Samples were prepared by mixing 5 µL of peptide sample with 5 µL of matrix solution (10 mg/mL α-cyano-4-hydroxy cinnamic acid in 50% ACN, 50% H2O and 0.1 % TFA). 1 µL of the sample/matrix solution was spotted onto a MALDI target plate and allowed to air dry for 30 mins. MALDI-MS spectra were acquired in the positive ion and linear modes. The mass range from m/z 2000 to 5000 was externally calibrated with polyethyleneglycol 2000.

2.5.2 Solubilisation of synthetic peptides in detergent micelles

The synthetic peptides were dissolved in detergent micelles prior to structural or oligomerisation experiments. During this research, the detergents used were purchased from Avanti Polar Lipids (Alabaster AL, USA) and included: dodecylphosphocholine (DPC), octylglucoside (OG) and lyso-palmitoyl phosphatidylglycerol (LPPG). Sodium dodecylsulfate (SDS) was also used, but was purchased from Sigma Aldrich (UK).

The concentration of detergent micelles in a detergent solution (**Table 2.7**) was calculated using the following equation:

$$c_{\text{micelle}} = (c_{\text{detergent}} - \text{cmc}) / AgrN ,$$

where c_{micelle} is the micelle concentration (M), $c_{\text{detergent}}$ is the detergent concentration (M), cmc is the critical micelle concentration (M), and $AgrN$ is the aggregation number. The aggregation number is the number of detergent molecules present in a micelle once the critical micelle concentration (cmc) has been reached, and the critical micelle concentration is the concentration of detergent at which micelles are spontaneously formed.

Table 2.7 - List and properties of biological detergents were used in this study (Sanders and Sonnichsen, 2006)**.**

Detergent	**Molecular weight (MW)**	**Critical Micelle Concentration (mM) (cmc)**	**Aggregation Number ($AgrN$)**
Dodecylphosphocholine (DPC)	352	1.5	50-60 (here used 56)
Octylglucoside (OG)	292	19-25	90
Lyso-palmitoyl phosphatidylglycerol (LPPG)	506	0.02-0.6	125
Sodium dodecylsulfate (SDS)	288	1-7	62-101

2.5.3 Circular Dichroism (CD)

Circular Dichroism (CD) is a widely used spectroscopic technique used for studying the structure of any optically active biomolecule (e.g. DNA, proteins). It measures differences in the absorption of left-handed versus right-handed polarized light which occur due to structural asymmetry in the molecule.

The CD spectra were measured using Jasco J715 and J815 spectropolarimeters (Jasco UK, Great Dunmow, UK) with 1.0 mm path-length quartz cuvettes (Starna, Optiglass Ltd, Hainault, UK). All spectra were recorded in the far UV spectral region, from 190 to 260 nm using a 2.0 nm spectral bandwidth, 0.2 nm step resolution, 100 nm min^{-1} scanning speed, and 1 sec response time.

All peptide samples were prepared in 50 mM sodium phosphate buffer (pH 7) and 100 mM NaCl, containing either 10 mM SDS, 3.74-91.1 mM DPC, 97-385 mM OG, or 25-50 mM LPPG. The final peptide concentrations were 40 μM in each sample. CD spectra were collected at room temperature. Data were averaged from 4 individual spectra and measurement of the buffer without peptide was

subtracted to obtain the final spectra. The secondary structure composition of the peptides was estimated from the CD spectra using CDSSTR (Johnson, 1999), for details see § 2.6.3.

2.5.4 Cross-linking

To determine the oligomeric state of TM peptides, SDS-PAGE analyses were carried out. Since SDS is a denaturing detergent, it breaks up non-covalent interactions, such as the TM-TM oligomerisation. For this reason, to be able to detect the higher order oligomeric species, TM peptides were chemically cross-linked.

It is known that the concentration of detergent can affect the dissociation constant (k_d) and thus the oligomeric states of transmembrane interactions (Fisher *et al.*, 1999). For this reason the cross-linking reactions were carried out for 20 µM solutions of the rCPT1 TM peptides dissolved in DPC micelles at micelle to peptide ratios ranging from 1:3 to 20:1 (M:P=1/3-20) (corresponding concentrations ranging from 1.89 to 23.9 mM, see in **Table 2.8**), LPPG micelles at M:P=2-10 (corresponding to LPPG concentrations ranging from 5 to 25 mM), OG micelles M:P=10-40 corresponding to OG concentrations ranging from 43 to 97 mM) and 15 mM SDS at M:P=4. All samples were prepared in 20 mM sodium phosphate and 150 mM NaCl buffer (pH 8). Bis[sulfosuccinimidyl]suberate (BS_3, Pierce (Thermo Scientific, UK)) was used to cross-link peptides in solution *via* primary amine groups according to the manufacturers protocol (for the BS_3 reaction mechanism, see **Figure 2.6**). The cross-linking reaction was terminated after 30 min by the addition of 1M Tris-HCl (pH 8) to a 50 mM final concentration. Un-crosslinked and SDS cross-linked samples were prepared as controls. All samples were analyzed by gel electrophoresis (see in § 2.1.5.1), and peptides were visualized on gels by staining either with coomassie blue and silver nitrate (see in § 2.1.5.2-2.1.5.3).

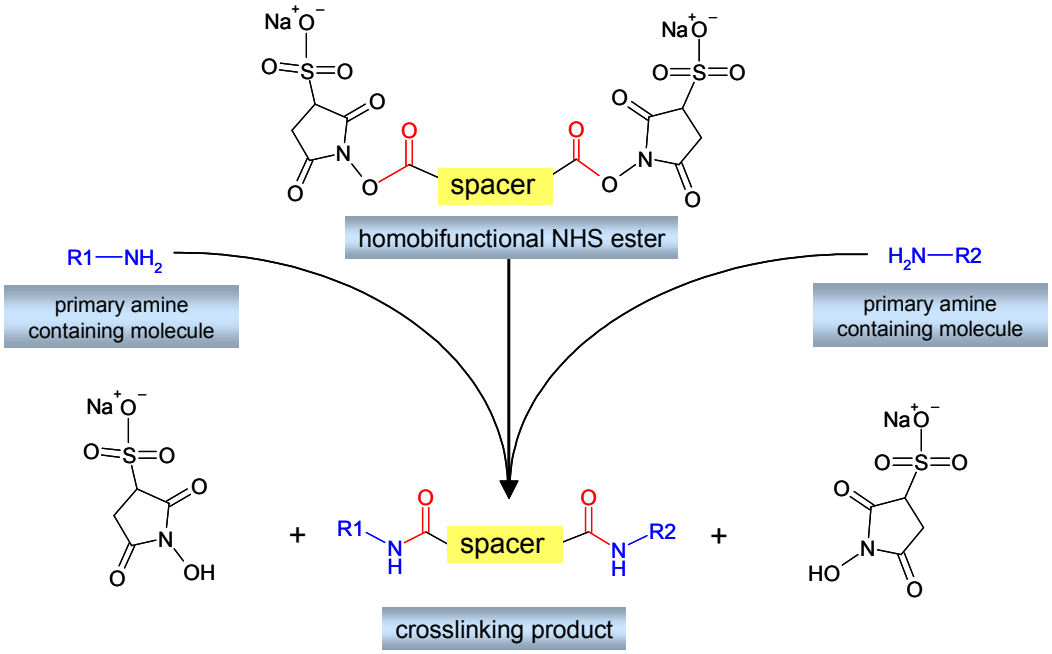

Figure 2.6 - The general reaction scheme of amine-reactive NHS ester crosslinkers. The bis[sulfosuccinimidyl]suberate, BS_3, also NHS ester, where spacer arm length is $(CH2)_6$, 11.4 Å.

Table 2.8 - The concentrations of the peptide and DPC detergent used in cross-linking experiments at different micelle to peptide ratios.

Micelle to Peptide ratio (M:P)	C peptide (μM)	C micelle (μM)	C DPC detergent (mM)
1:3	20	7	1.89
1:2	20	10	2.06
1:1	20	20	2.62
2:1	20	40	3.74
3:1	20	60	4.86
5:1	20	100	7.1
10:1	20	200	12.7
15:1	20	300	18.3
20:1	20	400	23.9

2.5.5 Analytical Ultracentrifugation (AUC)

A classical method, analytical ultracentrifugation became a very useful research technique in modern biochemistry and other (e.g. polymer science) fields for studying the solution-state behaviour of macromolecules (Laue and Stafford, 1999). It can provide information on the size and shape of biomolecules, and the stoichiometry of complex formation (assembly, disassembly), as well as equilibrium constants and thermodynamic parameters for self- and hetero-

associating systems. In an AUC experiment, UV optical spectroscopy is used to record absorption and interference data. There are two types of commonly used AUC experiments: sedimentation velocity (SV) and sedimentation equilibrium (SE).

2.5.5.1 Sedimentation velocity (SV)

Sedimentation velocity (SV) experiments were employed in this study as they provide information about the shape and size of peptides in solution. Due to the high rate of back diffusion expected from low molecular weight peptides, high speeds are sometimes required to obtain reliable SV data. In the present study, measurements were made at speeds of 40,000 rpm and/or 55,000 rpm to generate data with the required mass resolution.

To determine the size distribution of peptide samples, absorbance data collected during an SV experiment was analyzed with the SEDFIT software (§ 2.6.3) using the c(S) method (Schuck *et al.*, 2002). The size distribution profiles were then converted to a molecular mass distribution using the molecular mass of the peptide monomer.

The sedimentation velocity measurements were carried out on a Beckman XL-1/A analytical ultracentrifuge (Beckman Coulter, Fullerton CA, USA) housed in the Department of Biological Sciences, University of Birmingham (Birmingham, UK) and in the Biochemistry Department, University of Oxford (Oxford, UK). Peptide samples were prepared in 50 mM Tris-HCl (pH 7.5), containing 15 mM DPC 100 mM NaCl, and 52.2% D_2O (Sigma) to match the buoyant density of the detergent. Density matching is needed so that the solvent density matches the buoyant density of the detergent micelles, and the only contribution to the buoyant molecular weight is from the peptide (Kochendoerfer *et al.*, 1999; Salom *et al.*, 2000). Data were collected using absorbance optics set to 280 nm.

Data were collected at one or two peptide concentrations (see in **Table 2.9**) using a two chamber centerpiece at a speed of 40,000 rpm and a temperature of 25°C or 55,000 rpm and a temperature of 20°C. The AUC cells were set up and filled according to the manufacturer's instructions (**Figure 2.7**). 400 scans were recorded for each sample, with 50 seconds between each scan. The moving boundary was monitored by repetitive radial scanning at a constant step size of 0.003 cm at 280 nm using a UV absorption optical system.

The peptides' monomeric molecular masses are shown in **Table 2.9**. The buffer density was 1.0608 g mL^{-1}, the buffer viscosity was 1.186 cP, (values were measured by Dr Andrew Beevers). The partial specific volumes (**Table 2.9**) were calculated using SEDNTERP software (see in § 2.6.3).

Table 2.9 - Peptide parameters used for AUC-SV data analysis. PSV stands for partial specific volume.

TM domain of interest	Molecular weight (Da)	Peptide concentration (μM)	PSV (mLg^{-1}) at 25 °C	PSV (mLg^{-1}) at 20 °C
rCPT1A TM1	2957	40	0.7722	0.7701
rCPT1A TM2 wt	2689	62, 142	0.7792	0.7771
rCPT1A TM2 $G_{107}I$	2745	49, 98	0.7872	0.7851
rCPT1A TM2 $G_{107}G_{113}I$	2804	112	0.7949	0.7928
rCPT1B TM1	2963	83	0.7592	0.7571
rCPT1B TM2	2785	107	0.7730	0.7709

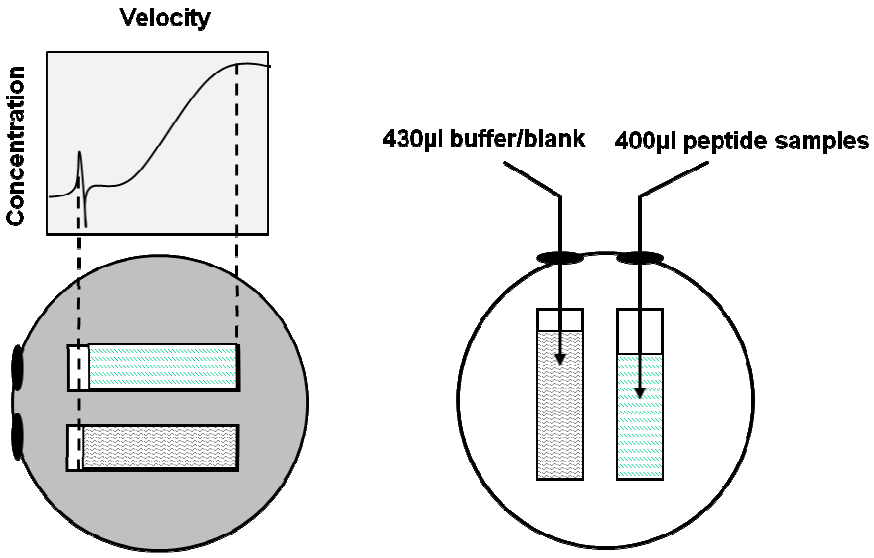

Figure 2.7 - Experimental setup of an analytical ultracentrifugation sedimentation velocity (AUC-SV) two chamber centre piece. The left panel shows a two-chamber cell during a SV experiment with the typical absorbance data. The loading setup of centre piece chambers is shown on the right hand side of the figure, where sample is loaded into the right chamber, and the reference solution (buffer) is loaded into the left chamber.

2.6 Software

2.6.1 Analysis of DNA sequences

SeqScanner: the sequencing data of all plasmids DNA was analysed using the free version of the Sequence Scanner program version 1.0 (downloadable from http://www.appliedbiosystems.com).

Clone Manager: For the design of cloning strategy and alignment of DNA sequences the Clone Manager version 5.02 software was used.

2.6.2 Analysis of protein sequences

ProtParam: Allows the computation of various physical and chemical parameters for a user entered sequence. The computed parameters include molecular weight, amino acid composition, atomic composition, extinction coefficient, aliphatic index and grand average of hydrophobicity (downloadable from http://www.expasy.ch/tools/protparam.html).

TMSTAT: Analysis of TM domains to identify helix-helix interaction motifs (Senes *et al.*, 2000). http://bioinfo.mbb.yale.edu/tmstat/.

ClustalW: Multiple sequence alignment of CPT1A and CPT1B proteins was carried out using Biology Workbench, http://workbench.sdsc.edu/.

2.6.3 Analysis of biophysical data

SEDNTERP: was used to estimate physical parameters are required for AUC data analysis, for example buffer density, buffer viscosity and the partial specific volume of peptides from their amino acid composition. The software developed by J. Philo, D. Hayes, and T. Laue, University of New Hampshire, USA, available at www.jphilo.mailway.com (Laue, 1992).

SEDFIT: was used for AUC-SV data analysis. The software is available at https://sedfitsedphat.nibib.nih.gov, (Schuck, 2000).

Dichroweb: Calculation of protein secondary structure from CD spectra (Whitmore and Wallace, 2008). The CDSSTR algorithm (Johnson, 1999; Sreerama and Woody, 2000) was used with the SP175 reference set (Lees *et al.*, 2006); see also http://dichroweb.cryst.bbk.ac.uk/html/home.shtml.

2.6.4 Molecular modelling

CHI: Structural calculations were performed using the CHI program (*C*NS searching of *h*elix *i*nteractions), the details of which have been described previously (Adams *et al.*, 1995; Adams *et al.*, 1996; Brunger *et al.*, 1998). The calculations were performed using an 8 node dual 2.66 GHz Xenon processor Linux cluster (Streamline Computing, Warwick).

CHI was used to create molecular models of all rCPT1A and rCPT1B TM domain homo- and hetero-oligomer structures. Using CHI, either two (for dimer), three (for trimer), or six (for hexamer) canonical α-helices containing TM domain sequence of interest were built. The starting geometries incorporated both right-handed (-25°) and left-handed (25°) crossing angles and an axis-to-axis distance between the helices of 10.4 Å. In a search of approximately symmetrical interactions, the helices were simultaneously rotated about their central axis in 45° increments from 0°-360°. After each rotation, molecular dynamics (MD) simulations were performed using simulated annealing of atomic coordinates. Four different MD simulations were performed for each starting geometry, and energy minimization of structures was carried out both before and after MD simulations. Groups of structures with a backbone RMSD of ≤1 Å were placed in clusters of 10 or more members, followed by a calculation of an average structure for each cluster and energy minimization. (The RMSD and cluster size was changed between 1.0-1.6 and 10-6, respectively, if the simulation did not produce meaningful results).

PyMOL: All peptide sequences present in this thesis were visualised and the figures produced using the PyMOL software (DeLano, 2002) (freely available from http://www.pymol.org).

CHAPTER 3

HOMO-OLIGOMERISATION OF CPT1A TRANSMEMBRANE DOMAINS

This chapter presents the results from biological assays and studies on synthetic peptides constituting the transmembrane domains of CPT1A. The self-association of both studied TM domains is observed, and the stoichiometry of assembly is determined in detergent micelles *in vitro.* Possible interacting sites between these helical peptides are proposed from *in silico* models.

3.1 Introduction

The kinetic characteristics of the two catalytically active isoforms of carnitine palmitoyltransferases, CPT1A and B, have been extensively studied since the late 1970s. Although they share a high degree of sequence similarity, CPT1A and B have been found to have significant differences in their substrate and inhibitor (carnitine and malonyl-CoA) binding sensitivity (Saggerson, 1982; Paulson *et al.*, 1984; Park and Cook, 1998). Furthermore, only the CPT1A isoform is found to alter its inhibitor binding sensitivity in different physiological states, where significant changes in membrane fluidity and composition are observed (Kolodziej and Zammit, 1990; Zammit *et al.*, 1998). These results highlighted the potential importance of transmembrane helix interactions in the enzyme's kinetics and folding of CPT1A, and that differences in transmembrane

helix-helix interactions may contribute to the differences in kinetics of the two CPT1 isoforms. Recently it has also been reported that CPT1A exists as an oligomeric complex in the OMM and that the N-terminal region of the protein containing TM1 and TM2 (residues 1-147 in the rat enzyme, rCPT1A) is involved in driving the oligomerisation of CPT1A (Faye *et al.*, 2007). Therefore, a closer study of the homo- and hetero-interactions of the TM domains in CPT1A could provide new understanding of the role of TM domains in enzyme folding and function.

The present chapter summarises the investigation of oligomerisation of each of the TM domains in CPT1A in isolation, carried out to identify what regions of the protein drive the oligomerisation and kinetics of the full-length enzyme. Here the self-association of each individual TM domain of rat CPT1A (rCPT1A) was studied in natural *E. coli* membranes using the TOXCAT (Russ and Engelman, 1999) and GALLEX (Schneider and Engelman, 2003) assays. Synthetic peptides corresponding to the TM sequences were used to obtain quantitative biophysical evidence of TM1 and TM2 oligomerisation, including the stoichiometry of assembly in detergent micelles. The results have enabled us to construct molecular models that highlight potential points of contact between TM helices and suggest that oligomer formation is favoured by the relative positioning of helix-helix interaction motifs within the predicted transmembrane domain helices.

3.2 Sequence analysis of CPT1A TM domains

The prediction of membrane spanning regions in CPT1A proteins was first carried out using the Uniprot online database (http://www.expasy.org), where TM1 and TM2 are indicated in the protein sequence of different species (highlighted in white in **Figure 3.1**). Additionally, the transmembrane hidden Markov model (TMHMM) software (Sonnhammer *et al.*, 1998) was used to predict the location of the transmembrane helices from the sequences, and these results are highlighted in colour in **Figure 3.1**.

3.2.1 Sequence conservation and helix-helix interaction motifs

The sequences of CPT1A TM domains (as predicted by the bioinformatics tool TMHMM) were further analysed to look for sequence conservation between species as well as known helix-helix interaction motifs. Multiple sequence alignments of the predicted TM sequences from a variety of species are shown in

Figure 3.2, where the sequence similarity across different species is 73.3% for CPT1A TM1 and 81.8% for TM2. TM domains of membrane proteins frequently contain sequence motifs that are known to both stabilise the proteins and provide structural plasticity by promoting TM helix-helix interactions. Moreover, different motifs within the same TM may separately promote hetero- or homo-interhelical associations (Gerber *et al.*, 2004).

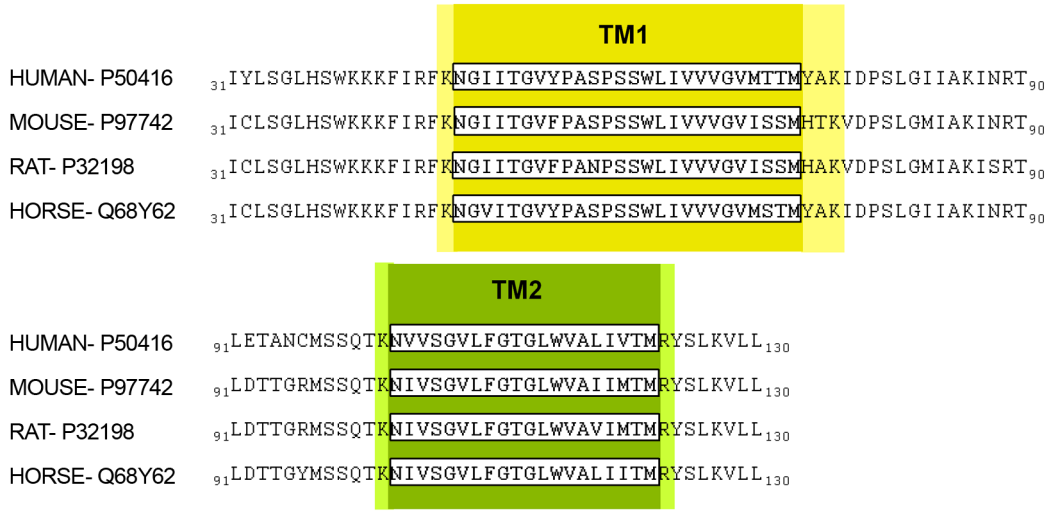

Figure 3.1 - Prediction of TM domain regions in CPT1A proteins from different species. Transmembrane domain regions defined by UniProt are in white brackets, highlighted with yellow and green, while residues highlighted with light yellow or light green were also predicted as part of TM domains by TMHMM. The UniProt codes of the analysed CPT1A proteins are shown on the left hand side.

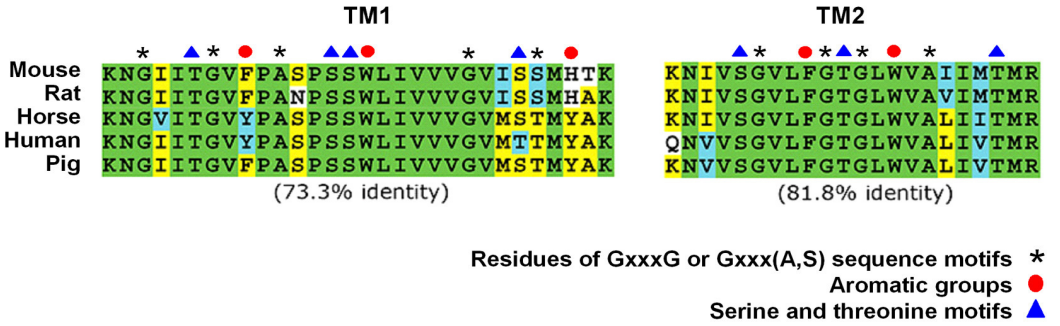

Figure 3.2 - Analysis of conserved residues and helix-helix interaction motifs in CPT1A TM1 and TM2. The sequence analyses of conserved residues were carried out using Biology Workbench http://workbench.sdsc.edu/. Completely conserved residues are labelled green, identical residues are labelled with yellow, similar residues with blue, and different residues with white. The sequence motifs are highlighted according to TMSTAT analysis.

3.3 *In vivo* oligomerisation of rCPT1A TM domains

Although previously reported data suggests that the TM2 domain plays a key role in oligomer formation of rCPT1A (Faye *et al.*, 2007), no direct measurements of self-association for either TM of rCPT1A had been reported at the start of the present work. To address this, we have examined the homo-oligomerisation of rCPT1A TM1 and TM2 in natural *E. coli* membranes using *in vivo* oligomerisation assays.

Studying lateral helix-helix interactions between transmembrane α-helices in a natural membrane environment has been made possible by several biological assays such as the ToxR system (Langosch *et al.*, 1996), TOXCAT (Russ and Engelman, 1999), POSSYCAT (Gurezka and Langosch, 2001) and GALLEX (Schneider and Engelman, 2003).

Previously, TOXCAT and GALLEX assays were successfully applied to the examination of several different TM homo- and hetero-interactions (Li *et al.*, 2004; Escher *et al.*, 2009). For this reason, in the present study both assays were initially used to measure homo-association of rCPT1A TM domains, providing complementary data. Here both TOXCAT and GALLEX assays were used to examine CPT1A TM domain oligomerisation and also to compare the two techniques. The GALLEX assay was further employed to measure hetero-association between TM1 and TM2 domains (see CHAPTER 6).

The TOXCAT assay is a ToxR-based transcriptional assay linked to chloramphenicol acetyltransferase (CAT) expression. The degree of TM association can be measured in terms of the CAT activity generated as a result of the homo-oligomerisation of TM domains in ToxR-TM-MBP chimera (where ToxR is a dimerisation-dependent DNA binding domain from *Vibrio cholerae* and MBP is maltose binding protein, for schematic figure and detailed description see Materials and Methods § 2.2). The sequence of the investigated TM domains was based on analyses of the full-length sequence of rat CPT1A (rCPT1A) using the bioinformatics program TMHMM to predict the location of TM domains (as described in § 3.2.1). Initial measurement of self-association of rCPT1A TM domains in TOXCAT chimera suggested that none of these sequences self-associate. However, previous studies suggest that the length of the TM cloned into the TOXCAT chimera can affect ToxR-based transcriptional activity (Langosch *et al.*, 1996; Li *et al.*, 2004). We undertook therefore a more extensive

investigation of how the length of the TM insert affected the association measured, and attempted to optimize the CAT activity by decreasing the length of the TM sequence in the chimera. The shorter rCPT1A TM sequences were designed taking into consideration the position of GxxxG motifs in the transmembrane segments.

In the GALLEX assay, the fundamental concepts of measuring TM homo-association are similar to those in the TOXCAT assay, but here a different LexA-TM-MBP chimera (where LexA is transcription factor) is expressed and the oligomerisation of the TM domain within the chimera results in the repression of β-galactosidase synthesis in *E. coli* cells. TM domain oligomerisation was characterized by the quantitative measurement of β-galactosidase (for schematic figure and detailed description see Materials and Methods § 2.3). The TM sequences cloned into GALLEX chimeras were originally designed with shorter TM lengths in agreement with the TOXCAT assay results mentioned above. Before the quantitative measurement of CAT activity (in TOXCAT assay) or β-galactosidase repression (in GALLEX assays), correct insertion of all chimeras was confirmed using NaOH extraction, *malE* complementation and spheroplast proteolysis assays as described in detail in § 2.2.2.

The above mentioned biological assays were performed using the TM domain of glycophorin A (GpA), a very well-characterized and strongly-dimerising TM domain, as a positive control and a dimerisation-defective point mutant ($G_{83}I$) as a negative control.

3.3.1 Homo-oligomerisation of transmembrane domain 1 (TM1)

The oligomerisation of rCPT1A TM1 was first measured using the TOXCAT assay. The initial sequence cloned into the TOXCAT chimera contained 27 residues (Lys_{47}-Met_{73}) from the TM domain (as predicted using TMHMM) and showed little or no ability to self-associate. When shortened to 24 and 21 residues (Ile_{50}-Val_{73}, Ile_{50}-Val_{73} respectively), the CAT activities of resulting chimeras were lower than that obtained for the negative control (**Figure 3.3**). The chimera containing the 21 residue TM1 insert also failed to grow on maltose minimal media plates when analysed using the *malE* complementation assay, but we could confirm the correct orientation of the chimera in the *E. coli* membrane using the spheroplast proteolysis assay (**Figure 3.4**).

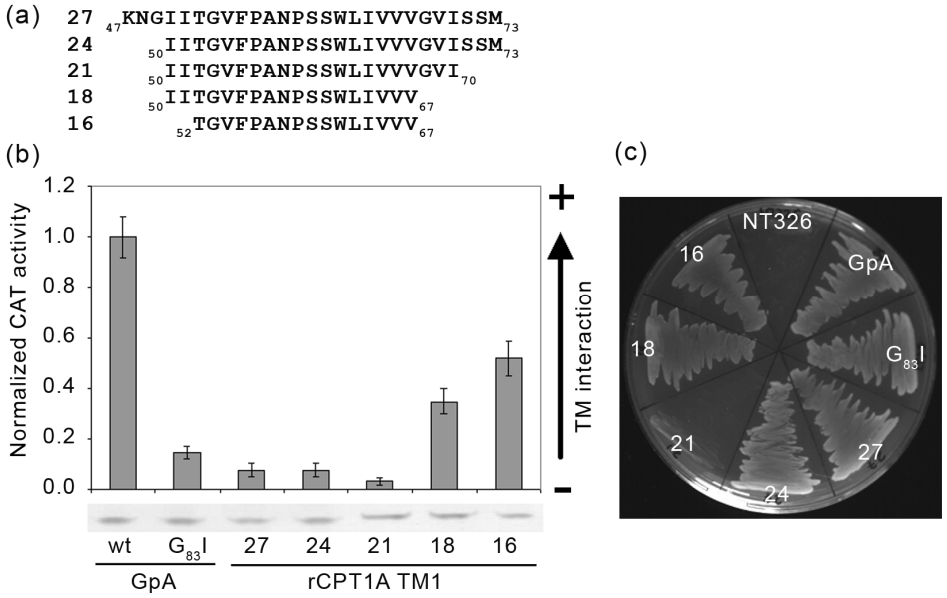

Figure 3.3 - Oligomerisation of rCPT1A TM1 (27, 24, 21, 18, 16) TOXCAT chimeras in *E. coli* membranes. (a) Transmembrane domain sequences of rCPT1A TM1 were cloned and analyzed using the TOXCAT assay. **(b)** CAT activities obtained for the different length rCPT1A TM1 inserts, and expression levels of each chimera detected by western blot analysis (using antibodies directed against MBP). All CAT activities are reported relative to the value obtained for wt GpA (positive control). Values are means (+/- standard deviation) for three or more independent measurements. **(c)** *malE* complementation to test the ToxR-TM1-MBP chimera's correct insertion and orientation.

The sequence of TM1 was further shortened to 18 and 16 residues (Ile_{50}-Val_{67}, Thr_{52}-Val_{67} respectively) and the resulting chimeras showed higher propensity to self-associate, yielding CAT activities of 35% and 53% of GpA levels, respectively. The self-association of rCPT1A TM1 studied using the TOXCAT assay suggests that shorter constructs of this sequence have the ability to form homo-oligomers (**Figure 3.3**).

Self-association of the rCPT1A TM1 domain was also studied using the GALLEX assay. In *wt* LexA-TM-MBP chimeras, different lengths of TM1 sequences were also tested. Reassuringly, TM1 inserts show the same length-dependent oligomerisation observed using the TOXCAT assay. However, the GALLEX assay suggests much stronger oligomerisation of the 21 residue construct as well as for the 18 and 16 residue sequences, which yielded results very similar to those obtained for wt GpA (**Figure 3.5**). The correct insertion and orientation of chimeras containing 21, 18 and 16 residues was confirmed by the spheroplast proteolysis assay (data not shown).

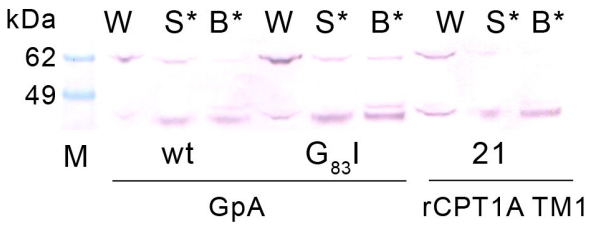

Figure 3.4 - Immunoblots of spheroplast proteolysis assay to investigate the topology of the ToxR-TM1(21)-MBP chimera. Chimeras were expressed in NT326 cells. The immunoblotting was carried out using antibodies directed against MBP. The correctly inserted chimeras were detected at 66 kDa (the full length chimera protein molecular weight) in W: whole cell fractions, and at 43 kDa (molecular weight of MBP) in S*: spheroplast treated with proteinase K and B*: lysed spheroplast treated with proteinase K fractions.

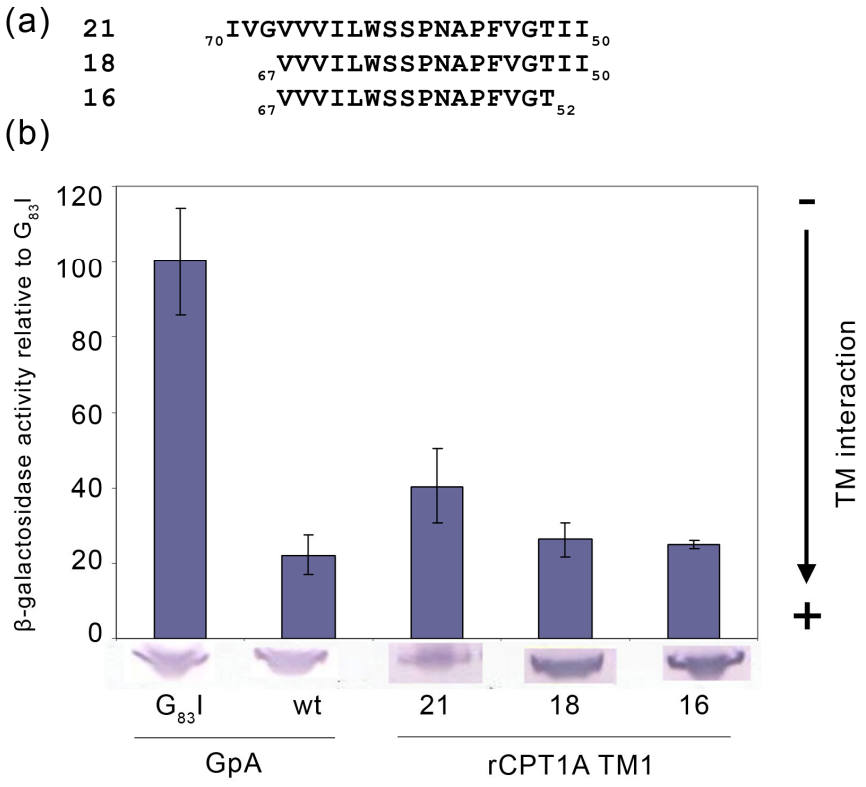

Figure 3.5 - Oligomerisation of rCPT1A TM1 (21, 18, and 16 amino acids in length) in GALLEX homo-oligomerisation assay. (a) The inverse sequences of rCPT1A TM1 were cloned into the pBLM vector to form the *wt* LexA-TM-MBP chimera. Chimeras were expressed in SU101 using 0.01 mM IPTG when analyzed using the GALLEX homo-oligomerisation assay. **(b)** The resulting β-galactosidase activities of GpA and rCPT1A TM1 chimeras. All activities are reported relative to the value obtained for GpA $G_{83}I$ (negative control). Values are means (+/- standard deviation) for three independent measurements. The expression levels of each chimera detected by western blot analysis.

In summary, results from both TOXCAT and GALLEX assays support the self-association of the rCPT1A TM1 domain in the *E. coli* membrane.

3.3.2 Homo-oligomerisation of transmembrane domain 2 (TM2)

In a similar manner as that described above, the TOXCAT assay was also used to measure self-association of rCPT1A TM2. The initial sequences of rCPT1A TM2 inserts containing 22 or 20 residues indicate no significant interaction, however after further optimization of the length of the TM domain insert, chimeras showed a much greater propensity to form homo-oligomers in the membrane. The CAT activity of a 16 amino acid TM2 insert (Ile_{104}-Ile_{119}) was approximately 47% of that observed for the positive control wt GpA (**Figure 3.6**).

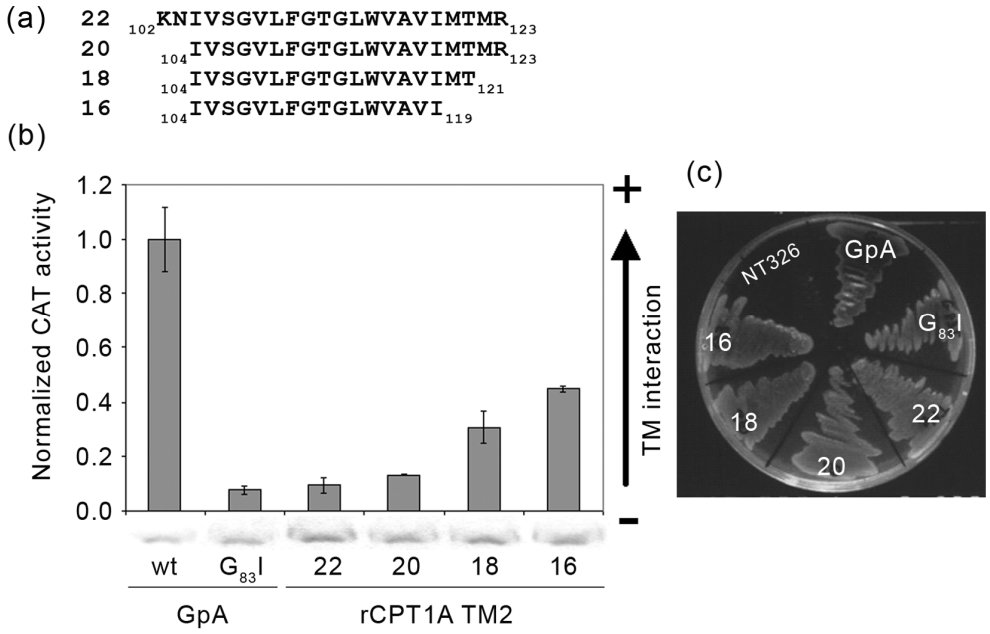

Figure 3.6 - Oligomerisation of rCPT1A TM2 (22, 20, 18, and 16 amino acids in length) TOXCAT chimeras in *E.coli* membranes. (a) Transmembrane domain sequences of rCPT1A TM2 were cloned and analyzed using the TOXCAT assay. **(b)** CAT activities obtained for the different length TM2 constructs, and expression levels of chimeras detected by western blot analysis. All CAT activities are reported relative to the value obtained for wt GpA (positive control). Values are means (+/- standard deviation) for three or more independent measurements. **(c)** *malE* complementation to confirm the ToxR-TM2-MBP chimeras correct insertion.

The 16 amino acid TM2 sequence, which yielded the strongest signal in the TOXCAT assay, was also cloned into the GALLEX *wt* LexA-TM-MBP chimera and the homo-oligomerisation assay was performed. The resulting *wt* LexA-TM2(16)-MBP chimera yielded β-galactosidase repression similar to that

observed for the positive control (GpA), which further validates the results obtained using TOXCAT (**Figure 3.7**).

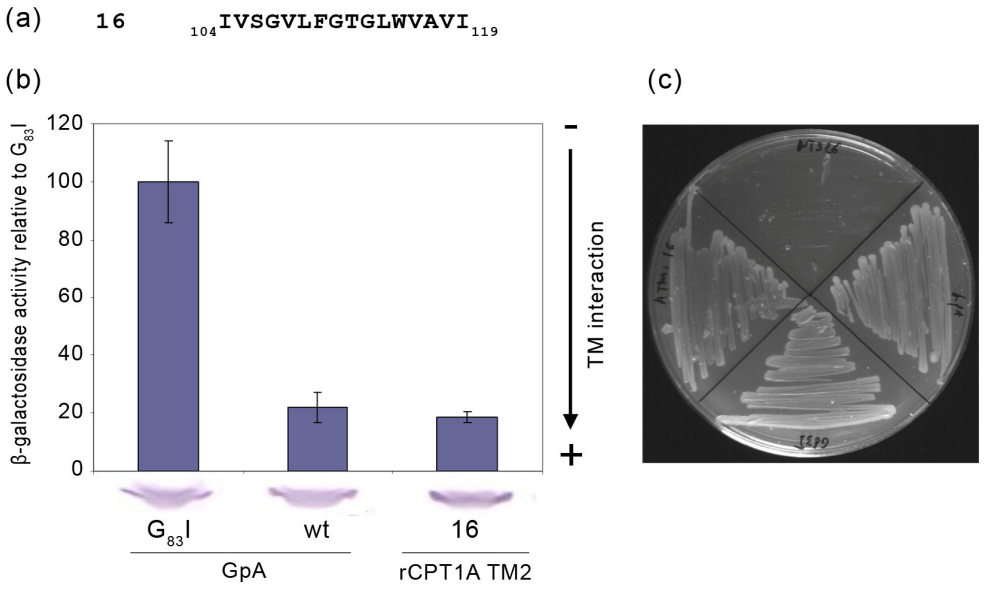

Figure 3.7 - Oligomerisation of rCPT1A TM2 (16 amino acids in length) in GALLEX homo-oligomerisation assay. (a) The sequence of rCPT1A TM2 was cloned into the pBLM vector to form the MBP-TM-*wt*LexA chimera. Chimeras were expressed in SU101 using 0.01 mM IPTG when analyzed by the GALLEX homo-oligomerisation assay. **(b)** The resulting β-galactosidase activities of GpA and rCPT1A TM2 chimera. All activities are reported relative to the value obtained for $GpAG_{83}I$ (negative control). Values are means (+/- standard deviation) for three independent measurements. The expression levels of chimeras detected by western blot analysis. **(c)** *malE* complementation assay results to confirm the correct insertion of the LexA-TM2-MBP chimera.

The correct insertion and orientation of all of the above-mentioned TM2 chimeras, analyzed using either the TOXCAT or GALLEX assays, was confirmed by growth on maltose minimal media plates in the *malE* complementation assay.

In summary, similarly to TM1, both homo-oligomerisation assays also suggest significant homo-oligomerisation of rCPT1A TM2.

3.4 *In vitro* oligomerisation of rCPT1A TM peptides

While the above presented oligomerisation studies provide a strong indication that the rCPT1A TM sequences can support self-association of these domains, the TOXCAT or GALLEX assay cannot report on the order of the oligomeric state achieved. Therefore, in order to validate the results of *in vivo* assays and characterise the oligomeric state(s) of the rCPT1A TM domains, *in vitro* approaches were used.

Synthetic peptides corresponding to the rCPT1A TM domains were investigated to establish whether the oligomeric states attained *in vitro* correspond to those observed for full-length rCPT1A (i.e. trimer and hexamer; (Faye *et al.*, 2007)).

The secondary structures of the synthetic peptides were first characterised in a number of detergents using circular dichroism (CD). To investigate the oligomeric state(s) of rCPT1A TM peptides, chemical cross-linking and analytical ultracentrifugation sedimentation velocity (AUC-SV) experiments were carried out (§ 2.4 and **Table 2.6**).

3.4.1 Purification of synthetic TM peptides

The crude synthetic peptides were purified by reversed-phase high performance liquid chromatography (RP-HPLC). Further details and peptide sequences can be found in § 2.4. The purity of the peptide fractions was confirmed by electrospray ionization time-of-flight mass spectroscopy (ESI-TOF-MS micrOTOF, Bruker). The deconvoluted mass spectra of rCPT1A TM1 and TM2 peptides are shown in **Figure 3.8** and **Figure 3.9**, respectively.

Table 3.1 - The amino acid sequences of rCPT1A TM1 and TM2 synthetic peptides used in this study. Non-native lysine residues are shown in bold.

TM domain of interest	Synthetic peptide sequence	Molecular weight (Da)
rCPT1A TM1	$COCH_3$-KNGIITGVFPANPSSWLIVVVGVISSM**K**-$CONH_2$	2957
rCPT1A TM2 wt	$COCH_3$-**K**KNIVSGVLFGTGLWVAVIMTMR**K**-$CONH_2$	2689

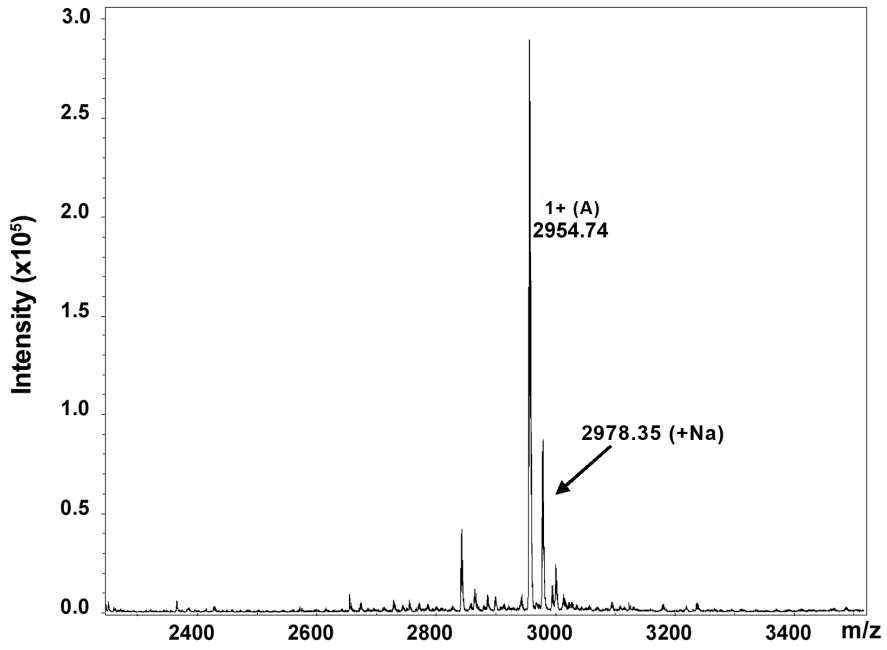

Figure 3.8 - Analysis of purified rCPT1A TM1 peptide by electrospray ionisation mass spectrometry (ESI-MS). The HPLC fractions containing the desired peptide were pooled and analyzed using ESI-MS. In the deconvoluted spectrum, the major peak corresponds to the rCPT1A TM1 peptide (2954 Da), and additional peaks correspond to sodium and solvent adducts.

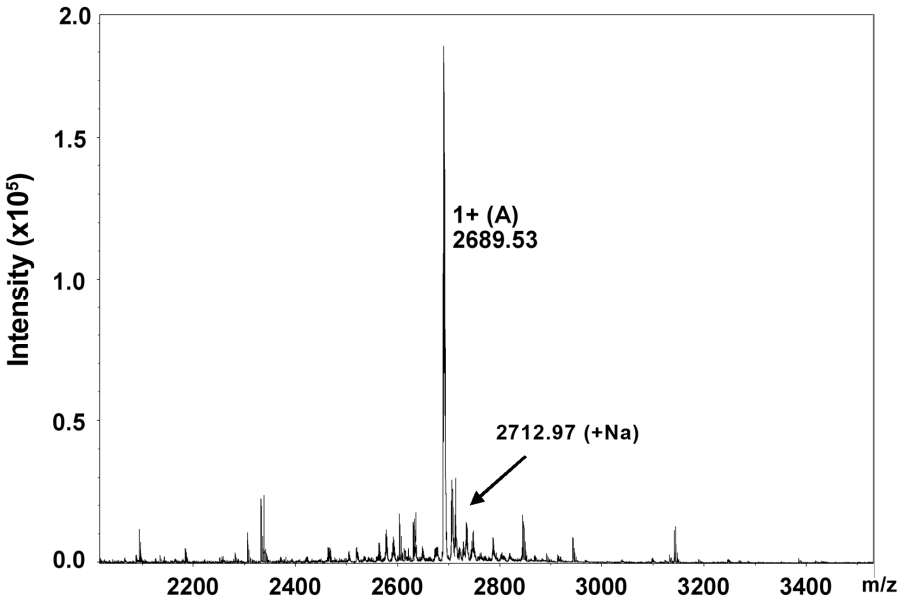

Figure 3.9 - Analysis of purified rCPT1A TM2 peptide by electrospray ionisation mass spectrometry (ESI-MS). The HPLC fractions containing the pure peptide were pooled and analyzed using ESI-MS. In the deconvoluted spectrum, the major peak corresponds to the rCPT1A TM2 peptide (2689 Da), and additional peaks correspond to sodium and solvent adducts.

3.4.2 Secondary structure of TM peptides

Before characterizing the oligomeric state, the secondary structure of the rCPT1A TM peptides was determined using circular dichroism (CD) spectroscopy (details in § 2.5.3). The analyses of secondary structure composition from the collected CD spectra were carried out by fitting of the data using the CDSSTR software (Johnson, 1999).

CD spectra were collected for the CPT1A TM1 peptide, and visual inspection of the spectra suggested that the peptide adopts mainly an α-helical secondary structure in the anionic and denaturing detergent sodium dodecylsulphate (SDS) at a 3:1 micelle to peptide ratio and in zwitterionic detergent, dodecyl-phosphocholine (DPC) micelles at 10:1 and 20:1 ratios. DPC was selected because it is a less denaturing detergent than SDS, and is amenable to a large range of biophysical methods (including analytical ultracentrifugation) (Li *et al.*, 2001; Oates *et al.*, 2008). However, at lower DPC micelle to peptide ratios (4:1 and 2:1), the peptide adopted a primarily β-sheet secondary structure, which we suggest arises from insoluble aggregates. Fitting of CD data using CDSSTR software confirmed that the rCPT1A TM1 peptide secondary structure composition in DPC is dependent on the micelle concentration (**Figure 3.10**). Secondary structure composition was calculated by fitting of the CD data between 200-260 nm. Data collected at lower wavelengths (190-200 nm) was not included in the fit due to the increased effects of light scattering of detergent micelles in this range, as evidenced by high tension (HT) values greater than 600 mV.

Despite the fact that results for TM1 have been presented here first, our initial CD experiments were actually carried out on the rCPT1A TM2 peptide, and in these initial experiments we screened a number of different detergent micelles to determine which were optimal for solubilisation of the TM peptides. Spectra were collected for the solubilised TM2 peptide in trifluoroethanol (TFE), SDS, octylglucoside (OG), a neutral and non-denaturing detergent, lyso-palmitoyl phosphatidylglycerol (LPPG), an anionic detergent, as well as in DPC. Apart from the spectra collected for the OG-solubilised peptide, all of the resulting spectra (**Figure 3.11**) displayed a characteristic α-helical profile, with negative absorption maxima at 208 and 222 nm, demonstrating that the peptides adopt an α-helical

secondary structure in TFE, SDS, LPPG and DPC micelles. In the case of OG, the spectra suggest more β-sheet content.

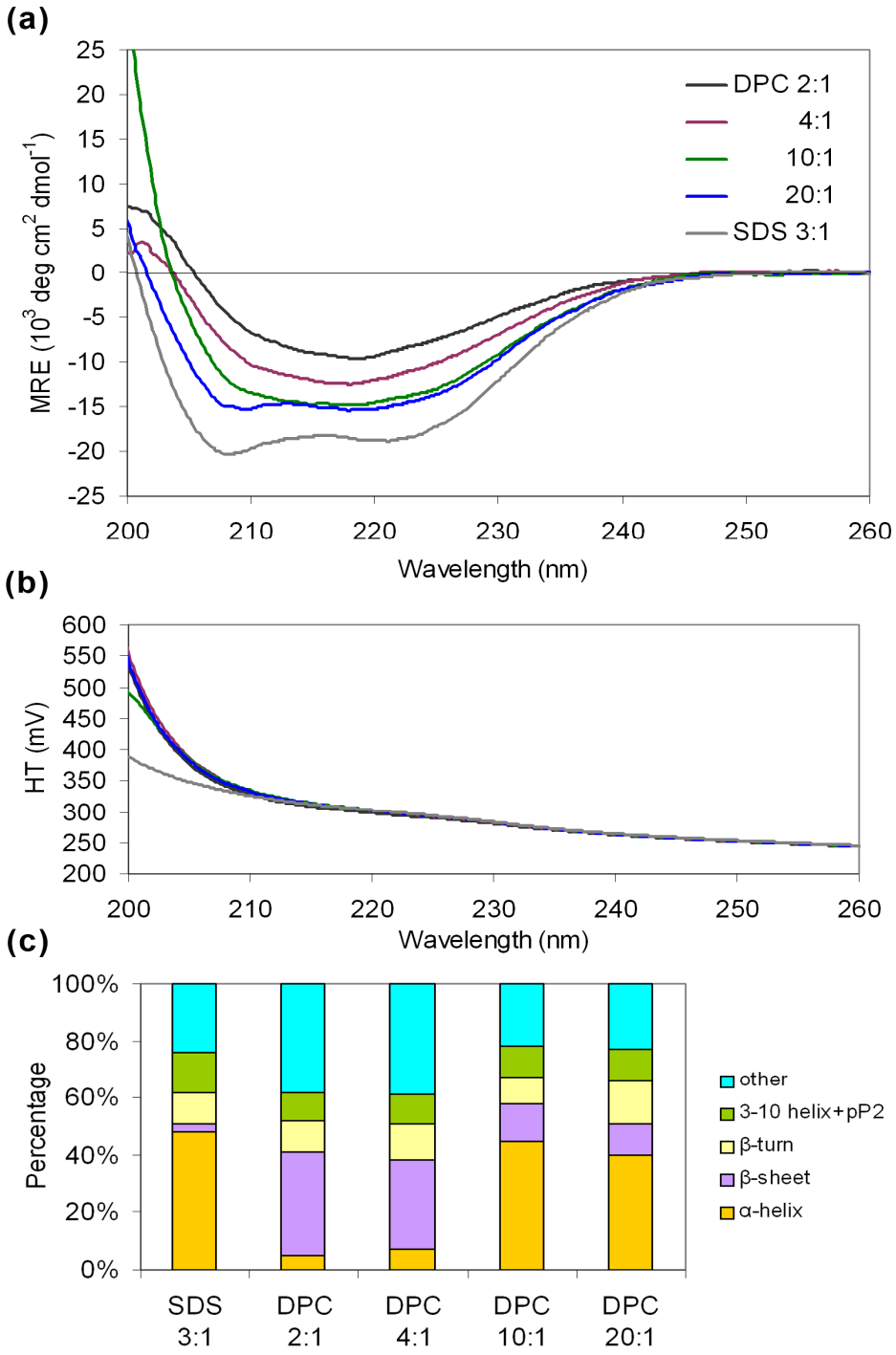

Figure 3.10 - The effect of DPC micelle concentration on the secondary structure of rCPT1A TM1 peptide. (a) CD spectra measured at different detergent micelle to peptide ratios, plotted in units of mean residue ellipticity (MRE). **(b)** High tension (HT) over the wavelength region specified in (a). **(c)** The secondary structure composition of the rCPT1A TM1 peptide estimated from the CD spectra shown in (a) using the CDSSTR software (Johnson, 1999).

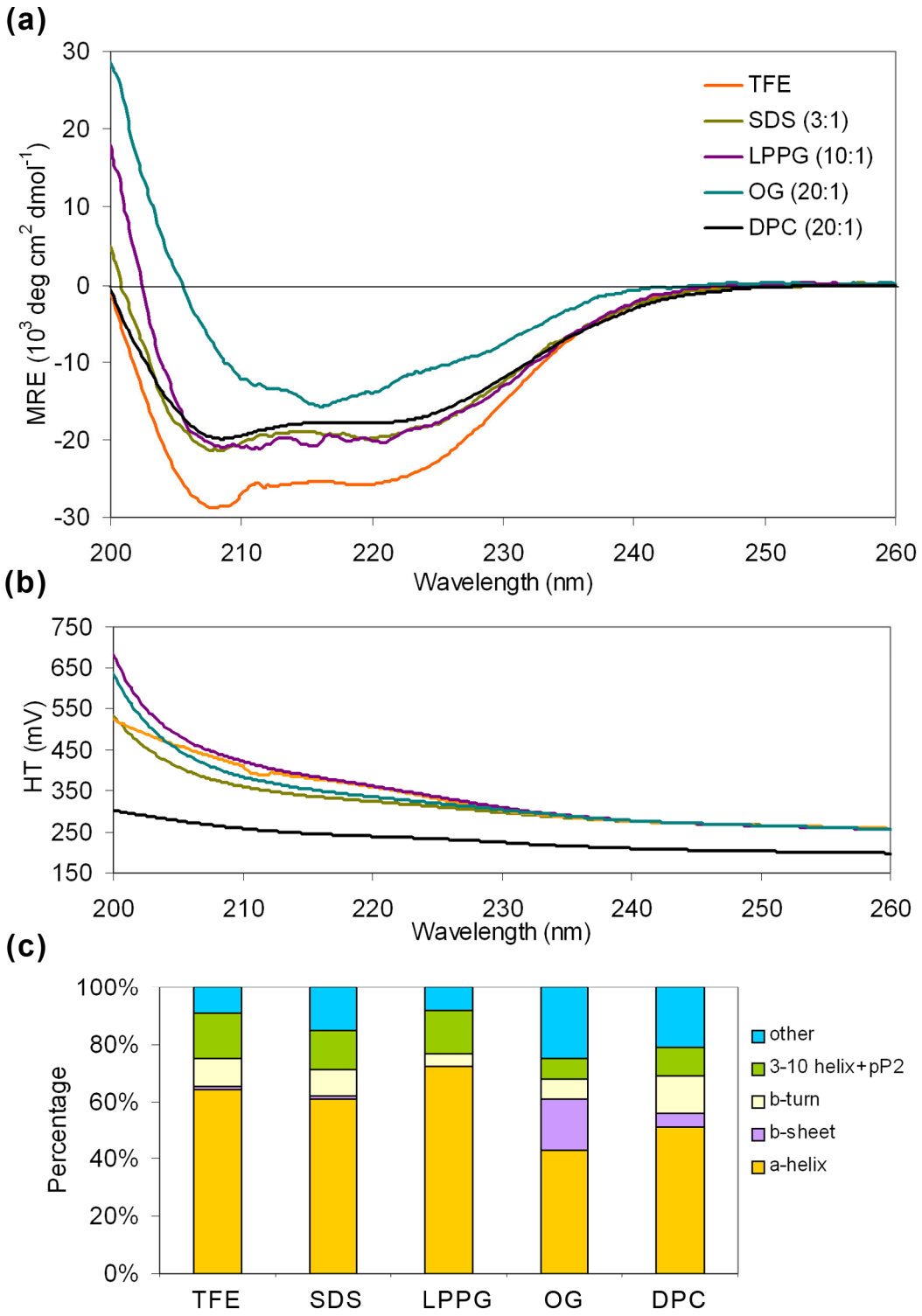

Figure 3.11 - The effect of TFE solvent and different detergent micelles (SDS, LPPG. OG, DPC) on the secondary structure of rCPT1A TM2 peptide. (a) CD spectra measured in different detergent micelles, plotted in units of mean residue ellipticity (MRE). **(b)** High tension (HT) over the wavelength region specified in (a). **(c)** The secondary structure composition of the rCPT1A TM2 peptide estimated from the CD spectra shown in (a) using the CDSSTR software (Johnson, 1999).

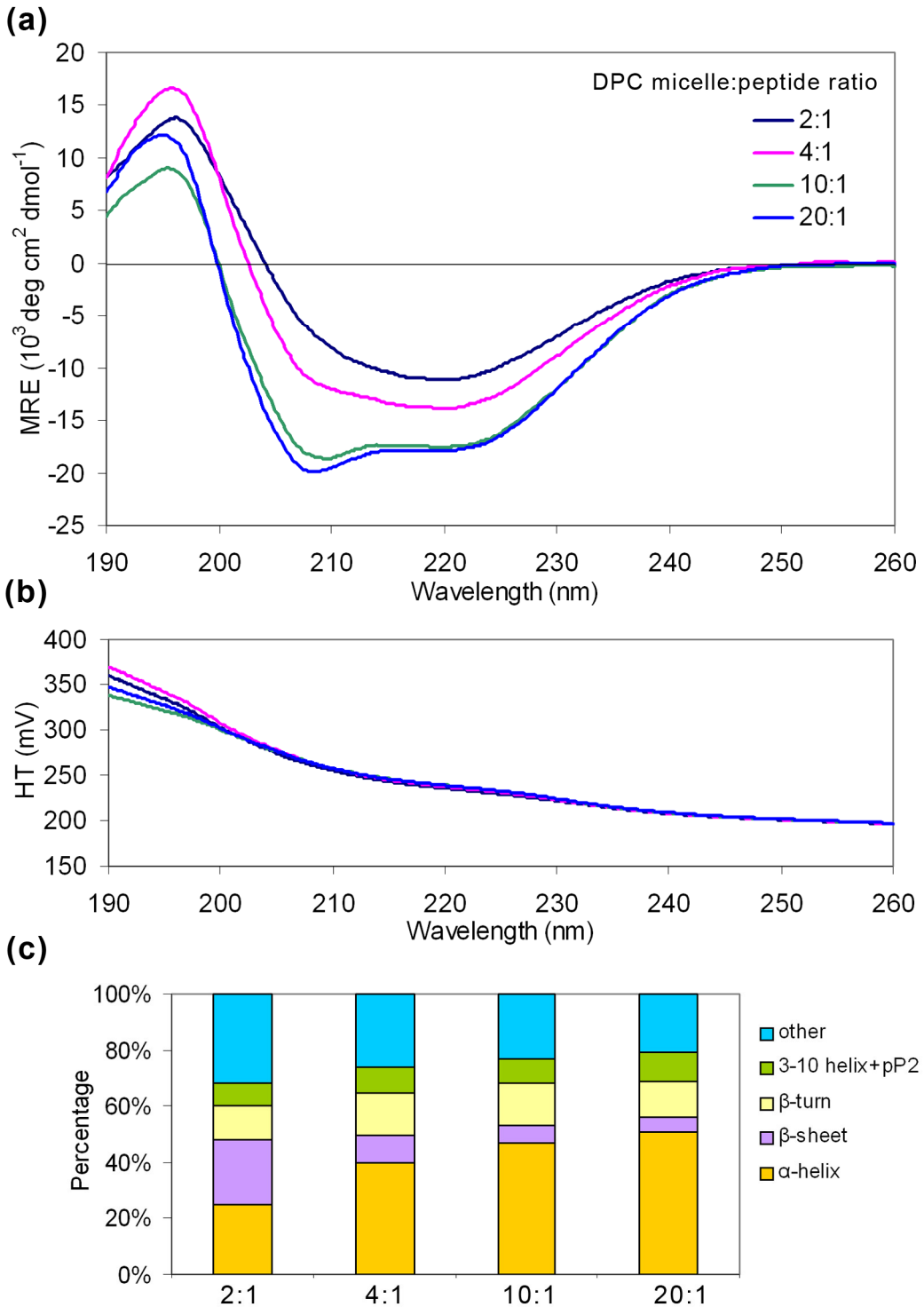

Figure 3.12 - The effect of DPC micelle concentration on the secondary structure of the rCPT1A TM2 peptide. (a) CD spectra measured at different detergent micelle to peptide ratios, plotted in units of mean residue ellipticity (MRE). **(b)** High tension (HT) over the wavelength region specified in (a). **(c)** The secondary structure composition of the rCPT1A TM2 peptide estimated from the CD spectra (190-260 nm) shown in (a) using the CDSSTR software (Johnson, 1999).

Fitting of CD data using CDSSTR software confirms that the CPT1A TM2 peptide is predominantly α-helical in TFE, SDS and LPPG, while it is primarily β-sheet in OG (**Figure 3.11**). Further investigation also revealed that, as observed for the CPT1A TM1 peptide, the helical character of the TM2 peptide is also dependent on the micelle concentration in DPC (**Figure 3.12**). Since the HT values were lower than 600, here the secondary structure of the rCPT1A TM2 peptide was calculated using the 190-260 nm data set as shown in **Figure 3.12**.

3.4.3 Determination of rCPT1A TM1 peptide oligomeric state

Synthetic peptides corresponding to rCPT1A TM1 and TM2 were solubilised in DPC micelles and then treated with the water-soluble chemical cross-linker bis[sulfosuccinimidyl] suberate (BS^3). BS^3 reacts specifically with the terminal $-NH_2$ of the peptide as well as the $-NH_2$ groups on lysine side chains, provided that the reactive groups are within 11.4 Å of one another (Staros, 1982). Cross-linking reactions were carried out at increasing DPC micelle to peptide (M:P) concentration ratios to investigate the effect of detergent concentrations on oligomeric state of TM peptides (Fisher *et al.*, 1999). Cross-linked species were analyzed using SDS-PAGE and visualized by staining with silver nitrate (for details see § 2.1.5.3).

The rCPT1 TM1 peptide (K_{47}-M_{73}, 2954 Da) was electrophoresed under denaturing conditions (SDS-PAGE) before and after treatment with a chemical crosslinker. When dissolved in SDS detergent, the TM1 peptide migrated as a monomeric species at ~3 kDa (**Figure 3.13 a** and **b**, cross-linked and un-cross-linked in the last two lanes), as expected from the ability of SDS to destabilize the non-covalent interactions involved in transmembrane oligomer formation (Fisher *et al.*, 2003). In order to investigate its oligomeric state in a less denaturing detergent, the peptide was dissolved in DPC detergent micelles followed by chemical cross-linking with BS^3 to covalently stabilize rCPT1A TM1 peptide oligomers in DPC micelles. Cross-linked species were visualized by SDS-PAGE analysis. The TM1 peptide produced a number of bands between the 6 and 14 kDa molecular weight markers, which corresponds to oligomeric states between trimer and pentamer. A broad band between 28-38 kDa was observed at the lowest detergent concentrations (M:P=1/3–2), suggesting the presence of higher order aggregates. As the detergent concentration was increased (M:P=3–5), only

trimer and tetramer species were observed, and at the highest detergent concentrations (M:P=10–20) only trimer species were detected (**Figure 3.13 b**). It is well-established that increasing detergent concentration can destabilize TM helix oligomers (Fisher *et al.*, 1999), and this behaviour is reconfirmed in this study of the CPT1A TM1 peptide. These results also suggest that the most stable oligomeric state for the TM1 peptide at all detergent concentrations is that of a trimer.

To confirm the specificity of the cross-linking reaction and investigate the strength of helix-helix interactions in SDS micelles, samples were also analysed in the absence of a cross-linker on SDS-PAGE. Although the bulk of the peptide migrated at the molecular weight of the monomer, we were surprised to find that the trimer species was also present on the gel, especially at the lowest detergent concentrations (**Figure 3.13 c**). According to the cross-linking experiments, the CPT1A TM1 peptide forms predominantly trimers when dissolved in DPC micelles.

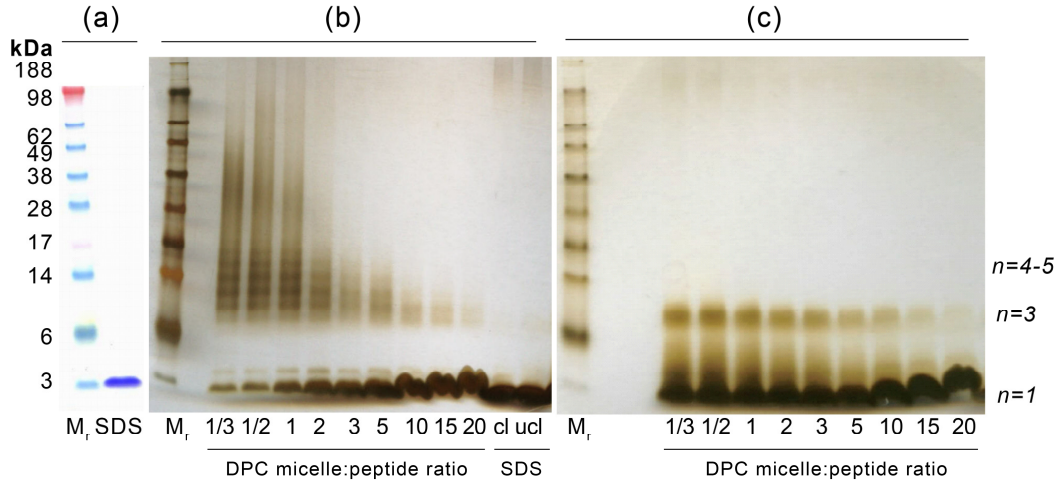

Figure 3.13 - SDS-PAGE analysis of chemically cross-linked rCPT1A TM1 peptide oligomerisation. (a) The molecular weight marker is shown in the left-hand lane. Peptide dissolved in SDS and visualised by coomassie staining. **(b)** BS^3-mediated cross-linking of peptides dissolved in DPC micelles. Cross-linking reactions were carried out in DPC detergent micelles at various micelle to peptide concentration ratios as indicated below each lane. Protein bands were visualized by staining with silver nitrate. Oligomeric states (e.g. trimer indicated by n=3) are indicated at the far right of the gels. **(c)** rCPT1A TM1 peptide in the absence of crosslinker migrates mainly as monomer, but bands corresponding to trimer were also detected at different DPC micelle concentrations, as visualized by silver nitrate staining.

In order to directly and more quantitatively study the oligomerisation behaviour of rCPT1A TM peptides, they were also studied in the absence of a cross-linker using analytical ultracentrifugation (AUC). For investigating the oligomeric state of the TM1 peptide, sedimentation velocity (SV) experiments were carried out at 25°C at a speed of 40,000 rpm (Department of Biochemistry, Birmingham University) and at 20°C at a speed of 55,000 rpm, (Department of Biochemistry, University of Oxford) using Beckman Optima XL-1/A ultracentrifuges (as described in § 2.5.5).

The data collected during the lower speed AUC-SV experiments (40,000 rpm) were analyzed. When the data were fit using the programme SEDFIT (Schuck, 2000), the sedimentation coefficient profile showed hexamer or higher order sedimenting species (aggregation) in rCPT1A TM1 samples (data not shown). Since the sizes of the sedimenting species were estimated to be ~ 3-15 kDa (based on what we learnt from our cross-linking experiments, **Figure 3.13** and § 3.4.3,), it was hoped that we could resolve any small molecular weight sedimenting species by carrying out further experiments at a higher speed (55,000 rpm). AUC-SV data were collected at 55,000 rpm at two different peptide concentrations, but only the lower concentration sample yielded a sedimentation profile of sufficient quality to be analyzed. The peptide concentration of this sample was 40 µM (M:P ratio ~ 6). The partial specific volume was 0.7701 mL g^{-1} (at 20°C). Sedimentation profiles were again fit using SEDFIT (Schuck, 2000) and the resulting sedimentation coefficient profile and fitting residuals are shown in **Figure 3.14**. The sedimenting species in the rCPT1A TM1 peptide sample were typically hexamers, centered at S=0.68. Upon conversion of this sedimentation coefficient to molecular mass, the peak mass value was 16.75 kDa, corresponding to hexamers. When compared with the calculated molecular weights for the TM1 hexamer (17.72 kDa), the experimental value agreed to within 5.5% of the theoretical values.

Although the higher speed AUC-SV data was in agreement with our results collected at lower speed, AUC did not detect the smaller species (trimer), which was observed previously by SDS-PAGE analysis (**Figure 3.13**). However, the absence of hexameric or higher order species on the cross-linking SDS-PAGE and the presence of SDS-stable trimers in the uncross-linked samples suggest that the hexamers detected with AUC-SV analyses are most likely dimers of trimers.

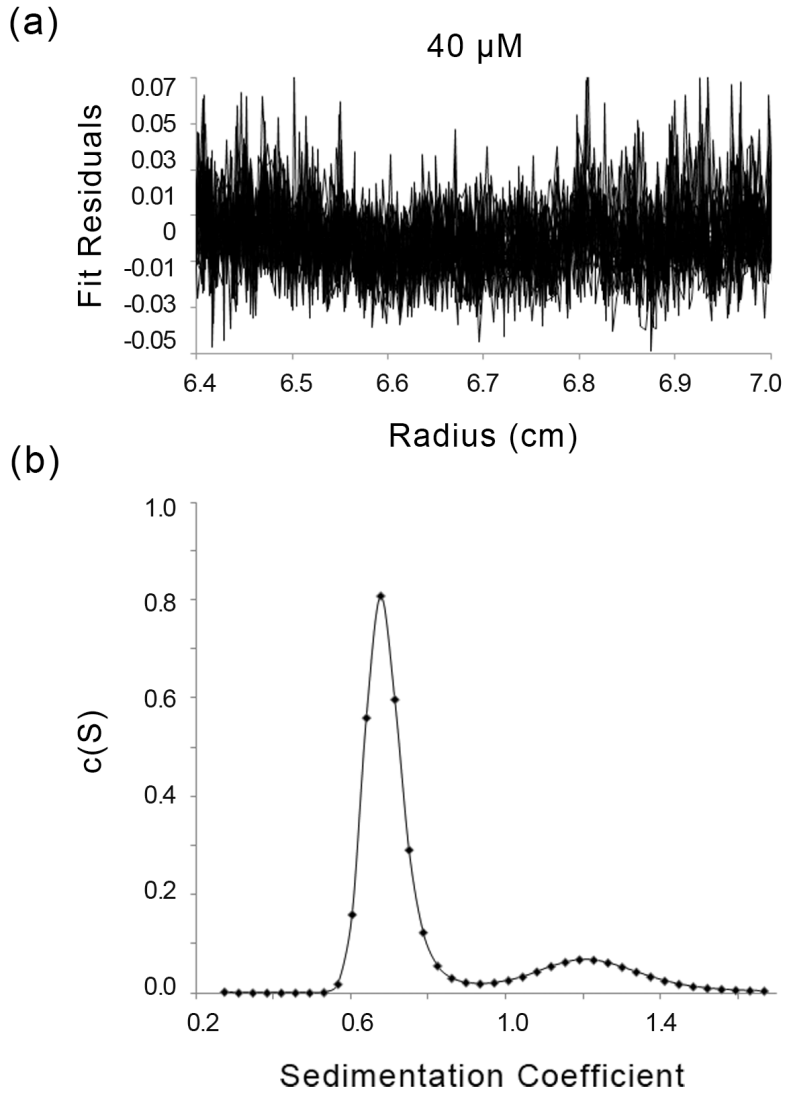

Figure 3.14 - Analytical ultracentrifugation analysis of rCPT1A TM1 synthetic peptide in DPC detergent solution. Sedimentation velocity data were obtained for TM1 peptide dissolved in buffer containing 15 mM DPC and 52.5% D_2O. **(a)** Residuals of the fitting process for samples containing 63 µM peptide. **(b)** Sedimentation coefficient distribution profiles for the peptide as calculated using the SEDFIT program.

3.4.4 The order of rCPT1A TM2 peptide oligomerisation

Similar to rCPT1A TM1, after significant homo-oligomerisation behaviour was observed for the rCPT1A TM2 domain using *in vivo* assays (see in § 3.3.2), further experiments were carried out to identify the order of TM2 oligomerisation. As before, cross-linking with BS^3 was initially used to assess the oligomeric state of the rCPT1A TM2 synthetic peptide (K_{102}-R_{123}, 2689 Da) dissolved in DPC micelles, and cross-linked species were visualized by SDS-PAGE analysis.

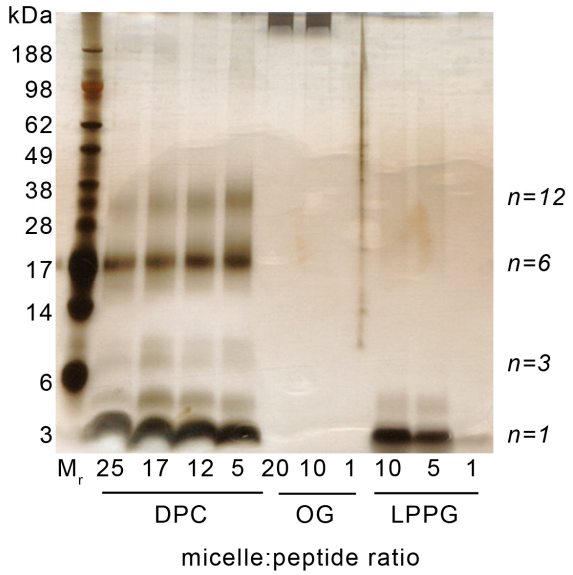

Figure 3.15 - SDS-PAGE analysis of chemically cross-linked rCPT1A TM2 peptide oligomerisation in different detergent micelles (DPC, OG, LPPG). Molecular weight marker is shown in the first left-hand lane. BS^3-mediated cross-linking of peptides were dissolved in DPC, OG and LPPG micelles. Cross-linking reactions were carried out in each detergent micelles at various micelle to peptide concentration ratios as indicated below each lane. Protein bands were visualized by staining with silver nitrate. Oligomeric states (e.g. trimer indicated by n=3) are shown at the far right of the gels.

The data shown in **Figure 3.15** indicates that the TM2 peptide migrates primarily as monomers (2.69 kDa), and hexamers (16.1 kDa) after cross-linking. In addition to these species, small concentrations of dimer, trimer and dodecamer species are also observed. In OG micelles, the peptide forms aggregates which sit in the wells, explaining the high β-sheet content (**Figure 3.11**) of the peptide CD spectra in this detergent. In LPPG micelles, the peptide is found to form predominantly monomers. For this reason, in further experiments throughout this work peptides were dissolved in DPC micelles when studied with the different techniques.

To test the reproducibility of the above results, and to investigate the effect of detergent concentration on the rCPT1A TM2 oligomeric states, the cross-linking reactions were carried out using M:P=1/3-20, DPC micelle to peptide ratios and M:P=4 SDS micelle to peptide ratio.

The cross-linking reaction samples (**Figure 3.16 b**) at 1/2 and 1/3 M:P ratios were overloaded on the gel however bands correspond to hexamer and dodecamer were detected as well as in M:P=1. No bands corresponding to lower-order oligomeric states (e.g. trimer) or monomer were evident in these lanes. As

the M:P ratio was increased to a value of 2, a monomer band could be observed (2.69 kDa) as well as weak bands corresponding to dimer (5.38 kDa) and trimer (8.07 kDa). Further increases in the M:P ratio resulted in increasing amounts of monomeric, dimeric and trimeric species, accompanied by decreasing populations of hexamers and dodecamers. The results shown in **Figure 3.16 b** demonstrate that the oligomeric states of the TM2 peptide differ with increasing detergent concentrations. The rapid loss of the dodecamer of TM2 with increasing M:P ratios suggests that this is the least stable species. The hexamer is evidently more stable, as its presence can be detected at all M:P ratios studied, although the concentration of hexamer is greatly reduced at M:P > 5. The oligomeric species that are most stable at the highest M:P ratios are the dimer and trimer. These two species (together with the monomer) steadily increased in concentration at high M:P ratios.

As a negative control, cross-linking was carried out with the peptide dissolved in SDS; as expected (Fisher *et al.*, 2003), only a band corresponding to the monomer was observed (**Figure 3.16 b**). TM2 peptide samples were also analysed in the absence of cross-linker on SDS-PAGE. At the lowest M:P ratios, SDS-stable hexamers and dodecamers are clearly detected (**Figure 3.16 c**). However, as the micelle concentration is increased, the high-order oligomers are rapidly destabilized and cannot be detected at M:P ratios above 3 (as shown in **Figure 3.16 c**). These results suggest an SDS-stable interaction (at least at low M:P ratios), and validate specificity of BS^3 cross-linking reaction.

To confirm the oligomeric state(s) of the rCPT1A TM2 peptide in the absence of a cross-linker, analytical ultracentrifugation studies were carried out. Here a speed of 40,000 rpm was sufficient to generate data with the required mass resolution for the analysis of the oligomeric state of the TM2 peptide. Two peptide concentrations were analyzed, 62 μM (M:P ~ 4) and 142 μM (M:P ~ 1), in buffered DPC solution. The fitting residuals for both concentrations are shown in **Figure 3.17 a-b** (sedimentation profiles not shown), corresponding to fits with RMSD values of 4.9×10^{-3} and 6.5×10^{-3}, respectively. The sedimentation coefficient profile for the higher of the two concentrations (**Figure 3.17 c**) contained two species centered at S=0.747 and S=1.15.

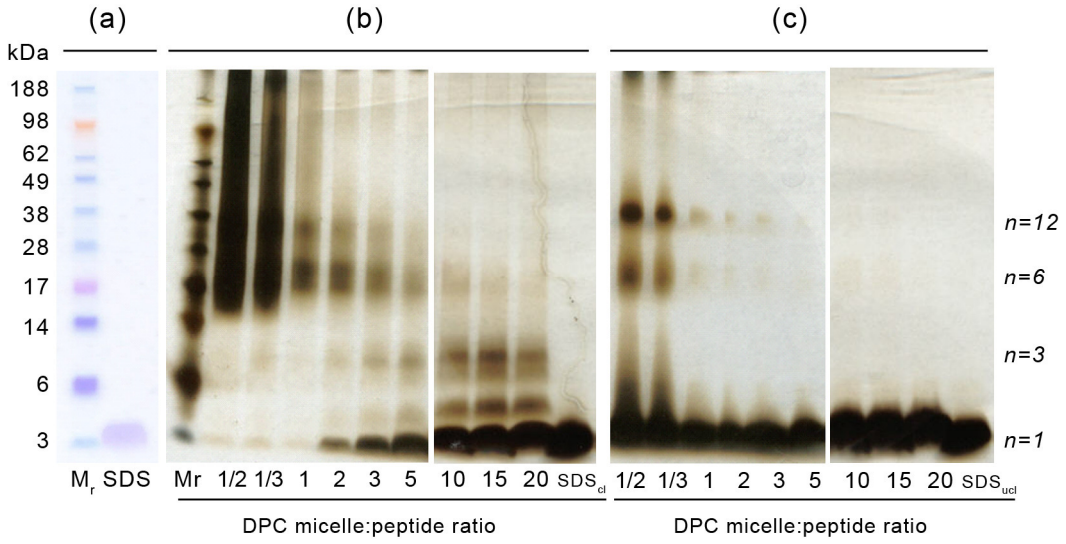

Figure 3.16 - SDS-PAGE analysis of chemically cross-linked rCPT1A TM2 peptide oligomerisation in DPC. (a) Molecular weight marker is shown in the first left-hand lane. Peptide dissolved in SDS and visualised by comassie staining. **(b)** BS^3-mediated cross-linking of peptides were dissolved in DPC micelles. Cross-linking reactions were carried out in DPC detergent micelles at various micelle to peptide concentration ratios as indicated below each lane. Protein bands were visualized by staining with silver nitrate. Oligomeric states (e.g. trimer indicated by n=3) are indicated at the far right of the gels. **(c)** rCPT1A TM2 peptide in the absence of a crosslinker.

Conversion of sedimentation coefficients to molecular mass yielded one peak at low peptide concentration, with a mass value of 16.3 kDa (hexamer), and two peaks at high peptide concentration, with mass values of 16.13 kDa and 30.85 kDa (corresponding to hexamer and dodecamer, respectively). When compared with the calculated molecular weights for the TM2 hexamer (16.1 kDa) and dodecamer (32.2 kDa), the experimental values agreed to within 4% of the theoretical values. This result agrees with the cross-linking results shown in **Figure 3.16** where, at M:P=1, only hexamers and dodecamers were present. At the lower concentration of peptide (M:P ratio ~ 4), the resulting sedimentation coefficient profile contained a single species centered at S=0.787, corresponding to a molecular mass for the TM2 peptide of 16.3 kDa, i.e. within 2% of the theoretical molecular weight of the hexamer (16.1 kDa). These data are in accordance with the results obtained after cross-linking at M:P ratios of 3 and 5. Within the range of these M:P ratios, the concentration of cross-linked dodecamer decreased significantly, while the hexamer remained detectable.

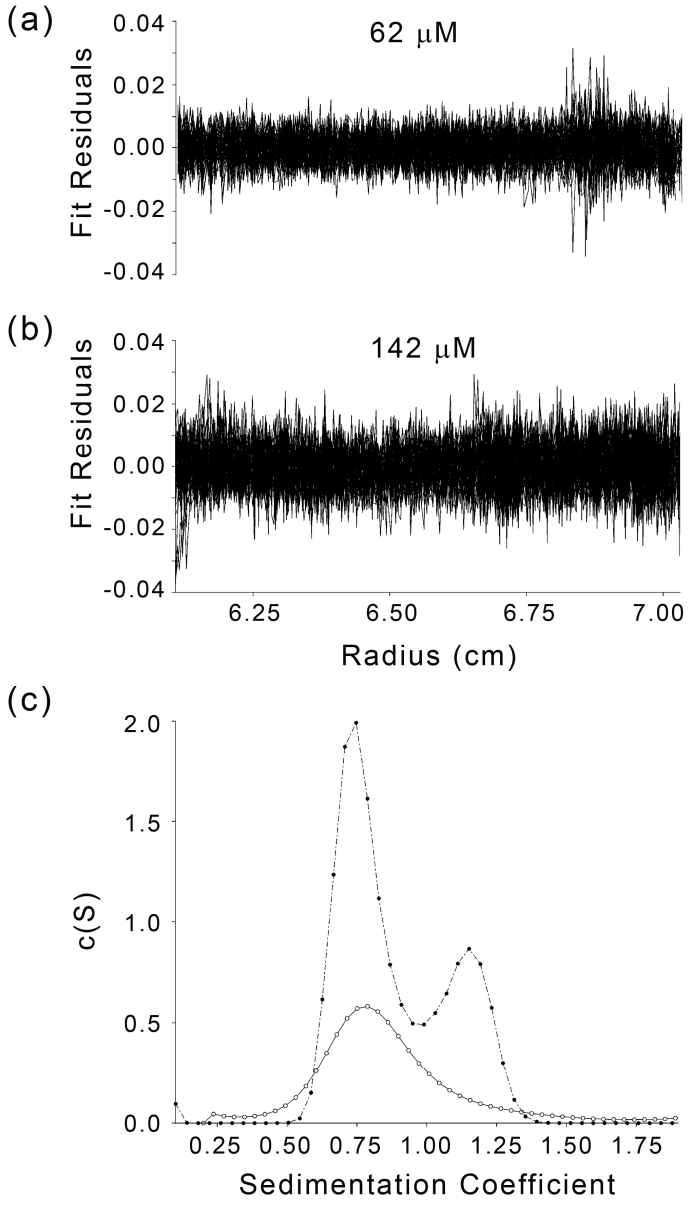

Figure 3.17 - Analytical ultracentrifugation analysis of rCPT1A TM2 derived peptide in DPC detergent solution. Sedimentation velocity data were obtained for TM2 peptide dissolved in buffer containing 15 mM DPC and 52.5% D_2O. Residuals of the fitting process for samples containing **(a)** 62 μM peptide and **(b)** 142 μM TM2 peptide. **(c)** Sedimentation coefficient distribution profiles for the peptide at concentrations of 62 μM (open circles) and 142 μM (closed circles) as calculated using the SEDFIT program.

Fitting of the data described above produced a frictional ratio of 1.88, suggesting a slightly elongated ellipsoidal shape for the hexamer as would be expected for a bundle of TM α-helices. Therefore, the SV data suggest that the TM2 peptide in DPC detergent solution exists as an equilibrium mixture of hexamers and dodecamers at the concentrations studied. The dodecamer species, which was

also detected in the cross-linking experiments, is present only at low M:P concentration ratios.

3.5 *In silico* models of rCPT1A TM oligomerisation

For further insight into the structural features of rCPT1A TM domains that may have a role in stabilising the observed oligomers, computational models were produced using the program 'CNS searching of helix interactions' (CHI), described in detail in § 2.6.4.

3.5.1 Modelling TM1 homo-oligomerisation

As previously discussed, the rCPT1A TM1 sequence contains several conserved motifs (**Figure 3.2**) that could support inter helical interactions. The helical wheel representation of the TM domain sequence (K_{47}-M_{73}) in **Figure 3.18 a-b** also indicates that GxxxG, Ser and Leu-Val-Ile motifs are present on the same helical interface.

Chemical cross-linking and AUC suggest that the 27 residue TM1 peptide primarily forms trimers in DPC and SDS micelles, while TOXCAT data also suggest that a shorter sequence of TM1, composed of only 16 amino acids, can also support strong self-association. Therefore, both the 27 (K_{47}-M_{73}) and 16 (T_{52}-V_{67}) TM1 residues were initially used to create dimer models in the program CHI to explore helix-helix interactions in the simplest possible model.

Full dimer searches were performed using the TM1 (K_{47}-M_{73}) sequence, and the results were clustered into 15 clusters with RMSD < 1.4 Å and a cluster size > 7, yielding two symmetric left-handed structures and one right-handed structure. In **Figure 3.18 c,** a model of a left-handed TM1 homo-dimer is shown where well-known helix interaction motifs pack at the helix-helix interface of the dimer. The G_{49} and G_{53} residues make up a GxxxG motif, bringing the top (N-termini) of the helices into close contact. The two Pro residues (P_{56} and P_{59}), known to disrupt the α-helical structure and form kinks (von Heijne, 1991; Nilsson *et al.*, 1998; Orzaez *et al.*, 2004), could explain the high β-sheet content of the TM1 peptide as indicated by the CD spectra (**Figure 3.10**). The Ser residues form interhelical hydrogen bonds (assigned in this case since the donor and acceptor were within 2.1 Å of one another) in the middle of the TM sequence. Finally, Leu_{63}-Val_{67}-Ile_{70} residues were also found to support the self association of the modelled TM1

helices by close packing at the bottom (C-termini) of the sequence. In addition, the CHI model of TM1 16 (T_{52}-V_{67}) proposed the possible role of an interhelical Ser hydrogen bond in the 16 residue chimera observed *in vivo* (see in § 3.3.2). As before, full dimer searches were performed using the TM1 (T_{52}-V_{67}) sequence, and the results were clustered into 18 clusters with RMSD < 1.2 Å and cluster size > 8, yielding two symmetric left-handed structures and one right-handed structure.

The 27 amino acid TM1 (K_{47}-M_{73}) sequence was also used to initiate a symmetrical trimer search to study the synthetic peptide oligomerisation behaviour observed using cross-linking and AUC (see in § 3.4.3) *in silico*. The symmetric trimer searches were performed using the TM1 (K_{47}-M_{73}) sequence, and the results were clustered into 6 clusters with RMSD < 1.5 Å and cluster size > 4, yielding two symmetric left-handed structures and four symmetric right-handed structures. The trimer model (cluster 1, left-handed, **Figure 3.18 e**), was selected because it contains well-known interaction motifs packing on the interface of the sequence. The structure suggests that the motifs packing against neighbouring helices are similar to those observed in the dimer model, promoting formation of a plausible left-handed helical bundle. In the trimer model, the Ser residues also form interhelical hydrogen bonds, in this case the donor and acceptor distances were within 2.2-4.1 Å of one another.

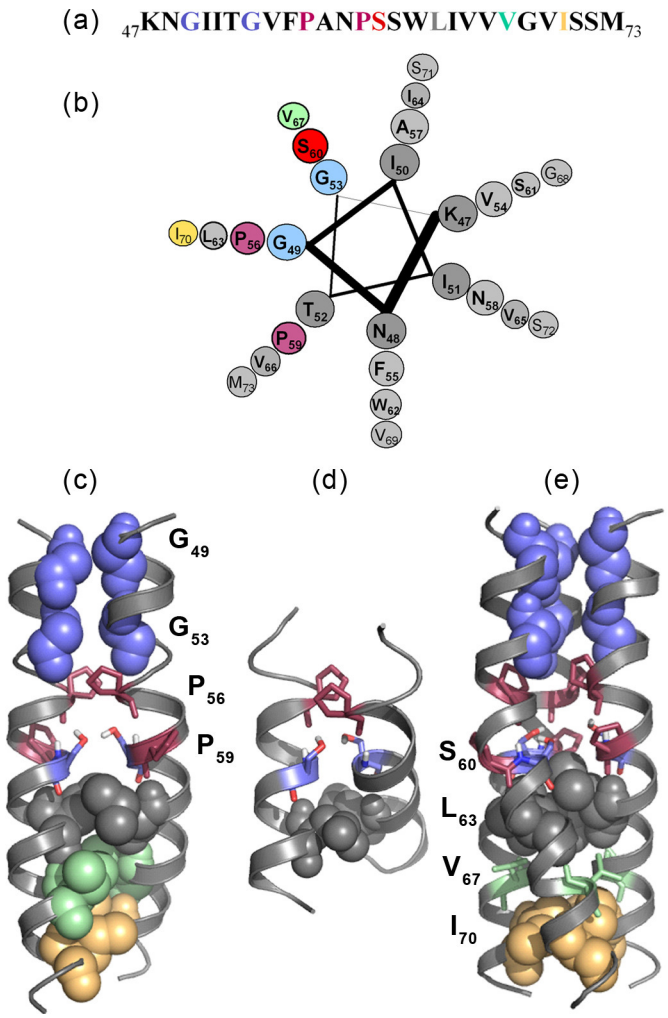

Figure 3.18 - Molecular models of rCPT1A TM1 oligomerisation.

(a) Amino acid sequence of rCPT1A TM1 domain (Lys_{47}-Met_{73}). **(b)** Helical wheel representation of the TM1 domain, where colour coded residues found on the same interface of the helix suggest well known helix interaction motifs. **(c)** CHI model of a 27 amino acid (K_{47}-M_{73}) left-handed, symmetrical dimer. **(d)** CHI model of 16 amino acid (T_{52}-V_{67}) left-handed, symmetrical dimer. **(e)** CHI model of the K_{47}-M_{73} trimer sequence (left-handed, symmetrical helical structure). In **(c)-(e)**, individual helices are represented as grey ribbon cartoons and residues are labelled as follows: G_{49} and G_{53}, highlighted as blue spheres, S_{60} as stick coloured by elements, L_{63} in grey, V_{67} in green, and I_{70} in yellow spheres.

3.5.2 Modelling TM2 homo-oligomerisation

CHI searches were performed on either three or six parallel α-helices containing the predicted sequence of TM2 to gain insight into the structural features that may have a role in stabilizing both the trimeric and hexameric forms of the synthetic peptide (see § 3.4.4). The trimer models suggest that the TM domain can form chemically plausible right- and left-handed coiled-coils. However, in the all of the trimer models obtained (**Figure 3.19**), the interaction interface contains

either a GxxxG motif (G_{107}, G_{111}) *or* a GxxxA motif (G_{113}, A_{117}), respectively. Both of these motifs are highly conserved in TM2 domains of the CPT1A isoform across all mammalian species (**Figure 3.2**), and are known to stabilize TM helix-helix interactions in several other membrane proteins (see § 3.2.1). The *in silico* models of the trimer of rCPT1A TM2 also suggest that this oligomer is capable of being stabilized by the interhelical hydrogen bonding of Thr_{112} (**Figure 3.19 c**). In the present analyses, hydrogen bonds were assigned whenever a hydrogen bond donor and acceptor were within 3 Å of one another.

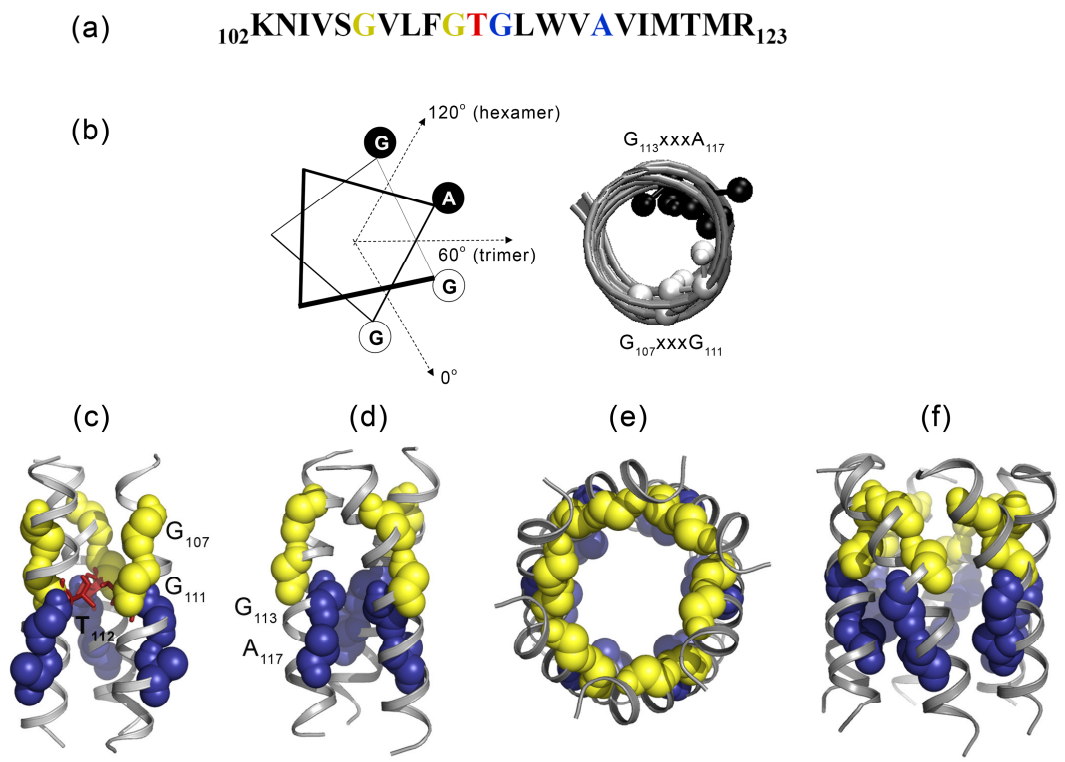

Figure 3.19 - Molecular models of rCPT1A TM2 trimers and hexamers.

(a) The amino acid sequence of rCPT1A TM2 (Lys_{102}-Arg_{123}) **(b)** Orientation of the GxxxG and GxxxA motifs relative to each other on a helical wheel (left panel) and in a canonical α-helix (built using CHI) containing residues K_{102}-R_{123} of TM2. Both models predict that the relative angle between the two motifs corresponds closely to the apex angles of a hexamer (120°). Also highlighted is the apex angle in a trimer (60°), which cannot accommodate both motifs. **(c)** Side view of a right-handed TM2 trimer, in which individual helices are represented as ribbons. In this model, the trimer is stabilized by packing of the GxxxG motifs (G_{107}, G_{111}, shown in yellow) against sidechains from an adjacent helix, as well as interhelical hydrogen bonding of Thr_{112} (shown in red, bond representation) at the centre of the bundle. **(d)** Model of a left-handed trimer in which the GxxxA motif (G_{113}, A_{117}, shown in dark blue) packs against the adjacent helix; while the GxxxG motif is predicted to be on the outside of the bundle. **(e)** Top-down view of the left-handed TM2 hexamer. **(f)** Side view of the left-handed TM2 hexamer, showing the simultaneous packing of both the GxxxG (yellow) and GxxxA (dark blue) motifs against adjacent TM helices. The hexamer is the only observed oligomeric state for which it is predicted that both of these oligomer-favouring TM-domain motifs are used to stabilise the quaternary structure of the peptide.

The modelling of the TM2 hexamer (**Figure 3.19 e-f**) suggests that TM2 can form a plausible left-handed helical bundle (no right-handed solutions were found) in which both the GxxxG and the GxxxA motifs pack against neighbouring helices. In this way, the stabilizing effects of both motifs can be exploited simultaneously through interactions with adjacent helices. This is possible only in a hexameric arrangement, which has apex angles of 120° - the predicted angle between the two motifs ($G_{107}xxxG_{111}$ and $G_{113}xxxA_{117}$) in the α-helical model of TM2 (depicted in **Figure 3.19 b**). Such simultaneous packing of the two motifs is not possible in the trimer, as the angle between the two motifs is such that they can never both pack at once (apex angles = 60^{o}), resulting in exclusion of one motif from interfacial interactions with the other two helices.

3.6 Summary

The lack of a detailed crystal structure for CPT1A proteins and the unknown role of the TM domains in the observed kinetic characteristics and protein complex formation has meant that this system provides an interesting problem to study. Therefore, within this project one of the main aims was to characterise and quantify the oligomerisation propensities of TM1 and TM2 in isolation. Using the TOXCAT and GALLEX biological assays, we have explored their oligomerisation *in vivo* (§ 3.3). Furthermore *in vitro* biophysical analyses (§ 3.4) performed on TM synthetic peptides corresponding to TM1 and TM2 not only quantified the order of oligomerisation, but also indicated the possible correspondence between the oligomerisation behaviour of rCPT1A *in vivo (Faye et al., 2007)*. Finally, *in silico* modelling of TM segments highlighted the GxxxG motif (and variants) and other well-known interaction motifs may be important in stabilizing the observed oligomers of CPT1A TM domains as shown in **Figure 3.2**, **Figure 3.18** and **Figure 3.19** (§ 3.5).

By studying different lengths of rCPT1A TM domain sequences, we further validate the previously observed behaviour of the TOXCAT and GALLEX assays, in which the association of chimeras could depend on the length of the TM sequence. The results of the quantitative CAT assays with the shorter length of ToxR-rCPT1A TM-MBP or *wt*LexA-rCPT1A TM-MBP chimeras strongly indicates that the length of the TM spanning region needs to be optimised when using these assays. Changes in CAT and β-galactosidase activities, measured for

rCPT1A TM chimeras suggest significant homo-oligomerisation of both rCPT1A TM1 and TM2 domains.

For the first time this work quantified the homo-oligomerisation of both rCPT1A TM domains. The synthetic peptide of TM1 was found to form trimer species in DPC micelles when cross-linked and hexamers (possibly dimer of trimers) when analyzed by AUC-SV. When the TM2 peptide was dissolved in DPC micelles and cross-linked with BS^3, oligomers corresponding to the hexamer were observed, suggesting that the TM2 sequence has inherent primary and secondary structural properties that favour hexamerisation. These results were supported by the AUC-SV experiments, when the TM2 peptide was found to sediment according to the size of the hexamer in the absence of cross-linker. The fact that the hexamer also appears to be a favoured oligomeric state *in vivo* (Faye *et al.*, 2007), suggests that these interactions are also important in the context of the full-length protein when this is stabilised within a lipid bilayer. This finding points to an interesting correlation between the oligomerisation behaviour of rCPT1A TM2 and that of the full-length protein and further, possibly supporting the hypothesis that rCPT1A oligomerisation may be initiated and/or regulated by its TM domain. The molecular modelling results also support the trimer and hexamer formation of TM2 and suggest the GxxxG(A) motifs role in developing these oligomeric structures.

Although the observed homo-oligomerisation described above suggests the possibility of a potential role of both rCPT1A TM domains in assembly of the full-length protein, the results obtained for TM2 were most consistent between the various techniques used. This consistency provided a strong foundation to further study the sequence dependent oligomerisation CPT1A TM2, as presented in the following CHAPTER 4.

Finally, it is important to note the reason for discrepancy between data presented in this chapter and in (Jenei *et al.*, 2009) about rCPT1A TM1 oligomerisation (paper attached at the end of this thesis). The chimeras of 18 and 16 residues long TM1 peptides were re-cloned and re-measured in TOXCAT assay after further CPT1A TM1 peptide studies raised the possibility of oligomerisation. Also, when the homo-oligomerisation of TM1 was measured using the GALLEX assay, the results also indicated the ability of TM1 oligomerisation.

CHAPTER 4

THE ROLE OF SEQUENCE MOTIFS IN CPT1A TM2 OLIGOMERISATION

Here the implications of mutagenesis strategies coupled with *in vivo* and *in vitro* biophysical methods are discussed on investigating sequence-dependent homo-oligomerisation of rCPT1A TM2. The results suggest a key role of GxxxG(A) motifs in stabilizing TM2 hexamers.

4.1 Introduction

Carnitine palmitoyltransferase 1A (CPT1A) is the key regulatory enzyme of fatty acid metabolism, since it catalyses the conversion of long chain acyl-CoA to acylcarnitine, and transports acyl-CoA from the cytosol into the mitochondrial matrix (§ 1.3.1, **Figure 1.6**). Its sensitivity to its inhibitor, malonyl-CoA, is modulated by intramolecular interactions, which depend on the properties of the mitochondrial outer membrane, such as fluidity (Kolodziej and Zammit, 1990) and lipid composition when altered by dietary lipids, fasting, and diabetes (Zammit *et al.*, 1998). The modulation of CPT1A sensitivity to malonyl-CoA is crucial in the hepatic response to dietary fat intake, obesity, fasting and diabetes (Zammit, 1999), and implies that CPT1A has a high degree of molecular plasticity (adopts a "flexible" structure). From these observations, it has been proposed that membrane-sensitive TM-TM interactions are central to CPT1A function.

Furthermore, a recent study suggests that the TM-domains, and specifically TM2, also drive the oligomerisation of CPT1A (Faye *et al.*, 2007). Thus, it was shown that full-length rCPT1A forms oligomeric complexes and the fundamental oligomeric unit was suggested to be a trimer, which associates into a dimer of trimers to yield hexamers. The protein-protein interactions that stabilize these complexes were narrowed down to a 51 amino acid stretch of CPT1A (residues 97-147) that includes TM2. When expressed as a fusion protein with dihydrofolate reductase (DHFR), this region induced the formation of hexamers (Faye *et al.*, 2007).

As discussed in CHAPTER 3, the formation of trimers and hexamers by rCPT1A was further traced to a group of 22 residues thought to comprise TM2 (Lys_{102}-Arg_{123}), which also form stable trimers and hexamers when studied *in vivo* and i*n vitro* (Jenei *et al.*, 2009). In this same study, molecular modelling results suggested that interaction of GxxxG(A) sequence motifs (see in § 3.5.2), might play a role in stabilizing hexamer and trimer formation. TM2 contains two such motifs (Gly_{107}xxxGly_{111} and Gly_{113}xxxAla_{117}), which are highly conserved among species (see in § 3.2.1, **Figure 3.2**). Molecular models also suggested that the polar Thr_{112}, located in the transmembrane domain, may also play a role in stabilizing rCPT1A TM2 homo-trimers by interhelical hydrogen bonding. Motifs containing Thr residues have been discussed previously in (§ 1.2.2). These observations point toward an important role for the TM2 domain in the oligomeric assembly of rCPT1A, and raise the question of whether there is any sequence specificity in TM2 oligomer formation.

Hence, the aim of the work presented in the current chapter is to examine the role of GxxxG(A) motifs and a Thr residue in the oligomerisation of rCPT1A TM2 using mutagenesis strategies coupled with *in vivo* and *in vitro* biophysical methods. In order to investigate sequence-dependent self-association, we designed single and double mutants of the conserved GxxxG and GxxxA motifs, as well as of the Thr_{112} residue, and measured TM helix-helix interactions using the TOXCAT assay. These data were compared to TOXCAT data collected previously for the wild-type rCPT1A TM2 domain. Synthetic peptides corresponding to highly disruptive single ($G_{107}I$) and double ($G_{107}IG_{113}I$) point mutants were also studied, and confirmed the key role of GxxxG(A) motifs in stabilizing TM2 hexamers.

4.2 Sequence specific self-association in vivo

In order to experimentally validate our previously reported model (obtained from molecular dynamics simulations) predicting that GxxxG and GxxxA motifs work together to stabilize the rCPT1A TM2 hexamer, systematic mutation of these motifs was carried out. The self-association of point mutant TM domains was measured using the TOXCAT assay, described in detail in § 2.2. Single and double point mutations of Gly or Ala to Ile were introduced in place of Gly_{107}, Gly_{111}, Gly_{113} and Ala_{117} within the rCPT1A TM2 sequence (as detailed in § 2.1.3.4). The resulting CAT activity for each mutant is shown in **Figure 4.1**, alongside the value obtained for the 16 amino acid sequence of wild-type rCPT1A TM2 (*wt* TM2).

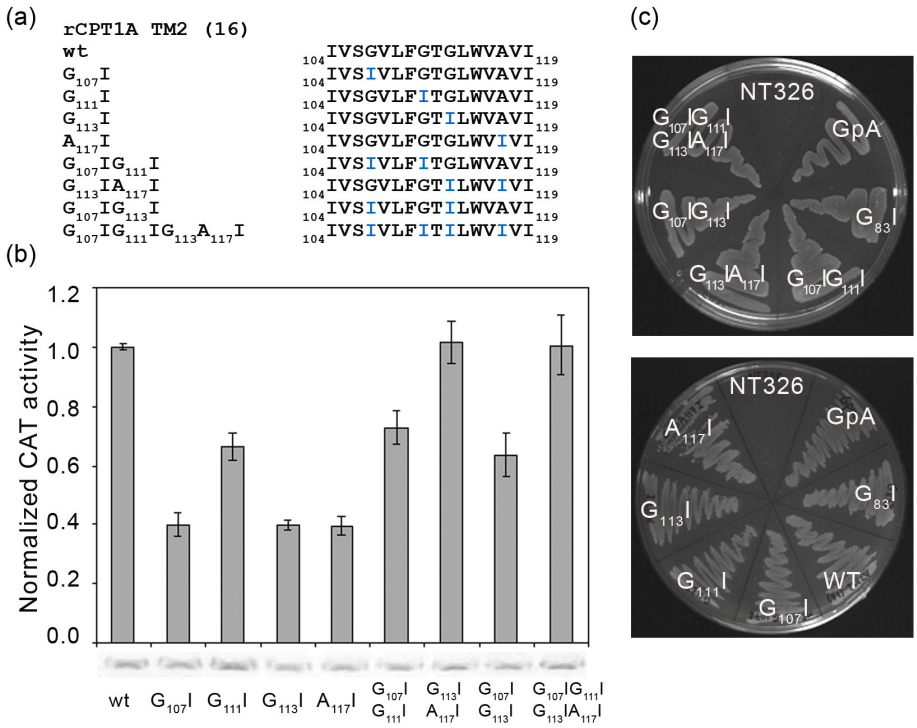

Figure 4.1 - Oligomerisation of rCPT1A TM2 (16 amino acids in length) and various GxxxG(A) mutants in TOXCAT chimeras in *E. coli* membranes. (a) Sequences of wt and point mutants rCPT1A TM2 analyzed using the TOXCAT assay. **(b)** CAT activities obtained in TOXCAT relative to wt rCPT1A TM2. Values are means (+/- standard deviation) for three or more independent measurements. **(c)** *malE* complementation to test the wild type and mutant ToxR-TM2-MBP chimera's correct insertion and orientation.

Here the positive (GpA) and negative ($G_{83}I$) controls are absent in order to compare the self-association of the various mutants more directly with that observed for *wt* TM2 (which were previously compared to these controls in § 3.3.2, **Figure 3.6**).

All of the single point mutants showed a marked decrease in self-association (as indicated by CAT activity) from wild-type levels. These single point mutants were found to have the most destabilizing effect on rCPT1A TM2 oligomerisation, with the $G_{107}I$, $G_{113}I$ and $A_{117}I$ mutants producing an approximately 60% reduction in CAT activity relative to the wild-type sequence. Surprisingly, the double mutants ($G_{107}IG_{111}I$ and $G_{107}IG_{113}I$) had a less significant effect on homo-oligomerisation, producing at most a ~20-30% reduction in CAT relative to the wild-type levels (**Figure 4.1**). This at first seems counter-intuitive, however previous experimental and computational results suggest that TM2 trimers may be stabilised by a single GxxxG(A) motif, whereas hexamers may require both motifs (§ 3.5.2) (Jenei *et al.*, 2009). Therefore, one explanation may be that the single mutants tested here may represent destabilized hexamers while the $G_{107}I$ $G_{111}I$ and $G_{113}I$ $A_{117}I$ mutants may form stable trimers which interact *via* the remaining unmutated GxxxG or GxxxA motifs (for visual clarification see **Figure 4.13**).

In addition, the complete substitution of all four residues in the GxxxG(A) motifs with Ile was also carried out, to create the $G_{107}I$ $G_{111}I$ $G_{113}I$ $A_{117}I$ (4xI) mutant. Surprisingly, this mutant produces CAT activities similar to that obtained for wild-type rCPT1A TM2. It is important to note that creation of the 4×I mutant resulted in a TM domain sequence where over 50% of the residues are Ile, Leu, or Val, residues that can stabilize helix-helix interactions by packing in a “leucine zipper” or heptad repeat motif (Gurezka *et al.*, 1999). Specifically, a potential heptad motif is created in the sequence by residues IxxIxxxIxILxxIxI, placing Ile and Leu residues at the *a* and *d* positions of the heptad motif (see in § 1.2.2). Because we have created this motif by extensive mutation of the sequence, the resulting CAT activities are difficult to interpret in comparison with *wt* TM2 interaction.

We also could not rule out the possibility that, as well as changes in oligomeric state (which are undetectable in TOXCAT), other motifs may also participate in helix-helix interactions. One residue of interest in TM2 was Thr_{112}, especially in the interpretation of the $G_{107}I$ $G_{113}I$ mutant where both GxxxG(A) motifs were disturbed, yet significant self-association was observed. To test whether the Thr

residue could stabilise TM2 self-association through formation of interhelical H-bonds, further TOXCAT experiments were carried out.

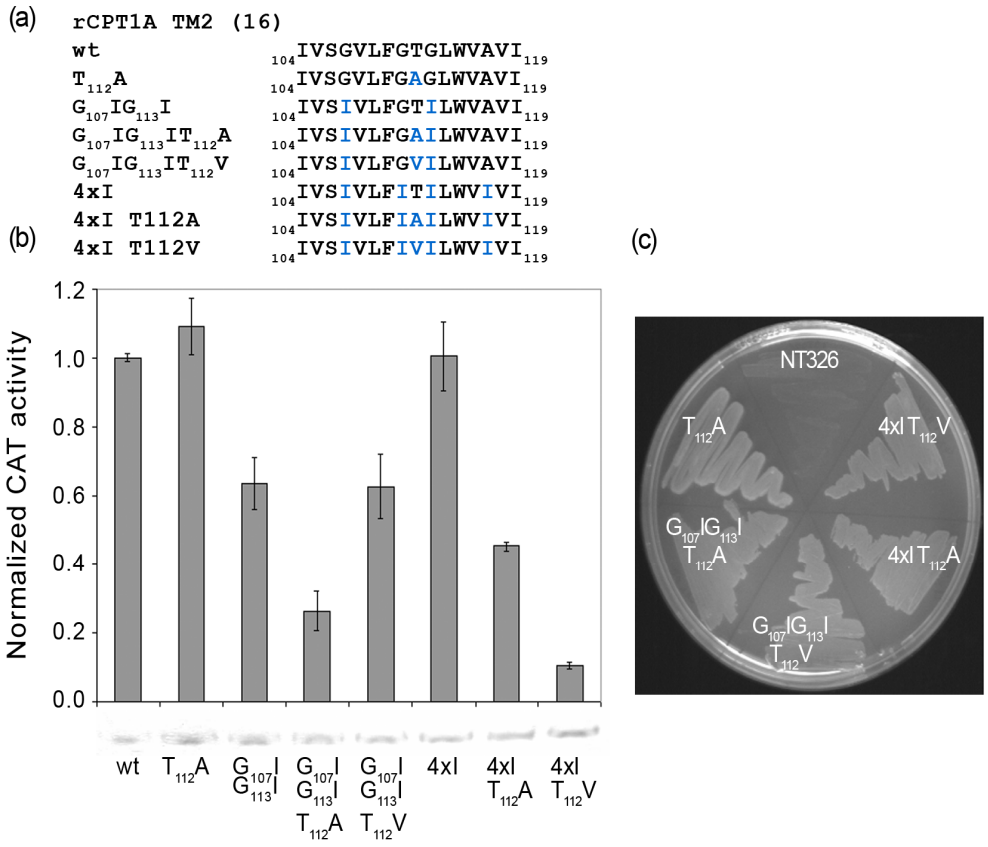

Figure 4.2 - Oligomerisation of rCPT1A TM2 (16 amino acids in length) and its GxxxG(A)-Thr mutants using the TOXCAT assay in *E. coli* membranes. (a) Sequences of wt and point mutants of rCPT1A TM2 analyzed in TOXCAT assay. **(b)** CAT activities obtained in TOXCAT relative to wt rCPT1A TM2. Values are means (+/- standard deviation) for three or more independent measurements. **(c)** *malE* complementation to test the wild type and mutant ToxR-TM2-MBP chimera's correct insertion and orientation.

To study the possible role of Thr in rCPT1A TM2 oligomerisation, Thr_{112} was mutated to Ala in the wild-type TM2 domain ($T_{112}A$) and self-association was again measured using the TOXCAT assay. The resulting CAT activity of this mutant is shown in **Figure 4.2**, and demonstrates that this residue on its own does not have a large effect on oligomerisation when both GxxxG(A) motifs are intact. However, when both GxxxG(A) motifs are disrupted, as they are in the $G_{107}IG_{113}I$ mutant, further mutation of Thr to Ala (to create the $G_{107}I$ $G_{113}I$ $T_{112}A$ mutant) results in a considerable decrease in self-association to ~30% of wild-

type levels. This suggests that, in the context of the $G_{107}IG_{113}I$ mutant sequence, Thr now contributes considerably to self-association. However, this contribution is unlikely to be entirely due to H-bond formation as replacing T_{112} with Val ($G_{107}I$ $G_{113}I$ $T_{112}V$, (**Figure 4.2**)) restores some CAT activity relative to the $G_{107}I$ $G_{113}I$ $T_{112}A$ mutant.

As discussed above, with the 4xI sequence mutation heptad repeat motif was created. The observed homo-oligomerisation of this sequence can also be stabilised by H-bond formation of the Thr_{112} residue. The data given in **Figure 4.2** also summarises mutagenesis strategies designed to test the effect of Thr_{112} mutation in the 4xI sequence. It is again important to see that mutation of 5 residues in a 16 amino acid sequence resulted a 31% different sequence and the CAT activities are difficult to interpret in comparison with *wt* TM2 interaction. However, it is interesting to note when 4xI was mutated jointly with Thr_{112}, the $4xIT_{112}A$, $4xIT_{112}V$ mutants yielded signals 90% smaller than *wt* TM2 or 4xI.

From the TOXCAT data presented in **Figure 4.1** and **Figure 4.2**, we can see that mutation of the GxxxG and GxxxA motifs in rCPT1A TM2 can result in a reduced self-association of this sequence. Furthermore, in certain sequence contexts (but not independently), mutation of Thr_{112} can also destabilise helix-helix interactions, suggesting this residue may also play a role in TM2 oligomer formation. These results are complicated by the fact that the TOXCAT assay cannot report on changes in oligomeric state, and an understanding of the oligomeric state is critical to elucidation of the role of key motifs. For this reason, further research was focused on the GxxxG(A) motifs role in wt TM2 oligomerisation by selecting mutants that not only have a minimal change in the sequence while yielding large effects on self-association in the TOXCAT assay, but also can be employed to systematically study the effect of both GxxxG and GxxxA motifs on oligomerisation. Therefore, the $G_{107}I$ and $G_{107}IG_{113}I$ mutants were further studied *in vitro* in order to quantitatively determine their oligomeric state.

4.3 GxxxG(A) driven oligomerisation of rCPT1A TM2

The *in vivo* oligomerisation study suggested that mutation of conserved GxxxG(A) motifs destabilises homo-oligomerisation of the second transmembrane domain in rCPT1A. In light of this result, synthetic peptides were used to more directly examine the possible differences in oligomerisation caused by mutation of these motifs. As described in CHAPTER 3, the oligomerisation of

the purified mutant peptides was studied by cross-linking and AUC. Molecular modelling was also used to help interpret the oligomerisation behaviour.

4.3.1 Purification of mutant peptides

The crude peptides were purified by RP-HPLC using a linear acetonitrile gradient with 0.1% trifluoroacetic acid as detailed in § 2.4. The HPLC fractions were analysed for the presence of pure peptide using ESI-MS, and fractions containing the pure peptide of interest were pooled for further analysis. The major species detected by ESI-MS are shown in **Figure 4.3** and **Figure 4.4**. In **Figure 4.3**, the major peak corresponded to pure G_{107}I peptide (2745 Da), with an additional peak corresponding to sodium adducts (2790 Da). The $G_{107}IG_{113}$I peptide was detected at 2802 Da, with an additional peak corresponding to sodium adducts (2847 Da) as shown in **Figure 4.4**. Sodium adducts have previously been observed in the purification of TM peptides (Rijkers *et al.*, 2005). The minor peak at ~2700 Da in this spectrum is likely a truncated peptide that co-purified with the major product.

4.3.2 Secondary structure of mutant peptides

To determine the secondary structure of the G_{107}I and $G_{107}IG_{113}$I peptides in detergent micelles, CD spectra were collected. The spectra were recorded for peptides solubilised in buffer containing SDS (at a M:P ratio of 3:1) and DPC detergent at different M:P ratios ranging from 2:1 to 20:1 (for details see § 2.5.3). Fitting of the data between 190 nm and 260 nm using the CDSSTR software (Johnson, 1999) indicates that the G_{107}I peptide is predominantly α-helical in DPC at a 20:1 M:P ratio and in SDS at a 3:1 ratio. Similar to the previously discussed peptides (§ 3.4.2), here the α-helical content of the peptide also depends on the micelle to peptide ratio. In the samples with M:P=2:1, 4:1 and 10:1, aggregation of the hydrophobic peptide decreases the α-helical content. This is especially true in samples with M:P=2:1 and 4:1, where the β-sheet content is higher than in any other sample.

Table 4.1 - The amino acid sequences of rCPT1A TM2 G_{107} and $G_{107}G_{113}$ synthetic peptides used in this study. Non-native lysine residues are shown in bold.

TM domain of interest	Synthetic peptide sequence	Molecular weight (Da)
rCPT1A TM2 G_{107}I	$COCH_3$-**K**KNIVSIVLFGTGLWVAVIMTMR**K**-$CONH_2$	2745
rCPT1A TM2 $G_{107}G_{113}$I	$COCH_3$-**K**KNIVSIVLFGTILWVAVIMTMR**K**-$CONH_2$	2804

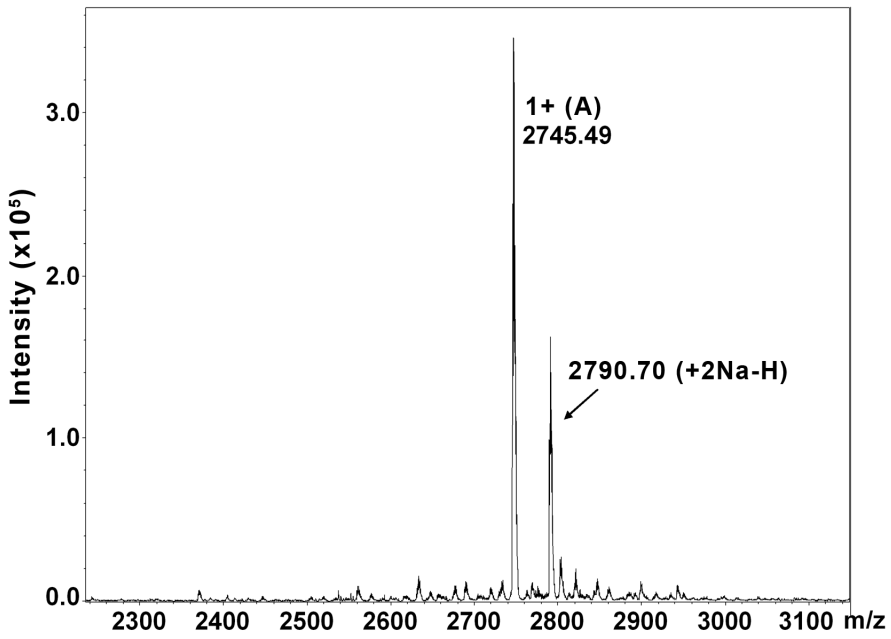

Figure 4.3 - Analysis of purified rCPT1A TM2 $G_{107}I$ peptide by electrospray ionisation mass spectrometry (ESI-MS). The HPLC fractions containing the pure peptide were pooled and analyzed using ESI-MS (Bruker MicroTOF). In the deconvoluted spectrum, the major peak corresponds to the rCPT1A TM2 $G_{107}I$ peptide (2745 Da), and additional peaks correspond to sodium and solvent adducts.

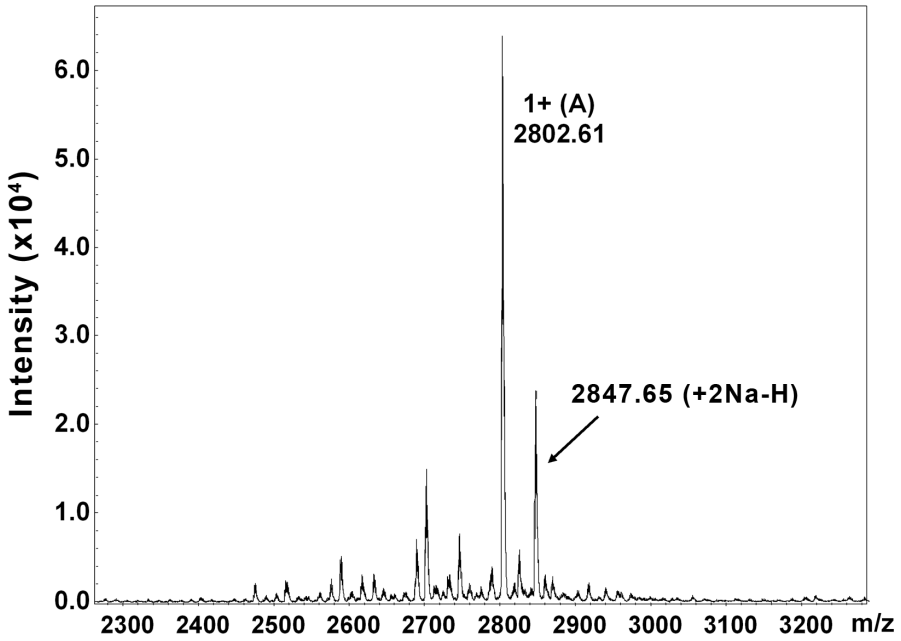

Figure 4.4 - Analysis of purified rCPT1A TM2 $G_{107}IG_{113}I$ peptide by electrospray ionisation mass spectrometry (ESI-MS). The HPLC fractions containing the pure peptide were pooled and analyzed using ESI-MS (Bruker MicroTOF). In the deconvoluted spectrum, the major peak corresponds to the rCPT1A TM2 $G_{107}I$ $G_{113}I$ peptide (2802 Da), and additional peaks correspond to sodium and solvent adducts.

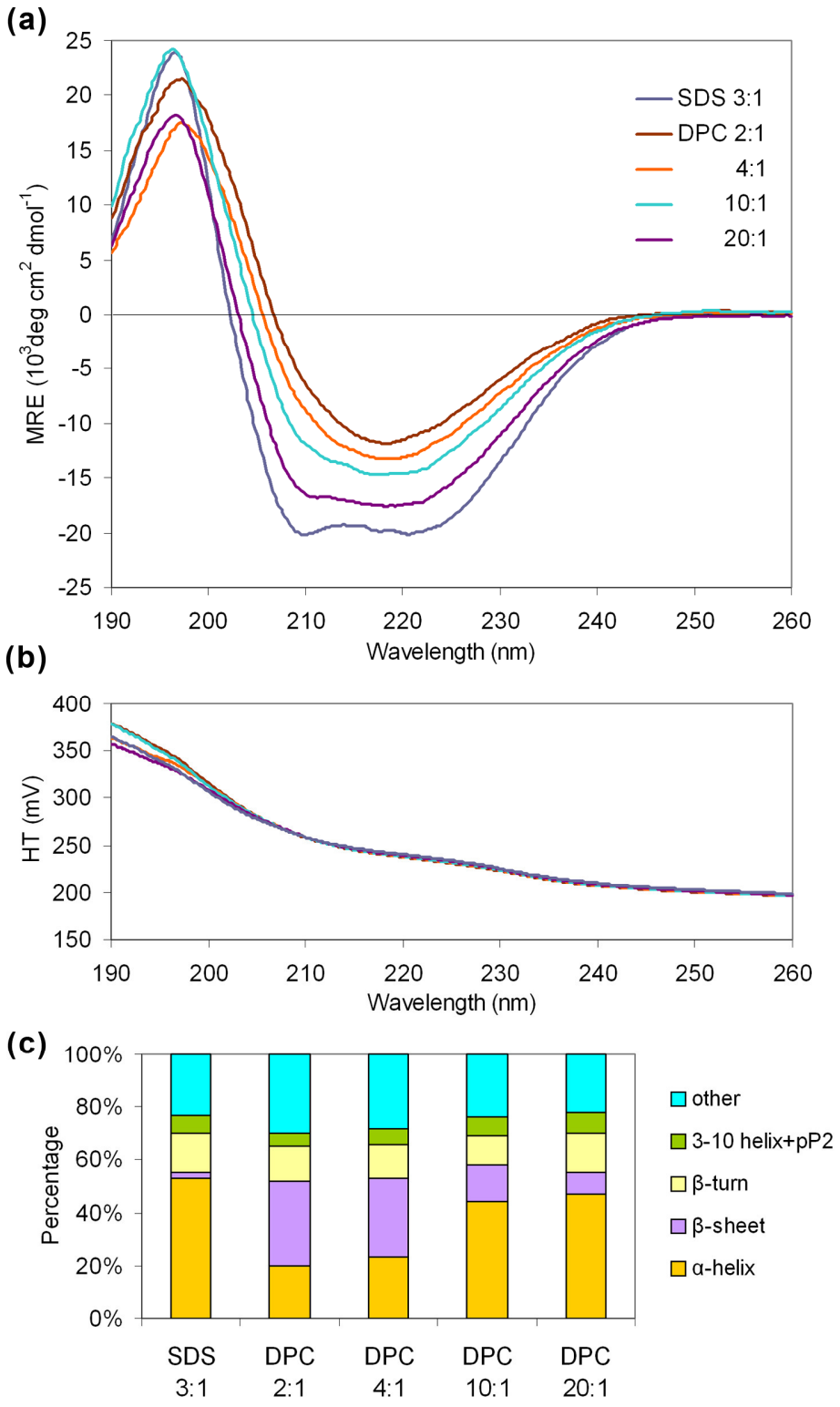

Figure 4.5 - The effect of DPC micelle concentration on the secondary structure of the rCPT1A TM2 G_{107}I peptide. (a) CD spectra measured at different detergent micelle to peptide ratios, plotted in units of mean residue ellipticity (MRE). **(b)** High tension (HT) over the wavelength region specified in (a). **(c)** The secondary structure composition of the rCPT1A TM2 G_{107}I peptide estimated from the CD spectra shown in (a) using the CDSSTR software (Johnson, 1999).

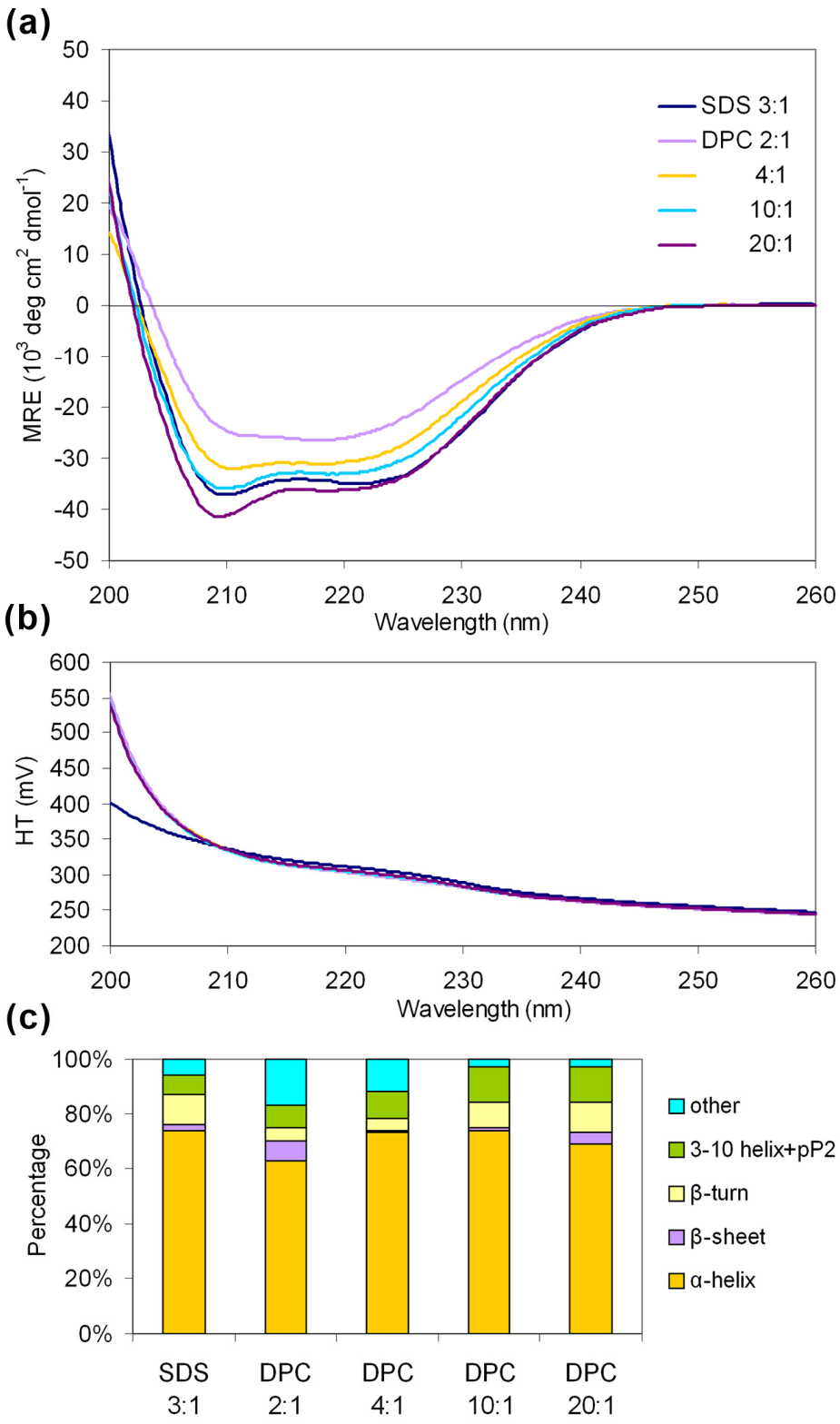

Figure 4.6 - The effect of DPC micelle concentration on the secondary structure of the rCPT1A TM2 G107IG113I peptide. (a) CD spectra measured at different detergent micelle to peptide ratios, plotted in units of mean residue ellipticity (MRE). **(b)** High tension (HT) over the wavelength region specified in (a). **(c)** The secondary structure composition of the rCPT1A TM2 G_{107}I G_{113}I peptide estimated from the CD spectra shown in (a) using the CDSSTR software (Johnson, 1999).

The CD spectra of the $G_{107}IG_{113}I$ peptide at all concentrations of DPC displayed the negative minima at 208 and 222 nm characteristic of an α-helical secondary structure. These features can be seen in the spectrum collected in SDS. The data indicate that the peptide does have a largely α-helical secondary structure in DPC detergent micelles. Additionally, the signal was not very accurate below 195 nm due to light scattering of the sample, therefore data were fit between 200 and 240 nm to calculate secondary structure content.

4.3.3 Oligomeric state of $G_{107}I$ mutant peptide

To compare the oligomeric states achieved by the $G_{107}I$ and $G_{107}IG_{113}I$ mutant peptides to that of the wild-type TM2 peptide, chemical cross-linking was initially used. Similar to our previous experiments (§ 3.4.4), the mutant peptides were dissolved in different concentrations of DPC micelles and subsequently cross-linked with the amine-reactive cross-linker, BS^3. The different oligomeric species were detected on SDS-PAGE and visualized by staining with silver nitrate.

Cross-linking of the $G_{107}I$ peptide resulted in one main band migrating at approximately the molecular mass of the trimeric species (MW ~8.23 kDa; between the 6-14 kDa molecular weight markers). In addition, at low detergent concentrations a second band was observed migrating at the approximate molecular mass of the pentamer/hexamer (~13.73 kDa; between molecular marker 14-17 kDa). Increasing the M:P ratio did not destabilize the trimer, but it destabilized the formation of higher oligomeric species, while the concentration of monomeric species was only increased slightly (**Figure 4.7 a**). The above oligomerisation pattern is also in agreement with the $G_{107}I$ peptide secondary structure composition. In the light of the secondary structure calculated from CD spectra (**Figure 4.5**), lanes of M:P>5 contain more helical peptide, while lanes where M:P<10 the peptide also form β-sheet (aggregation typically at M:P=1/3-2). As shown in **Figure 4.7 b**, the un-cross-linked peptide samples at all micelle concentrations migrate mainly as monomers. In addition, a weak band at the approximate molecular weight of the pentamer species was also detected at low detergent concentrations (M:P=1/3-5).

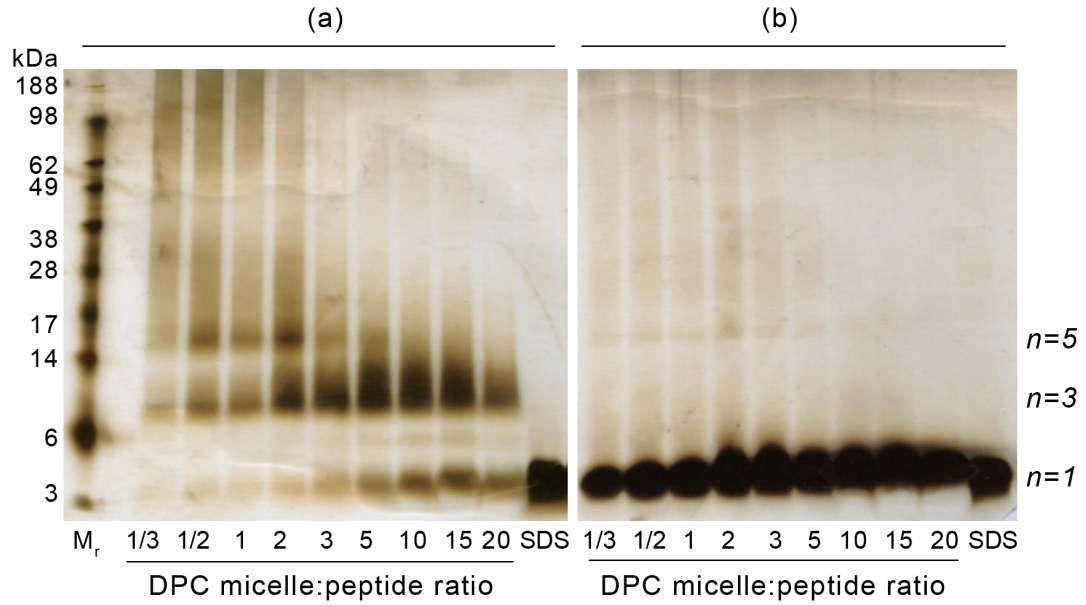

Figure 4.7 - SDS-PAGE analyses of chemically cross-linked rCPT1A TM2 $G_{107}I$ peptide oligomers. (a) The molecular weight marker is shown in the left-hand lane. The BS^3-mediated cross-linking of peptides dissolved in DPC micelles. Cross-linking reactions were carried out in DPC (or SDS, last lane M:P=4) detergent micelles at various M:P concentration ratios as indicated below each lane. **(b)** rCPT1A TM2 $G_{107}I$ peptide in the absence of crosslinker migrates mainly as monomer. In figure, protein bands were visualized by staining with silver nitrate. Oligomeric states (e.g. trimer indicated by n=3) are indicated at the far right of the gels.

To test the reproducibility of the above cross-linking experiment, and also to directly compare the oligomerisation of the single point mutant $G_{107}I$ peptide to the *wt* rCPT1A TM2 peptide, the cross-linked peptides were analysed on the same gel. The difference between the oligomeric species formed by the *wt* and $G_{107}I$ peptides at different DPC concentrations is clearly visible using SDS-PAGE (**Figure 4.8)**. As previously discussed in § 3.4.4, *wt* rCPT1A TM2 forms predominantly hexamers and here the $G_{107}I$ peptide was observed to form predominantly trimeric species.

This finding suggests that disrupting the first GxxxG motif results in destabilisation of the hexamer to form mostly trimers, but also a small proportion of pentamers. This result is in good agreement with our previously discussed model (§ 3.5.2), proposing that rCPT1A TM2 trimers could be stabilized by a single GxxxG(A) motif.

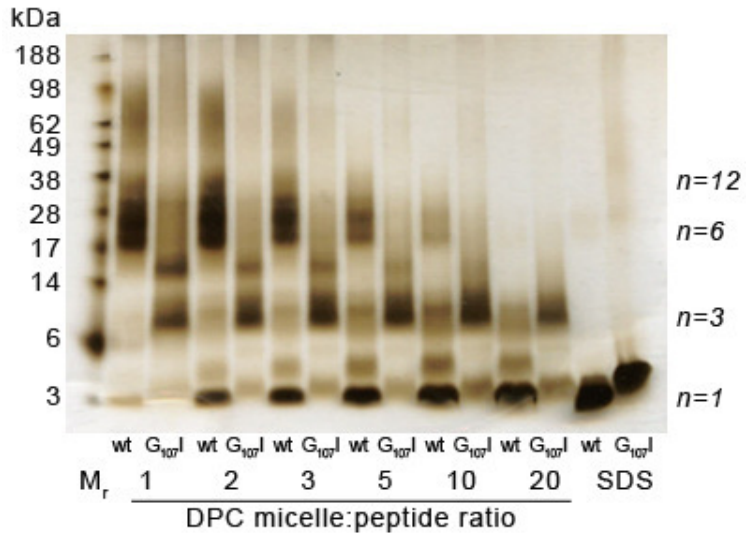

Figure 4.8 - SDS-PAGE visualisation of the cross-linked wt rCPT1A TM2 peptide side-by-side with the cross-linked $G_{107}I$ mutant peptide. A clear difference in the oligomerisation pattern is observed.

To further study the oligomeric species formed by the $G_{107}I$ peptide, AUC experiments were carried out. AUC-SV data were collected at two different peptide concentrations, 49 and 98 μM (M:P ratio ~ 5 and 2.5), at 55,000 rpm and 20°C (University of Oxford). Sedimentation profiles were fit using SEDFIT (Schuck, 2000) and the resulting sedimentation coefficient profile and fitting residuals are shown in **Figure 4.9**. Two species were detected in the fit data, with the major peak centered at S=0.46 and a minor peak centered at S=0.8. Conversion of the sedimentation coefficient to molecular mass, the peak at S=0.46 corresponds to a rCPT1A TM2 $G_{107}I$ peptide species with a molecular mass of 11.25 kDa (98 μM sample) and 9.8 kDa (49 μM sample), which most closely corresponds to tetramers. The calculated mass of a $G_{107}I$ tetramer is 10.98 kDa, agreeing within 2.4% (98 μM) and 11% (49 μM) of the theoretical values. The minor peak at S=0.8 for both concentrations corresponds to octamer species with a molecular mass of ~ 22 kDa (probably dimer of tetramers).

While from our cross-linking experiments we conclude the peptide forms mostly trimers, here we detected predominantly tetramer species during sedimentation of the sample. The discrepancy could be the result of the speed of the AUC-SV experiment, which resulted in error in the data analysis where smaller molecular species (monomer, trimer, pentamer) were not resolved.

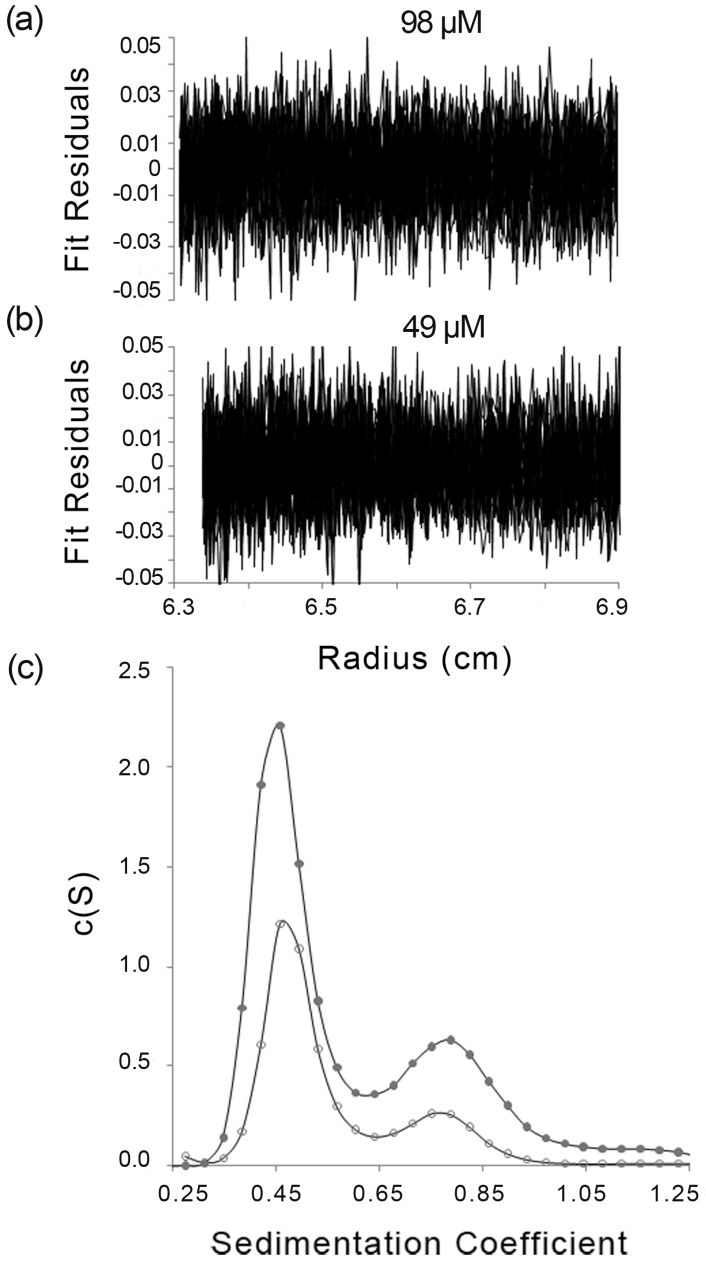

Figure 4.9 - Analytical ultracentrifugation analysis of rCPT1A TM2 $G_{107}I$ synthetic peptide in DPC detergent solution. Sedimentation velocity data were obtained for TM2 $G_{107}I$ peptide dissolved in buffer containing 15 mM DPC and 52.5% D_2O. **(a)** Residuals of the fitting process for samples containing 49 and **(b)** 98 µM peptide. **(c)** Sedimentation coefficient distribution profiles for the peptide concentrations of 49 µM (open circles) and 98 µM (closed circles) as calculated using the SEDFIT program.

Taken together, both cross-linking and AUC experiments suggest the rCPT1A TM2 $G_{107}I$ peptide forms lower molecular weight oligomeric species than the wild-type peptide in DPC micelles, and strongly support the possible role of the N-terminal GxxxG motif in the previously observed TM2 oligomerisation.

4.3.4 Oligomeric state of the G107IG113I double mutant peptide

To continue the examination a second point mutation was introduced within the peptide sequence in order to further investigate the role of both GxxxG(A) motifs in rCPT1A TM2 oligomerisation. This mutation created the sequence $G_{107}IG_{113}I$, where both motifs were disrupted by mutating their first glycine residues (G_{107}xxxG and G_{113}xxxA) to isoleucine. The oligomerisation of the resulting peptide ($G_{107}IG_{113}I$) was studied, in comparison with the *wt* rCPT1A TM2 peptide, using cross-linking and AUC analyses.

The results for the double mutant ($G_{107}IG_{113}I$) peptide are shown in **Figure 4.10 a**, where a ladder of bands is observed after cross-linking. The strongest bands were initially assigned to monomer (n=1, MW=2.8 kDa), dimer (n=2, MW=5.6 kDa), trimer (n=3, MW=8.4 kDa), and tetramer (n=4, MW=11.21 kDa) species.

When the oligomerisation of the single $G_{107}I$ (lanes labelled *s* for *single mutant*) and double $G_{107}IG_{113}I$ mutant (lanes labelled *d* for *double mutant*) peptides were directly compared with that of the wild-type TM2 (lanes labelled *w*) as shown in **Figure 4.12,** it is clear that the three peptides behave differently with respect to their oligomeric states. At low M:P ratios it is seen that, while the wild-type sequence forms primarily hexamers (as discussed previously in § 3.4.4 and in reference (Jenei *et al.*, 2009)), the mutant peptides form smaller oligomers. At high M:P ratios, the *wt* peptide hexamer is destabilised and it exists mainly as monomer, with a small concentration of dimeric and trimeric species. In contrast, both mutant peptides still form stable trimers and the $G_{107}IG_{113}I$ mutant also forms monomers and dimers whose populations increase at higher M:P ratios.

These results reflect the possible role of GxxxG(A) motifs in stabilising the rCPT1A TM2 hexamer. When the G_{107}xxxG_{111} or both the G_{107}xxxG_{111} and G_{113}xxxA_{117} motifs are absent, the sequence does not form hexamers at any of the M:P ratios studied. Furthermore, mutation of the G_{107}xxxG_{111} motif in the $G_{107}I$ peptide resulted in formation of a very stable trimer at all detergent concentrations studied, suggesting that the G_{113}xxxA motif is involved in stabilising the timer. Since the concentration of trimeric species for the double mutant peptide decreases at higher M:P ratios, we can say that trimers formed by the $G_{107}IG_{113}I$ mutant peptide are not as stable as trimers formed by the single mutant sequence.

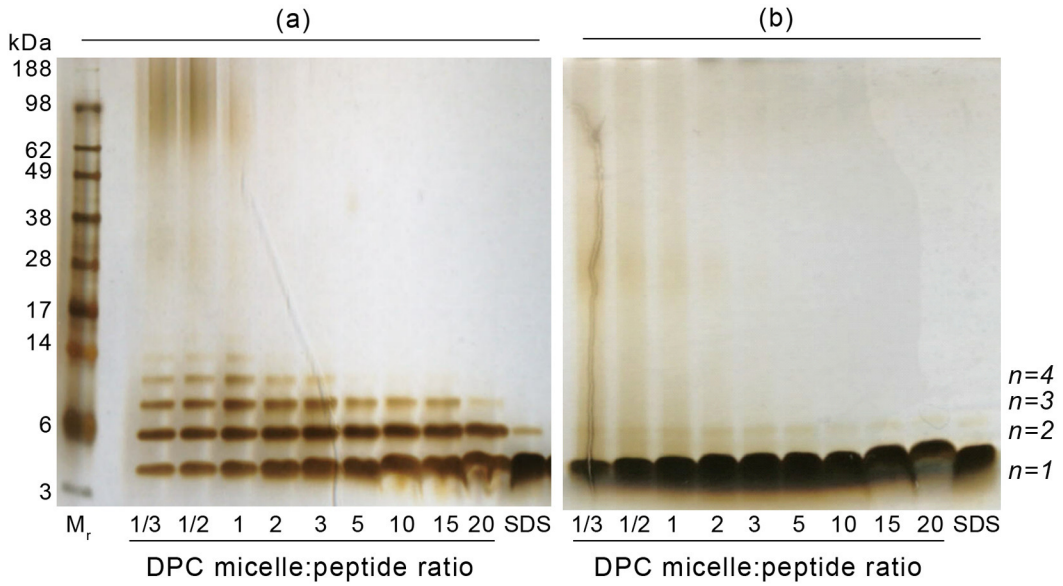

Figure 4.10 - SDS-PAGE analyses of chemically cross-linked rCPT1A TM2 $G_{107}IG_{113}I$ peptide oligomerisation. (a) The molecular weight marker is shown in the left-hand lane. The BS^3-mediated cross-linking of peptides dissolved in DPC micelles. Cross-linking reactions were carried out in DPC (or SDS, last lane M:P=4) detergent micelles at various M:P concentration ratios as indicated below each lane. **(b)** rCPT1A TM2 $G_{107}I$ peptide in the absence of crosslinker migrates mainly as monomer. In figure, protein bands were visualized by staining with silver nitrate. Oligomeric states (e.g. trimer indicated by n=3) are indicated at the far right of the gels.

In addition, oligomerisation of $G_{107}IG_{113}I$ peptide was also studied using AUC-SV. The experiment was carried out at 40,000 rpm, 25°C (Birmingham University), the peptide sample concentration was 112 μM (M:P ratio ~ 2.2). Fitting of the sedimentation velocity data resulted in a single peak at S=0.42 (**Figure 4.11**). Conversion of this sedimentation coefficient to molecular mass resulted in a $G_{107}IG_{113}I$ peptide species with a mass of 7205 kDa. When compared with the calculated molecular weights for the dimer (5604 kDa) and trimer (8406 kDa), the experimental value agreed to within 12% and 14% of the theoretical values, respectively. This suggests that, in the AUC experiment, the peptide exists as a mixture of smaller molecular size oligomeric species (monomer, dimer, and trimer). This result agrees with the results of cross-linking **Figure 4.12**, where the monomer, dimer and trimer species of $G_{107}IG_{113}I$ were detected in similar concentrations.

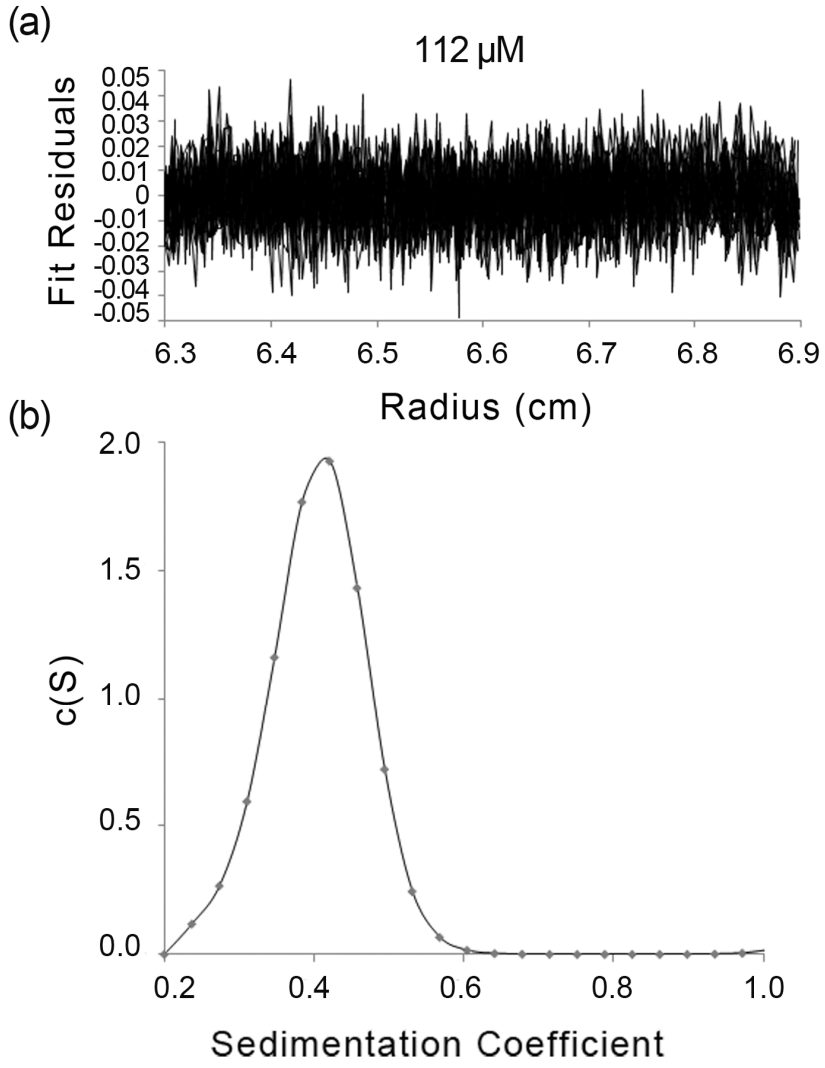

Figure 4.11 - Analytical ultracentrifugation analysis of a double mutant, rCPT1A TM2 $G_{107}I$ $G_{113}I$ synthetic peptide in DPC detergent solution. Sedimentation velocity data were obtained for TM2 $G_{107}I$ $G_{113}I$ peptide dissolved in buffer containing 15 mM DPC and 52.5% D_2O. **(a)** Residuals of the fitting process for samples containing 112 µM peptide. **(b)** Sedimentation coefficient distribution profiles for the peptide as calculated using the SEDFIT program.

These observations provide further evidence to support our hypothesis that formation of rCPT1A TM2 hexamers depends on the presence of GxxxG(A) motifs, and mutation of these motifs results in significant changes in the oligomeric states formed by the TM sequence.

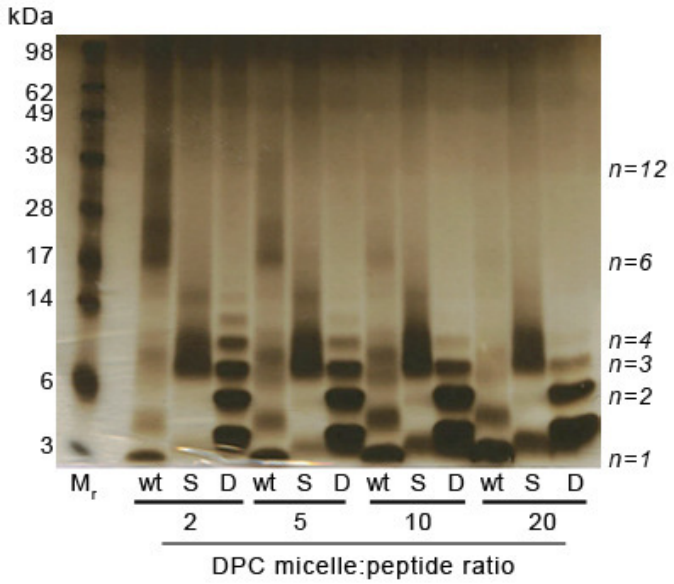

Figure 4.12 - SDS-PAGE gel analyses of chemically cross-linked wild type rCPT1A TM2 (w) peptide and its point mutants $G_{107}I$ (s) and $G1_{07}IG_{113}I$ (d). BS^3-mediated cross-linking of peptides was carried out in DPC detergent micelles at various micelle to peptide concentration ratios as indicated below each lane. The molecular weight marker is shown in the far left-hand lane. Proteins were visualized by staining with silver nitrate. Oligomeric states (e.g. trimer indicated by n=3) are indicated at the far right of the gels.

4.4 Modelling the sequence dependent oligomerisation

As discussed above in sections § 4.3.3 and § 4.3.4, our experimental data (TOXCAT, cross-linking and AUC) suggest that mutation of GxxxG(A) interaction motifs within the rCPT1A TM2 peptide sequence changes its oligomerisation behaviour. Thus, molecular models of the primary oligomeric complexes formed by the mutant peptides ($G_{107}I$ trimers and $G_{107}IG_{113}I$ dimers and trimers) were created using CHI (§ 2.6.4).

In modelling the $G_{107}I$ trimer, symmetric trimer searches were performed for helices containing the rCPT1A TM2 $G_{107}I$ (K_{102}-R_{123}) sequence. The results were clustered into 7 structures with RMSD < 1.2 Å and a cluster size > 8. The interacting residues were analysed in all 7 structures, and typically two types of conformations were found. Similar to the previously (§ 3.5.2) discussed wt rCPT1A TM2 oligomerisation model (**Figure 3.19**), in the $G_{107}I$ trimer the interaction interfaces also contain either the mutated IxxxG motif (I_{107}, G_{111}) *or* a the GxxxA motif (G_{113}, A_{117}), respectively. The models shown in **Figure 4.13 a-b** provide further evidence that the $G_{107}I$ mutant TM2 sequence can form stable trimer complexes.

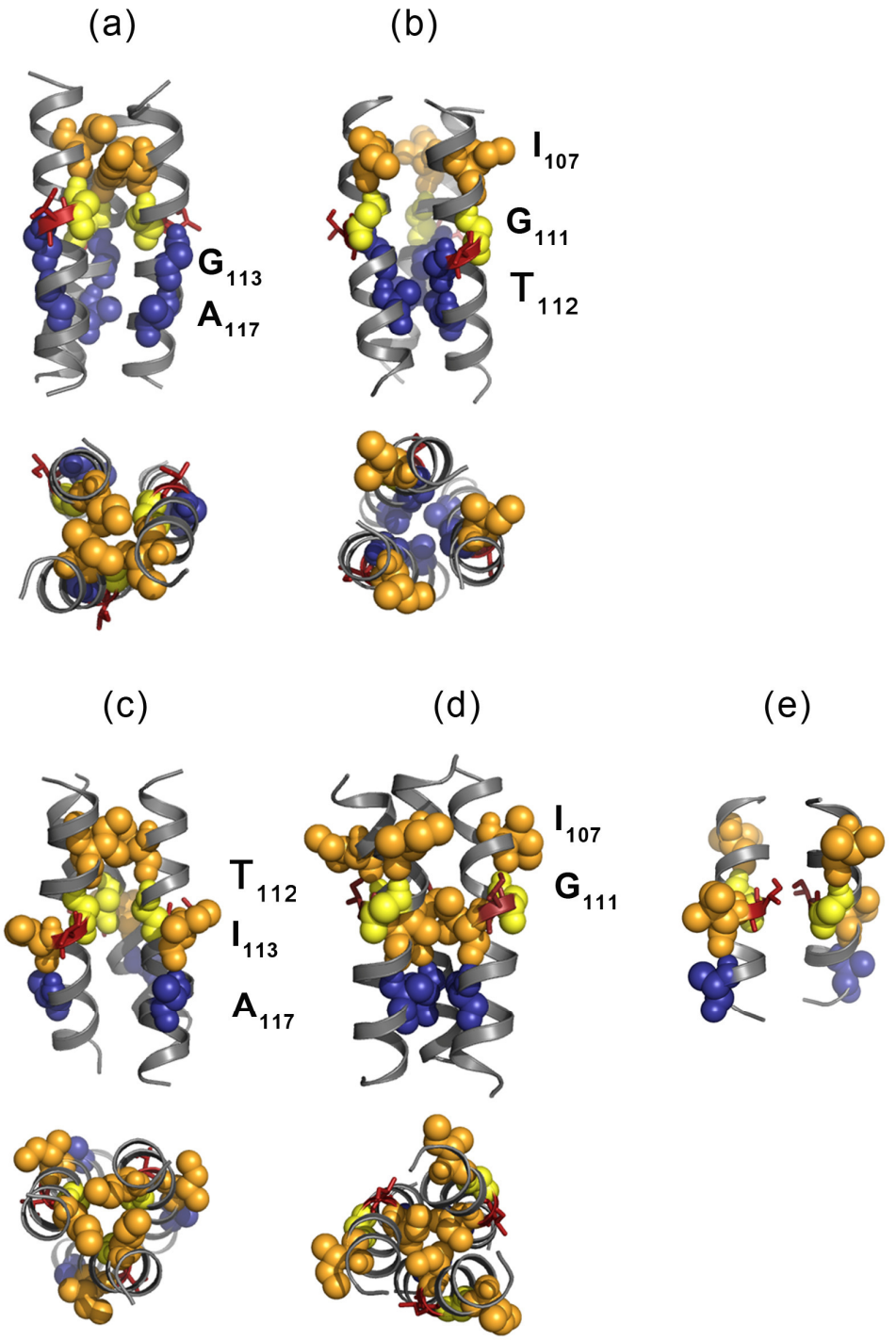

Figure 4.13 - Molecular models of rCPT1A TM2 mutants, $G_{107}I$ and $G_{107}IG_{113}I$ oligomerisation. (a) Side and top view of $G_{107}I$ trimer model, when $I_{107}xxxG_{111}$ or **(b)** $I_{113}xxxA_{117}$ falls on the helical interface and form the helix interaction. **(c)** Side and top view of $G_{107}I$ $G_{113}I$ trimer model when $I_{107}xxxG_{111}$ motif or **(d)** $I_{113}xxxA_{117}$ falls on the helical interface. **(e)** Side view of $G_{107}I$ $G_{113}I$ dimer model, where T_{112} residues form interhelical hydrogen bond on the helical interface and form the helix interaction. **(a)-(e)** In all structures, sequence corresponds to rCPT1A TM2 (Lys_{102}-Arg_{123}) including the actual mutation(s). Individual helices are represented as grey ribbon cartoons and residues are labelled as follows: the mutated residues I_{107} and I_{113}, highlighted as orange spheres, G_{111} and A_{117} or G_{113} shown in yellow and blue spheres respectively. Thr_{112} residues are shown as sticks, coloured in red.

In modelling $G_{107}IG_{113}I$ trimers, the same approach was used, with symmetric trimer searches carried out for helices containing the rCPT1A TM2 $G_{107}IG_{113}I$ (K_{102}-R_{123}) sequence. Results were clustered into 10 clusters. From these structures, two typical structures were obtained as shown in **Figure 4.13 c-d** containing either the IxxxG motif (I_{107}, G_{111}) *or* the IxxxA motif (I_{113}, A_{117}), respectively, at the helix-helix interface. In addition, in the $G_{107}IG_{113}I$ trimer model shown in **Figure 4.13 d**, the Val_{105}-Leu_{109} residues (not highlighted) were also found at the interface. These residues together with Ile_{113} support the self association of the modelled helices by close packing at the N-terminus of the sequence.

In the dimer model of the $G_{107}IG_{113}I$ peptide, Thr_{112} residues were found on the helical interface (**Figure 4.13 e**). This model suggests that the dimer is stabilized by the interhelical hydrogen bonding (1.7 Å), which could also explain the above presented TOXCAT mutagenesis results, where the $G_{107}IG_{113}IThr_{112}A$ mutant sequence causes a decrease in self-association, as compared to the wild-type rCPT1A TM2 (**Figure 4.2**).

4.5 Summary

A region containing the second TM domain (residues 97-147) of the rCPT1A enzyme was previously found to have an important role in oligomerisation of the full-length protein (Faye *et al.*, 2007). In the previous chapter, TM2 was studied in isolation (*in vivo, in vitro* and *in silico*), and was found to assemble into a hexamer-trimer oligomeric complex, mirroring the behaviour of the full length enzyme (§ 3.3.2).

The research presented in this chapter sought to study the sequence specificity of the observed oligomerisation behaviour of rCPT1A TM2. To verify the role of well-known GxxxG(A) sequence motifs, the TOXCAT assay was initially used to analyse mutants of the TM2 domain. Building on these results, the oligomerisation of two mutant synthetic peptides ($G_{107}I$ and $G_{107}IG_{113}I$) was also studied. Finally, we constructed molecular models highlighting potential points of contact between TM helices and suggesting that oligomer formation is favoured by the relative positioning of tightly-packed GxxxG and GxxxA motifs within the predicted TM2 helix.

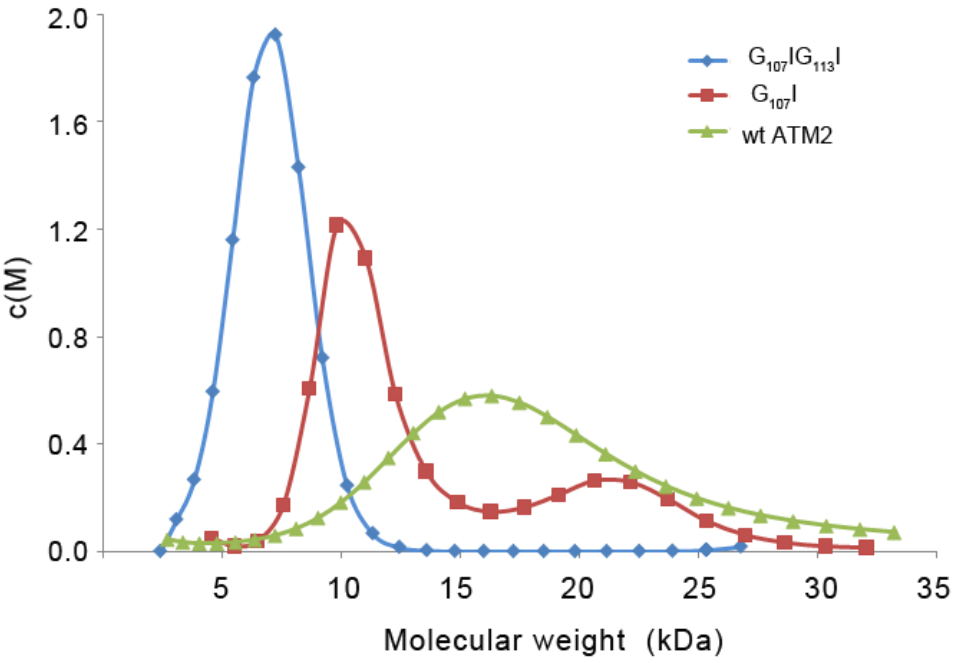

Figure 4.14 - Single and double mutation of GxxxG(A) motifs changes the size of the rCPT1A TM2 peptide complex. Molar mass distribution profiles of $G_{107}I$ (49 μM), $G_{113}I$ $G_{107}I$ (112 μM), and rCPT1A TM2 (62 μM) peptide samples calculated using SEDFIT.

The systematic mutagenesis of sequence motifs $G_{103}xxxG_{111}$, $G_{113}xxxA_{117}$ and Thr_{112} within TM2 established potential residues involved in helix interaction, when mutant sequences showed weaker oligomerisation than the wt TM2 in TOXCAT chimera. Mutations of $G_{107}I$ and $G_{107}IG_{113}I$ reduced the measured CAT activity by ~50%. Since these two mutants would provide critical information on the role of the two motifs, without making more than two mutations in the sequence, they were selected for further study *in vitro* (§ 4.2).

Synthetic peptides of the $G_{107}I$ and $G_{107}IG_{113}I$ mutants were studied using cross-linking and AUC, and significant differences were found in peptide oligomerisation, compared to the *wt* rCPT1A TM2 (§ 4.3.3 and 4.3.4). Both mutant peptides were found to form oligomeric species smaller than hexamers. The $G_{107}I$ peptide (mutation of the N-terminal $G_{107}xxxG_{111}$ motif) forms a stable trimer, which we suggest is stabilised *via* the undisturbed $G_{113}xxxA_{117}$ motif. In addition, the $G_{107}IG_{113}I$ peptide formed trimers in AUC experiments, but equivalent amounts of dimer and monomer species were detected by cross-linking (**Figure 4.10**). According to our *in silico* models, the oligomers formed by

the mutant peptides are likely to be stabilized by interhelical hydrogen bonding of Thr_{112} residues or close packing of Val-Leu-Ile residues (**Figure 4.13**).

Furthermore AUC experiments confirmed that mutation of GxxxG and GxxxA motifs changes rCPT1A TM2 oligomerisation. The mutant peptides found to sediment according to lower molecular weight species compared to the wild type peptide (**Figure 4.14**).

The above presented results give rise to further questions, such as how important are these motifs in the full length protein complex formation, and how these mutations would influence the protein assembly and function. These questions will be investigated in the future by introducing these mutations in the full-length protein and studying its effect on the complex formation and the enzyme function.

CHAPTER 5

HOMO-OLIGOMERISATION OF CPT1B TRANSMEMBRANE DOMAINS

This chapter presents the results from biological assays and studies on synthetic peptides constituting the transmembrane domains of CPT1B. The homo-oligomerisaton of both studied TM domains is observed, together with the stoichiometry of assembly in detergent micelles *in vitro,* and possible interacting sites between these helical peptides are proposed from *in silico* models.

5.1 Introduction

The carnitine palmitoyltransferase I (CPT1) enzyme has another important catalytically active isoform, CPT1B. Also called the M-isoform (muscle isoform), CPT1B occurs in skeletal and cardiac muscle mitochondria and in other particularly high fatty acid oxidative capacity tissues (e.g. brown adipose tissue) (McGarry and Brown, 1997). The sequence of CPT1B is very similar (63%) to CPT1A, but there is an important kinetic difference between the two, namely their inhibitor sensitivity. In contrast to CPT1A (which has been discussed in detail previously in § 3.1 and § 4.1), the CPT1B isoform is much more sensitive to inhibition by malonyl-CoA, and has a permanently high malonyl-CoA sensitivity which is not modulated by physiological state, suggesting that this molecule

adopts a more “active” but “rigid” structure (Mynatt *et al.*, 1992; Saggerson *et al.*, 1992). These observations suggest that there are molecular differences in the two isoforms which govern their inhibitor binding through different intramolecular interactions and could explain their different kinetic behaviour.

The difference in the kinetic behaviour of the two isoforms can be investigated by focusing on molecular differences between CPT1A and CPT1B. If we consider their differences in molecular plasticity and kinetic response to changes in physiological state, both of which are governed by changes in the membrane such as lipid fluidity and lipid composition in the mitochondrial outer membrane, the study can be narrowed down to differences in the structure or interactions of the transmembrane (TM) domains. Differences in TM helix-helix interactions could explain why the two isoforms have different degrees of molecular flexibility and have such different kinetic behaviour, despite the large similarity in their sequences and topologies.

The CPT1B isoform has no crystal structure or homology molecular model. There are no published data about the oligomerisation of the full length protein. However, the similarity in the protein sequence and topology indicates the possibility of complex formation similar to CPT1A.

The work presented in this chapter was designed to explore the TM homo-oligomerisation of the CPT1B TM domains, and compare it to that observed for CPT1A focusing on differences that might explain their different kinetic behaviour. For direct comparison, the same techniques were used as described for CPT1A in CHAPTERS 3 and 4. *In vivo* TOXCAT and GALLEX assays and *in vitro* peptide homo-oligomerisation and oligomeric state studies, together with molecular models, were used to determine important interaction motifs in CPT1B TM1 and TM2.

5.2 Sequence conservation and helix-helix interaction motifs in CPT1B TM domains

The two TM domains in CPT1B were defined using the UniProt database (www.expasy.org), highlighted in grey, with the sequence in white brackets, and using the TMHMM software (TM1 highlighted blue and TM2 highlighted in purple), as shown in **Figure 5.1**.

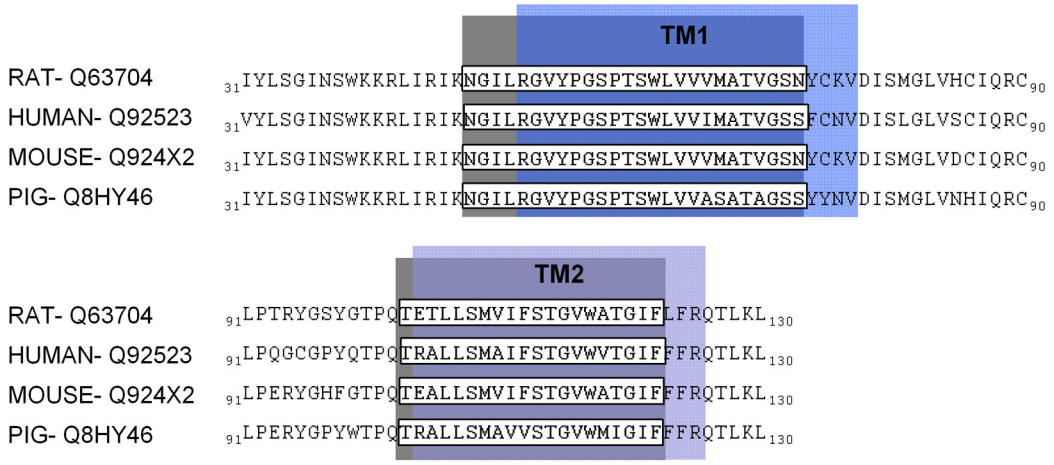

Figure 5.1 - Prediction of TM domain regions in CPT1B proteins from different species. TMs were predicted using the UniProt database and the TMHMM software. The sequence of CPT1B TM1 is highlighted in grey and blue, while that of TM2 is highlighted in grey and purple. TMs defined by UniProt are in brackets, residues highlighted with blue or purple were also predicted as part of TM by TMHMM (Sonnhammer *et al.*, 1998). (The UniProt codes (from www.expasy.org) of the analysed CPT1B proteins are shown on the left hand side.)

Using the TM domain sequences identified by TMHMM, the TM domains were further analysed to study the sequence conservation across different species, as well as the presence of known interaction motifs. TM domains of membrane proteins frequently contain sequence motifs that are known to stabilise the helix-helix interactions (for more details, see § 1.2.2 and § 3.2.1).

As shown in **Figure 5.2**, the sequence identities of CPT1B TM1 and CPT1B TM2 were 73.1% and 50%, respectively, when comparing four different mammalian species. The sequence identity of TM1 is very similar to that found for CPT1A TM1, and it also has similar helix-helix interaction motifs such as GxxxG, GxxxS, and motifs of polar Thr and Ser residues. In contrast, CPT1B TM2 sequence is about 23% more variable than CPT1A TM2 (see in **Figure 3.2**), when compared across different species, but the largest difference observed for this TM domain is the absence of any "*small*-xxx-*small*" interaction motifs. This TM sequence, however, does contain aromatic Phe residues and polar Ser and Thr residues (both of which are potential sites of TM helix-helix interactions), as shown in **Figure 5.2.**

Figure 5.2 - Analysis of conserved residues and helix-helix interaction motifs in CPT1B TM1 and TM2. Sequence analyses of conserved residues were carried out using the Biology Workbench software (http://workbench.sdsc.edu). Completely conserved residues are labelled green, identical residues are labelled with yellow, similar residues with blue, and different residues with white. The sequence motifs are highlighted according to TMSTAT.

This simple sequence analysis already suggests differences in the two isoforms, and we can see that the sequence of CPT1B TM2 contains no potential "GxxxG-like" interaction motifs and is much less conserved than any other TMs investigated.

5.3 *In vivo* oligomerisation of rCPT1B TM domains

5.3.1 Self-association of transmembrane domain 1 (TM1)

The TOXCAT assay was used to study the CPT1B TM1 domain self-association in the *E. coli* inner membrane. The TM domain sequences originally designed for the rCPT1B TM1 length optimization experiments were: Arg_{52}-Lys_{76}, Tyr_{55}-Lys_{76} and Tyr_{55}-Tyr_{74}, shown in **Figure 5.3 a,** and were 25, 22 and 20 amino acids in length. These chimeras all failed the *malE* complementation assay, **Figure 5.3 c**, suggesting that they were incorrectly inserted into the inner membrane. Chimeras containing TM1 sequences with lengths of 25 and 22 amino acids were tested with the CAT assay, but did not show oligomerisation **Figure 5.3 b**.

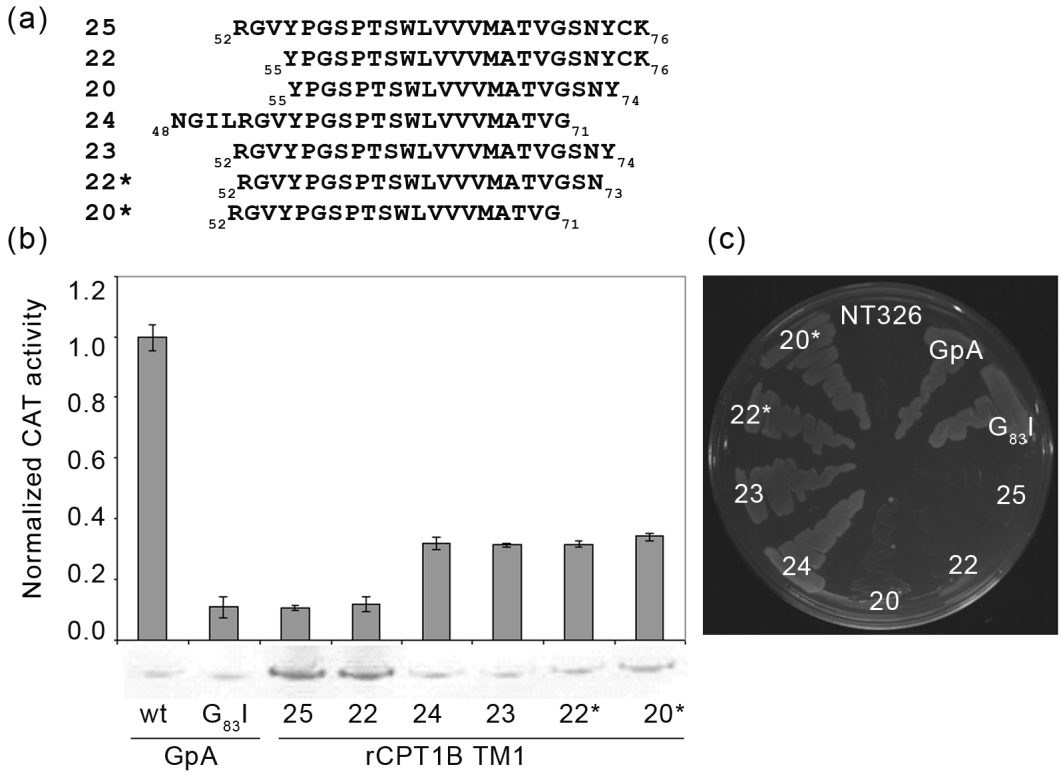

Figure 5.3 - Oligomerisation of TOXCAT chimeras containing rCPT1B TM1 domain sequences of varying length (25, 22, 24, 23, 22*, 20* residues) in *E. coli* membranes. **(a)** Transmembrane domain sequences of rCPT1B TM1 cloned and analyzed in TOXCAT assay. **(b)** The resulting CAT activities of rCPT1B TM1 length optimization study. CAT activities obtained for the different lengths of rCPT1B TM1 and expression level of chimeras detected by western blot analysis (using antibodies directed against MBP). All CAT activities are reported relative to the value obtained for wt GpA (positive control). Values are means (+/- standard deviation) for three or more independent measurements. **(c)** malE complementation to test for correct insertion of ToxR-TM1-MBP chimeras.

Interestingly, rCPT1B TM1 sequences Asn_{48}-Gly_{71} (24 residues in length), Arg_{52}-Tyr_{74} (23 residues), Arg_{52}-Asn_{73} (22*) and Arg_{52}-Gly_{71} (20*) were correctly inserted (**Figure 5.3 c**) across the membrane and yielded approximately 32-39% of CAT activities compared to the positive control *wt* GpA (**Figure 5.3 b**).

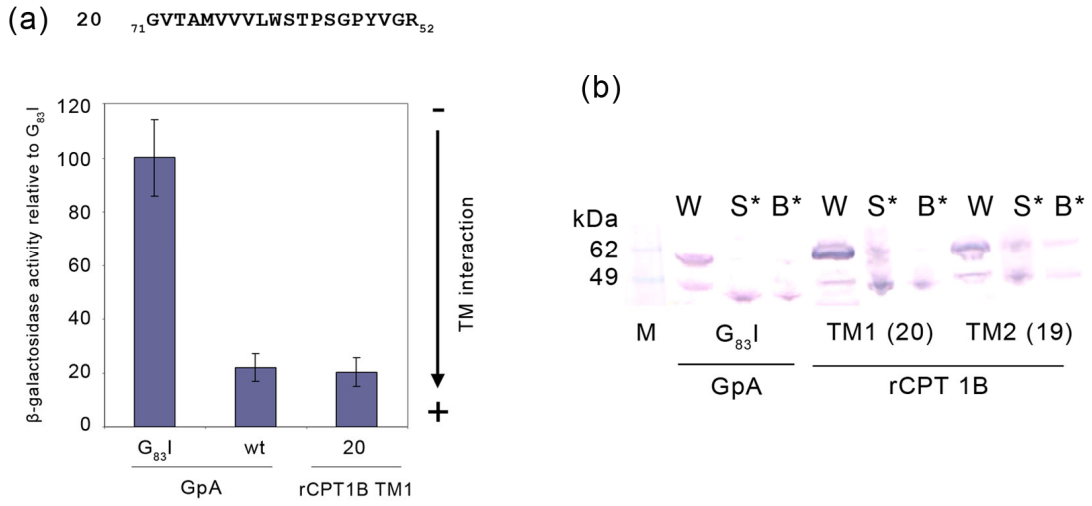

Figure 5.4 - Oligomerisation of rCPT1B TM1 (20) in GALLEX homo-oligomerisation assay. (a) The inverse sequences of rCPT1A TM1 were cloned into pBLM vector in *wt* LexA-TM-MBP chimera (Gly_{71}-Arg_{52}). Chimeras were expressed in SU101 using 0.01 mM IPTG when analyzed by GALLEX-homo assay. All activities are reported relative to the value obtained for $GpAG_{83}I$ (negative control). Values are means (+/- standard deviation) for three independent measurements. **(b)** Immunoblot of spheroplast proteolysis assay to test topology of rCPT1B LexA-TM1-MBP chimeras expressed in NT326 cells. Immunoblotting was carried out using antibodies directed against MBP. The correctly inserted chimeras were detected at 66kDa (full length chimeric protein) in whole cell fractions (W), and at 43 kDa (MBP molecular weight) in spheroplasts treated with proteinase K (S*) and lysed spheroplast treated with proteinase K (B*) fractions.

In addition, the self-association of the rCPT1B TM1 domain sequence Arg_{52}-Gly_{71} was also studied using the GALLEX assay (**Figure 5.4 a**). This sequence was selected because it was the shortest (previous reports suggest that TM domain lengths of $\leq$ 19 amino acids are usually successful in this assay) of those which gave a positive CAT signal. The chimera w*t* LexA-TM1-MBP failed to grow in the *malE* complementation assay (data not shown), but the spheroplast proteolysis assay (**Figure 5.4 b**) again confirmed the correct insertion and orientation. In the GALLEX chimera rCPT1B TM1, oligomerisation was found to be similar to the *wt* GpA positive control (**Figure 5.4 a**). These results support the results obtained from TOXCAT (i.e. CPT1B TM1 has a propensity to self-associate), however the strength of this association relative to GpA appears to be much larger when measured in GALLEX.

5.3.2 Self-association of transmembrane domain 2 (TM2)

The length optimisation of rCPT1B TM2 in the TOXCAT assay resulted in only one TM domain construct, containing residues Leu_{106}-Arg_{125} (20 residues in length; see **Figure 5.5 a**), which showed both correct insertion and self-association. Interestingly, the TOXCAT signal was similar to that obtained for rCPT1B TM1 20 (Arg_{52}-Gly_{71}) (**Figure 5.3 b**) yielding CAT activities approximately 31% of those observed for the positive control *wt* GpA (see in **Figure 5.5 b**).

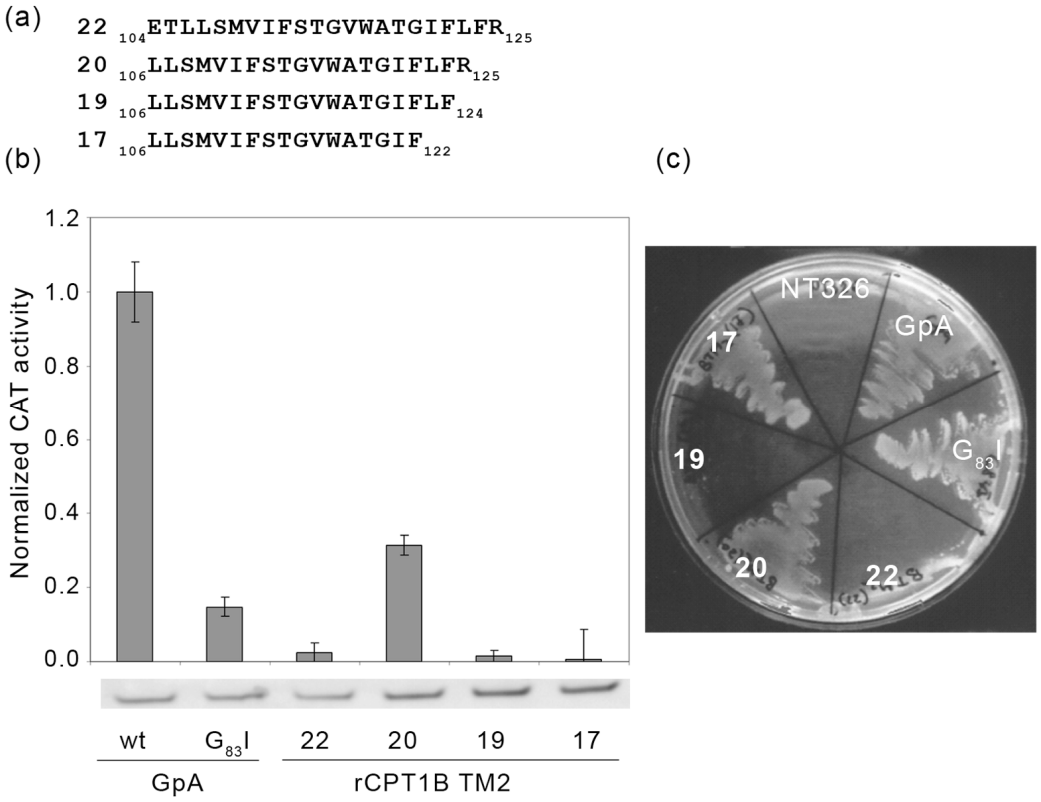

Figure 5.5 - Oligomerisation of rCPT1B TM2 (22, 20, 19, 17) TOXCAT chimeras in *E. coli* membranes. (a) Transmembrane domain sequences of rCPT1B TM1 cloned and analyzed in TOXCAT assay. **(b)** The resulting CAT activities of rCPT1B TM1 length optimization study. CAT activities obtained for the different length of rCPT1B TM1 and expression level of chimeras detected by western blot analysis (using antibodies directed against MBP). All CAT activities are reported relative to the value obtained for wt GpA (positive control). Values are means (+/- standard deviation) for three or more independent measurements. **(c)** malE complementation to test the ToxR-TM1-MBP chimeras correct insertion.

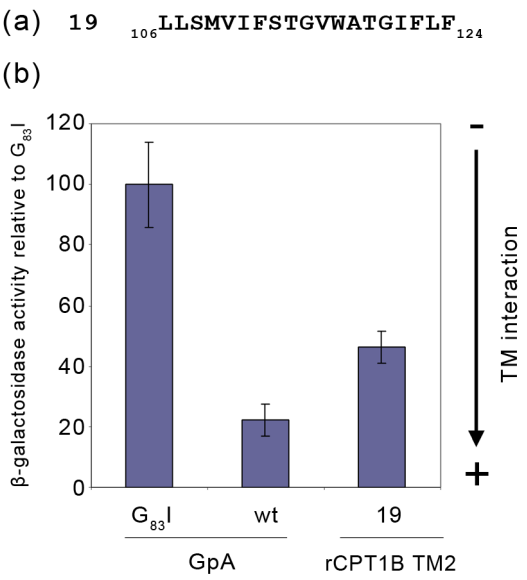

Figure 5.6 - Oligomerisation of rCPT1B TM2 (19) in GALLEX homo-oligomerisation assay. (a) The inverse sequences of rCPT1A TM1 were cloned into pBLM vector in *wt* LexA-TM-MBP chimera. Chimeras were expressed in SU101 using 0.01 mM IPTG when analyzed by GALLEX-homo assay. **(b)** The resulting β-galactosidase activities of GpA and rCPT1A TM1 chimeras. All activities are reported relative to the value obtained for $GpAG_{83}I$ (negative control). Values are means (+/- standard deviation) for three independent measurements.

In the case of the 22 (Glu_{104}-Arg_{125}) and 19 (Leu_{106}-Phe_{124}) amino acid sequences, the very low signals detected (**Figure 5.5 b**) were most probably the result of incorrect insertion of the chimeras. Furthermore, the 17 (Leu_{106}-Phe_{122}) amino acid sequence which was correctly inserted according to the *malE* complementation assay (and membrane association with NaOH extraction) still yielded low signals despite numerous independent measurements. In comparison, both rCPT1A TM domains showed the strongest interaction at an optimal TM domain length of 16 residues (§ 3.3.1 and § 3.3.2), while here the rCPT1B TM2 length of 20 residues (Arg_{52}-Gly_{71}) was found to correctly span the *E. coli* membrane and oligomerise in the TOXCAT assay. To confirm rCPT1B TM2 homo-oligomerisation, GALLEX experiments were also designed.

Based on our TOXCAT results, the rCPT1B TM2 20 residue (Leu_{106}-Arg_{125}) sequence was initially used for cloning, but ligation of this oligonucleotide into the pBLM plasmid failed after multiple attempts. However the 19 residue (Leu_{106}-Phe_{124}) sequence was successfully cloned into pBLM. The resulting chimera was also correctly expressed and inserted into the membrane as tested with the spheroplast proteolysis assay (shown in **Figure 5.4 b**). The GALLEX chimera containing rCPT1B TM2 (19) yielded approximately 46% β-galactosidase activity

compared to the negative control GpA $G_{83}I$, which suggests stronger oligomerisation than the 20 residue Leu_{106}-Arg_{125} sequence analysed using the TOXCAT assay (**Figure 5.5 b**), but not as strong as the positive control GpA in **Figure 5.6 b**.

5.4 *In vitro* oligomerisation of rCPT1B TM peptides

The above presented oligomerisation studies of rCPT1B TM sequences suggested that these domains can self-associate in a natural membrane. In order to validate the results of *in vivo* assays and investigate the oligomeric state(s) formed by the rCPT1B TM domains, *in vitro* approaches were used. Synthetic peptides corresponding to rCPT1B TM domains were purified and their secondary structures were characterised in DPC detergent micelles using circular dichroism (CD) spectroscopy. To investigate the oligomeric state of rCPT1B TM peptides, chemical cross-linking and analytical ultracentrifugation sedimentation velocity (AUC-SV) experiments were carried out. (For peptide sequences and details see § 2.4-2.5, **Table 2.6**).

5.4.1 Purification and structural analyses of synthetic TM peptides

The crude synthetic peptides were purified by reversed-phase high performance liquid chromatography (RP-HPLC) as discussed in detail in § 2.4. To verify the peptides' purity and correct molecular weight, matrix-assisted laser desorption ionization-time of flight mass spectroscopy (MALDI-TOF-MS, Bruker) was used. The deconvoluted mass spectra of rCPT1B TM1 and TM2 peptides are shown in **Figure 5.7** and **Figure 5.8**.

Table 5.1 - The amino acid sequences of rCPT1B TM1 and TM2 synthetic peptides used in this study. Non-native lysine residues are shown in bold.

TM domain of interest	Synthetic peptide sequence	Molecular weight (Da)
rCPT1B TM1	$COCH_3$-**K**ILRGVYPGSPTSWLVVVMATVGSNY**K**-$CONH_2$	2963
rCPT1B TM2	$COCH_3$-**K**ETLLSMVIFSTGVWATGIFLFR**K**-$CONH_2$	2785

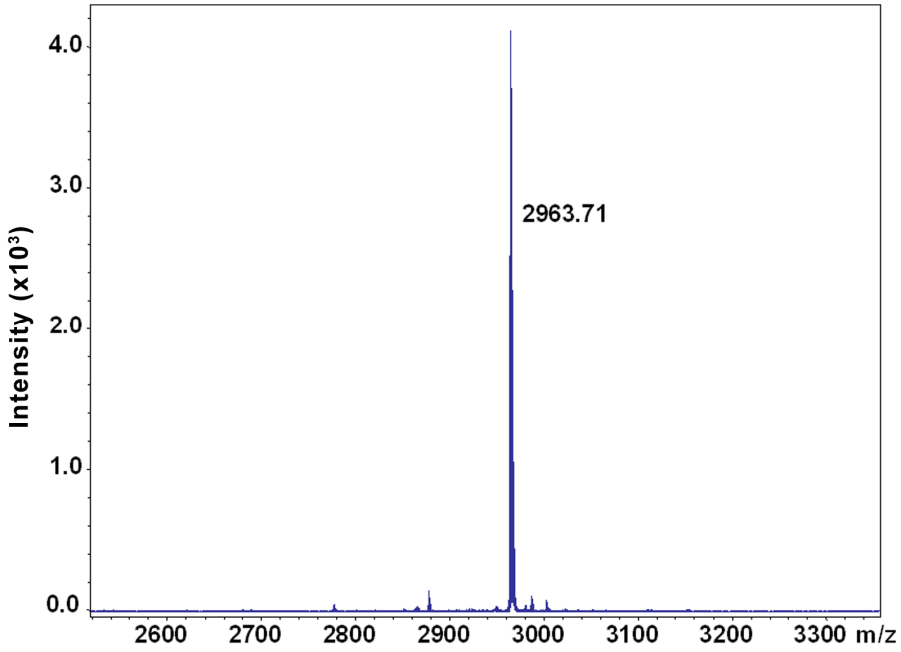

Figure 5.7 - Analysis of purified rCPT1B TM1 peptide by matrix-assisted laser desorption ionization-time of light mass spectrometry (MALDI-TOF-MS). The HPLC fractions containing the pure peptide were pooled and analyzed using MALDI-TOF-MS. In the spectrum, the major peak corresponds to the rCPT1B TM1 peptide (2963 Da).

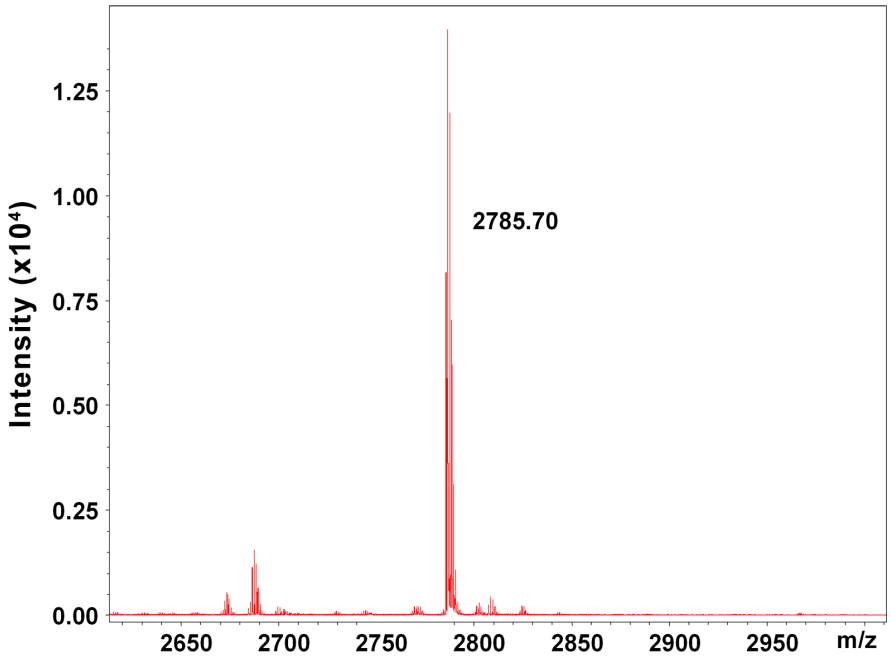

Figure 5.8 - Analysis of purified rCPT1B TM2 peptide by MALDI-TOF-MS. The HPLC fractions containing the pure peptide were pooled and analyzed using MALDI-TOF-MS. In the spectrum, the major peak corresponds to the rCPT1B TM2 peptide (2785 Da), and additional peaks correspond to truncated peptides that co-purified with the major product.

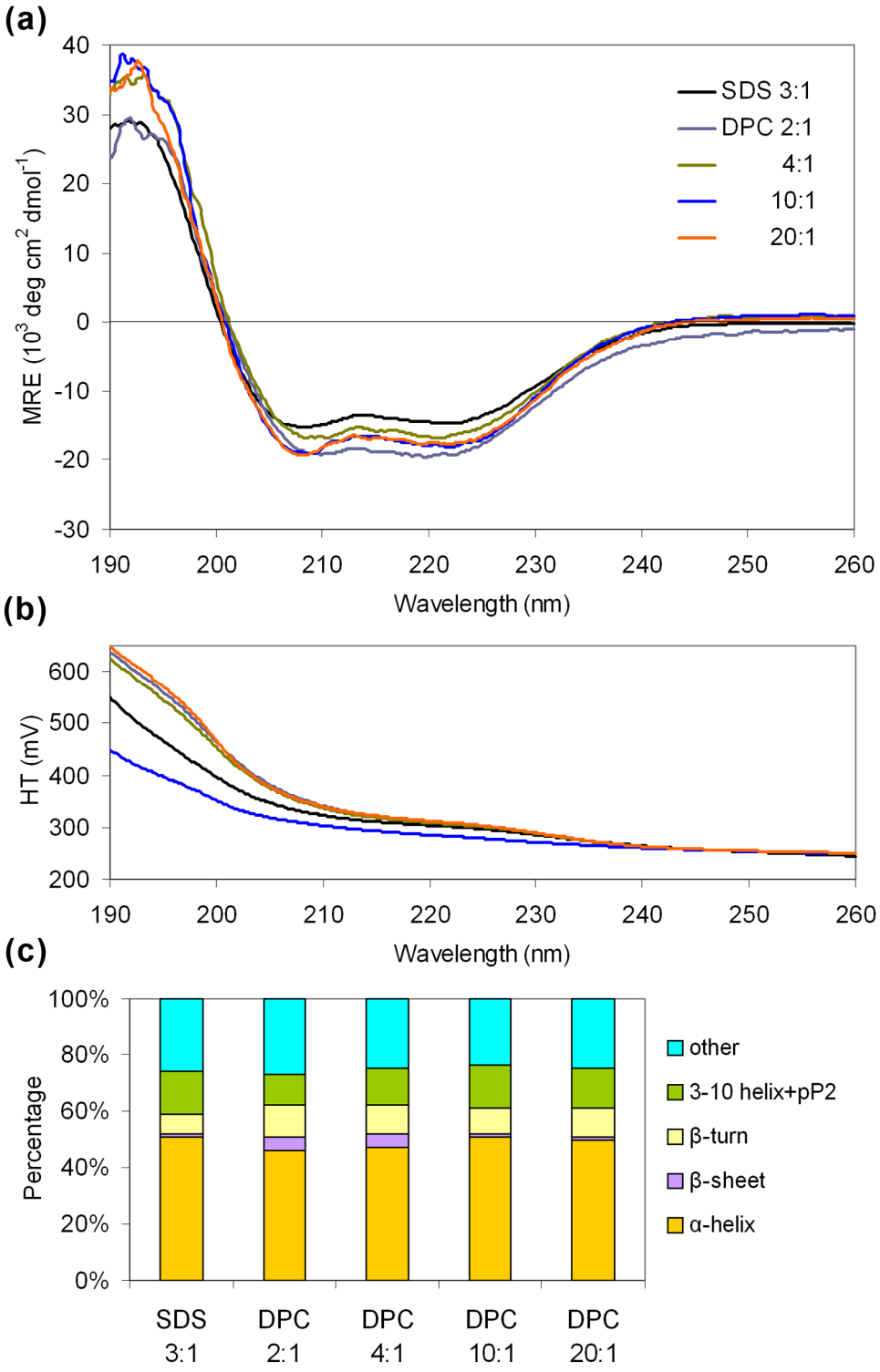

Figure 5.9 - The effect of DPC micelle concentration on the secondary structure of rCPT1B TM1 peptide. (a) CD spectra measured at different detergent micelle to peptide ratios, plotted in units of mean residue ellipticity (MRE). **(b)** High tension (HT) over the wavelength region specified in (a). **(c)** The secondary structure composition of the rCPT1B TM1 peptide estimated from fitting of the CD spectra shown in (a) using the CDSSTR software (Johnson, 1999). Secondary structure composition was calculated by fitting of the CD data between 190-260 nm.

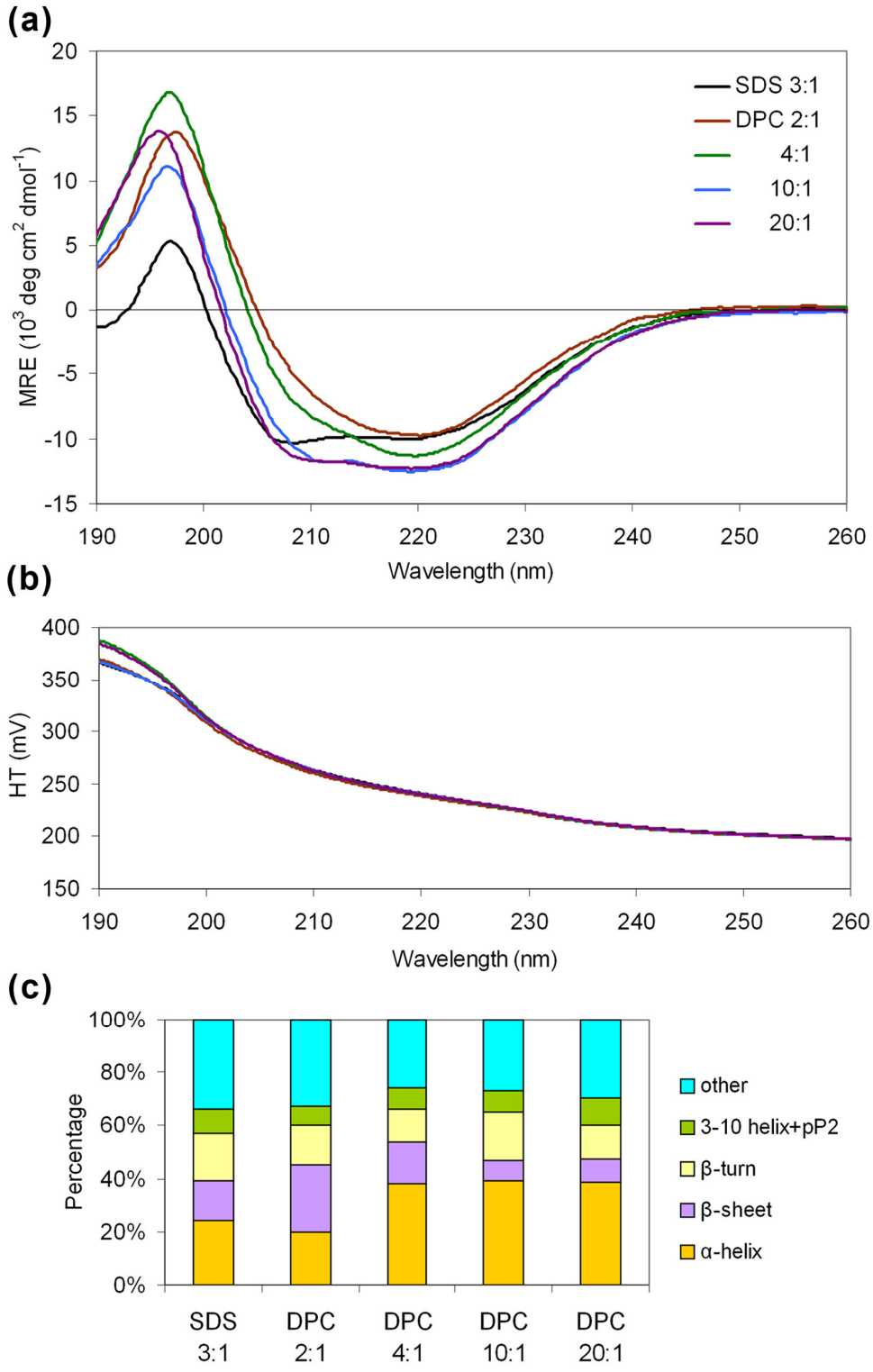

Figure 5.10 - The effect of DPC micelle concentration on the secondary structure of rCPT1B TM2 peptide. (a) CD spectra measured at different detergent micelle to peptide ratios, plotted in units of mean residue ellipticity (MRE). **(b)** High tension (HT) over the wavelength region specified in (a). **(c)** The secondary structure composition of the rCPT1B TM2 peptide estimated from fitting of the CD spectra shown in (a) using the CDSSTR software (Johnson, 1999). Secondary structure composition was calculated by fitting of the CD data between 190-260 nm.

CD spectra were then collected to determine whether the peptides were properly folded in DPC micelles. CD spectra collected at different micelle concentrations indicated that the rCPT1B TM1 peptide adopts mainly α-helical secondary structure (46-51%) at all different M:P ratios (**Figure 5.9**).

In contrast, the rCPT1B TM2 peptide at lower peptide to micelle ratios (in SDS 3:1 and in DPC 2:1) adopted a primarily β-sheet secondary structure (shown in **Figure 5.10**), which we suggest arises from insoluble aggregates. At higher, 4:1-20:1 ratios the α-helical content of the peptide samples was 39%. One possible explanation of the observed differences between the secondary structure content of the rCPT1B peptides is that the TM2 sequence is more hydrophobic than TM1, making it more prone to aggregation (the TM2 sequence contains three phenylalanine residues and one tryptophan residue). The hydrophobicity values were calculated according to the relative hydrophobicity of the amino acid residues, as determined by the retention time in RP-HPLC (Liu and Deber, 1998).

5.4.2 Determination of rCPT1B TM1 peptide oligomeric state

To study the oligomeric state(s) achieved by the rCPT1B TM1 peptide in detergent micelles, chemical cross-linking and AUC experiments were carried out. The synthetic peptide derived from rCPT1B TM1 (mentioned above; MW=2963 kDa) was solubilised in DPC micelles and treated with the water-soluble chemical cross-linker BS^3. Cross-linked species were visualized by SDS-PAGE analysis (**Figure 5.11 a**). The TM1 peptide produced a number of bands between the 6 and 17 kDa molecular weight markers, which corresponds to oligomeric states between trimer and pentamer. A broad band between 28-49 kDa was observed at the lowest detergent concentrations (M:P=1/3–1), suggesting the presence of higher order aggregated states for very low detergent concentrations. As the detergent concentration was increased (M:P=2–5), only trimer and tetramer species were observed, which were destabilised by increasing the detergent concentrations to M:P=10–20, where only monomer species were detected. A double band migrating slightly above the expected monomer molecular weight could be seen at all M:P ratios, and may correspond to two different monomer conformations or to the monomer complexed with different numbers of cross-linker molecules.

Also shown in **Figure 5.11 a,** is the result from cross-linking the TM1 peptide in SDS. The resulting single band corresponding to the molecular weight of the

monomer confirmed the specificity of the cross-linking reaction in DPC. The peptide was also analysed in the absence of cross-linker in SDS (M:P=3) and DPC micelles (M:P=2 and 5) on SDS-PAGE, as shown in **Figure 5.11 b**. Again, only monomeric species were observed, suggesting that this peptide cannot form SDS-stable oligomers.

It is interesting to note that the results of the rCPT1B TM1 peptide cross-linking experiments closely mirror those obtained with the rCPT1A TM1 peptide in § 3.3.1, **Figure 3.13** which suggests strong similarities in the oligomerisation properties of this region of both enzymes.

The rCPT1B TM1 peptide oligomerisation was also studied in the absence of a cross-linker by AUC-SV. Initially, data were collected at the speed of 40,000 rpm, 25°C (Birmingham University), but when analysed, the sedimentation coefficient distribution indicated that the majority of the peptide forms mostly higher order species larger than 18-22 kDa, which was probably due to aggregation (data not shown).

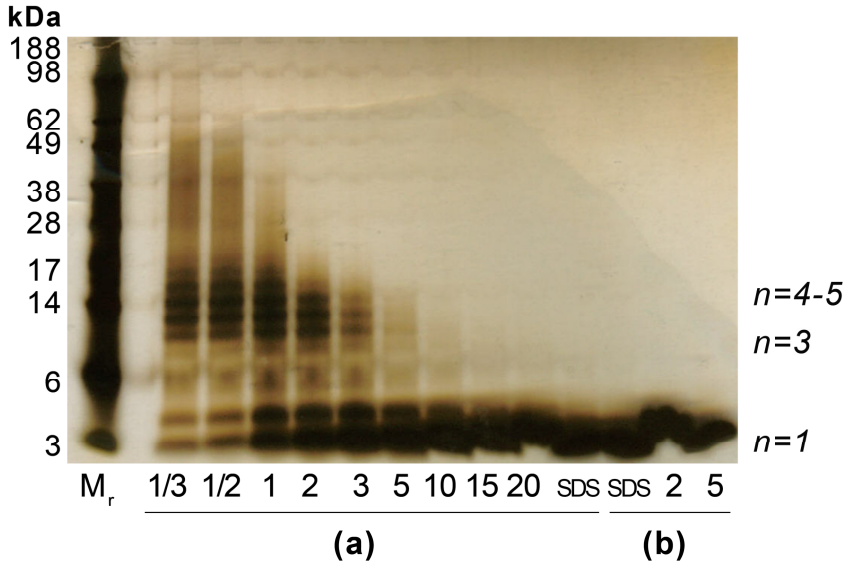

Figure 5.11 - SDS-PAGE analysis of chemically cross-linked rCPT1B TM1 peptide oligomerisation. The molecular weight marker is shown in the left-hand lane (M_r). **(a)** BS^3-mediated cross-linking of peptides dissolved in DPC micelles. Cross-linking reactions were carried out in DPC detergent micelles at various micelle to peptide concentration ratios as indicated below each lane. Protein bands were visualized by staining with silver nitrate. Oligomeric states (e.g. trimer indicated by n=3 are indicated at the far right of the gels. **(b)** rCPT1B TM1 peptide in the absence of crosslinker migrates mainly as monomer in SDS micelles at M:P=4, and in DPC micelles at M:P=2 and 5.

With new sample preparation, and using 55,000 rpm, 20°C (Oxford University), we collected a better resolved data set (**Figure 5.12**). The sedimentation coefficient profile for the 83 µM concentration contained one species centered at S=0.71 (at RMSD value of 1.7×10^{-2}), corresponding to a molecular mass of 14.35 kDa, near the mass of the pentameric species. When compared with the calculated molecular weights for the TM1 pentamer (14.8 kDa), the experimental values agreed to within 4% of the theoretical values.

Among all species observed by the previous cross-linking experiment (shown in **Figure 5.11**), only the pentameric species could be detected by AUC-SV at this speed. The smaller complexes were probably also present in the solution, but undetectable under the above mentioned experimental conditions with AUC.

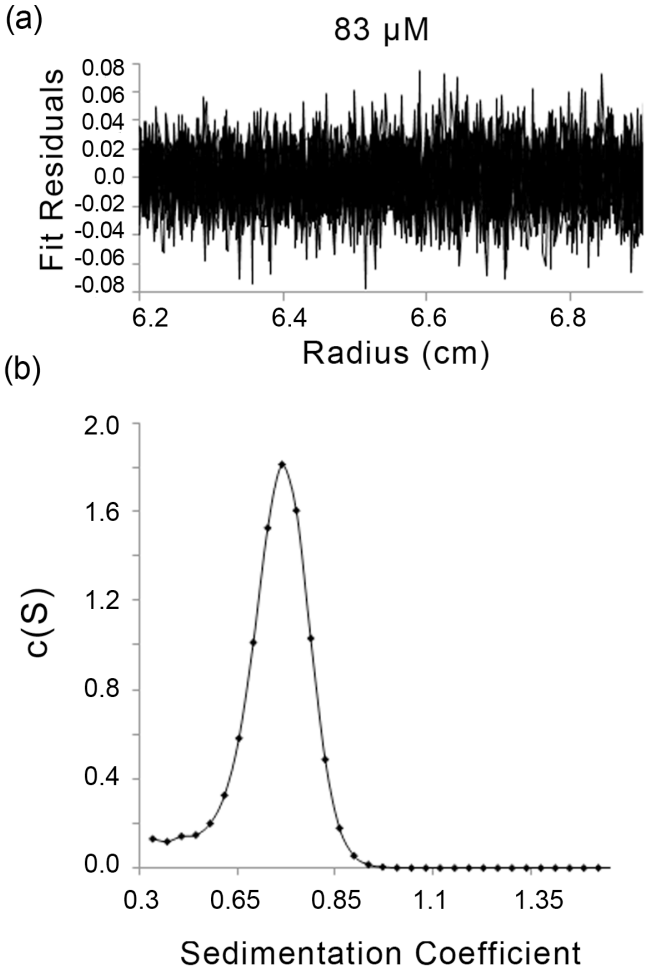

Figure 5.12 - Analytical ultracentrifugation analysis of rCPT1B TM1 derived peptide in DPC detergent solution. Sedimentation velocity data obtained for TM1 peptide dissolved in buffer containing 15 mM DPC and 52.5% D_2O. **(a)** Residuals of the fitting process for samples containing 83 µM peptide (M:P ratio ~3). **(b)** Sedimentation coefficient distribution profiles for the peptide as calculated using the SEDFIT program.

5.4.3 The order of rCPT1B TM2 peptide oligomerisation

To study oligomerisation of rCPT1B TM2, the peptide derived from this domain (MW=2785 kDa) was also cross-linked and analysed using SDS-PAGE, shown in **Figure 5.13**. The oligomeric species detected across all M:P ratios runs slightly above the 6 kDa molecular weight marker, suggesting the presence of a TM2 trimer (8355 kDa) rather than a dimer (5570 kDa). As mentioned above, the oligomer appears as a closely spaced pair of bands, most clearly shown at M:P=10 and 20, that may represent two different trimer conformations or the trimer species complexed with different numbers of cross linker molecules. Increasing the micelle concentration resulted in a higher concentration of monomer and less aggregation, but the trimer band concentration did not change. This suggests that the rCPT1B TM2 peptide forms stable trimers in DPC micelles (**Figure 5.13 a**).

The result from cross-linking the TM2 peptide in SDS is shown in **Figure 5.13 a** (lanes labelled SDS), and confirms the specificity of the cross-linking reaction in DPC. Analyses of the peptide in the absence of cross-linker in SDS and DPC micelles again yielded only monomer bands (**Figure 5.13 b**), demonstrating that this peptide also cannot form SDS-stable oligomers.

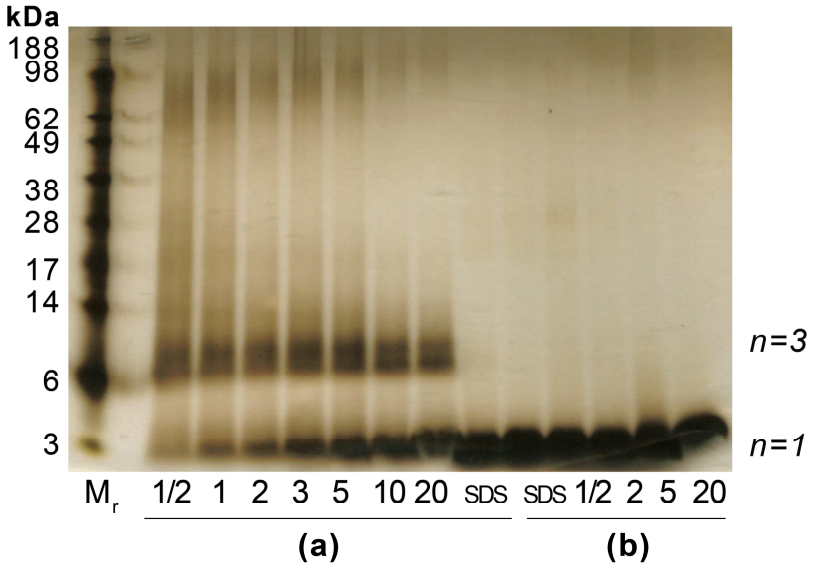

Figure 5.13 - SDS-PAGE analysis of chemically cross-linked rCPT1B TM2 peptide oligomerisation. The molecular weight marker is shown in the left-hand lane (M_r). **(a)** BS^3-mediated cross-linking of peptides dissolved in DPC micelles. Cross-linking reactions were carried out in DPC detergent micelles at various micelle to peptide concentration ratios as indicated below each lane. Protein bands were visualized by staining with silver nitrate. Oligomeric states are indicated at the far right of the gels. **(b)** rCPT1B TM2 peptide in the absence of crosslinker migrates as monomer.

In order to more quantitatively determine the oligomeric state of the rCPT1B TM2 domain, samples were also analysed by AUC-SV. The data were collected at a peptide concentration of 107 μM (M:P ratio ~ 2), at 55,000 rpm and 20°C (University of Oxford). The residuals of the fit and sedimentation coefficient profile are shown in **Figure 5.14**. The major peak of the resulting sedimentation coefficient profile was centered at S= 0.33, while a minor peak was also typically present at S=0.94 (**Figure 5.14 b**). Converting the sedimentation coefficient to molecular mass distribution indicated molecular weights for the peaks of 6.48 kDa and 30.9 kDa, respectively. According to the molecular weight of the peaks, the majority of the peptides sedimented as dimers in the absence of cross-linker molecules (agreeing to within 15% of the theoretical value of 5.57kDa). The minor peak with higher molecular weight was probably due to aggregation in the sample caused by the high hydrophobicity of the peptide (as discussed in § 5.4.1).

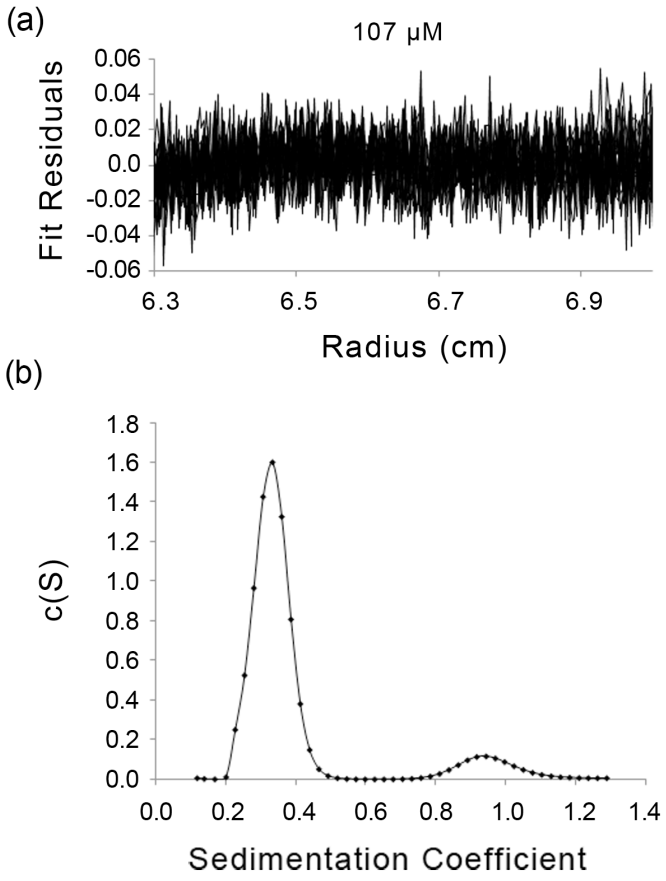

Figure 5.14 - Analytical ultracentrifugation analysis of rCPT1B TM2 derived peptide in DPC detergent solution. Sedimentation velocity data were obtained for TM2 peptide dissolved in buffer containing 15 mM DPC and 52.5% D_2O. **(a)** Residuals of the fitting process for samples containing 107 μM peptide (M:P ratio ~2). **(b)** Sedimentation coefficient distribution profiles for the peptide as calculated using the SEDFIT program.

5.5 *In silico* models of rCPT1B TM oligomerisation

The experimental data discussed above suggests that both TM domains of rCPT1B are able to form homo-oligomers *in vivo* and *in vitro*. The observed oligomerisation behaviour was further studied by *in silico* modelling of homo-dimers and homo-trimers for each TM domain using CHI. The modelled sequences were identical to the peptide sequences (TM1: Ile_{50}-Tyr_{74} and TM2: Glu_{104}-Arg_{125}). Modelling these structures enables us to determine possible interacting residues and motifs responsible for the observed oligomerisation.

5.5.1 Modelling TM1 homo-oligomerisation

The analysis of CPT1B TM1 domain already indicated several interaction motifs (GxxxG and Ser, Thr) within the sequence (§ 5.2). In the following models we examined their significance in rCPT1B TM1 homo-oligomerisation.

First, for the simplest model of homo-interaction, a TM1 dimer was built and simulated. The results were clustered into 5 clusters with RMSD < 1.2 Å and a cluster size > 8 structures. The interacting residues within two symmetric clusters were assessed. **Figure 5.15 a** shows the cluster containing left handed helical dimer structures, while **Figure 5.15 b** illustrates the structure for the cluster containing right handed dimers. In the dimer model shown in **Figure 5.15 a**, four residue pairs (both R_{52}-$Y_{55,}$ T_{69} -T_{69} and S_{72}-N_{73}) form interhelical H-bonds of lengths 1.7-1.9 Å. The right handed dimer model shown in **Figure 5.15 b** has the $G_{53}xxxG_{57}$ motif packed in the interface of the helices, bending them towards each other. In this model two pairs (S_{61}-S_{61} and T_{69} -S_{72}) of H-bonds also stabilise the helix-helix interaction. The donor and acceptor distances are within 1.8 Å of one another for these H-bonds.

As trimer formation of rCPT1B TM1 was previously observed by cross-linking (**Figure 5.11**), we have also attempted to model the homo-trimer structure.

rCPT1B TM1: $_{50}$ILRGVYPGSPTSWLVVVMATVGSNY$_{74}$

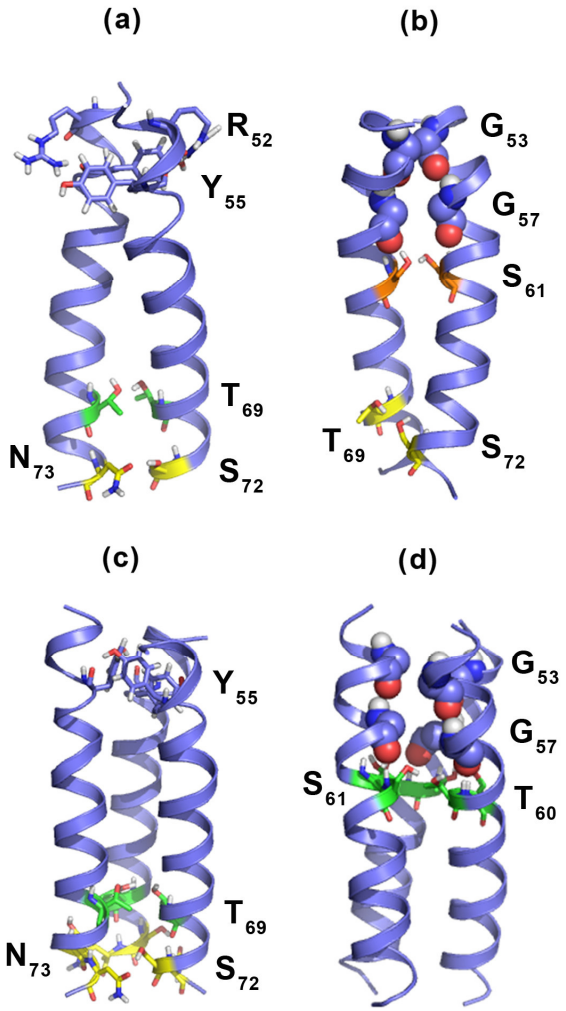

Figure 5.15 - Likely interaction motifs in rCPT1B TM1 (a-b) homo-dimer and (c-d) homo-trimer CHI models. (a) Left-handed, symmetrical dimer model. **(b)** Right-handed, symmetrical dimer model. **(c)-(d)** Left handed symmetrical trimer models. Individual helices are represented as blue ribbon cartoons and residues are labelled as follows: **(a)** R_{52} and Y_{55} shown as sticks, coloured by element (blue carbons), T_{69} (green carbons), S_{72} and N_{73} (yellow carbons). **(b)** G_{53} and G_{57}, highlighted as blue spheres, S_{61} shown as sticks coloured by elements (orange carbons), T_{69} and S_{72} (yellow carbons). **(c)** Y_{55} shown as sticks coloured by elements (blue carbons), T_{69} (green carbons) S_{72} and N_{73} (yellow carbons). **(d)** G_{53} and G_{57}, highlighted as spheres coloured by element, T_{60} and S_{61} residues are shown as sticks, coloured by element (green carbons).

The structures found during the CHI search were arranged into 9 clusters, according to the criteria RMSD < 1.8 Å and cluster size > 4. All structures were analysed and typically two types of conformations were found. Interestingly, these were similar to that detailed for the dimer models: in **Figure 5.15 c** there are interhelical H-bonds (1.7-2 Å) between the $Y_{55,}$ T_{69} and S_{72}-N_{73} residues, while

in the other model shown in **Figure 5.15 d**, the $G_{53}xxxG_{57}$ motif and a H-bond (1.8 Å) between S_{61}-T_{60} residues is formed at the helix-helix interfaces to stabilise the trimer structure.

Similarly to that observed for the rCPT1A TM1 domain (§ 3.5.1), in the rCPT1B TM1 models discussed here the same P_{56} and P_{59} residues (not highlighted) also disrupt the helical structure by forming proline kinks, but only for the conformations where the $G_{53}xxxG_{57}$ motifs are not at the interface.

While chemical cross-linking and AUC (§ 5.4.2) experiments suggest that the TM1 peptide forms pentameric species, the CHI simulation using RMSD < 1.8 Å and a cluster size > 4 did not produce any pentameric structures. This may be due to the simulation software producing highly strained initial structures, making it impossible for the molecular dynamics to maintain a pentameric configuration. Using more sophisticated force fields and providing non-strained initial structures could be a way to investigate the stability of similar oligomers in the future.

5.5.2 Modelling TM2 homo-oligomerisation

The rCPT1B sequence is different from any previously modelled sequences, as it is the only one from the investigated TM domains containing no *GxxxG like* motifs, but it contains several aromatic and Thr, Ser residues. CHI searches were performed on either two or three parallel α-helices containing rCPT1B TM2 to study the structural features that may have a role in stabilizing both the trimeric (detected by cross-linking, § 5.4.3) and dimeric (observed by AUC, § 5.4.3) forms of the synthetic peptide.

The dimer model was simulated using RMSD < 1.0 Å and a cluster size > 10. The simulation resulted in 3 clusters, from which the energy plot of the right handed cluster was sufficiently good to analyse further. L_{106} and V_{110} residues interact on the helix interface of the structure shown in **Figure 5.16 a**, constituting a possible heptad motif. We found no other known interaction motifs or any other interacting residues on the interface in the TM2 dimer model.

rCPT1B TM2:$_{104}$ETLLSMVIFSTGVWATGIFLFR$_{125}$

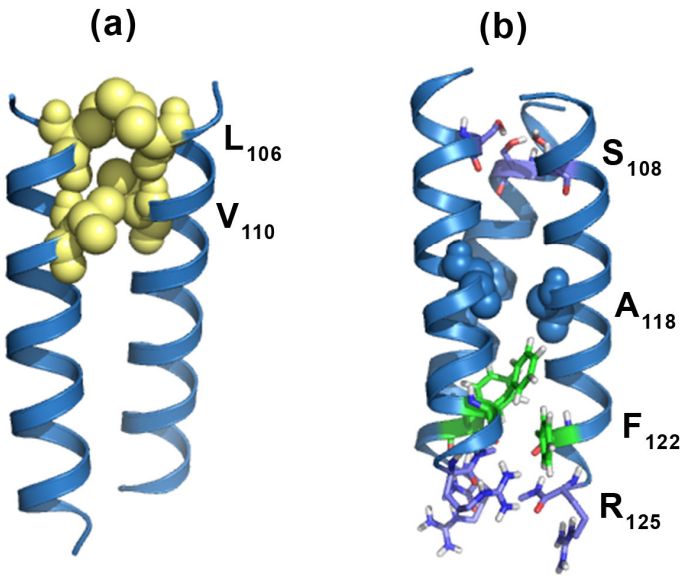

Figure 5.16 - Possible interhelical interactions in rCPT1B TM2 (a) homo-dimer and (b) homo-trimer CHI models. In **(a)-(b)**, individual helices are represented as blue ribbon cartoons. **(a)** Model for the homo-dimer, we see packing of L_{106} and V_{110} which highlighted as yellow spheres. **(b)** Homo-trimer model, where we see packing of A_{118} highlighted as blue spheres S_{108}, F_{122} and R_{125} highlighted as stick coloured by elements.

For the modelling of rCPT1B timers, symmetric trimer searches were carried out with helices containing the rCPT1B TM2 sequence. We clustered the structures according to RMSD < 1.5 Å and cluster size > 6. This resulted in one right handed coiled coil with the above parameters. In this cluster, the interface of the trimer model contains S_{108}, and R_{125} residues forming interhelical H-bonds (1.7 Å), small A_{118} residues and F_{122} forming hydrophobic interactions (see in **Figure 5.16 b**).

Molecular modelling of the TM homo-oligomerisation in CPT1B highlighted several sequence motifs, which are likely to play a role in stabilising self-association of these TM domains. In the future, these results could be used as a starting point for designing mutagenesis experiments, similar to what was already carried out for rCPT1A TM2 (CHAPTER 4).

5.6 Summary

It is not known whether the full length CPT1B also exists as an oligomer in muscle mitochondria. In the previous chapter we found correlation between oligomerisation of full length CPT1A and the oligomerisation of its TM domains. This finding might be helpful in highlighting differences between the oligomerisation of the two isoforms by comparing the self-association behaviour of their TM domains. By studying the self-association of the TM domains, based on our previous results, we could compare the TM oligomerisation of the two isoforms directly. Biological assays and biophysics techniques were used to identify the oligomerisation properties of rCPT1B TM domains. Both of the rCPT1B TM domains showed self-association.

Interestingly, we have found some similarity in the oligomerisation behaviour of rCPT1A and rCPT1B TM1 domains. When studying their corresponding synthetic peptides with chemical cross-linking, both form similarly sized species (n=3-5) with a very similar pattern according to SDS-PAGE analysis (see **Figure 3.13** and **Figure 5.11**). The observed similarity could be due to their sequence similarity (GxxxG like motifs, proline residues). However, the TM2 domain of rCPT1B behaved very differently from its counterpart in CPT1A, forming dimers and trimers as opposed to the hexamers formed by rCPT1A TM2. The sequence motifs in the TM2 domains are also significantly different in the two isoforms, and molecular modelling showed different interactions between their amino acids.

The above observations do suggest that the CPT1B isoform is able to form oligomeric complexes. The oligomeric state of CPT1B could be different from that of CPT1A, as their TM2 domains have significantly different oligomerisation behaviour. In CPT1A oligomerisation the TM2 domain was found to have key role in forming hexamers (Faye *et al.*, 2007). If the same applies to CPT1B, the oligomerisation of the full length CPT1B will be different. If for example, CPT1B would form trimer complexes, and the different sizes of the protein complexes for CPT1A and CPT1B would explain their different enzyme kinetics. However, the hypothesis needs more data to directly compare the complex and possible chanell formation for these proteins.

The investigation of TM domain interaction in CPT1A and CPT1B still has one more aspect we need to consider, namely the hetero interaction of TM1-TM2 domains, which is discussed in the following CHAPTER 6.

CHAPTER 6

HETERO, TM1-TM2 INTERACTIONS IN CPT1 ISOFORMS

In this chapter the possibility of hetero-oligomerisation between TM1 and TM2 domains is studied. Using the GALLEX assay, interactions of TM1-TM2 were identified in both CPT1A and CPT1B, and by modelling the appropriate peptide sequences, interaction motifs playing a possible role in stabilising the oligomers are proposed.

6.1 Introduction

As previously discussed, intramolecular interactions in CPT1A (but not in CPT1B) are modulated by changes in the properties of the mitochondrial outer membrane (Kolodziej and Zammit, 1990; Zammit *et al.*, 1998). The absence of a similar response by CPT1B to a change in physiological state suggests that TM1-TM2 interactions may be fundamentally different in this isoform. When we studied the homo-oligomerisation of the TM domains of these isoforms, each TM helix was found to form higher order homo-oligomeric complexes. According to our molecular modelling results, the homo-oligomerisation in each TM domain occurred *via* different interaction interfaces and sequence motifs in the isoforms' TM domains. The variety of interacting residues and motifs within one TM helix suggests the possibility that hetero-oligomerisation may also occur (Gerber *et al.*, 2004) between TM1 and TM2 in the isoforms. Therefore, the experiments described in this chapter were designed to investigate whether intramolecular

interactions involving known motifs within TM1 and TM2 of CPT1A and B are involved in hetero-association of the two TM domains. Furthermore, here differences in TM1-TM2 interactions in the two isoforms are examined which would explain their different kinetic characteristics. In order to examine the TM1-TM2 hetero-interactions in both isoforms, the GALLEX biological assay was used in combination with molecular modelling.

6.2 *In vivo* TM domain hetero-oligomerisation

The GALLEX biological assay (for details see § 2.3) can be used to study hetero-association between different TM domains (Schneider and Engelman, 2003). To investigate hetero-interaction of two different transmembrane helices, the assay uses two separately expressed chimeras (wt LexA-iTM1-MBP and *mut* LexA-TM2-MBP). The TM domain sequences in the GALLEX chimera were designed according to the results of the TOXCAT and GALLEX assays presented in CHAPTER 3 and CHAPTER 5, respectively. Here we have inverted the sequences of the rCPT1A and rCPT1B TM1 domains in order to achieve an antiparallel orientation of the different TM domains (TM1 and TM2) in the membrane, as would be found in the native full length CPT1 proteins.

To measure TM1-TM2 hetero-oligomerisation, TM2 domains of interest were cloned into the pALM148 vector used to transform the SU202 strain of *E. coli*. This was followed by a second transformation with the pBLM100 plasmid, which encoded the chimera containing the appropriate TM1 domain (inverted TM1 sequences were used to gain antiparallel orientation). Both TM1 and TM2 plasmids were previously used to perform the GALLEX homo-oligomerisation assays (see in CHAPTER 3 and CHAPTER 5). Here the two chimeras were expressed simultaneously in the SU202 strain of *E. coli* to perform β-galactosidase assay.

Initially, experiments were carried out to test different lengths of the TM1 and TM2 sequences, however as discussed CHAPTER 3 and CHAPTER 5, several of the chimera did not correctly insert into the *E .coli* membrane when studied with the control assays (*malE* complementation and proteolysis in spheroplasts). This length optimisation finally resulted in the transmembrane domain sequence pairs shown in **Figure 6.1 a** that were analysed using the GALLEX hetero-association assay. Before the quantitative measurement of β-galactosidase repression was carried out, the correct membrane insertion and topology of the chimeric proteins

was confirmed using the NaOH assay, the *malE* complementation assay, and the proteolysis in spheroplasts assay (all as described in § 2.2.2 and § 2.3.2). The NaOH assay confirmed that all chimeras were associating with the *E. coli* inner membrane (data not shown). According to the *malE* complementation assay, not all the constructs were inserted in the correct orientation into the *E. coli* inner membrane. While the rCPT1A TM2 (16) sequence and the positive and negative controls (GpA and $G_{83}I$) did grow on the maltose minimal media plates, cells transformed with the rCPT1B TM2-containing plasmid did not grow (see in **Figure 6.1 c**). For this reason, further characterisation was performed using the spheroplast assay to confirm the correct orientation of the chimera *mut* LexA-rCPT1B TM2 (19)-MBP (**Figure 6.1 d**). The correct orientation and insertion of w*t* LexA-TM1-MBP chimeras of rCPT1A TM1 or rCPT1B TM1 (with the inverted TM1 sequences) were previously discussed and illustrated in **Figure 3.5** and **Figure 5.4**, respectively.

Hetero-oligomerisation of the TM1-TM2 chimeras was measured at two different IPTG concentrations (0.1 and 0.01 mM) within the optimal range for induced chimeric protein expression (Finger *et al.*, 2006). The measured β-galactosidase activities are shown in **Figure 6.1 b.** The TM1-TM2 hetero oligomerisation measurements produced β-galactosidase activities for rCPTA and rCPT1B of 29% and 31%, respectively, relative to the $G_{83}I$ negative control when 0.1 mM IPTG was used in the growth medium. These results demonstrate, for the first time, that the TM domains of both isoforms can take part in TM1-TM2 hetero-interactions. The relative β-galactosidase activity obtained using 0.01 mM IPTG resulted in less hetero-association, with rCPTA and rCPT1B displaying 45% and 64% of the activity observed for G83I, respectively. This reduction of hetero-association is expected at a reduced IPTG concentration, as less protein is expressed. However, working at this lower concentration still yields significant repression of β-galactosidase (and thus significant helix-helix interactions) and has the added benefit of revealing subtle differences between the two isoforms that were obscured at higher protein concentrations (i.e. 0.1 mM IPTG). The above results demonstrate that significant hetero-oligomerisation occurs between TM1 and TM2 domains in both rCPT1 isoforms. The results obtained upon moderate induction of the two protein chimeras (0.01 mM IPTG) also suggest that the TM1-TM2 interactions are stronger in the CPT 1A isoform, revealing a key difference in two isoforms that may be linked to their different kinetic behaviour.

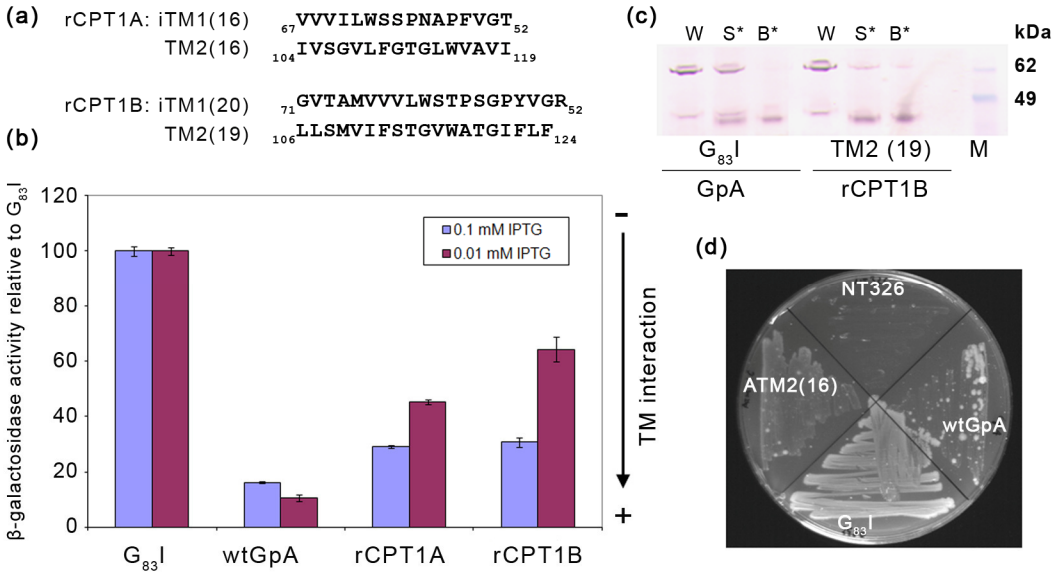

Figure 6.1 - Hetero-oligomerisation of TM1-TM2 in rCPT1A and rCPT1B. (a) TM domain sequences cloned into the GALLEX plasmids. (b) The resulting β-galactosidase activities of GpA, G83I, and rCPT1A TM1 chimeras. The β-galactosidase activities obtained for the different lengths of rCPT1A TM1 and relative expression levels of chimeras were detected by western blot analysis. All activities are reported relative to the value obtained for GpA $G_{83}I$ (negative control). Values are means (+/- standard deviation) for three independent measurements. (c) Immunoblots of spheroplast proteolysis assay to test topology of LexA- rCPT1B TM2 (19)-MBP chimera. Chimeras were expressed in NT326 cells. The immunoblotting was carried out using antibodies directed against MBP. The correctly inserted chimeras were detected at 66 kDa (at the molecular weight of the full length chimeric protein) in whole cell fractions (W), and at 43 kDa (molecular weight of MBP) in spheroplasts treated with proteinase K (S*) and lysed spheroplasts treated with proteinase K (B*) fractions. (d) *malE* complementation assay to test for correct insertion and orientation of the *mut* LexA-rCPT1A TM2 (16)-MBP chimera.

6.3 Molecular models of hetero interactions

The primary aim of modelling the TM1-TM2 hetero-interactions *in silico* in CPT1 proteins was to highlight potential residues or sequence motifs that could support the above observed oligomerisation behaviour, and design mutants for future experiments. As the experimental data shown in Fig. 6.1 demonstrate differences in the strength of TM1-TM2 hetero-oligomerisation in the two isoforms, modelling may also help to highlight differences in the interacting residues which could further our understanding of the CPT1 isoform's different enzyme kinetics. Molecular modelling was performed using the CNS searching of helix interactions (CHI) software (described in detail in § 2.6.4). The CHI models were built to take it into account both the full length TM domains in CPT1A and B, and also the actual lengths of TM domains studied in the GALLEX hetero-assay. To estimate the hetero-interactions in all of the structures presented below, a full CHI search

was used and results were clustered into groups of structures with an RMSD of 1.2 and a minimum cluster size of 8 members.

The CHI search of hetero-interactions between rCPT1A TM1 (T_{52}-V_{67}) - iTM2 (I_{119}-I_{104}) yielded 22 clusters, when these shortened sequences were modelled. One left-handed structure (cluster 9) was found to form a *knobs into holes* type interaction by closely packing residues (Lemmon and Engelman, 1994; Gurezka *et al.*, 1999; Harrington and Ben-Tal, 2009), with L_{114} of TM2 packing against V_{54} - A_{57} of TM1 and I_{64} of TM1 packing between G_{111} – G_{107} of TM2 as shown in **Figure 6.2 a**. This interaction is one example of a hetero TM interaction that could explain the observed GALLEX results, formed through close packing interactions that bring the two helices into close contact. When the full length TM sequences of rCPT1A TM1 (K_{47}-M_{73}) – iTM2 (R_{123}-K_{102}) were used for modelling, a full CHI search was again carried out, and results were clustered into groups of structures with an RMSD of 1.2 and a minimum cluster size of 14 members.

By modelling the hetero-association of full length TM domains, we find that one of the structures (left handed, cluster 2) again shows the helices packing through a knobs into holes type close packing of Ile/Val of TM1 to Ile residues (I51/V54 - I119) of TM2 and hydrogen bonding of Asn-Thr residues of TM1 and TM2, respectively (N58-T112: 1.9 Å) as shown in **Figure 6.2 b**. Interestingly, both G_{107}xxxG_{111} and G_{113}xxxA_{117} motifs in the rCPT1A TM2 sequence are present on the outside of the packing interface of the TM2 helix, motifs that have been previously found to drive TM2-TM2 homo-oligomerisation. This observation opens up the possibility that homo- and hetero-interactions could occur at the same time *via* different residues in CPT1A and could stabilise protein complex formation.

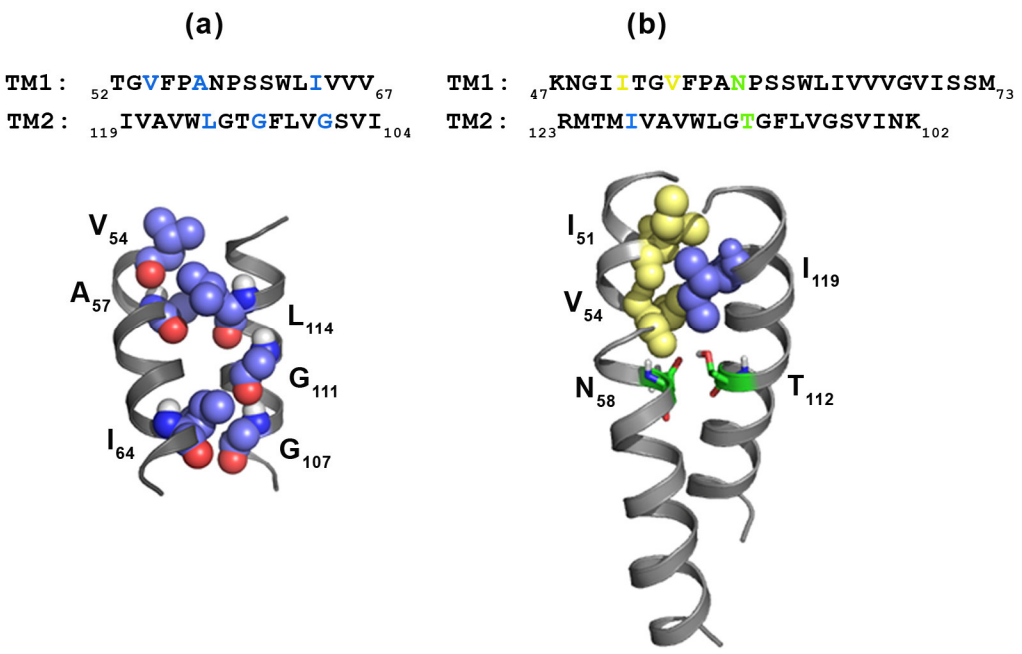

Figure 6.2 - **CHI models of possible hetero interactions of TM1-TM2 within the rCPT1A protein.** Amino acid sequences and CHI models of (a) rCPT1A TM1 (T_{52}-V_{67}) - iTM2 (I_{119}-I_{104}) (b) rCPT1A TM1 (K_{47}-M_{73}) – iTM2 (R_{123}-K_{102}) interaction. Individual helices are represented as grey ribbon cartoons and residues are labelled as follows: (a) interacting residues highlighted as spheres coloured by element (b) I_{119} highlighted as blue while I_{51} and V_{54} highlighted as yellow spheres, N_{58} and T_{112} hydrogen bonding residues are labelled as sticks and coloured by elements.

The rCPT1B hetero-interaction was also studied, and the CHI search results were clustered into 18 clusters when the shorter iTM1 (G_{71}-R_{52}) - TM2 (L_{106}-F_{124}) (i.e. GALLEX assay equivalent) sequences were modelled. The models of these shorter sequences suggest that interhelical hydrogen bonds can be formed between Ser residues (S_{61} of TM1-S_{113} of TM2 within 2.1 Å of one another) and also small Gly residues can pack between TM1-TM2 helices (G_{57} -G_{53} to G_{120}) as shown in **Figure 6.3 a**.

When the full length TM sequences were used, the modelling resulted in 22 structures for rCPT1B iTM1 (Y_{74}-I_{50}) –TM2 (E_{104}-R_{125}). In one of the left-handed clusters, as shown in **Figure 6.3 b,** the helices are associating *via* hydrogen bonding between Y_{74} of TM1 and T_{105} of TM2 (1.9 Å) and close packing of Ile/Val in TM1 to Ile residues in TM2 (V_{66} /L_{63} to I_{111}).

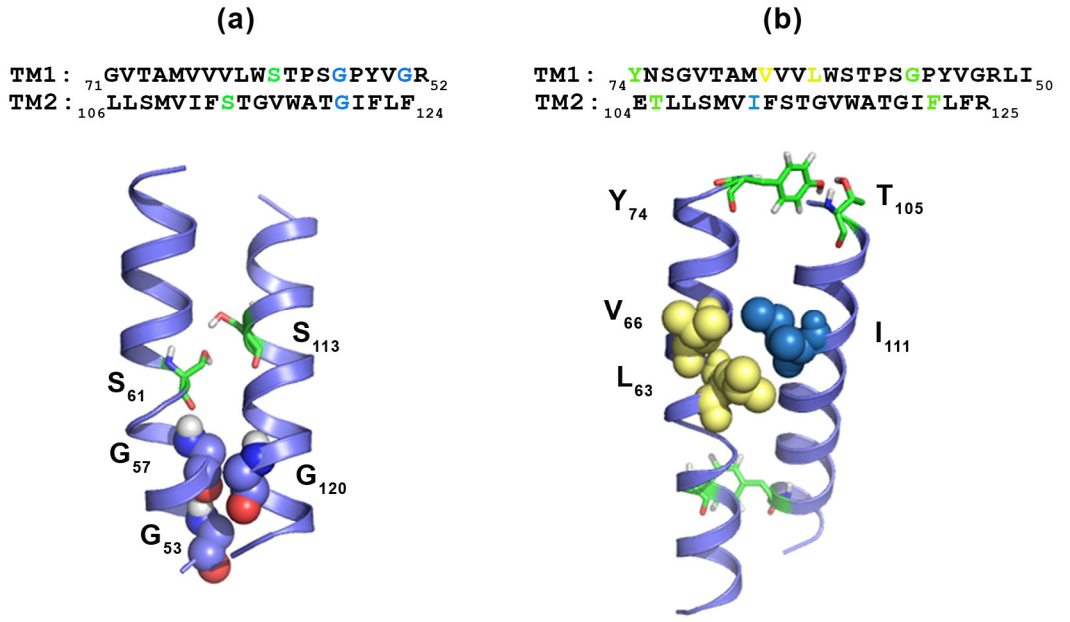

Figure 6.3 - CHI models of possible hetero interactions of TM1-TM2 within the rCPT1B protein. Amino acid sequences and CHI models of (a) rCPT1B iTM1 (G_{71}-R_{52}) - TM2 (L_{106}-F_{124}), (b) rCPT1B iTM1 (Y_{74}-I_{50}) –TM2 (E_{104}-R_{125}) interactions. Individual helices are represented as blue ribbon cartoons and residues are labelled as follows: (a) interacting residues: G_{57}, G_{53} and G_{120} highlighted as spheres coloured by element, hydrogen bonding residues S_{61} and S_{113} are labelled as sticks and coloured by elements. (b) I_{111} highlighted as blue while V_{66} and L_{63} highlighted as yellow spheres, Y_{74} and T_{105} hydrogen bonding residues are labelled as sticks and coloured by elements.

The above models present possible sites of TM1-TM2 interactions that will be investigated experimentally in the future *via* mutagenesis. These results should, of course, be interpreted with caution and must be investigated *in vivo* since the conformation of the TM domains in the full-length protein as inserted into the OMM, as well as the positions of TM1-TM2 relative to each other, could be different which could change the interacting residues and their position. Furthermore, several other combinations of well-known interaction motifs are present in the two sequences which could support the hetero interaction.

6.4 Summary

To complement our homo-oligomerisation studies (CHAPTERS 3-5), in this chapter we investigated the possibility of TM1-TM2 interactions in CPT1 A and B for the first time. Using the GALLEX assay we studied the two different TM1-TM2 interactions in isolation in *E. coli* membranes. The possible contacts between the TM domains were investigated by molecular modelling (CHI).

It is known that changes in CPT1A enzyme kinetics, possibly due to changes in protein structure, occur in response to changes in composition and fluidity of the OMM, suggesting a larger flexibility of this protein, while CPT1B is believed to adopt a more rigid structure that is less sensitive to the membrane environment. This data could suggest that the TM1-TM2 interactions in CPT1B are stronger than those in CPT1A, and therefore more stable in a variety of membrane environments. Alternatively, if the TM1-TM2 interactions in CPT1B were weak, significant changes in these interactions may not be observed upon changing the membrane structure. While we found evidence for TM1-TM2 hetero-interactions in both isoforms using the GALLEX biological assay, the data reported in this chapter cannot prove that the interaction strengths are different in the two isoforms. Only at the lowest protein expression levels do we see a difference, where the TM1-TM2 interaction in CPT1B was slightly weaker than that for CPT1A. In this system, we also need to consider that while the enzyme is in the OMM, both homo and hetero interactions could occur at the same time through TM1 and TM2. Thus, to be able to accurately detect possible differences in hetero oligomerisation, the competition of the two types of interactions (homo, hetero) needs to be taken into account. Further *in vitro* analyses of the observed interactions have to be carried out along with their effects on the folding and enzyme kinetics of the full length protein and mutagenesis of the involved residues.

CHAPTER 7

CONCLUSIONS

Carnitine palmitoyltransferase 1 enzymes responsible for the regulation of mitochondrial fatty acid oxidation have a central role in many cellular mechanisms such as energy homeostasis (in heart and skeletal muscle (Eaton *et al.*, 2001)) or insulin secretion (in pancreatic β-cells (Chen *et al.*, 1994)), and thus are central in cell function (Zammit, 2008). The structural characterization of CPT1 is difficult because of its association with the mitochondrial membrane. Previous studies of the structure-function relationship in CPT1 proposed that the TM1-TM2 interactions affect the inter-cytosolic domain interactions, and hence the kinetics of the enzyme (Zammit *et al.*, 2001). The lack of a detailed crystal structure for these proteins and the unknown but likely role of the TM domains in their observed kinetic characteristics has meant that this system provides an interesting problem to study. In addition, it has been reported that CPT1A forms protein complexes (Faye *et al.*, 2007). At present one of the most significant problems in CPT1 research is the investigation of TM domain structure and oligomerisation and its role in the function of CPT1, which is fundamentally important in the design of pharmacological strategies aimed at the modulation of the activities of these enzymes in conditions such as diabetes (Giannessi *et al.*, 2001).

The aim of this PhD research was to systematically investigate the homo- and hetero- transmembrane domain (TM) interactions, which are involved in modulating folding and driving oligomerisation of the carnitine palmitoyltransferase enzymes, CPT1A and CPT1B. The project involved using different biochemical and biophysical techniques (*in vivo* oligomerisation assays,

chemical cross-linking, circular dichroism and analytical ultracentrifugation) to characterise TM derived peptides.

In the following sections the results presented, their significance and future directions are summarised.

Self-association of CPT1A and CPT1B TM domains

The initial question of the present research was whether the transmembrane spanning regions of CPT1A and CPT1B can form homo-oligomers. For this reason, we first studied the TM sequences using the *in vivo* TOXCAT and GALLEX assays. We observed homo-oligomerisation of these TM domains within natural, *E. coli* membranes. In addition, our experiments also indicated that the length of the TM spanning region greatly affected the results of these assays, which supports previous observations (Li *et al.*, 2004). In light of these results, further investigations were carried out to quantify the oligomerisation propensities of the investigated TM domains. We used synthetic peptides and examined them by *in vitro* biophysical techniques. Cross-linking and AUC experiments both gave strong indications that the TM domains of both isoforms form oligomers, as summarised in **Table 7.1**.

Our work demonstrates, for the first time, that the CPT1A and CPT1B TM spanning regions homo-oligomerise, and quantifies the oligomeric states they can achieve. Since the examined TM segments all contain well-known interaction motifs (§ 1.2.2), we used *in silico* modelling to highlight the interacting residues on the helix-helix interface of the resulting structures. The residues that are of potential importance in stabilizing the observed oligomers are indicated in **Table 7.1**.

In the case of the CPT1A isoform, our results not only quantified the order of its oligomerisation, but also indicated a strong link between the oligomerisation behaviour of TM2 and the *in vivo* oligomerisation of full length rCPT1A. The rCPT1A TM2 domain was found to have a key role in forming the native protein hexamer and trimer when studied *in vivo* (Faye *et al.*, 2007). Here we observed that the synthetic CPT1A TM2 peptide also forms hexamers and trimers when the TM sequence was studied in isolation by cross-linking and AUC-SV. Such close correspondence between the oligomerisation behaviour of the full length rCPT1A

in vivo and those of TM2 segment *in vitro* provided further evidence that TM2 is a site of potentially important protein-protein interactions (Jenei *et al.*, 2009).

While there is a good indication that the oligomeric state formed by TM2 correlates with the full length protein complex (Faye *et al.*, 2007; Jenei *et al.*, 2009), it is not known whether the full length rCPT1B also exists as an oligomer in muscle mitochondria. This raises the question of whether the oligomerisation observed for the rCPT1B TM2 reflects the folding and assembly of full length rCPT1B *in vivo*.

Table 7.1 - Summary of the observed transmembrane helix oligomerisation behaviour.

	CPT1A		CPT1B	
Oligomerisation observed by:	TM1	TM2	TM1	TM2
TOXCAT/GALLEX	+	+	+	+
Cross-linking	3 - 5	3 , 6, 12	3 - 5	3
AUC	5	6 ,12	5	2
Interacting residues observed using CHI modelling: In homo-oligomeric structures:	G_{49}-$G_{53,}$ S_{60}, L_{63}-V_{67}-I_{70}	G_{107}-G_{111} or G_{113}-A_{117}, T_{112}	$R_{52,}$ Y_{55}, $T_{69,}$ S_{72} - N_{73} or G_{53}-G_{57}, T_{60} -S_{61} or T_{69} -S_{72}	L_{106}, V_{110} or $A_{118,}$ S_{108}, F_{122}, R_{125}
In hetero-oligomeric structures interfacial residues:	TM1: V_{54} A_{57} I_{64} TM2: L_{114} G_{111} G_{107} or TM1: I_{51} V_{54} N_{58} TM2: I_{119} T_{112}		TM1: G_{53} G_{57} S_{61} TM2: G_{113} S_{120} or TM1: L_{63} V_{66} Y_{74} TM2: I_{111} T_{105}	

We have found strong similarities between the oligomerisation behaviour of rCPT1A and rCPT1B TM1 domains, when studying their corresponding synthetic peptides with chemical cross-linking or AUC-SV (see **Table 7.1**). However, the TM2 domain of rCPT1B behaved very differently from that of rCPT1A, forming dimers and trimers as opposed to the hexamers formed by rCPT1A TM2. The sequence motifs in the TM2 domains are also significantly different in the two isoforms, and molecular modelling showed different interactions between their amino acids. If TM helix-helix interactions are important in the folding and

enzyme kinetics of CPT1A and B, the above observations suggest that CPT1B would form different oligomers than CPT1A and may display different TM1-TM2 interactions as well. For example, if CPT1B forms oligomeric complexes in the OMM, and its oligomerisation is driven by TM2-TM2 interactions (as suggested for CPT1A), then its oligomeric state would likely be different from that of CPT1A. However, confirming this hypothesis requires more data to directly compare the complex formation for these proteins (see Future directions).

Sequence specificity of the self-association of rCPT1A TM2

As CPT1A oligomerisation appears to be driven primarily by interactions between its TM2 domains, to further explore this effect we investigated the sequence motifs that drive TM2-TM2 interactions. *In silico* models presented in CHAPTER 3 suggest that rCPT1A TM2 oligomerisation to trimers and hexamers is likely driven by the $Gly_{107}xxxGly_{111}$ and $Gly_{113}xxxAla_{117}$ motifs, while Thr_{112} could also have a stabilising effect. To verify the possible role of these sequence motifs we used mutagenesis strategies coupled with *in vivo* and *in vitro* biophysical methods.

Systematic mutagenesis of sequence motifs $G_{103}xxxG_{111}$, $G_{113}xxxA_{117}$ and Thr_{112} was performed using TOXCAT assay. The mutations of $G_{107}I$ and $G_{107}IG_{113}I$ reduced helix interaction by ~50%, without making more than two mutations in the sequence, and these mutations were selected for further studies *in vitro*. Synthetic peptides of the $G_{107}I$ and $G_{107}IG_{113}I$ mutants were both found to form oligomeric species smaller than the *wt* rCPT1A TM2 hexamers, with the most consistent oligomeric state observed for both mutants being the trimer species.

In conclusion, the results presented in CHAPTER 4 propose that the GxxxG(A) motifs play a role in rCPT1A TM2 oligomerisation and also give rise to further questions about the role of these recognised motifs in full length protein assembly and function.

Interaction of TM1-TM2 domains in CPT1A and CPT1B

This work also reports the first direct measurements of TM1-TM2 oligomerisation in these proteins. The data presented in CHAPTER 6 provides evidence for the hetero-interactions of the TM domains in both isoforms.

The interaction between TM domains (both homo and hetero) is believed to be central to the function of CPT1 enzymes. In order to provide evidence for the TM domains hetero oligomerisation in CPT1A and CPT1B the *in vivo* GALLEX assay was used. We showed that TM1 and TM2 domains in both isoforms are capable of interacting in a natural (*E. coli*) membrane environment, and *in silico* models were built to find possible interacting residues supporting TM1-TM2 interactions (see **Table 7.1**). These results could be correlated with folding and enzyme kinetics of the full length CPT1A and CPT1B proteins. However, to verify the observed interactions, further analyses have to be carried out (see in Future directions).

Future directions

Based on our current experimental results strongly supporting interactions between TM domains, the exact role of such interactions in the tertiary structure of CPT1A and CPT1B proteins and in the previously proposed channel formation is still unclear. As shown in **Figure 7.1**, the observed TM helix-helix interactions can be described by several different models that summarize their potential role in driving oligomerisation of the native enzymes into both trimers (as observed for CPT1A and CPT1B TM2) and hexamers (as observed for CPT1A).

For this reason, further *in vitro* analyses would help us to better understand whether these sequences are responsible for forming homo, hetero or both types of interactions, and the role of the suggested interaction motifs also needs to be verified by mutagenesis. The hetero interactions need further investigation as well, because at this point the data reported for TM1-TM2 hetero oligomerisation cannot prove that the interaction strengths are different in the two isoforms. Different interaction strengths would explain the difference in the kinetic behaviour of the isoforms.

To translate our oligomerisation studies of isolated TM domains into biologically relevant data, mutations that resulted in significant disruption in the observed interactions need to be transferred into the full-length proteins. For example, in case of the CPT1A, mutations of $G_{107}I$ and $G_{107}IG_{113}I$ need to be tested. For CPT1B, the oligomerisation of the full length protein needs to be clarified and the role of sequence motifs has to be investigated prior to carrying out mutagenesis of the full-length protein. Analysis of these full-length mutants will yield crucial

information on the functional consequences of altered TM homo- or hetero-interactions.

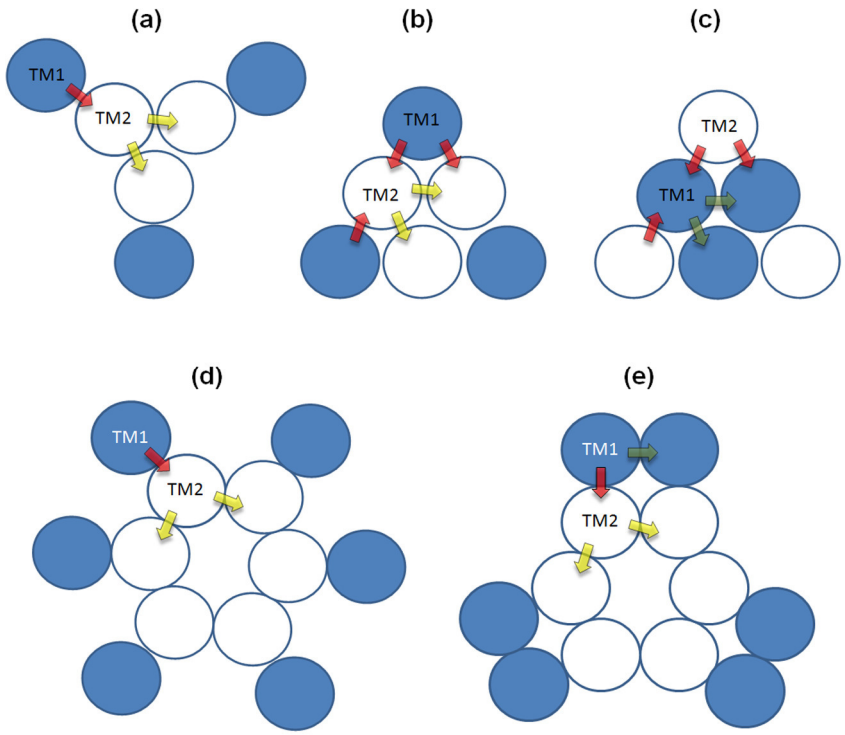

Figure 7.1 - Models of TM interactions in likely CPT1 complex formation. Hetero interactions of TM1-TM2 are indicated as red arrows, while homo-interactions of TM1-TM1 as green and TM2-TM2 as yellow arrows. The trimer and hexamer models shown were preferred considering based on the already observed CPT1A oligomerisation by Faye and colleagues (Faye *et al.*, 2007).

REFERENCES

Adams, P. D., I. T. Arkin, D. M. Engelman and A. T. Brunger (1995). Computational searching and mutagenesis suggest a structure for the pentameric transmembrane domain of phospholamban. *Nat Struct Biol* **2**(2): 154-62.

Adams, P. D., D. M. Engelman and A. T. Brunger (1996). Improved prediction for the structure of the dimeric transmembrane domain of glycophorin A obtained through global searching. *Proteins* **26**(3): 257-61.

Bibi, E. and H. R. Kaback (1990). In vivo expression of the lacY gene in two segments leads to functional lac permease. *Proc Natl Acad Sci U S A* **87**(11): 4325-9.

Bowie, J. U. (2005). Solving the membrane protein folding problem. *Nature* **438**(7068): 581-9.

Brunger, A. T., P. D. Adams, G. M. Clore, W. L. DeLano, P. Gros, R. W. Grosse-Kunstleve, J. S. Jiang, J. Kuszewski, M. Nilges, N. S. Pannu, R. J. Read, L. M. Rice, T. Simonson and G. L. Warren (1998). Crystallography & NMR system: A new software suite for macromolecular structure determination. *Acta Crystallogr D Biol Crystallogr* **54**(Pt 5): 905-21.

Chapman, R., C. Sidrauski and P. Walter (1998). Intracellular signaling from the endoplasmic reticulum to the nucleus. *Annu Rev Cell Dev Biol* **14**: 459-85.

Chen, C. P. and B. Rost (2002). State-of-the-art in membrane protein prediction. *Appl Bioinformatics* **1**(1): 21-35.

Chen, H. and D. A. Kendall (1995). Artificial transmembrane segments. Requirements for stop transfer and polypeptide orientation. *J. Biol. Chem.* **270**(23): 14115-14122.

Chen, S., A. Ogawa, M. Ohneda, R. H. Unger, D. W. Foster and J. D. McGarry (1994). More direct evidence for a malonyl-CoA-carnitine palmitoyltransferase I interaction as a key event in pancreatic beta-cell signaling. *Diabetes* **43**(7): 878-83.

Dai, Y., M. J. Wolfgang, S. H. Cha and M. D. Lane (2007). Localization and effect of ectopic expression of CPT1c in CNS feeding centers. *Biochem Biophys Res Commun* **359**(3): 469-74.

Dawson, J. P., R. A. Melnyk, C. M. Deber and D. M. Engelman (2003). Sequence context strongly modulates association of polar residues in transmembrane helices. *J Mol Biol* **331**(1): 255-62.

Dawson, J. P., J. S. Weinger and D. M. Engelman (2002). Motifs of serine and threonine can drive association of transmembrane helices. *J Mol Biol* **316**(3): 799-805.

DeLano, W. L. (2002). The PyMOL Molecular Graphics System. *DeLano Scientific*.

Ding, F. X., H. Xie, B. Arshava, J. M. Becker and F. Naider (2001). ATR-FTIR study of the structure and orientation of transmembrane domains of the

Saccharomyces cerevisiae alpha-mating factor receptor in phospholipids. *Biochemistry* **40**(30): 8945-54.

Dmitrova, M., G. Younes-Cauet, P. Oertel-Buchheit, D. Porte, M. Schnarr and M. Granger-Schnarr (1998). A new LexA-based genetic system for monitoring and analyzing protein heterodimerization in Escherichia coli. *Mol Gen Genet* **257**(2): 205-12.

Dougherty, D. A. (1996). Cation-pi interactions in chemistry and biology: a new view of benzene, Phe, Tyr, and Trp. *Science* **271**(5246): 163-8.

Doura, A. K., F. J. Kobus, L. Dubrovsky, E. Hibbard and K. G. Fleming (2004). Sequence context modulates the stability of a GxxxG-mediated transmembrane helix-helix dimer. *J Mol Biol* **341**(4): 991-8.

Eaton, S., K. Bartlett and P. A. Quant (2001). Carnitine palmitoyl transferase I and the control of beta-oxidation in heart mitochondria. *Biochem Biophys Res Commun* **285**(2): 537-9.

Engelman, D. M., Y. Chen, C. N. Chin, A. R. Curran, A. M. Dixon, A. D. Dupuy, A. S. Lee, U. Lehnert, E. E. Matthews, Y. K. Reshetnyak, A. Senes and J. L. Popot (2003). Membrane protein folding: beyond the two stage model. *FEBS Lett* **555**(1): 122-5.

Escher, C., F. Cymer and D. Schneider (2009). Two GxxxG-like motifs facilitate promiscuous interactions of the human ErbB transmembrane domains. *J Mol Biol* **389**(1): 10-6.

Faye, A., K. Borthwick, C. Esnous, N. T. Price, S. Gobin, V. N. Jackson, V. A. Zammit, J. Girard and C. Prip-Buus (2005). Demonstration of N- and C-terminal domain intramolecular interactions in rat liver carnitine palmitoyltransferase 1 that determine its degree of malonyl-CoA sensitivity. *Biochem J* **387**(Pt 1): 67-76.

Faye, A., C. Esnous, N. T. Price, M. A. Onfray, J. Girard and C. Prip-Buus (2007). Rat liver carnitine palmitoyltransferase 1 forms an oligomeric complex within the outer mitochondrial membrane. *J Biol Chem* **282**(37): 26908-16.

Finger, C., T. Volkmer, A. Prodohl, D. E. Otzen, D. M. Engelman and D. Schneider (2006). The stability of transmembrane helix interactions measured in a biological membrane. *J Mol Biol* **358**(5): 1221-8.

Fisher, L. E., D. M. Engelman and J. N. Sturgis (1999). Detergents modulate dimerization, but not helicity, of the glycophorin A transmembrane domain. *J Mol Biol* **293**(3): 639-51.

Fisher, L. E., D. M. Engelman and J. N. Sturgis (2003). Effect of detergents on the association of the glycophorin a transmembrane helix. *Biophys J* **85**(5): 3097-105.

Fleishman, S. J. and N. Ben-Tal (2002). A novel scoring function for predicting the conformations of tightly packed pairs of transmembrane alpha-helices. *J Mol Biol* **321**(2): 363-78.

Fleming, K. G., A. L. Ackerman and D. M. Engelman (1997). The effect of point mutations on the free energy of transmembrane alpha-helix dimerization. *J Mol Biol* **272**(2): 266-75.

Fleming, K. G., C. C. Ren, A. K. Doura, M. E. Eisley, F. J. Kobus and A. M. Stanley (2004). Thermodynamics of glycophorin A transmembrane helix dimerization in C14 betaine micelles. *Biophys Chem* **108**(1-3): 43-9.

Fraser, F., C. G. Corstorphine and V. A. Zammit (1997). Topology of carnitine palmitoyltransferase I in the mitochondrial outer membrane. *Biochem J* **323 (Pt 3)**: 711-8.

Gaddie, K. J. and T. L. Kirley (2009). Conserved polar residues stabilize transmembrane domains and promote oligomerization in human nucleoside triphosphate diphosphohydrolase 3. *Biochemistry* **48**(40): 9437-47.

Gerber, D., N. Sal-Man and Y. Shai (2004). Two motifs within a transmembrane domain, one for homodimerization and the other for heterodimerization. *J Biol Chem* **279**(20): 21177-82.

Giannessi, F., P. Chiodi, M. Marzi, P. Minetti, P. Pessotto, F. De Angelis, E. Tassoni, R. Conti, F. Giorgi, M. Mabilia, N. Dell'Uomo, S. Muck, M. O. Tinti, P. Carminati and A. Arduini (2001). Reversible carnitine palmitoyltransferase inhibitors with broad chemical diversity as potential antidiabetic agents. *J Med Chem* **44**(15): 2383-6.

Granseth, E., S. Seppala, M. Rapp, D. O. Daley and G. Von Heijne (2007). Membrane protein structural biology--how far can the bugs take us? *Mol Membr Biol* **24**(5-6): 329-32.

Grantham, B. D. and V. A. Zammit (1986). Restoration of the properties of carnitine palmitoyltransferase I in liver mitochondria during re-feeding of starved rats. *Biochem J* **239**(2): 485-8.

Groves, J. D. and M. J. Tanner (1995). Co-expressed complementary fragments of the human red cell anion exchanger (band 3, AE1) generate stilbene disulfonate-sensitive anion transport. *J Biol Chem* **270**(16): 9097-105.

Gurezka, R., R. Laage, B. Brosig and D. Langosch (1999). A heptad motif of leucine residues found in membrane proteins can drive self-assembly of artificial transmembrane segments. *J Biol Chem* **274**(14): 9265-70.

Gurezka, R. and D. Langosch (2001). In vitro selection of membrane-spanning leucine zipper protein-protein interaction motifs using POSSYCCAT. *J Biol Chem* **276**(49): 45580-7.

Harrington, S. E. and N. Ben-Tal (2009). Structural determinants of transmembrane helical proteins. *Structure* **17**(8): 1092-103.

Jackson, V. N., J. M. Cameron, F. Fraser, V. A. Zammit and N. T. Price (2000). Use of six chimeric proteins to investigate the role of intramolecular interactions in determining the kinetics of carnitine palmitoyltransferase I isoforms. *J Biol Chem* **275**(26): 19560-6.

Jackson, V. N., N. T. Price and V. A. Zammit (2001). Specificity of the interactions between Glu-3, Ser-24, and Gln-30 within the N-terminal segment of rat liver mitochondrial overt carnitine palmitoyltransferase (L-CPT I) in determining the malonyl-CoA sensitivity of the enzyme. *Biochemistry* **40**(48): 14629-34.

Jenei, Z. A., K. Borthwick, V. A. Zammit and A. M. Dixon (2009). Self-association of transmembrane domain 2 (TM2), but not TM1, in carnitine palmitoyltransferase 1A: role of GXXXG(A) motifs. *J Biol Chem* **284**(11): 6988-97.

Johnson, R. M., K. Hecht and C. M. Deber (2007). Aromatic and cation-pi interactions enhance helix-helix association in a membrane environment. *Biochemistry* **46**(32): 9208-14.

Johnson, W. C. (1999). Analyzing protein circular dichroism spectra for accurate secondary structures. *Proteins* **35**(3): 307-12.

Kochendoerfer, G. G., D. Salom, J. D. Lear, R. Wilk-Orescan, S. B. Kent and W. F. DeGrado (1999). Total chemical synthesis of the integral membrane protein influenza A virus M2: role of its C-terminal domain in tetramer assembly. *Biochemistry* **38**(37): 11905-13.

Kolodziej, M. P. and V. A. Zammit (1990). Sensitivity of inhibition of rat liver mitochondrial outer-membrane carnitine palmitoyltransferase by malonyl-CoA to chemical- and temperature-induced changes in membrane fluidity. *Biochem J* **272**(2): 421-5.

Langosch, D., B. Brosig, H. Kolmar and H. J. Fritz (1996). Dimerisation of the glycophorin A transmembrane segment in membranes probed with the ToxR transcription activator. *J Mol Biol* **263**(4): 525-30.

Langosch, D. and J. Heringa (1998). Interaction of transmembrane helices by a knobs-into-holes packing characteristic of soluble coiled coils. *Proteins* **31**(2): 150-9.

Laue, T. M., Shah, B. D., Ridgeway, T. M., and Pelletier, S. L. (1992). SEDNTERP. Analytical Ultracentrifugation in Biochemistry and Polymer Science. S. E. Harding, Rowe, A. J., and Horton, J. C., Royal Society of Chemistry, Cambridge**:** 90–125.

Laue, T. M. and W. F. Stafford, 3rd (1999). Modern applications of analytical ultracentrifugation. *Annu Rev Biophys Biomol Struct* **28**: 75-100.

Lavrentyev, E. N., S. G. Matta and G. A. Cook (2004). Expression of three carnitine palmitoyltransferase-I isoforms in 10 regions of the rat brain during feeding, fasting, and diabetes. *Biochem Biophys Res Commun* **315**(1): 174-8.

Lazarova, T., K. A. Brewin, K. Stoeber and C. R. Robinson (2004). Characterization of peptides corresponding to the seven transmembrane domains of human adenosine A2a receptor. *Biochemistry* **43**(40): 12945-54.

Lees, J. G., A. J. Miles, F. Wien and B. A. Wallace (2006). A reference database for circular dichroism spectroscopy covering fold and secondary structure space. *Bioinformatics* **22**(16): 1955-62.

Lemmon, M. A. and D. M. Engelman (1994). Specificity and promiscuity in membrane helix interactions. *Q Rev Biophys* **27**(2): 157-218.

Lemmon, M. A., J. M. Flanagan, J. F. Hunt, B. D. Adair, B. J. Bormann, C. E. Dempsey and D. M. Engelman (1992). Glycophorin A dimerization is driven by specific interactions between transmembrane alpha-helices. *J Biol Chem* **267**(11): 7683-9.

Li, R., C. R. Babu, J. D. Lear, A. J. Wand, J. S. Bennett and W. F. DeGrado (2001). Oligomerization of the integrin alphaIIbbeta3: roles of the transmembrane and cytoplasmic domains. *Proc Natl Acad Sci U S A* **98**(22): 12462-7.

Li, R., R. Gorelik, V. Nanda, P. B. Law, J. D. Lear, W. F. DeGrado and J. S. Bennett (2004). Dimerization of the transmembrane domain of Integrin alphaIIb subunit in cell membranes. *J Biol Chem* **279**(25): 26666-73.

Liao, M. J., K. S. Huang and H. G. Khorana (1984). Regeneration of native bacteriorhodopsin structure from fragments. *J Biol Chem* **259**(7): 4200-4.

Liu, L. P. and C. M. Deber (1998). Guidelines for membrane protein engineering derived from de novo designed model peptides. *Biopolymers* **47**(1): 41-62.

Liu, W., E. Crocker, D. J. Siminovitch and S. O. Smith (2003). Role of side-chain conformational entropy in transmembrane helix dimerization of glycophorin A. *Biophys J* **84**(2 Pt 1): 1263-71.

MacKenzie, K. R. and K. G. Fleming (2008). Association energetics of membrane spanning alpha-helices. *Curr Opin Struct Biol* **18**(4): 412-9.

MacKenzie, K. R., J. H. Prestegard and D. M. Engelman (1997). A transmembrane helix dimer: structure and implications. *Science* **276**(5309): 131-3.

McGarry, J. D. and N. F. Brown (1997). The mitochondrial carnitine palmitoyltransferase system. From concept to molecular analysis. *Eur J Biochem* **244**(1): 1-14.

McGarry, J. D. and N. F. Brown (2000). Reconstitution of purified, active and malonyl-CoA-sensitive rat liver carnitine palmitoyltransferase I: relationship between membrane environment and malonyl-CoA sensitivity. *Biochem J* **349**(Pt 1): 179-87.

Melnyk, R. A., A. W. Partridge, J. Yip, Y. Wu, N. K. Goto and C. M. Deber (2003). Polar residue tagging of transmembrane peptides. *Biopolymers* **71**(6): 675-85.

Merril, C. R., M. L. Dunau and D. Goldman (1981). A rapid sensitive silver stain for polypeptides in polyacrylamide gels. *Anal Biochem* **110**(1): 201-7.

Merril, C. R. and M. E. Pratt (1986). A silver stain for the rapid quantitative detection of proteins or nucleic acids on membranes or thin layer plates. *Anal Biochem* **156**(1): 96-110.

Morillas, M., P. Gomez-Puertas, B. Rubi, J. Clotet, J. Arino, A. Valencia, F. G. Hegardt, D. Serra and G. Asins (2002). Structural model of a malonyl-CoA-binding site of carnitine octanoyltransferase and carnitine palmitoyltransferase I: mutational analysis of a malonyl-CoA affinity domain. *J Biol Chem* **277**(13): 11473-80.

Mynatt, R. L., M. D. Lappi and G. A. Cook (1992). Myocardial carnitine palmitoyltransferase of the mitochondrial outer membrane is not altered by fasting. *Biochim Biophys Acta* **1128**(1): 105-11.

Nilsson, I., A. Saaf, P. Whitley, G. Gafvelin, C. Waller and G. von Heijne (1998). Proline-induced disruption of a transmembrane alpha-helix in its natural environment. *J Mol Biol* **284**(4): 1165-75.

Nilsson, I. and G. von Heijne (1998). Breaking the camel's back: proline-induced turns in a model transmembrane helix. *J Mol Biol* **284**(4): 1185-9.

Oates, J., M. Hicks, T. R. Dafforn, D. DiMaio and A. M. Dixon (2008). In vitro dimerization of the bovine papillomavirus E5 protein transmembrane domain. *Biochemistry* **47**(34): 8985-92.

Orzaez, M., J. Salgado, A. Gimenez-Giner, E. Perez-Paya and I. Mingarro (2004). Influence of proline residues in transmembrane helix packing. *J Mol Biol* **335**(2): 631-40.

Park, E. A. and G. A. Cook (1998). Differential regulation in the heart of mitochondrial carnitine palmitoyltransferase-I muscle and liver isoforms. *Mol Cell Biochem* **180**(1-2): 27-32.

Paulson, D. J., K. M. Ward and A. L. Shug (1984). Malonyl CoA inhibition of carnitine palmityltransferase in rat heart mitochondria. *FEBS Lett* **176**(2): 381-4.

Popot, J. L. and D. M. Engelman (1990). Membrane protein folding and oligomerization: the two-stage model. *Biochemistry* **29**(17): 4031-7.

Popot, J. L., S. E. Gerchman and D. M. Engelman (1987). Refolding of bacteriorhodopsin in lipid bilayers. A thermodynamically controlled two-stage process. *J Mol Biol* **198**(4): 655-76.

Price, N., F. van der Leij, V. Jackson, C. Corstorphine, R. Thomson, A. Sorensen and V. Zammit (2002). A novel brain-expressed protein related to carnitine palmitoyltransferase I. *Genomics* **80**(4): 433-42.

Rabilloud, T. (1990). Mechanisms of protein silver staining in polyacrylamide gels: a 10-year synthesis. *Electrophoresis* **11**(10): 785-94.

Ridge, K. D., S. S. Lee and L. L. Yao (1995). In vivo assembly of rhodopsin from expressed polypeptide fragments. *Proc Natl Acad Sci U S A* **92**(8): 3204-8.

Rijkers, D. T. S., J. A. W. Kruijtzer, J. A. Killian and R. M. J. Liskamp (2005). A convenient solid phase synthesis of S-palmitoyl transmembrane peptides. *Tetrahedron Letters* **46**(19): 3341-3345.

Ruan, W., V. Becker, U. Klingmuller and D. Langosch (2004). The interface between self-assembling erythropoietin receptor transmembrane segments corresponds to a membrane-spanning leucine zipper. *J Biol Chem* **279**(5): 3273-9.

Russ, W. P. and D. M. Engelman (1999). TOXCAT: a measure of transmembrane helix association in a biological membrane. *Proc Natl Acad Sci U S A* **96**(3): 863-8.

Russ, W. P. and D. M. Engelman (2000). The GxxxG motif: a framework for transmembrane helix-helix association. *J Mol Biol* **296**(3): 911-9.

Saggerson, D., I. Ghadiminejad and M. Awan (1992). Regulation of mitochondrial carnitine palmitoyl transferases from liver and extrahepatic tissues. *Advances in Enzyme Regulation* **32**: 285-306.

Saggerson, E. D. (1982). Carnitine acyltransferase activities in rat liver and heart measured with palmitoyl-CoA and octanoyl-CoA. Latency, effects of K+, bivalent metal ions and malonyl-CoA. *Biochem J* **202**(2): 397-405.

Sal-Man, N., D. Gerber, I. Bloch and Y. Shai (2007). Specificity in transmembrane helix-helix interactions mediated by aromatic residues. *J Biol Chem* **282**(27): 19753-61.

Sal-Man, N., D. Gerber and Y. Shai (2004). The composition rather than position of polar residues (QxxS) drives aspartate receptor transmembrane domain dimerization in vivo. *Biochemistry* **43**(8): 2309-13.

Salom, D., B. R. Hill, J. D. Lear and W. F. DeGrado (2000). pH-dependent tetramerization and amantadine binding of the transmembrane helix of M2 from the influenza A virus. *Biochemistry* **39**(46): 14160-70.

Sambrook, J. and D. W. Russel (2001). Molecular Cloning - A Laboratory Manual., Cold Spring Habour, N.Y.: Cold Spring Habour Laboratory Press.

.

Sanders, C. R. and J. K. Myers (2004). Disease-related misassembly of membrane proteins. *Annu Rev Biophys Biomol Struct* **33**: 25-51.

Sanders, C. R. and J. K. Nagy (2000). Misfolding of membrane proteins in health and disease: the lady or the tiger? *Curr Opin Struct Biol* **10**(4): 438-42.

Sanders, C. R. and F. Sonnichsen (2006). Solution NMR of membrane proteins: practice and challenges. *Magn Reson Chem* **44 Spec No**: S24-40.

Schneider, D. and D. M. Engelman (2003). GALLEX, a measurement of heterologous association of transmembrane helices in a biological membrane. *J Biol Chem* **278**(5): 3105-11.

Schneider, D. and D. M. Engelman (2004). Motifs of two small residues can assist but are not sufficient to mediate transmembrane helix interactions. *J Mol Biol* **343**(4): 799-804.

Schuck, P. (2000). Size-distribution analysis of macromolecules by sedimentation velocity ultracentrifugation and Lamm equation modeling. *Biophys J* **78**(3): 1606-1619.

Schuck, P., M. A. Perugini, N. R. Gonzales, G. J. Howlett and D. Schubert (2002). Size-distribution analysis of proteins by analytical ultracentrifugation: strategies and application to model systems. *Biophys J* **82**(2): 1096-111.

Senes, A., D. E. Engel and W. F. DeGrado (2004). Folding of helical membrane proteins: the role of polar, GxxxG-like and proline motifs. *Curr Opin Struct Biol* **14**(4): 465-79.

Senes, A., M. Gerstein and D. M. Engelman (2000). Statistical analysis of amino acid patterns in transmembrane helices: the GxxxG motif occurs frequently and in association with beta-branched residues at neighboring positions. *J Mol Biol* **296**(3): 921-36.

Seubert, N., Y. Royer, J. Staerk, K. F. Kubatzky, V. Moucadel, S. Krishnakumar, S. O. Smith and S. N. Constantinescu (2003). Active and inactive orientations of the transmembrane and cytosolic domains of the erythropoietin receptor dimer. *Mol Cell* **12**(5): 1239-50.

Shi, J., H. Zhu, D. N. Arvidson and G. Woldegiorgis (1999). A single amino acid change (substitution of glutamate 3 with alanine) in the N-terminal region of rat liver carnitine palmitoyltransferase I abolishes malonyl-CoA inhibition and high affinity binding. *J Biol Chem* **274**(14): 9421-6.

Simmerman, H. K., Y. M. Kobayashi, J. M. Autry and L. R. Jones (1996). A leucine zipper stabilizes the pentameric membrane domain of phospholamban and forms a coiled-coil pore structure. *J Biol Chem* **271**(10): 5941-6.

Singer, S. J. and G. L. Nicolson (1972). The fluid mosaic model of the structure of cell membranes. *Science* **175**(23): 720-31.

Sonnhammer, E. L., G. von Heijne and A. Krogh (1998). A hidden Markov model for predicting transmembrane helices in protein sequences. *Proc Int Conf Intell Syst Mol Biol* **6**: 175-82.

Sreerama, N. and R. W. Woody (2000). Estimation of protein secondary structure from circular dichroism spectra: comparison of CONTIN,

SELCON, and CDSSTR methods with an expanded reference set. *Anal Biochem* **287**(2): 252-60.

Staros, J. V. (1982). N-hydroxysulfosuccinimide active esters: bis(N-hydroxysulfosuccinimide) esters of two dicarboxylic acids are hydrophilic, membrane-impermeant, protein cross-linkers. *Biochemistry* **21**(17): 3950-5.

Switzer, R. C., 3rd, C. R. Merril and S. Shifrin (1979). A highly sensitive silver stain for detecting proteins and peptides in polyacrylamide gels. *Anal Biochem* **98**(1): 231-7.

Tamm, L. K., H. Hong and B. Liang (2004). Folding and assembly of beta-barrel membrane proteins. *Biochim Biophys Acta* **1666**(1-2): 250-63.

Treptow, N. A. and H. A. Shuman (1985). Genetic evidence for substrate and periplasmic-binding-protein recognition by the MalF and MalG proteins, cytoplasmic membrane components of the Escherichia coli maltose transport system. *J Bacteriol* **163**(2): 654-60.

Treutlein, H. R., M. A. Lemmon, D. M. Engelman and A. T. Brunger (1992). The glycophorin A transmembrane domain dimer: sequence-specific propensity for a right-handed supercoil of helices. *Biochemistry* **31**(51): 12726-32.

van der Leij, F. R., A. M. Kram, B. Bartelds, H. Roelofsen, G. B. Smid, J. Takens, V. A. Zammit and J. R. Kuipers (1999). Cytological evidence that the C-terminus of carnitine palmitoyltransferase I is on the cytosolic face of the mitochondrial outer membrane. *Biochem J* **341 (Pt 3)**: 777-84.

von Heijne, G. (1991). Proline kinks in transmembrane alpha-helices. *J Mol Biol* **218**(3): 499-503.

von Heijne, G. (1996). Principles of membrane protein assembly and structure. *Prog Biophys Mol Biol* **66**(2): 113-39.

Walters, R. F. and W. F. DeGrado (2006). Helix-packing motifs in membrane proteins. *Proc Natl Acad Sci U S A* **103**(37): 13658-63.

White, S. H. (2003). Translocons, thermodynamics, and the folding of membrane proteins. *FEBS Lett* **555**(1): 116-21.

White, S. H. and W. C. Wimley (1999). Membrane protein folding and stability: physical principles. *Annu Rev Biophys Biomol Struct* **28**: 319-65.

Whitmore, L. and B. A. Wallace (2008). Protein secondary structure analyses from circular dichroism spectroscopy: methods and reference databases. *Biopolymers* **89**(5): 392-400.

Wimley, W. C. (2003). The versatile beta-barrel membrane protein. *Curr Opin Struct Biol* **13**(4): 404-11.

Wolfgang, M. J., T. Kurama, Y. Dai, A. Suwa, M. Asaumi, S. Matsumoto, S. H. Cha, T. Shimokawa and M. D. Lane (2006). The brain-specific carnitine palmitoyltransferase-1c regulates energy homeostasis. *Proc Natl Acad Sci U S A* **103**(19): 7282-7.

Zammit, V. A. (1999). The malonyl-CoA-long-chain acyl-CoA axis in the maintenance of mammalian cell function. *Biochem J* **343 Pt 3**: 505-15.

Zammit, V. A. (2008). Carnitine palmitoyltransferase 1: central to cell function. *IUBMB Life* **60**(5): 347-54.

Zammit, V. A., C. G. Corstorphine, M. P. Kolodziej and F. Fraser (1998). Lipid molecular order in liver mitochondrial outer membranes, and sensitivity of carnitine palmitoyltransferase I to malonyl-CoA. *Lipids* **33**(4): 371-6.

Zammit, V. A., N. T. Price, F. Fraser and V. N. Jackson (2001). Structure-function relationships of the liver and muscle isoforms of carnitine palmitoyltransferase I. *Biochem Soc Trans* **29**(Pt 2): 287-92.

Zhou, F. X., M. J. Cocco, W. P. Russ, A. T. Brunger and D. M. Engelman (2000). Interhelical hydrogen bonding drives strong interactions in membrane proteins. *Nat Struct Biol* **7**(2): 154-60.

Zhou, F. X., H. J. Merianos, A. T. Brunger and D. M. Engelman (2001). Polar residues drive association of polyleucine transmembrane helices. *Proc Natl Acad Sci U S A* **98**(5): 2250-5.

APPENDIX

Appendix 1: Oligonucleotide sequences were used to modify pCC-KAN plasmid vector. DNA letter coding*: C=cytosine, G= guanine, A=adenine, T=thymine.* Colour coding: Gly or Ala to Ile mutations are highlighted with yellow, Thr to Ala mutations are highlighted with green and Thr to Val mutations are highlighted with purple. The oligonucleotide sequences shown in capital letters were used as quick change primers, while sequences shown in lower case letters were used as primers for ligation reaction. Rows highlighted with blue correspond to rCPT1A TM1, with green to rCPT1A TM2, with purple to rCPT1B TM1, and with orange to rCPT1B TM2 primers.

Primer	Sequence 5' to 3'
rCPT1A TM1(27)for	**ctagc** aaa aac ggc att att acc ggc gtg ttt ccg gcg aac ccg agc agc tgg ctg att gtg gtg gtg ggc gtg att agc agc atg **gg**
rCPT1A TM1(27)rev	**gatccc** cat gct gct aat cac gcc cac cac cac aat cag cca gct gct cgg gtt cgc cgg aaa cac gcc ggt aat aat gcc gtt ttt **g**
rCPT1A TM1(24)for	**GGGAATCGAGCTAGCATTATTACCGGCGTG**
rCPT1A TM1(24)rev	**CACGCCGGTAATAATGCTAGCTCGATTCCC**
rCPT1A TM1(21)for	**GTGGTGGGCGTGATTGGGATCCTGATCAAC**
rCPT1A TM1(21)rev	**GTTGATCAGGATCCCAATCACGCCCACCAC**
rCPT1A TM1(18)for	**ctagc** att att acc ggc gtg ttt ccg gcg aac ccg agc agc tgg ctg att gtg gtg gtg **gg**
rCPT1A TM1(18)rev	**gatccc** cac cac cac aat cag cca gct gct cgg gtt cgc cgg aaa cac gcc ggt aat aat **g**
rCPT1A TM1(16)for	**ctagc** acc ggc gtg ttt ccg gcg aac ccg agc agc tgg ctg att gtg gtg gtg **gg**
rCPT1A TM1(16)rev	**gatccc** cac cac cac aat cag cca gct gct cgg gtt cgc cgg aaa cac gcc ggt **g**
rCPT1A TM2(22)for	**ctagc** aaa aac att gtg agc ggc gtg ctg ttt ggc acc ggc ctg tgg gtg gcg gtg att atg acc atg cgc **gg**
rCPT1A TM2(22)rev	**gatccc** gcg cat ggt cat aat cac cgc cac cca cag gcc ggt gcc aaa cag cac gcc gct cac aat gtt ttt **g**
rCPT1A TM2(20)for	**GCGGTGATTATGACCGGGATCCTGATCAAC**
rCPT1A TM2(20)rev	**GTTGATCAGGATCCCGGTCATAATCACCGC**

Primer	Sequence 5' to 3'
rCPT1A TM2(18)for	**GGGAATCGAGCTAGCATTGTGAGCGGCGTG**
rCPT1A TM2(18)rev	**CACGCCGCTCACAATGCTAGCTCGATTCCC**
rCPT1A TM2(16)for	**CTGTGGGTGGCGGTGATTGGGATCCTGATCAAC**
rCPT1A TM2(16)rev	**GTTGATCAGGATCCCAATCACCGCCACCCACAG**
rCPT1A TM2(16)_G107Ifor	**CTAGCATTGTGAGCATTGTGCTGTTTGGCAC**
rCPT1A TM2(16)_G107Irev	**GTGCCAAACAGCACAATGCTCACAATGCTAG**
rCPT1A TM2(16)_G111Ifor	**ctagc** att gtg agc ggc gtg ctg ttt att acc ggc ctg tgg gtg gcg gtg att **gg**
rCPT1A TM2(16)_G111Irev	**gatccc** aat cac cgc cac cca cag gcc ggt aat aaa cag cac gcc gct cac aat **g**
rCPT1A TM2(16)_G113Ifor	**CTGTTTGGCACCATTCTGTGGGTGGCG**
rCPT1A TM2(16)_G113Irev	**CGCCACCCACAGAATGGTGCCAAACAG**
rCPT1A TM2(16)_A117Ifor	**GGCCTGTGGGTGATTGTGATTGGGATC**
rCPT1A TM2(16)_A117Irev	**GATCCCAATCACAATCACCCACAGGCC**
rCPT1A TM2(16)_G107IG111Ifor	**ctagc** att gtg agc att gtg ctg ttt att acc ggc ctg tgg gtg gcg gtg att **gg**
rCPT1A TM2(16)_G107IG111Irev	**gatccc** aat cac cgc cac cca cag gcc ggt aat aaa cag cac aat gct cac aat **g**
rCPT1A TM2(16) _G113IA117Ifor	**CCATTCTGTGGGTGATTGTGATTGGGATCC**
rCPT1A TM2(16) _G113IA117Irev	**GGATCCCAATCACAATCACCCACAGAATGG**
rCPT1A TM2(16)_G107IG113Ifor	**CTGTTTGGCACCATTCTGTGGGTGGCG**

Primer	Sequence 5' to 3'
rCPT1A TM2(16)_G107IG113Irev	CGCCACCCACAGAATGGTGCCAAACAG
rCPT1A TM2(16)_G107IG111IG113IA117Ifor	ctagc att gtg agc att gtg ctg ttt att acc att ctg tgg gtg att gtg att gg
rCPT1A TM2(16)_G107IG111IG113IA117Irev	gatccc aat cac aat cac cca cag aat ggt aat aaa cag cac aat gct cac aat g
rCPT1A TM2(16) _T112Afor	GTGCTGTTTGGCGCCGGCCTGTGGGTG
rCPT1A TM2(16) _T112Arev	CACCCACAGGCCGGCGCCAAACAGCAC
rCPT1A TM2(16)_G107IG113IT112Afor	GCATTGTGCTGTTTGGCGCCATTCTGTGGGTGGCGG
rCPT1A TM2(16)_G107IG113IT112Arev	CCGCCACCCACAGAATGGCGCCAAACAGCACAATGC
rCPT1A TM2(16)_G107IG113IT112Vfor	GCATTGTGCTGTTTGGCGTGATTCTGTGGGTGGCGG
rCPT1A TM2(16)_G107IG113IT112Vrev	CCGCCACCCACAGAATCACGCCAAACAGCACAATGC
rCPT1A TM2(16)_G107IG111IG113IA117IT112Afor	GTGCTGTTTATTGCCATTCTGTGGGTG
rCPT1A TM2(16)_G107IG111IG113IA117IT112Arev	CACCCACAGAATGGCAATAAACAGCAC
rCPT1A TM2(16)_G107IG111IG113IA117IT112Vfor	GTGCTGTTTATTGTGATTCTGTGGGTG
rCPT1A TM2(16)_G107IG111IG113IA117IT112Vrev	CACCCACAGAATCACAATAAACAGCAC
rCPT1B TM1(25)for	ctagc cgc ggc gtg tat ccg ggc agc ccg acc agc tgg ctg gtg gtg gtg atg gcg acc gtg ggc agc aac tat tgc aaa gg
rCPT1B TM1(25)rev	gatccc ttt gca ata gtt gct gcc cac cct cgc cat cac cac cac cag cca gct ggt cgg gct gcc cgg ata cac gcc gcg g
rCPT1B TM1(22)for	GGGAATCGAGCTAGCTATCCGGGCAGCCCG
rCPT1B TM1(22)rev	CGGGCTGCCCGGATAGCTAGCTCGATTCCC

Primer	Sequence 5' to 3'
rCPT1B TM1(24)for	**GAATCGAGCTAGCAATGGCATCCTGCGCGGCGTGTATC**
rCPT1B TM1(24)rev	**GATACACGCCGCGCAGGATGCCATTGCTAGCTCGATTC**
rCPT1B TM1(23)for	**GTGGGCAGCAACTATGGGATCCTGATCAAC**
rCPT1B TM1(23)rev	**GTTGATCAGGATCCCATAGTTGCTGCCCAC**
rCPT1B TM1(22*)for	**CGTGGGCAGCAACGGGATCCTGATC**
rCPT1B TM1(22*)rev	**GATCAGGATCCCGTTGCTGCCCACG**
rCPT1B TM1(20*)for	**GGCGACCGTGGGCGGGATCCTGATC**
rCPT1B TM1(20*)rev	**GATCAGGATCCCGCCCACGGTCGCC**
rCPT1B TM2(22)for	**ctagc** gaa acc ctg ctg agc atg gtg att ttt agc acc ggc gtg tgg gcg acc ggc att ttt ctg ttt cgc **gg**
rCPT1B TM2(22)rev	**gatcc**c gcg aaa cag aaa aat gcc ggt cgc cca cac gcc ggt gct aaa aat cac cat gct cag cag ggt ttc **g**
rCPT1B TM2(20)for	**GGGAATCGAGCTAGCCTGCTGAGCATGGTG**
rCPT1B TM2(20)rev	**CACCATGCTCAGCAGGCTAGCTCGATTCCC**
rCPT1B TM2(19)for	**CCGGCATTTTTCTGTTTGGGATCCTGATCAACCC**
rCPT1B TM2(19)rev	**GGGTTGATCAGGATCCCAAACAGAAAAATGCCGG**
rCPT1B TM2(17)for	**GCGACCGGCATTTTTGGGATCCTGATCAAC**
rCPT1B TM2(17)rev	**GTTGATCAGGATCCCAAAAATGCCGGTCGC**

Appendix 2: Oligonucleotide sequences were used to modify pALM148 or pBLM100 plasmid vectors.
DNA letter coding*: C=cytosine, G= guanine, =A=adenine, T=thymine.*

Primer	Sequence 5' to 3'
rCPT1A iTM1(21)for	**c**g att gtg ggc gtg gtg gtg att ctg tgg agc agc ccg aac gcg ccg ttt gtg ggc acc att att **a**
rCPT1A iTM1(21)for	**ctagt** aat aat ggt gcc cac aaa cgg cgc gtt cgg gct gct cca cag aat cac cac cac gcc cac aat **cgagct**
rCPT1A iTM1(18)for	**c**g gtg gtg gtg att ctg tgg agc agc ccg aac gcg ccg ttt gtg ggc acc att att **a**
rCPTA iTM1(18)rev	**ctagt** aat aat ggt gcc cac aaa cgg cgc gtt cgg gct gct cca cag aat cac cac cac **cgagct**
rCPT1A iTM1(16)for	**c**g gtg gtg gtg att ctg tgg agc agc ccg aac gcg ccg ttt gtg ggc acc **a**
rCPT1A iTM1(16)rev	**ctagt** ggt gcc cac aaa cgg cgc gtt cgg gct gct cca cag aat cac cac cac **cgagct**
rCPT1A TM2(16)for	**c**g att gtg agc ggc gtg ctg ttt ggc acc ggc ctg tgg gtg gcg gtg att **a**
rCPT1A TM2(16)rev	**ctagt** aat cac cgc cac cca cag gcc ggt gcc aaa cag cac gcc gct cac aat **cgagct**
rCPT1B iTM1(20)for	**c**g ggc gtg acc gcg atg gtg gtg gtg ctg tgg agc acc ccg agc ggc ccg tat gtg ggc cgt **a**
rCPT1B iTM1(20)rev	**ctagt** acg gcc cac ata cgg gcc gct cgg ggt gct cca cag cac cac cac cat cgc ggt cac gcc **cgagct**
rCPT1B TM2(19)for	**c**g ctg ctg agc atg gtg att ttt agc acc ggc gtg tgg gcg acc ggc att ttt ctg ttt **a**
rCPT1B TM2(19)rev	**ctagt** aaa cag aaa aat gcc ggt cgc cca cac gcc ggt gct aaa aat cac cat gct cag cag **cgagct**

THE JOURNAL OF BIOLOGICAL CHEMISTRY VOL. 284, NO. 11, pp. 6988–6997, March 13, 2009

Self-association of Transmembrane Domain 2 (TM2), but Not TM1, in Carnitine Palmitoyltransferase 1A

*ROLE OF GXXXG(A) MOTIFS**

Received for publication, November 7, 2008, and in revised form, December 17, 2008 Published, JBC Papers in Press, January 9, 2009, DOI 10.1074/jbc.M808487200

Zsuzsanna A. Jenei[‡], Karen Borthwick[§], Victor A. Zammit[§], and Ann M. Dixon[‡1]

From the [‡]Department of Chemistry and [§]Clinical Sciences Research Institute, Warwick Medical School, University of Warwick, Coventry CV4 7AL, United Kingdom

Carnitine palmitoyltransferase 1 (CPT1) controls the rate of entry of long-chain fatty acids into the mitochondrial matrix for β-oxidation and has been reported to exist as an oligomer. We have investigated the *in vivo* oligomerization of full-length rat CPT1A (rCPT1A) along with those of the N-terminal truncation/deletion mutants Δ(1–82), Δ(1–18), and Δ(19–30) expressed in yeast mitochondria. The data indicate that in liver mitochondria *in vivo* CPT1A exists as a hexamer but that during preparation and storage of mitochondria the order of oligomerization is rapidly reduced to the trimer, such that a mixture of hexamer and trimer is observed in isolated mitochondria *in vitro*. Mutants bearing deletions of different segments of the N terminus (including the more N-terminal of the two transmembrane domains) have the same pattern of oligomerization when expressed in yeast mitochondria. The self-association of the individual rCPT1A transmembrane (TM) domains (TM1, TM2) was also studied using the TOXCAT assay (which measures TM self-association in the *Escherichia coli* inner membrane). There was minimal self-association of the sequence corresponding to TM1 but significant self-association of TM2 in TOXCAT. Chemical cross-linking and analytical ultracentrifugation of a TM2-derived synthetic peptide showed oligomerization with a similar trimer/hexamer equilibrium to that observed for native rCPT1A in isolated mitochondria. Therefore, there was a correlation between the oligomerization behavior of TM2 peptide and that of the full-length protein. *In silico* molecular modeling of rCPT1A TM2 highlighted the favorable orientation of G*XXX*G and G*XXX*A motifs in the formation of the TM2 hexamer.

Carnitine palmitoyltransferase 1 (CPT1)[2] catalyzes the reaction that exerts the strongest control over the rate of mitochondrial long-chain fatty acid β-oxidation (1). Changes in mitochondrial function, particularly their ability to oxidize fatty acids, accompany the development of obesity and pre-diabetes (2). The activity of CPT1 also determines the availability of one of its substrates, long-chain acyl-CoA, in the cytosol such that when the rate of fatty acid oxidation is low, there is increased availability of acyl-CoA esters which are highly active intermediates involved in complex lipid synthesis (3), activation of inflammatory pathways (4), and activation of ion channels (particularly the K^+_{ATP} channel (5)), actions that have the potential to result in important cellular effects (6). Therefore, regulation of CPT1 activity is important not only in determining the rate of fatty acid oxidation but in the maintenance of a multiplicity of cell functions (7).

CPT1A is one of three isoforms of CPT1 that are products of distinct genes that share considerable sequence similarity (~65%) (8). It is a polytopic membrane protein of the mitochondrial outer membrane (9, 10) having two transmembrane domains (TM1, TM2) that link the large C-terminal (catalytic, 602-residue) and N-terminal (regulatory, 47-residue) segments of the molecule (9). The N- and C-terminal regions are exposed on the cytosolic face of the membrane; the functional consequences of this topology have been described previously (11). In CPT1A, interactions between the N- and C-terminal domains of the protein are central to the regulation of the activity of the enzyme and particularly the modulation of its sensitivity to the physiological inhibitor, malonyl-CoA (11). The close interaction between the N- and C-terminal segments has been demonstrated via intramolecular cross-linking studies (12) and supported by recent *in silico* molecular modeling of human CPT1A (13). The TM domains play an important role in mediating and modulating N-C interactions (12) as does the loop linking the two TMs (14, 15).

More recently, it has been reported that rat CPT1A exists as an oligomer and that the N-terminal region of the protein containing TM1 and TM2 (residues 1–147 in the rat enzyme, rCPT1A) is involved in driving the oligomerization of CPT1A (16). Thus, it was shown that full-length rCPT1A (whether in rat liver mitochondria or when expressed heterologously in the yeast *Pichia pastoris*) forms oligomeric complexes when analyzed using gel filtration chromatography or Blue Native (BN)-PAGE. The fundamental oligomeric unit was suggested to be the trimer, which associates into a dimer of trimers to yield hexamers (16). The protein-protein interactions that stabilize these complexes were narrowed down to a 51-amino acid stretch of CPT1A (residues 97–147) that includes TM2 and a

* This work was supported by a Diabetes UK grant (to V. A. Z. and A. M. D.) and by a Warwick University Postgraduate Research Fellowship (to Z. J.). The costs of publication of this article were defrayed in part by the payment of page charges. This article must therefore be hereby marked "*advertisement*" in accordance with 18 U.S.C. Section 1734 solely to indicate this fact.

[1] To whom correspondence should be addressed. Tel.: 44-24761-50037; Fax: 44-24765-24112; E-mail: ann.dixon@warwick.ac.uk.

[2] The abbreviations used are: CPT1, carnitine palmitoyltransferase 1; rCPT1A, rat CPT1A; CD, circular dichroism; DPC, dodecylphosphocholine; TM, transmembrane; MES, (2-(*N*-morpholino)-ethanesulfonic acid); CAT, chloramphenicol acetyltransferase; GpA, glycophorin A; BN, Blue Native; Bis-Tris, 2-[bis(2-hydroxyethyl)amino]-2-(hydroxymethyl)propane-1,3-diol; BS^3, bis[sulfosuccinimidyl]suberate; M:P, micelle:peptide.

non-cleavable matrix-targeting signal sequence. When expressed as a fusion protein with dihydrofolate reductase, this region induced the formation of hexamers. However, any complementary role of the oligomerization behavior of rat CPT1A TM1 could not be investigated (16). These observations point toward an important role for the TM domains in the oligomeric assembly of rCPT1A. This role can be conceptualized using the "two-stage model" of membrane protein folding (17) which describes the side-by-side interactions of TM α-helices in the plane of the bilayer as strong determinants of correct folding and assembly of membrane proteins.

In the present study we have investigated the role of the TMs in the oligomerization of full-length rCPT1A. Self-association of each individual TM domain was studied directly in natural membranes (*Escherichia coli*) using the TOXCAT assay (18). The resulting data indicate that whereas TM2 has a strong propensity for homo-oligomerization, TM1 does not. A synthetic peptide corresponding to the TM2 sequence of rat CPT1A was used to obtain quantitative biophysical evidence of TM2-peptide oligomerization, including the stoichiometry of assembly in detergent micelles. The results have enabled us to construct molecular models that highlight potential points of contact between TM2 helices and suggest that oligomer formation is favored by the relative positioning of tightly packing G*XXX*G and G*XXX*A motifs within the predicted TM2 helix.

EXPERIMENTAL PROCEDURES

Preparation of Rat Liver Mitochondria—Mitochondria were prepared from livers of fed male Wistar rats. The liver was rapidly excised from the rat and placed in 20 ml of ice-cold homogenization medium containing 300 mM sucrose, 5 mM Tris-HCl, 1 mM EDTA (pH 7.4). All procedures were carried out at 4 °C. The liver was minced using scissors and washed 2–3 times in ice-cold medium. The minced liver was homogenized using a Porter-Elvenheim Teflon glass homogenizer. The homogenates were centrifuged at 500 × *g* for 10 min to remove debris. The supernatant was then decanted and centrifuged at 12,000 × *g* for 10 min. The resultant crude mitochondrial fraction was collected and resuspended in a medium containing 300 mM sucrose, 5 mM Tris, 1 mM EDTA (pH 7.4), and gently resuspended. After this, the mitochondria were sedimented by centrifuging at 9000 × *g* for 10 min to give a mitochondrial fraction. For rapid preparation of the mitochondria, the second centrifugation step was omitted.

Preparation of P. pastoris Mitochondria—Yeast cultures were grown for 24 h at 30 °C with shaking at 200 rpm. All initial steps were carried out at room temperature. Cells were collected by centrifugation at 4000 × *g* for 5 min, and the resultant pellet was weighed. The appropriate amounts of Tris-SO_4^{2-} (2 ml g^{-1} yeast) and dithiothreitol (3.084 mg g^{-1} yeast) were added. The mixture was incubated at 30 °C for 10–15 min with shaking at 150 rpm. The cells were then sedimented by centrifugation as before and washed in 1.2 M sorbitol/20 mM potassium phosphate buffer (pH 7.4). This pellet was resuspended in 30 ml of 1.2 M sorbitol, 20 mM potassium phosphate, and zymolase was added (3.4 mg g^{-1}). The cells were incubated at 30 °C with shaking (150 rpm) for 20 min. All subsequent steps were carried out at 4 °C. An equal volume of mannitol buffer (0.6 M mannitol, 1 mM KCl, 10 mM MES, and 0.5 mM EDTA) was added containing a mixture of protease inhibitors (Roche Applied Science) as recommended by the manufacturer. Spheroplasts were collected by sedimentation and washed in the mannitol-containing buffered medium. The pellet was then resuspended in 20 ml of the same medium and homogenized using a Porter-Elvenheim Teflon glass homogenizer. Homogenates were centrifuged at 800 × *g* for 10 min to remove debris. The supernatant was then decanted and further centrifuged at 12,000 × *g* for 15 min to obtain the mitochondrial fraction. The pellet was washed and resuspended in a medium containing 0.6 M sorbitol and 20 mM Hepes (pH 7.4).

Blue Native PAGE of CPT1A—Samples were prepared and subjected to Blue Native PAGE using the Novex Bis-Tris gel system (Invitrogen). Briefly 100 μg of mitochondrial fraction were collected by centrifugation for 12 min at 12,000 × *g* in a cooled centrifuge at 4 °C and resuspended in 100 μl of Native sample buffer (Invitrogen) containing 0.5% digitonin. After solubilization for 15 min on ice, the extracts were centrifuged for 30 min at 50,000 × *g*, and the supernatants were recovered and supplemented with 0.5 μl of G-250 additive (Invitrogen) for each 10 μl of extract before electrophoresis on 4–16% gradient Novex Bis-Tris gels (Invitrogen). The calibration standard kit used was comprised of eight proteins with a molecular mass covering the range between 20 and 1200 kDa.

Western Blot Analysis—Separated proteins were blotted onto polyvinylidene difluoride membranes using Tris-glycine transfer buffer. After transfer, the membrane was washed for 15 min in 8% acetic acid and allowed to air-dry. The membrane was then washed in methanol, and proteins were detected as described previously using the ECL detection system (Pierce). The antibodies used were antipeptide antibodies raised against the Arg^{428}-Lys^{441} sequence within the C-segment of rat CPT1A (19).

TOXCAT Assay and Construction of Chimera—The self-association of rCPT1A transmembrane domains in a natural membrane was studied using the TOXCAT assay, the details of which have been described previously (18). Briefly, TOXCAT employs a chimeric protein in which the α-helical TM domain of interest is inserted between the N-terminal DNA binding domain of ToxR, a dimerization-dependent transcriptional activator, and maltose-binding protein, a monomeric periplasmic anchor protein. The fusion protein is constitutively expressed in *E. coli* together with a chloramphenicol acetyltransferase (CAT) reporter gene under the control of a ToxR-responsive *ctx* promoter. Oligomerization of the TM domains within the bacterial inner membrane results in oligomerization of the ToxR domain, transcriptional activation of the *ctx* promoter, and CAT expression. The amount of CAT expressed in this system is proportional to the strength of oligomerization of the TM domains. The expression vectors (pccKAN, pccGpA-wt, and pccGpA-G83I) and *E. coli* strain NT326 were kindly provided by Prof. Donald M. Engelman. TOXCAT chimera were constructed according to a reported protocol (18) and expressed in *E. coli*. Before performing the assay, membrane insertion of all constructs was confirmed using sodium hydroxide washes (20), and correct orientation of the TOXCAT constructs in the membrane was confirmed through protease sen-

sitivity in a spheroplast assay (18). Similar expression levels for all constructs were confirmed via Western analysis against the maltose-binding protein domain before performing CAT assays. The CAT assays were performed using the FAST CAT kit (Molecular Probes and Invitrogen).

Peptide Synthesis and Purification—A peptide corresponding to the second TM domain (TM2) of CPT1A was synthesized at the Keck Facility, Yale University using Fmoc (*N*-(9-fluorenyl)methoxycarbonyl) chemistry. The sequence of the TM2 peptide was $COCH_3$-KKNIVSGVLFGTGLWVAVIMT-MRK-$CONH_2$, containing residues Lys^{102}-Arg^{123} as well as non-native lysine residues (to aid solubility) and end-caps on the C and N termini (M_r = 2689 Da). The peptide was purified by reversed-phase high performance liquid chromatography using a linear acetonitrile gradient from 30 to 100% containing 0.1% trifluoroacetic acid on a Phenomenex C4 semipreparative column. The purity of pooled peptide fractions was confirmed by electrospray ionization time-of-flight mass spectroscopy (ESI-TOF-MS microTOF, Bruker) before subsequent lyophilization. Peptides were stored as dry powders until use.

Circular Dichroism (CD)—CD spectra were measured using a Jasco J715 spectropolarimeter (Jasco UK, Great Dunmow, UK) and 1.0-mm path-length quartz cuvettes (Starna, Optiglass Ltd, Hainault, UK). All spectra were recorded from 190 to 260 nm (data below 200 nm are not shown due to high noise of light scattering) using a 2.0-nm spectral bandwidth, 0.2-nm step resolution, 100-nm min^{-1} scanning speed, and 1-s response time. The TM2 peptide was prepared in 50 mM sodium phosphate buffer (pH 7) containing 10 mM SDS or 46 mM dodecylphosphocholine (DPC) (Avanti Polar Lipids, Alabaster AL) and 100 mM NaCl to a final peptide concentration of 40 μM. CD spectra were collected at room temperature.

Peptide Cross-linking in Detergents—Cross-linking reactions were carried out for 20 μM solutions of the TM2 peptide dissolved in DPC micelles at peptide:micelle ratios ranging from 1 to 20 (corresponding to DPC concentrations ranging from 2.7 to 24 mM). All samples were prepared in 20 mM sodium phosphate buffer and 150 mM NaCl (pH 8). Bis[sulfosuccinimidyl]-suberate (BS^3, Pierce) was used to cross-link the peptide in solution via primary amine groups according to the manufacturer's protocol. The cross-linking reaction was terminated after 30 min by the addition of 1 M Tris-HCl (pH 8). Uncross-linked and SDS cross-linked samples were prepared as controls. All samples were analyzed by gel electrophoresis, and peptides were visualized on gels by staining either with Coomassie Blue or with silver nitrate.

Analytical Ultracentrifugation—Sedimentation velocity measurements were carried out on a Beckman XL-1/A analytical ultracentrifuge (Beckman Coulter, Fullerton CA) housed in the Department of Biological Sciences, University of Birmingham, Birmingham, UK. TM2 peptide samples were prepared in 50 mM Tris-HCl (pH 7.5), containing 15 mM DPC (Avanti Polar Lipids), 100 mM NaCl, and 52.5% D_2O (Cambridge Isotope Laboratories, Andover MA) to match the buoyant density of the detergent. When the solvent matches the buoyant density of the detergent micelles, the only contribution to the buoyant molecular weight is from the peptide, as described (21).

Data were collected using absorbance optics set to 280 nm at two peptide concentrations (142 and 62 μM) using a double-sector centerpiece at a speed of 40,000 rpm and a temperature of 25 °C. 400 scans were recorded for each sample, with 50 s between each scan. The moving boundary was monitored by repetitive radial scanning at a constant step size of 0.003 cm at 280 nm using a UV absorption optical system. Fitting of the resulting profiles was achieved using SEDFIT (22) to generate a continuous sedimentation coefficient distribution, which was subsequently converted to a molecular mass distribution using a peptide monomeric molecular mass of 2689 Da, a buffer density of 1.05971 g ml^{-1}, a buffer viscosity of 1.0267 centipoise, and a partial specific volume of 0.7792 ml g^{-1} (calculated using SEDNTERP).

Computational Searches Using CHI—Structural calculations were performed using the CNS searching of helix interactions (CHI) package, the details of which have been described previously (23–25), on an 8-node dual 2.66-GHz Xenon processor Linux cluster (Streamline Computing, Warwick). CHI was used to create models of rCPT1A TM2 homotrimers and homohexamers. Using CHI, either three (for trimer) or six (for hexamer) canonical α-helices containing residues Lys^{102}-Arg^{123} of TM2 were built. The starting geometries incorporated both right-handed (−25°) and left-handed (25°) crossing angles and an axis-to-axis distance between the helices of 10.4 Å. In a search of approximately symmetrical interactions, the helices were simultaneously rotated about their central axis in 45° increments from 0° to 360°. After each rotation, molecular dynamics simulations were performed using simulated annealing of atomic coordinates. Four different molecular dynamics simulations were performed for each starting geometry, and energy minimization of structures was carried out both before and after molecular dynamics simulations. Groups of structures with a backbone root-mean-square deviation of ≤1 Å were placed in clusters of 10 or more members followed by a calculation of an average structure for each cluster and energy minimization.

RESULTS

Oligomerization of Full-length and Truncated rCPT1A

The oligomeric states of native rCPT1A in both intact rat liver mitochondria or expressed in mitochondria of the yeast *P. pastoris* were studied in addition to those of several yeast-expressed N-terminal truncation/deletion mutants (Δ1–82, Δ1–18, Δ19–30) to investigate which regions of the protein contribute to oligomer formation. A schematic of the various regions of rCPT1A is shown in Fig. 1*a*. The digitonin-solubilized mitochondrial extracts were analyzed using BN-PAGE followed by Western blotting and immunodetection with anti-peptide antibody raised against the C-terminal segment of the protein (19) (Fig. 1*b*). In both rat liver and yeast extracts, Western blotting revealed bands at ~264 and 528 kDa corresponding to rCPT1A trimers and hexamers, respectively. In preliminary experiments, extracts prepared in digitonin or 1% Triton-X-100 gave the same results (data not shown). Subsequent experiments were performed using only digitonin extraction. The results are at variance with previously published BN-PAGE

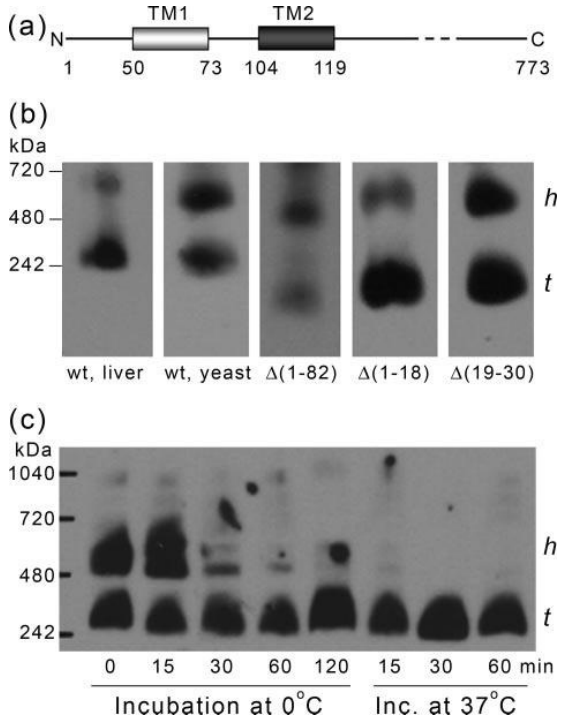

FIGURE 1. **Oligomerization patterns of native rCPT1A and N-terminal truncation and deletion mutants.** *a*, schematic representation of the rCPT1A sequence showing the relative positions of the two TM domains with respect to the N and C termini. *b*, Western blots of mitochondrial proteins separated by BN-PAGE probed with an antipeptide antibody raised against Arg^{428}-Lys^{441} within the C-terminal segment of rCPT1A. The figure shows blots for rat liver mitochondria (expressing native rCPT1A) and N-terminal truncation/deletion mutants of rCPT1A (Δ(1–82), Δ(1–18), and Δ(19–30)) expressed in the yeast *P. pastoris*, as indicated. These mutants were chosen for their wide range of the sensitivity of their catalytic activities to malonyl-CoA inhibition (see text). In all blots the proteins appear to form hexamers (*h*) or trimers (*t*). *wt*, wild type. *c*, BN-PAGE analyses of proteins extracted from rapidly prepared rat liver mitochondria (see "Results") that were subsequently stored either at 0 °C or 37 °C for the times indicated. Blots are representative of two to four separate experiments.

analyses of CPT1A, where only hexamers were observed (16). In that same study, however, the investigators observed only trimers when detergent extracts were analyzed by gel filtration. In the present studies all three deletion/truncation mutants migrated as a mixture of trimers and hexamers, with resolved bands observed at the appropriate molecular weights for the mutants studied (Fig. 1*b*). Our observation of both trimers and hexamers in samples analyzed by the same technique (BN-PAGE) indicates that the two oligomeric forms co-exist, at least *in vitro*. Furthermore, the data show that truncation (Δ1–18) and deletion (Δ19–30) mutants that differ widely in their kinetic characteristics from those of the native protein (26) (particularly their malonyl-CoA sensitivity) have the same oligomerization pattern (mixture of hexamers and trimers) as that of the native rCPT1A. Moreover, we have confirmed the previous finding that deletion of the N-terminal sequence including TM1 has no effect on oligomerization of the protein (although in the present data both trimers and hexamers were observed). This agrees with the suggestion that TM2 may provide the driving force for rCPT1A oligomeric assembly (16).

As the BN-PAGE results given in Fig. 1*b* differ from previous results in that both trimers and hexamers of rCPT1A were present in digitonin extracts of mitochondria isolated from rat liver and *P. pastoris*, we addressed the question of whether the trimer/hexamer ratio was altered during preparation of the mitochondria, as this would be indicative of whether the two oligomeric forms exist in equilibrium or whether one is preferentially present *in vivo*. Therefore, crude mitochondrial fractions were prepared as rapidly as possible from rat liver followed by storage at either 0 or 37 °C before extraction with digitonin, BN-PAGE analyses of the proteins, and Western blotting. The data shown in Fig. 1*c* indicate that when mitochondria were kept at 0 °C for less than 30 min, both trimers and hexamers were observed. However, at longer incubation times ($t \geq 30$ min; $T = 0$ °C) the proportion of CPT1A present as the hexamer was rapidly diminished, whereas that of the trimer was increased. When mitochondria were stored at 37 °C, the hexamer was not observed at all (even after the shortest incubation times), and only the trimer was detected. These data suggest that rCPT1A may exist mainly as hexamers in the rat liver mitochondrial outer membrane *in vivo* and that changes in the mitochondrial membrane that occur during isolation and storage result in rapid destabilization of the higher order oligomeric state.

Self-association of the Individual TM Domains rCPT1A

Although the present data and those published previously (16) strongly suggest that TM2 plays a key role in oligomer formation of rCPT1A, no direct measurements of self-association for either TM of rCPT1A have been reported. To address this, we have examined the homo-oligomerization of rCPT1A TM1 and TM2 using the TOXCAT assay, a ToxR-based transcriptional assay linked to CAT expression. TOXCAT is a method used to quantify the ability of individual TM domains to self-associate in a natural (*E. coli*) membrane bilayer and in which the degree of association can be measured in terms of the CAT activity generated as a result of the homo-oligomerization of TM domains (18) (see "Experimental Procedures"). The sequences corresponding to the respective TM domains of rCPT1A that were investigated using TOXCAT are shown in Fig. 2*a*. The selection of these sequences was based on an analysis of the full-length sequence of rCPT1A using the bioinformatics program TMHMM (27, 28) to predict the location of TM domains. TOXCAT data were also obtained for a positive control (the TM domain of glycophorin A (GpA), which is known to dimerize strongly (29)), and a negative control, GpA-G83I, a dimerization-impaired mutant. The data are shown in Fig. 2*b*. Comparison of the rCPT1A TM1 signal in the TOXCAT assay to that of the controls indicated that TM1 has very little propensity to self-associate. Indeed, TM1 yielded homo-oligomerization-dependent CAT activities that were lower than those produced by the negative control (GpA-G83I). Conversely, rCPT1A TM2 showed a higher propensity to form homo-oligomers, yielding CAT activities approximately half those observed for the TM domain of GpA.

It is important to note that the TM-spanning regions for TM1- and TM2-containing TOXCAT constructs are very different in length; the TM1 insert contained 24 amino acids,

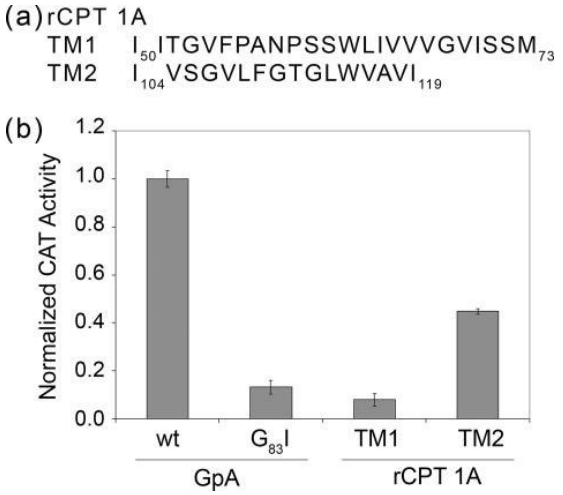

FIGURE 2. **Oligomerization of transmembrane domain sequences of rCPT1A in *E. coli* membranes.** *a*, rCPT1A transmembrane domain sequences (as predicted by TMHMM (27, 28)) that were analyzed using TOXCAT assays. *wt*, wild type. *b*, CAT activities obtained in the TOXCAT assay for the TM1 and TM2 domains of rCPT1A and for positive (GpA) and negative (GpA-G83I mutant) controls. All CAT activities are reported relative to the value obtained for GpA. Values are the means (±S.D.) for three or more independent measurements.

whereas the TM2 insert contained 16 amino acids. It has been shown previously that in a similar assay the length of the TM can affect ToxR-based transcriptional activity (30). To test whether differences in the lengths of TM1 and TM2 lead to an artificial difference in CAT activity, additional TOXCAT constructs were prepared. The TM1 sequence was shortened to 21, 20, 18, and 16 residues and tested in the assay (data not shown). TM1 inserts shorter than 21 residues failed to insert into the *E. coli* membrane, and the construct containing a 21-residue TM1 (Ile^{50}–Ile^{70}) yielded a signal ~50% smaller than that shown in Fig. 2*b*, thus confirming that TM1 has little or no ability to self-associate.

Therefore, these data support the inferences from the present BN-PAGE data on rCPT1A(Δ1–82) and those obtained previously (16) that TM2 is the only one of the TM domains of CPT1A that is required for homo-oligomerization of the protein. In view of these observations, only the oligomerization of TM2 was studied further.

Secondary Structure of TM2 Peptide

A synthetic peptide corresponding to TM2 (residues Lys^{102}-Arg^{123}, Fig. 3*a*) was studied to determine whether the oligomeric states attained *in vitro* correspond to those observed for full-length rCPT1A in rat liver mitochondria and in heterologously expressed rCPT1A. In synthesizing the peptide, lysine residues were added to the sequence at both its N and C termini to aid solubility and to reduce nonspecific aggregation, an approach that has been shown in several previous studies not to affect the properties of strongly interacting TM domain peptides (31–33). The secondary structure of the TM2 peptide in detergents was characterized using CD spectroscopy. CD spectra were collected for the TM2 peptide solubilized in (*a*) SDS, an anionic and denaturing detergent and (*b*) DPC, a zwitterionic detergent known to be less denaturing than SDS. The resulting spectra (Fig. 3*b*) were indicative of a characteristic α-helical profile, with negative absorption maxima at 208 and 222 nm, demonstrating that the TM2 peptide adopts an α-helical secondary structure in both SDS and DPC micelles.

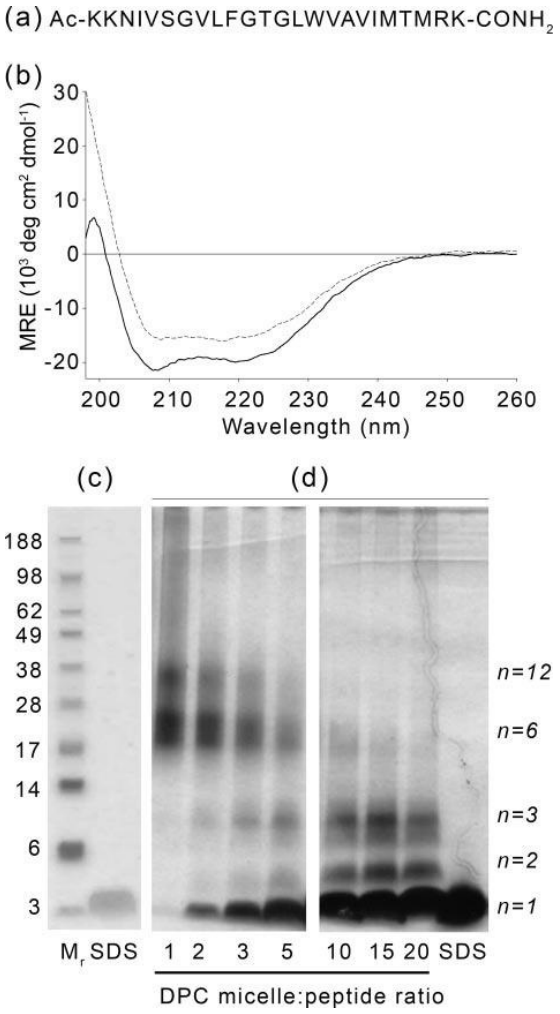

FIGURE 3. **Analysis of higher order structures of a rCPT1A TM2-derived peptide in detergent solutions.** *a*, amino acid sequence of the synthetic peptide used for biophysical studies, corresponding to rCPT1A TM2 (see the legend to Fig. 1) with additional Lys residues at its C and N termini to aid solubility and avoid nonspecific aggregation (see "Results"). *b*, CD spectra of the TM2 peptide in SDS (*solid line*) and DPC (*broken line*) detergent micelles. *c*, SDS-PAGE analysis of the TM2 peptide dissolved in DPC micelles, visualized using Coomassie-G250. *d*, BS^3-mediated cross-linking of TM2 peptide dissolved in DPC micelles. Cross-linking reactions were carried out in DPC detergent micelles at various micelle:peptide concentration ratios as indicated *below each lane*. Molecular weight markers are shown in the far *left-hand lane*. Protein bands were visualized by staining with silver nitrate. Oligomeric states (*e.g.* dimer indicated by $n = 2$) are indicated at the *far right of the gels*. A negative control reaction in which cross-linking was carried out for the peptide dissolved in SDS buffer is shown in the *last lane*.

Oligomeric State of rCPT1A TM2 Peptide

Chemical Cross-linking—Although providing a strong indication that the sequence of TM2 can support self-association of this domain, the TOXCAT assay cannot report on the order of

the oligomeric state achieved. Therefore, to characterize the oligomeric state(s) of the rCPT1A TM2 domain, *in vitro* approaches were used. The synthetic peptide corresponding to TM2 (see above) was electrophoresed under denaturing conditions (SDS-PAGE) before and after treatment with a chemical cross-linker. As shown in Fig. 3*c*, in the absence of cross-linker the peptide migrated as the monomeric species in SDS detergent. To investigate its oligomeric state in a less denaturing detergent, the peptide was dissolved in DPC detergent micelles and then treated with the water-soluble chemical cross-linker BS^3, which reacts specifically with the terminal NH_2 of the peptide as well as the NH_2 groups on lysine side chains provided that the reactive groups are within 11.4 Å of one another (34). Cross-linking reactions were carried out at increasing DPC micelle:peptide (M:P) concentration ratios to investigate the effect of detergent concentrations on oligomeric state. Cross-linked species were analyzed using SDS-PAGE and visualized by staining with silver nitrate (Fig. 3*d*). At the lowest detergent micelle:protein ratio (M:P = 1), bands corresponding to the hexamer (16.1 kDa) and dodecamer (32.2 kDa) were observed. No bands corresponding to lower-order oligomeric states (*e.g.* trimer) or monomer were evident. As the M:P ratio was increased to a value of 2, a monomer band could be observed (2.69 kDa) as well as weak bands corresponding to dimer (or potentially monomer plus bound BS^3, 5.38 kDa) and trimer (8.07 kDa). Further increases in the M:P ratio resulted in increasing amounts of monomeric, dimeric, and trimeric species accompanied by decreasing populations of hexamers and dodecamers. The results shown in Fig. 3*d* demonstrate that the oligomeric states of the TM2 peptide differ with increasing detergent concentrations. It is well established that increasing detergent concentration can destabilize TM helix oligomers (35). The rapid loss of the dodecamer of TM2 with increasing M:P ratios suggests that this is the least stable species. The hexamer is evidently more stable, as its presence can be detected at all M:P ratios studied, although the concentration of hexamer is greatly reduced at M:P > 5. The oligomeric species that are most stable at the highest M:P ratios are the dimer and trimer. These two species (together with the monomer) steadily increased in concentration at high M:P ratios. As a negative control, cross-linking was carried out with the peptide dissolved in SDS; as expected, only a band corresponding to the monomer was observed (Fig. 3*d*).

Analytical Ultracentrifugation—The oligomeric state of the TM2 peptide was also studied in the absence of cross-linker using analytical ultracentrifugation. Sedimentation velocity experiments were employed in this study as they provide information about the shape and size of peptides in solution. Because of the high rate of back diffusion expected from low molecular weight peptides, high speeds are sometimes required to obtain reliable sedimentation velocity data. In the present studies, a speed of 40,000 rpm was sufficient to generate data with the required mass resolution for the analysis of the oligomeric state of the TM2 peptide. Two peptide concentrations were analyzed, 62 μM (M:P $\sim$ 4) and 142 μM (M:P $\sim$ 1) in buffered DPC solution. The fitting residuals for both concentrations are shown in Figs. 4, *a* and *b* (sedimentation profiles not shown), corresponding to fits with root-mean-square deviation

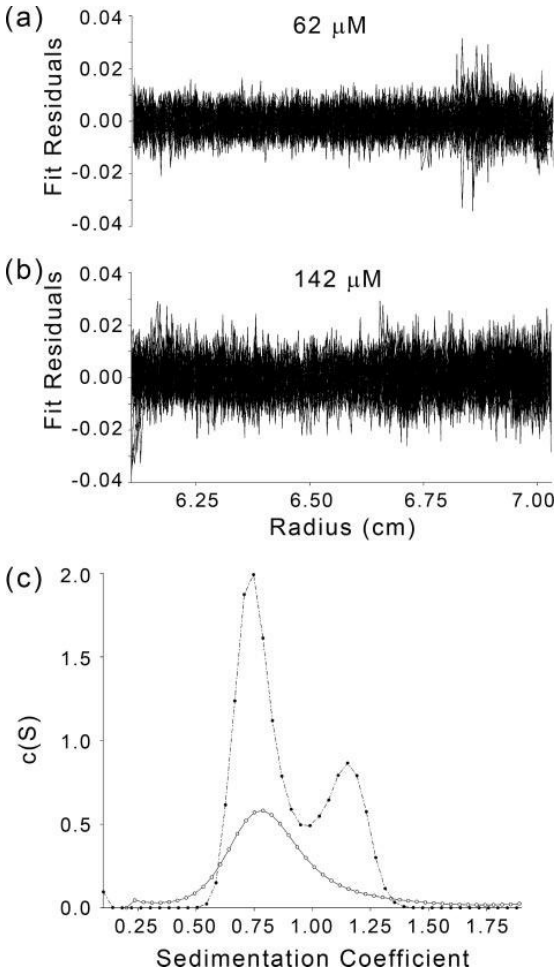

FIGURE 4. **Analytical ultracentrifugation analysis of rCPT1A TM2-derived peptide in detergent solution.** Sedimentation velocity data were obtained for the TM2 peptide dissolved in buffer containing 15 mM DPC and 52.5% D_2O. Residuals of the fitting process for samples containing 62 μM peptide (*a*) and 142 μM TM2 peptide (*b*). *c*, sedimentation coefficient distribution profiles for the peptide at concentrations of 62 μM (*open circles*) and 142 μM (*closed circles*) as calculated using the SEDFIT program (22). Conversion of sedimentation coefficients to molecular mass yielded one peak at low peptide concentration, with a mass value of 16.3 kDa (hexamer) and two peaks at high peptide concentration with mass values of 16.13 and 30.85 kDa (corresponding to hexamer and dodecamer, respectively).

values of 4.9×10^{-3} and 6.5×10^{-3}, respectively. The sedimentation coefficient profile for the higher of the two concentrations (Fig. 4*c*) contained two species centered at $S = 0.747$ and $S = 1.15$, corresponding to a molecular mass for the TM2 peptide of 16.1 and 30.9 kDa. When compared with the calculated molecular weights for the TM2 hexamer (16.1 kDa) and dodecamer (32.2 kDa), the experimental values agreed to within 4% of the theoretical values. This result agrees with the cross-linking results shown in Fig. 3*d*, where at M:P = 1, only hexamers and dodecamers were present. At the lower concentration of peptide (M:P ratio $\sim$ 4), the resulting sedimentation coefficient profile contained a single species centered at $S = 0.787$ (Fig. 4*c*), corresponding to a molecular mass for the TM2 peptide of 16.3 kDa, *i.e.* within 2% of the theoretical molecular

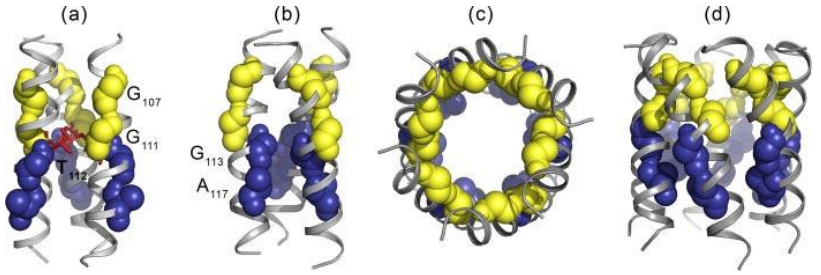

FIGURE 5. **Molecular models of CPT1A TM2 trimers and hexamers.** Molecular models of CPT1A TM2 trimers and hexamers were created using the program CHI (see "Experimental Procedures"). *a*, side view of a right-handed TM2 trimer in which individual helices are represented as *ribbons*. In this model the trimer is stabilized by packing of the G*XXX*G motifs (Gly^{107}, Gly^{111}, shown in *yellow*) against side chains from an adjacent helix as well as interhelical hydrogen bonding of Thr^{112} (shown in *red*, bond representation) at the center of the bundle. *b*, model of a left-handed trimer in which the G*XXX*A motif (Gly^{113}, A^{117}, shown in *dark blue*) packs against the adjacent helix, whereas the G*XXX*G motif is predicted to be on the outside of the bundle. *c*, top-down view of the left-handed TM2 hexamer. *d*, side view of the left-handed TM2 hexamer, showing the simultaneous packing of both the G*XXX*G (*yellow*) and G*XXX*A (*dark blue*) motifs against adjacent TM helices. The hexamer is the only observed oligomeric state for which it is predicted that both of these oligomer-favoring TM domain motifs are used to stabilize the quaternary structure of the peptide.

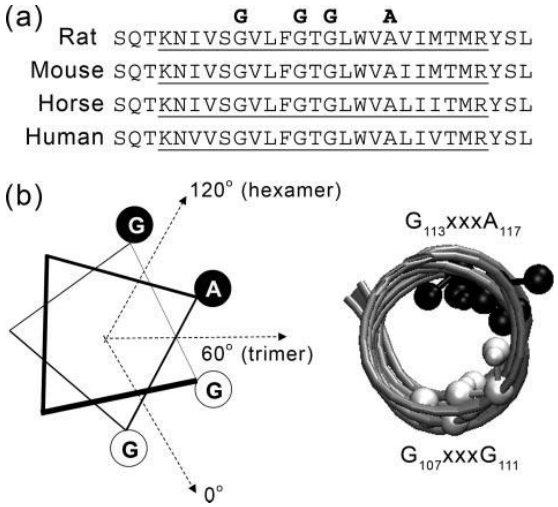

FIGURE 6. **Conservation of G*XXX*G and G*XXX*A motifs in the TM2 sequences of CPT1A from several mammalian species and their proposed role in hexamer formation.** *a*, alignment of the sequences of the predicted TM2 domains for CPT1A proteins sequenced to date. The TM domain is very highly conserved, as are the highlighted G*XXX*G and G*XXX*A motifs. *b*, orientation of the G*XXX*G and G*XXX*A motifs relative to each other on a helical wheel (*left panel*) and in a canonical α-helix (built using CHI; see "Experimental Procedures") containing residues Lys^{102}-Arg^{123} of TM2. Both models predict that the relative angle between the two motifs corresponds closely to the apex angles of a hexamer (120°). Also highlighted is the apex angle in a trimer (60°), which cannot accommodate both motifs.

weight of the hexamer (16.1 kDa). These data are in accordance with the results obtained after cross-linking at M:P ratios of 3 and 5 (Fig. 3*d*). Within the range of these M:P ratios, the concentration of cross-linked dodecamer decreased significantly, whereas the hexamer remained detectable.

Fitting of the data described above produced a frictional ratio of 1.88, suggesting a slightly elongated ellipsoidal shape for the hexamer as would be expected for a bundle of TM α-helices. Therefore, the sedimentation velocity data suggest that the TM2 peptide in DPC detergent solution exists as an equilibrium mixture of hexamers and dodecamers at the concentrations studied. The dodecamer species, which was also detected in the cross-linking experiments, is present only at low micelle:peptide concentration ratios.

Structural Models of TM2 Trimers and Hexamers

The results presented here establish that TM2 can associate to form hexamers and trimers, directly mirroring the behavior of the full-length rCPT1A both in freshly prepared rat liver mitochondria and in mitochondria isolated from yeast in which the protein (and its mutants) were heterologously expressed. To gain insight into the structural features of TM2 that may have a role in stabilizing both the trimeric and hexameric forms of the peptide, computational models were produced using the program CHI (see "Experimental Procedures"). CHI searches were performed on the basis of either three or six parallel α-helices containing the predicted sequence of the TM2 peptide. The trimer models suggest that the TM domain can form chemically plausible right- and left-handed coiled coils. However, in the all of the trimer models obtained (Fig. 5, *a* and *b*), the interaction interface contains either a G*XXX*G motif ($Gly107$, Gly^{111}) *or* a G*XXX*A motif (Gly^{113}, Ala^{117}), respectively. Both of these motifs are highly conserved in TM2 domains of the CPT1A isoform across all mammalian species (Fig. 6*a*) and are known to stabilize TM helix-helix interactions in several other membrane proteins (see "Discussion") (36–38). The *in silico* models of the trimer of rCPT1A TM2 also suggest that this oligomer is capable of being stabilized by the interhelical hydrogen bonding of Thr^{112}, as observed in other interacting TM domains (39) (in the present analyses, hydrogen bonds were assigned whenever a hydrogen bond donor and acceptor were within 3 Å of one another).

The modeling of the TM2 hexamer (Fig. 5*c*) suggests that TM2 can form a plausible left-handed helical bundle (no right-handed solutions were found) in which both the G*XXX*G and the G*XXX*A motifs pack against neighboring helices (Fig. 5*d*). In this way the stabilizing effects of both motifs can be exploited simultaneously through interactions with adjacent helices. This is possible only in a hexameric arrangement, which has apex angles of 120°, the predicted angle between the two motifs in the α-helical model of TM2 (Fig. 6*b*). Such simultaneous packing of the two motifs is not possible in the trimer, as the angle between the two motifs is such that they can never both pack at once (apex angles = 60°), resulting in exclusion of one motif from interfacial interactions with the other two helices (Fig. 6*b*).

DISCUSSION

Oligomer Formation in Natural Membranes—The involvement of the TM domains of CPT1A in the regulation of its activity and its sensitivity to malonyl-CoA has been strongly inferred for some time through numerous findings on the modulation of the interaction between the N- and C-terminal seg-

ments (for review, see Ref 40). This interaction between the N- and C-terminal segments of the molecule has now been modeled using *in silico* techniques based on homology with other transferases for which x-ray crystal structures have been determined (13). Moreover, we have shown that such a role for TM1-TM2 interactions occurs very much in the context of protein-lipid interactions, making CPT1A sensitive to changes in lipid composition that accompany changes in diet and pathophysiological state (*e.g.* diabetes, fasting) (15). Previous studies have also raised the possibility of an additional role for the TM domains, namely that of driving the oligomerization of CPT1A (16). In those studies, analysis of the native protein either in rat liver mitochondria or that expressed heterologously in yeast yielded either trimeric or hexameric oligomers in a manner that suggested that the fundamental oligomeric state is the trimer and that the hexamer results from the dimerization of the trimer (16). In general, trimers were observed after gel filtration, whereas hexamers were observed after Blue Native gel electrophoresis (16). The CPT1A protein N-terminally truncated at residue 82 (*i.e.* lacking TM1 but retaining most of the loop region and TM2 (9)) was similarly found to yield only trimers. Although these data indicated that TM2 was sufficient for oligomerization to occur, they did not exclude the possibility that TM1 plays an additional/complementary role in oligomerization and may be interpreted as indicating that TM1 may determine the order of oligomerization. Therefore, in our studies, in addition to characterization of the oligomeric characteristics of the native rCPT1A and truncation/deletion mutants, we have quantified the oligomerization propensities of both TM1 and TM2 in isolation using the TOXCAT assay and have explored in more detail the biophysical properties of TM2 (which is the only one to give a substantial signal in TOXCAT) with respect to its oligomerization properties.

Importantly, our experiments on CPT1A in rat liver mitochondria and the native protein expressed heterologously in yeast mitochondria showed that both trimers and hexamers can be detected using the same technique (Blue-Native gel electrophoresis). Similar observations were made for all the truncation and deletion mutants tested when expressed in yeast (Fig. 1*b*). In particular, contrary to previous observations (16), we found that the (Δ1–82) CPT1A truncation mutant also exists in a mixture of the two oligomeric states (Fig. 1*b*). These observations suggested that the two oligomeric forms may exist in equilibrium *in vivo*. However, our time-course experiments on rapidly prepared rat liver mitochondria suggest that *in vivo* CPT1A is likely to occur as a hexamer which de-oligomerizes rapidly during preparation of subcellular fractions and especially with storage of the mitochondria, particularly at 37 °C. The observations obtained on rapidly fractionated rat liver tissue indicate that the trimer (although stabilized by non-covalent interactions that we have modeled; see below) may not be a physiologically relevant entity but may arise as an artifact during the necessarily lengthy preparation of purified mitochondrial fractions by differential centrifugation (this study) or on self-forming gradients (16).

It has also been observed that there was no difference in the order of oligomerization of CPT1A in rat liver mitochondria isolated from animals in different physiological states (fasting, diabetic) known to result in a wide range of sensitivities of the enzyme to malonyl-CoA inhibition (16). Therefore, in this study we have tested this observation directly by studying the oligomerization state of mutants that contained deletion mutations within the N-terminal 47 amino acid residues that have previously been shown (see *e.g.* Ref. 26) to display a range of several orders of magnitude in their malonyl-CoA sensitivities. The data in Fig. 1*b* show that we always observed similar proportions of trimer and hexamer irrespective of which N-terminal mutant was studied. This strengthens the evidence that malonyl-CoA sensitivity is independent of the quaternary structure of CPT1A and is instead determined by intramolecular (N-C) interactions (40) to which TM1-TM2 (hetero-oligomeric) interactions are likely to be central.

Self-association of TM2, but Not TM1, Reflects the Oligomerization of the Native Protein—The above interpretations are supported by the biophysical experiments we performed on the peptide corresponding to TM2 *in vitro*. The experimental demonstration using TOXCAT that only TM2 has homo-oligomerization potential enabled us to focus on the biophysical properties of a peptide corresponding to this TM. When the TM2 peptide was dissolved in DPC micelles and cross-linked with BS^3, oligomers corresponding to the hexamer were observed, suggesting that the TM2 sequence has inherent primary and secondary structural properties that favor hexamerization. The fact that the hexamer also appears to be a favored oligomeric state *in vivo* suggests that these interactions are also important in the context of the full-length protein when this is stabilized within a lipid bilayer. De-oligomerization to the trimeric form occurs rapidly during preparation and storage of mitochondria (when disruption of contacts with other intracellular systems, loss of contact site density (20) and changes in outer membrane lipid composition because of phospholipase activity are known to occur). It is likely that de-oligomerization to the trimeric form of the native rCPT1A protein is also favored during digitonin- or Triton X-100 solubilization of mitochondria, in preparation for BN-PAGE or gel filtration (16). In this context, it is of interest to note that when the size of the molecular entity C-terminal of TM2 was much smaller than that of native CPT1A (*e.g.* the truncated CPT1A- dihydrofolate reductase chimera, CPT1A-(97–147) dihydrofolate reductase), only the respective hexamer was observed (16). This suggests that whereas TM2-driven oligomerization results in the hexamer as a default quaternary structure for the native protein, the large C-terminal domain of the native protein imposes intermolecular constraints within that oligomeric structure that are overcome only within the mitochondrial outer membrane *in vivo* and which result in the relatively rapid deoligomerization to the trimer.

Such close correspondence between the oligomerization behavior of rCPT1A *in vivo* and those of TM2 *in vitro* provide further evidence that TM2 plays a central role in the oligomerization of the native protein, as suggested by the strong propensity of this TM to oligomerize in *E. coli* inner membrane (in the TOXCAT assay).

Molecular Modeling of the Role of the GXXXG(A) Motifs in TM2 Oligomerization—As discussed above, the hexamer of rCPT1A is likely to be the most important oligomeric form of

rCPT1A *in vivo*, although the inability to prepare mitochondria sufficiently rapidly from intact rat liver does not allow a definitive exclusion of the co-existence of the trimer. Certainly, the hexameric form of TM2 is the predominant species when the corresponding peptide is studied in DPC-micelle solution; other oligomeric states are observed only at very low or very high M:P ratios. The molecular models shown in Fig. 5 illustrate predicted conformations that may be adopted by the TM2 trimers and hexamers. Importantly, Fig. 5*d* highlights the possible role of the G*XXX*G and G*XXX*A motifs present within TM2 (and conserved in all CPT1A proteins sequenced to date) in stabilizing the hexameric structure. In both of these motifs, Gly or other small residues (*e.g.* Ala) are found four residues apart (one turn of the helix) and, therefore, appear on the same helical face. The presence of a "patch" of these small residues allows the helices to pack tightly together, and this close-packing stabilizes helix-helix interactions (36, 41, 42).

The angular separation of the G*XXX*G and G*XXX*A motifs within the predicted helical structure of TM2 (Fig. 6*b*) is approximately equal to the apex angles of a hexagon (120°). Therefore, in the hexamer both motifs could theoretically pack against adjacent TM2 helices, hence favoring this oligomeric form. However, in the native protein, intermolecular steric hindrance may destabilize this tertiary structure such that during preparation of mitochondria the trimer is formed (Fig. 1*c*). This is also evidenced by data showing that when a smaller molecular entity replaced the bulky C-terminal segment of native rCPT1A with the structure of dihydrofolate reductase, only hexamers were observed (16). Although further work is required to confirm the mechanism of association, G*XXX*G and G*XXX*A motifs are well known to contribute to TM interactions.

The trimer, although appearing not to be the physiologically relevant quaternary structure of rCPT1A, is predicted to be stabilized by the possible close packing of at least one of the G*XXX*G or G*XXX*A motifs and by interhelical hydrogen bonding, as shown in Figs. 5, *a* and *b*. The relative disposition of the G*XXX*G or G*XXX*A motifs within the predicted α-helical structure of TM2 is incompatible with favorable packing of both of these motifs simultaneously in the formation of homo-trimers, which would require an angle of ~60° (Fig. 6*b*).

Functional Significance of CPT1A Oligomerization—Previous data (16) as well as data from the present study raise the question as to the function of CPT1A hexamer formation. It has been suggested that oligomerization (to form trimers or a dimer of trimers) may be a mechanism for the formation of a channel in the mitochondrial outer membrane through which the acylcarnitine product of the reaction catalyzed by CPT1 may gain access to the intermembrane space (16). The molecular models in Fig. 5 suggest that the hexamer (but not the trimer) is capable of forming a pore of significant dimensions; however, validation of its possible function as a channel for acylcarnitines awaits further study. In this context, two considerations are pertinent. First, we have previously shown by performing functional target size analysis on CPT1A in whole rat liver mitochondrial and purified outer membranes that the functional size of rCPT1A (*i.e.* the size of the molecular entity required for catalytic activity) is the same as that of the monomeric molecular mass (~88 kDa) of the protein (43). Therefore, in the rat liver mitochondrial outer membrane each monomer within the hexameric form would function as an independent entity in terms of its catalytic function. Second, if as suggested (16) the putative channel formed by the oligomerization of CPT1A were necessitated by the inability of porin (VDAC1) to allow acylcarnitine esters access into the intermembrane space (a prospect raised previously (44)), it would need to be suggested that either this effect of porin is unidirectional or that transport of acylcarnitines out of mitochondria (which is considerable) also occurs necessarily through the putative pore/channel created by CPT1A oligomerization. These are now testable hypotheses, and the present studies suggesting that stabilization of TM2 hexamerization by G*XXX*G and G*XXX*A interactions may be central to rCPT1A oligomerization will enable further studies on CPT1A mutants that are unable to oligomerize. These should be useful in obtaining information regarding the function of CPT1A oligomerization with respect to long-chain fatty acyl moiety entry into intact mitochondria.

Acknowledgments—We thank Prof. D. M. Engelman for kindly providing the expression vectors and E. coli strain for the TOXCAT assay, J. Crawford for peptide synthesis, R. Parslow for assistance with analytical ultracentrifugation, Dr. D. Scott for helpful discussions and training in SEDFIT, G. W. King for many helpful discussions regarding chemical cross-linking, and Prof. A. Rodger for access to circular dichroism instrumentation.

REFERENCES

1. Drynan, L., Quant, P. A., and Zammit, V. A. (1996) *Biochem. J.* **317,** 791–795
2. Reznick, R. M., and Shulman, G. I. (2006) *J. Physiol. (Lond.)* **574,** 33–39
3. Turner, N., Bruce, C. R., Beale, S. M., Hoehn, K. L., So, T., Rolph, M. S., and Cooney, G. J. (2007) *Diabetes* **56,** 2085–2092
4. Wellen, K. E., and Hotamisligil, G. S. (2005) *J. Clin. Investig.* **115,** 1111–1119
5. Branstrom, R., Aspinwall, C. A., Valimaki, S., Ostensson, C. G., Tibell, A., Eckhard, M., Brandhorst, H., Corkey, B. E., Berggren, P. O., and Larsson, O. (2004) *Diabetologia* **47,** 277–283
6. Zammit, V. A. (1999) *Biochem. J.* **343,** 505–515
7. Zammit, V. A. (2008) *IUBMB Life* **60,** 347–354
8. McGarry, J. D., and Brown, N. F. (1997) *Eur. J. Biochem.* **244,** 1–14
9. Fraser, F., Corstorphine, C. G., and Zammit, V. A. (1997) *Biochem. J.* **323,** 711–718
10. Fraser, F., and Zammit, V. A. (1998) *Biochem. J.* **329,** 225–229
11. Zammit, V. (1999) *Prog. Lipid Res.* **38,** 199–224
12. Faye, A., Borthwick, K., Esnous, C., Price, N. T., Gobin, S., Jackson, V. N., Zammit, V. A., Girard, J., and Prip-Buus, C. (2005) *Biochem. J.* **387,** 67–76
13. Lopez-Vinas, E., Bentebibel, A., Gurunathan, C., Morillas, M., de Arriaga, D., Serra, D., Asins, G., Hegardt, F. G., and Gomez-Puertas, P. (2007) *J. Biol. Chem.* **282,** 18212–18224
14. Kolodziej, M. P., and Zammit, V. A. (1990) *Biochem. J.* **272,** 421–425
15. Zammit, V. A., Corstorphine, C. G., Kolodziej, M. P., and Fraser, F. (1998) *Lipids* **33,** 371–376
16. Faye, A., Esnous, C., Price, N. T., Onfray, M. A., Girard, J., and Prip-Buus, C. (2007) *J. Biol. Chem.* **282,** 26908–26916
17. Popot, J. L., and Engelman, D. M. (1990) *Biochemistry* **29,** 4031–4037
18. Russ, W. P., and Engelman, D. M. (1999) *Proc. Natl. Acad. Sci. U. S. A.* **96,** 863–868
19. Kolodziej, M. P., Crilly, P. J., Corstorphine, C. G., and Zammit, V. A. (1992) *Biochem. J.* **282,** 415–421
20. Chen, H., and Kendall, D. A. (1995) *J. Biol. Chem.* **270,** 14115–14122

21. Kochendoerfer, G. G., Salom, D., Lear, J. D., Wilk-Orescan, R., Kent, S. B., and DeGrado, W. F. (1999) *Biochemistry* **38,** 11905–11913
22. Schuck, P. (2000) *Biophys. J.* **78,** 1606–1619
23. Adams, P. D., Arkin, I. T., Engelman, D. M., and Brunger, A. T. (1995) *Nat. Struct. Biol.* **2,** 154–162
24. Adams, P. D., Engelman, D. M., and Brunger, A. T. (1996) *Proteins* **26,** 257–261
25. Brunger, A. T., Adams, P. D., Clore, G. M., DeLano, W. L., Gros, P., Grosse-Kunstleve, R. W., Jiang, J. S., Kuszewski, J., Nilges, M., Pannu, N. S., Read, R. J., Rice, L. M., Simonson, T., and Warren, G. L. (1998) *Acta Crystallogr. D Biol. Crystallogr.* **54,** 905–921
26. Jackson, V. N., Zammit, V. A., and Price, N. T. (2000) *J. Biol. Chem.* **275,** 38410–38416
27. Krogh, A., Larsson, B., von Heijne, G., and Sonnhammer, E. L. (2001) *J. Mol. Biol.* **305,** 567–580
28. Sonnhammer, E. L., von Heijne, G., and Krogh, A. (1998) *Proc. Int. Conf. Intell. Syst. Mol. Biol.* **6,** 175–182
29. Lemmon, M. A., Flanagan, J. M., Hunt, J. F., Adair, B. D., Bormann, B.-J., Dempsey, C. E., and Engelman, D. M. (1992) *J. Biol. Chem.* **267,** 7683–7689
30. Langosch, D., Brosig, B., Kolmar, H., and Fritz, H. J. (1996) *J. Mol. Biol.* **263,** 525–530
31. Ding, F. X., Xie, H., Arshava, B., Becker, J. M., and Naider, F. (2001) *Biochemistry* **40,** 8945–8954
32. Lazarova, T., Brewin, K. A., Stoeber, K., and Robinson, C. R. (2004) *Biochemistry* **43,** 12945–12954
33. Melnyk, R. A., Partridge, A. W., Yip, J., Wu, Y., Goto, N. K., and Deber, C. M. (2003) *Biopolymers* **71,** 675–685
34. Staros, J. V. (1982) *Biochemistry* **21,** 3950–3955
35. Fisher, L. E., Engelman, D. M., and Sturgis, J. N. (1999) *J. Mol. Biol.* **293,** 639–651
36. Russ, W. P., and Engelman, D. M. (2000) *J. Mol. Biol.* **296,** 911–919
37. Senes, A., Engel, D. E., and DeGrado, W. F. (2004) *Curr. Opin. Struct. Biol.* **14,** 465–479
38. Schneider, D., and Engelman, D. M. (2004) *J. Mol. Biol.* **343,** 799–804
39. Dawson, J. P., Weinger, J. S., and Engelman, D. M. (2002) *J. Mol. Biol.* **316,** 799–805
40. Zammit, V. A., Fraser, F., and Corstorphine, C. G. (1997) *Adv. Enzyme Regul.* **37,** 295–317
41. Mendrola, J. M., Berger, M. B., King, M. C., and Lemmon, M. A. (2002) *J. Biol. Chem.* **277,** 4704–4712
42. Schneider, D., and Engelman, D. (2004) *J. Biol. Chem.* **279,** 9840–9846
43. Zammit, V. A., Corstorphine, C. G., and Kolodziej, M. P. (1989) *Biochem. J.* **263,** 89–95
44. Turkaly, P., Kerner, J., and Hoppel, C. (1999) *FEBS Lett.* **460,** 241–245